A Three-Dimensional Population Balance Model of Granulation Processes Employing Mechanistic Kernels

Jonathan Ming-Hin Poon

July 2008

A thesis submitted for the degree of
the University of London and
Diploma of Membership of Imperial College

Centre for Process Systems Engineering
Department of Chemical Engineering
Imperial College London
United Kingdom

BIBL. LONDON UNIV.

Abstract

Granulation is a process for agglomeration where powder material is combined with liquid binder solution to facilitate the formation of larger, free-flowing granules. Granulation has become a mainstream process amongst the industries with applicability in numerous areas, which include the pharmaceuticals, mineral processing, fertilisers and in the production of a range of commodity products. A major driving force for the production of granules from their ungranulated counterparts arises from the economic savings i.e., increased bulk density permits savings to be made in transportation and storage. Furthermore, granules may be tailored to possess certain desirable attributes that will suit their final application.

Granulation is an example of a process that exhibits complex interactions between the underlying granulation phenomena such as nucleation, consolidation, aggregation and breakage. In addition, the granule properties are distributed heterogeneously across the entire particle population, posing as a particular challenge in generating a mathematical model that is able to accurately describe the granulation behaviour. The modelling approach used in this study is different from common practices, which tend to rely on heuristics and empiricism for the operation of the granulation process. This empirical approach signifies a disconnect from our understanding of the underlying physics of the process, and is an impediment towards the efficient operation of granulation processes. The work presented in this thesis attempts to address this disconnect by applying a three-dimensional population balance with mechanistic representations for the underlying granulation rate processes. The population balance framework is ideally suited for this particular process, as it enables the evolution of the granules to be tracked with respect to differentiating particle traits, e.g. the granule size distribution. The selection of the distributed particle properties is influenced by the importance of these particle properties on the end granule product, and also by their influence on key process mechanisms.

A novel mechanistic nucleation kernel is developed incorporating fundamental material

properties pertaining to the powder substrate and the liquid binder solution. The model form of the nucleation kernel is formulated by drawing a parallel with the collision/transition state theory. There are few literature reports on the inclusion of nucleation phenomena in the population balance models of granulation processes, let alone a mechanistic nucleation model. This study is one of the first in this regard. The recent recognition of the importance of the wetting kinetics and the nucleation thermodynamics on the nucleation phenomenon has been factored into the nucleation kernel by explicitly accounting for the effects of the liquid flow rate and the physicochemical properties of the material properties (surface tension. contact angle, and spreading coefficient).

Batch granulation experiments were conducted obtaining granule measurements with respect to the size distribution, porosity and fractional binder content. Preliminary results for the validation of the population balance model with the experiment-measurements showed a good agreement, providing partial *albeit* valuable validation of the population balance model. This is also one of the first studies to model and validate a three-dimensional population balance model for granulation.

Model based analyses were also carried out under a variety of processing conditions, which included the effects of changing formulations, droplet size effects, feed size distribution and the effects of powder and binder properties. The proposed model demonstrated the interactions for a range of feed formulations in tandem with granulating operating conditions, establishing qualitative agreement with similar findings derived from past experimental studies. These qualitative agreements along with the quantitative validation mentioned above give positive insight into the predictive capability of the model.

Acknowledgments

There have been many people that have contributed to my research and have supported me during my time spent at Imperial College London. Firstly, I would like to express my deepest thanks to my supervisor, Dr. Charles Immanuel for providing me with the opportunity to work on this project, providing me with encouragement and support throughout as well as fulfilling a childhood dream of going to Australia. Thank you. I would also like to thank Dr. Frantisek Stepanek for the early support during the initial stages of my research. I would like to thank our collaborators from the University of Queensland and the University of California at Santa Barbara, to name but a few, Prof. Frank Doyle III, Prof. Ian Cameron, Prof. Jim Litster, Mr. David Page, Dr. Fu-Yang Wang, Dr. Lian Liu, Dr. Rachel Smith, without them the three month stint in Brisbane would not have been possible. To Thomas Glaser and Constantijn Sanders, we shared great times during the project and during our time exploring Brisbane. I would like to especially thank Prof. Jim Litster and his family for inviting us to their barbecue which made our time in Brisbane all the more enjoyable.

I would like to thank my parents and my brother Thomas for providing me with continued support during the troughs and peaks over the years. I would like to also thank my aunties for always putting a smile on my face whenever we visit, especially to Kwai-Heung and Kwai-Fan for their contagious humour. To my friends Jacob, Laleh, Murthy, Nuno, Alexandros, Diogo, Carolyn, Michaela, Senait, Cristina and Jerry. Finally, I would like to express my deepest thanks to all my friends within our research group. To Rohit, for continually making new nick names for me. To Nicola, truly you are an inspiration to all for not succumbing to the pressures in life. Your carefree attitude is something to be desired. To Stephen, for providing much needed comic relief over the past few years and perhaps the most interesting of all characters your past was a true revelation. To Mark, for being incredibly intelligent and giving the time to advise us whenever we needed it. To Bruno and Javier, although we didn't meet up as often I nevertheless enjoyed your company.

Nomenclature

Roman symbols

A	cross-sectional area of pellet
A_0	constant
β^*	size dependent part of the aggregation kernel
β_0	size independent part of the aggregation kernel
β	aggregation kernel
Ca	dimensionless capillary number
c	constant
c_1	constant
D_d	droplet diameter
D_p	particle diameter
D_{op}	original pellet diameter
$\bar{D}_p$	average particle diameter
F	particle density function
F_{load}	force
H	pellet height at a particular time instance
H_0	initial height of the granular pellet
k_{nuc}	nucleation kernel
k	Boltzmann constant
l_{sat}	liquid saturation of the granule
LS	fractional binder content
N_p	number of primary particles
N_A	Avogadro number
p	refers to the particle
Q	liquid binder flow rate

r	particle radius
r_d	droplet radius
R	ideal gas constant
R_{pore}	pore radius
$\Re_{nuc}$	rate of nucleation
$\Re_{aggre}$	rate of aggregation
$\Re_{break}$	rate of breakage
St_{def}	dimensionless Stoke's deformation number
Str^*	dimensionless peak flow stress
T	granulation operating temperature
u_0	relative collision velocity
V	volume
V_0	volume of a single droplet
$V_{penetrate}$	volume of binder droplet that penetrates into the powder bed
$V(t)$, V_{up}	volume of binder droplet remaining on the powder surface at time t
W	Fuch's stability ratio
W_{CS}	work of cohesion for a solid
W_{CL}	work of cohesion for a liquid
W_A	work of adhesion for an interface
x	fraction of primary particles

Greek symbols

ε	particle porosity
ε_{eff}	effective porosity of the granule
$\dot{\varepsilon}$	strain rate
λ	spreading coefficient
μ	viscosity of the liquid binder
Ψ_a	dimensionless spray flux
ρ_s	particle density
ρ_l	liquid binder density
ϕ	particle shape factor
σ	stress

θ	contact angle made between the solid-liquid interface
γ	interfacial energy
v_{platen}	velocity of platen
ζ	natural strain

Subscripts

S	denotes the solid phase
L	denotes the liquid phase
G	denotes the gas phase
n, nuc	refers to the nuclei particle

Superscripts

upp	upper limit of particle size

Abbreviations

API	active pharmaceutical ingredient
PSD	particle size distribution
GSD	granule size distribution
PBE	population balance equation

Contents

Abstract **2**

Acknowledgments 4

Nomenclature 5

Table of Contents 8

List of Tables 12

List of Figures **20**

1 Introduction **22**

1.1 Granulation process 22

1.1.1 Introduction 22

1.1.2 Granulation mechanisms 26

1.1.3 Concluding remarks 29

1.2 Thesis objectives 30

1.3 Thesis outline 31

2 Literature survey **33**

2.1 Physics and mechanisms of the granulation process 33

2.2 Numerical solution techniques 43

2.3 Controllability of granulation processes 51

2.4 Summary 55

3 Formulation of the population balance **58**

3.1 Introduction 58

3.2 Derivation of the population balance equation 59
3.2.1 Higher-dimensional population balances 60
3.2.2 Description of sub-rate processes 62
3.2.3 Two-dimensional visualisation 64
3.3 Model extensions to other scenarios 65
3.4 Introducing a mechanistic representation of the aggregation kernel 67
3.5 Mechanistic formulation of the nucleation kernel 70
3.5.1 Review of the nucleation phenomenon 70
3.5.2 Formulation properties 72
3.5.3 Development of the nucleation kernel 76
3.5.4 Numerical method for multi-dimensional population balance models . 85
3.6 Model simulation results and discussions 87
3.6.1 Seeded granulation: aggregation and consolidation 87
3.6.2 Combined nucleation, aggregation and consolidation 89
3.6.3 Parametric sensitivities and perturbation studies 93
3.6.4 Process sensitivities with spray flux simulations 97
3.7 Conclusion 101

4 Batch granulation experiments and model validation 105
4.1 Introduction 105
4.2 Model inputs under mechanistic kernels 106
4.3 Experimental 107
4.3.1 Materials 107
4.3.2 Particle size analysis 110
4.3.3 Porosimetry 110
4.3.4 Spectrophotometry 110
4.3.5 Dynamic strength of moist powder compacts 111
4.3.6 Granulation experiments 111
4.4 Results and discussions 113
4.4.1 Effects of moisture content and drum loading 114
4.4.2 Dimensional analysis 123
4.5 Summary 127

5 Studies of granulation variables on process inferences **129**

5.1 Introduction 129

5.2 Formulation properties and process conditions 131

5.2.1 Effects of formulation properties 131

5.2.2 Effects of feed size distribution 138

5.2.3 Manipulation of process conditions 140

5.3 Summary 142

6 Conclusions and recommendations **145**

6.1 Conclusions 145

6.2 Recommendations 147

List of Publications and Presentations **150**

Bibliography **153**

A Dimensionless spray flux derivation **165**

A.1 Dimensionless spray flux 165

A.2 Model extension of the dimensionless spray flux 167

B Analytical techniques **169**

B.1 Particle size analysis 169

B.2 Porosimetry 169

B.3 Fractional binder content determination 169

B.3.1 Calibration curve 170

B.3.2 Procedure for binder content determination 172

C Material properties **174**

C.1 Liquid binder property measurements 174

C.1.1 Binder-substrate contact angle 174

C.1.2 Binder viscosity 176

D Dynamic strength - axial compression test methodology **177**

D.1 Preparation for axial compression 177

D.2 Dimensional analysis with Str* and Ca 179

E Batch granulation data **182**

F Population balance model **195**

F.1 Determination of phenomenological kernel parameters 195

F.2 Population balance model degrees of freedom 196

List of Figures

1.1 Schematic of a rotary drum granulator. 24

1.2 Schematic of a Lödige mixer granulator. This particular granulator unit has chopper blades to facilitate the break-up of any material build-up against the internal walls of the equipment. Adapted from Hoornaert et al. (1998). 24

1.3 Schematic of a fluidised bed granulator with three possible configurations for the spray system: (i) top-spray, (ii) tangential-spray and (iii) bottom-spray. Adapted from Salman et al. (2007). 25

1.4 Schematic of a continuous granulation circuit employed in the fertiliser industry. Adapted from Ennis (1996). 27

1.5 Schematic of the different liquid saturation states that exist for liquid-bound granules of varying liquid binder-to-powder ratios (Combined findings from Rhodes (1990) and York and Rowe (1994)). Adapted from Iveson et al. (2001). 28

1.6 Modern view of the granulation process comprised of three predominant growth mechanisms: (a) wetting and nucleation, (b) consolidation and coalescence, and (c) attrition and breakage. Adapted from Iveson et al. (2001). 29

2.1 Schematic representation for the methods of nucleation based on the immersion (SMIH) and distribution (SMDH) hypothesis proposed by Schaefer and Mathiesen (1996a). Adapted from Schaefer and Mathiesen (1996a). 35

2.2 The nucleation regime map describes three regimes: (a) the droplet controlled regime, (b) the intermediate regime and (c) the mechanical dispersion regime. Different granule formation characteristics are exhibited within each type of regime domain. Adapted from Hapgood (2000). 37

2.3 Schematic of a collinear binary collision between two granules separated by a distance h, with a representative collision velocity of U. The particles shown here have a diameter d_g, surface asperity of height h_a and are coated with a thin binder liquid layer of thickness h_b. Adapted from Ennis et al. (1991). . . 41

2.4 Discretised grid indicating the pivots (x_i) and a hypothetical new born particle partitioned between the two pivots such that two pre-chosen properties are conserved. The grid shown here is for illustration purposes only, and need not be linear. Instead a geometric, or arbitrarily discretised grid may be used. Adapted from Kumar and Ramkrishna (1996a). 44

2.5 A graphical illustration with interpretation of the weights (W) and the respective nodes (the abscissas, ζ) used in the quadrature approximation to the actual distribution function. 48

3.1 Schematic of a finite element (rth finite element) discretised along the respective internal coordinate axis. The particles are shown here convecting along the coordinate axis with a convective velocity, GR, passing across the finite element boundary interface. 60

3.2 Establishing the relationships for the granule properties (l_{sat}, w, ε) from the three internal state variables of a granule: solid volume (S), liquid volume (L) and volume of air (G). Adapted from Verkoeijen et al. (2002). 64

3.3 Illustration showing the assignment of particles with corresponding size and fractional binder content for a two-dimensional visualisation of the particle distribution. 65

3.4 Schematic representation for type I and type II coalescence (Liu et al., 2000). The representative collision velocity between the two particles is denoted by u_0. For type I coalescence (i), the particles' initial kinetic energy is fully dissipated in the viscous binder layer ($u_1 \leq 0$). In type II coalescence, particle surfaces collide as the kinetic energy is greater than can be dissipated in the viscous binder layer (forward path). The particles begin to rebound from one another due to inherent elastic energy, which is dissipated during the retraction phase. There is again viscous losses through the binder layer, which bring the particles to rest ($u_3 \leq 0$) thereby preventing complete particle separation (reverse path). Adapted from Liu et al. (2000). 69

3.5 Schematic illustration of the nucleation process. (a) binder droplet formation. (b) droplet coalescence and overlap, (c) binder dispersion via wetting and capillary penetration, (d) mechanical dispersion of the binder droplet. Adapted from Litster and Ennis (2004). 72

3.6 Schematic depicting the work of cohesion for homogenous phases and the work of adhesion for composite interfaces for solid and liquid systems. The solid and liquid phases are denoted by S and L respectively. Adapted from York (1995). 74

3.7 Schematic of a liquid binder droplet placed on the surface of the powder bed mass. The solid, liquid and vapour/gas phase is denoted by S, L and V respectively. The interfacial surface energies between solid-vapour, liquid-vapour and solid-liquid are denoted by γ^{SV}, γ^{LV} and γ^{SL} respectively. Adapted from Litster and Ennis (2004). 74

3.8 Schematic depiction illustrating the fluid flow through powder beds for (a) well-packed powder compact and (b) loosely packed powder. In loosely packed powder, the possibility of macrovoids is higher. These pockets serve to impede fluid flow whereby pores that terminate at macrovoids with a radius much greater than its own will effectively block the progression of flow beyond that point. Adapted from Hapgood et al. (2002). 79

3.9 Schematic representation of (a) decreasing drawing area and (b) constant drawing area. Adapted from Marmur (1988). 82

3.10 Schematic representation of the nucleation mechanism. The unpenetrated volume of droplet that remains on the powder surface is denoted by $V_{up} = V(t)$. 83

3.11 Schematic representation of the hierarchical two-tier algorithm (Immanuel and Doyle III, 2003). 87

3.12 Time profiles of the average particle size (a); and the total number of particles (b), due to combined aggregation and consolidation. 89

3.13 Time evolution of the granule PSD due to combined aggregation and consolidation. 90

3.14 Three-dimensional plots at two time instances of 3.3 min and 6.7 min; (a) and (c) show the particle distributions with respect to the solid volume and the liquid volume for a gas volume of $8.7 \times 10^{-15}\,\mathrm{m}^3$; (b) and (d) show the particle distributions with respect to the solid volume and the gas volume for a liquid volume of $1.2 \times 10^{-14}\,\mathrm{m}^3$. 91

3.15 The initial seed of primary particles. 92

3.16 Time profile of the average particle size (a); and the early time profile of primary particles (b) with progress of nucleation along with consolidation and aggregation. 93

3.17 Time evolution of the granule size distribution under combined nucleation, aggregation and consolidation: (a) $t = 8 \times 10^{-3}\,\mathrm{s}$, (b) $t = 2 \times 10^{-2}\,\mathrm{s}$, (c) $t = 5 \times 10^{-2}\,\mathrm{s}$, (d) $t = 1 \times 10^{-1}\,\mathrm{s}$, (e) $t = 4 \times 10^{-1}\,\mathrm{s}$, (f) $t = 1\,\mathrm{s}$. 94

3.18 Effect of primary particle distribution on the process. 95

3.19 Comparison of the granule size distribution for different feed size primary particles at three different times: (a) and (b) $t = 2\times10^{-2}\,\mathrm{s}$; (c) and (d) $t = 5\times10^{-2}\,\mathrm{s}$; (e) and (f) $t = 1 \times 10^{-1}\,\mathrm{s}$. 96

3.20 Comparison of the end-point granule size distribution for the mono-sized primary particles (a) and the four-sized primary particles (b). 97

3.21 Effect of bed turnover rate relative to binder penetration rate, conceptually analysed in terms of the fraction of unpenetrated binder droplet. 98

3.22 The end-point particle size distribution obtained for the cases where the bed turnover rate is larger than the binder penetration rate into the bed, thereby leaving some unpenetrated binder liquid on the surface (a) 10% unpenetrated surface liquid; (b) 40% unpenetrated surface liquid; (c) 60% unpenetrated surface liquid. The unpenetrated surface liquid is uniformly partitioned into all the particles and nuclei. Compare against Figure 3.17f for the case with complete binder penetration into the bed. 99

3.23 Comparison of time profiles for the evolution of the average granule size subject to the influences of nucleation with aggregation and granule consolidation (a); and the time evolution of the average nucleus diameter during early nucleation for powder velocities 0.33 m/s ($\Psi_a = 0.54$), 2.1 m/s ($\Psi_a = 0.09$) and 7.8 m/s ($\Psi_a = 0.02$). 100

3.24 Time profiles for the depletion of primary particles during granule nucleation (a), and the overall decrease in the total number of granules in the system as a combined result of nucleation, aggregation and consolidation (b). for powder velocities 0.33 m/s ($\Psi_a = 0.54$), 2.1 m/s ($\Psi_a = 0.09$) and 7.8 m/s ($\Psi_a = 0.02$). 102

3.25 The end-point granule size distribution for three cases where the powder velocity was set to 0.33 m/s, 2.1 m/s and 7.8 m/s, which corresponds to a dimensionless spray flux of $\Psi_a = 0.54$, $\Psi_a = 0.09$ and $\Psi_a = 0.02$, respectively. . . . 103

4.1 Scanning electron micrograph images for primary particles of calcite powder at magnifications of ×200 (a) and ×1213 (b). Both the particle size and shape of the primary particles can be seen as non-spherical and rough. 109

4.2 Volume distribution of primary particles from the calcite powder. 109

4.3 Model prediction for the total number of particles (a) and a comparison between model predictions and batch granulation experiments for the evolution of the average granule diameter (b) for the case with a binder-to-solids ratio of 0.11 and a drum load of 1.5 kg of $CaCO_3$ powder (case 1). 116

4.4 Comparison between model predictions and batch granulation experiments for time profiles of the average fractional binder content (a), and the average granule porosity of the granules (b) for the case where the binder-to-solids ratio is 0.11 and a drum load of 1.5 kg of $CaCO_3$ powder (case 1). 116

4.5 Distribution profile for the fractional binder content across the granule size range. Three cases are shown for target binder-to-solid ratio (LS) of 0.11 and 0.12 for initial powder loading of 1.5 kg, the third case corresponds to a LS = 0.11 with a drum loading of 1.75 kg. 118

4.6 Comparison between model predictions on the granule size distribution at various time instances with data derived from batch granulation experiments for the case where the binder-to-solids ratio of 0.11 and a drum load of 1.5 kg of $CaCO_3$ powder (case 1). 119

4.7 Comparison between model predictions on the distribution of granule porosity at various time instances with data derived from batch granulation experiments for the case where the binder-to-solids ratio of 0.11 and a drum load of 1.5 kg of $CaCO_3$ powder (case 1). 120

4.8 Two-dimensional visualisation for the evolution of the granule size distribution at varying time instances, where the particle size and the fractional binder content are shown along each coordinate axes. The results correspond to a binder-to-solids ratio of 0.11 and a drum load of 1.5 kg of $CaCO_3$ powder (case 1). 121

4.9 Comparison between model predictions on the granule size distribution at various time instances with data derived from batch granulation experiments for the case where the binder-to-solids ratio of 0.12 and a drum load of 1.5 kg of $CaCO_3$ powder (case 2). 122

4.10 Comparison between model predictions on the distribution of granule porosity at various time instances with data derived from batch granulation experiments for the case where the binder-to-solids ratio of 0.12 and a drum load of 1.5 kg of $CaCO_3$ powder (case 1). 123

4.11 Comparison between model predictions on the granule size distribution at various time instances with data derived from batch granulation experiments for the case where the binder-to-solids ratio of 0.11 and a drum load of 1.75 kg of $CaCO_3$ powder (case 3). 124

4.12 Evolution of the average granule diameter, fractional binder content and the average granule porosity for cases 1, 2 and 3 with comparisons made between model predictions and data derived from batch granulation experiments. Cases 1 and 2 correspond to a binder-to-solids ratio of 0.11 and 0.12, respectively, and an initial drum load of 1.5 kg with $CaCO_3$ powder. Case 3 corresponds to a target binder-to-solids ratio of 0.11 with an initial drum load of 1.75 kg with $CaCO_3$ powder. 125

4.13 Profile of the stress against the natural strain (a) and (b) the peak flow stress against varying strain rates for preformed $CaCO_3$ pellets with a fractional binder content of 0.12. 126

4.14 Profile of the dimensionless strength (Str^*) against the capillary number (Ca) for $CaCO_3$ pellets with fractional binder content of 0.12. 126

5.1 Profile of the average granule diameter (a) and the total number of particles (b) over the course of a one hour simulated granulation process for different granulation recipes. 134

5.2 Profile of the average nucleus diameter (a) and the total primary particles (b) for different granulation recipes. 136
5.3 Comparison of the end-point granule size distribution for different formulations used as the granulation recipe for a one hour batch processing time. 137
5.4 Profile of the average granule size (a) and of the evolution of the average granule nucleus (b) for a granulation formulation of glass ballotini-PEG 200. Effective powder porosities of $\varepsilon_{eff} = 0.2$ and $\varepsilon_{eff} = 0.07$ were used, where in both cases, the initial primary particle size was 85.3 μm. A further case was studied where, for the same granulation recipe, smaller constituent particles were used with a size of 65.4 μm and with $\varepsilon_{eff} = 0.07$. 138
5.5 Time profiles for the evolution of the average granule size (a) and the nuclei particle size (b) for a glass ballotini-NDBS formulation. 139
5.6 Time profile of the depletion of primary particles within each type of initial powder feed consisting of mono-sized, two-sized and four-sized powder feed during the nucleation period. 140
5.7 Profile of the average granule size under the influence of varying droplet sizes. 141
5.8 Evolution of the granule nucleus size (a) and the total number of particles (b) under varying droplet sizes. 141
5.9 Simulated granule size distributions at varying time instances using a granulation recipe consisting of glass ballotini-NDBS for droplet sizes of 83.7 μm and 55.8 μm. 143
5.10 Comparison of the end-point particle size distributions for the two cases corresponding to droplet sizes of: 83.7 μm and 55.8 μm. 144

6.1 Schematic illustration of the multi-scale links in the granulation process, with important granulation interactions linked to process operations and formulation properties to the end granule properties (Ramachandran et al., 2008). . . 147

A.1 Illustration of the powder surface passing through the spray zone. The shape of the spray is depicted as line spray, which can be carried out using a flat fan nozzle configuration. The width of the powder bed is w moving through the spray zone with velocity v. The powder flux is defined as $\dot{A} = v \times w$ (m^2/s). . 166

B.1 Absorption spectrum for the blue dye component for solution strengths varying from 0.05%-2%. The optimum peak absorption for the dye occurs at a wavelength of 630 nm. A standard solution of dye with a concentration of 8.9 g/L represents 100% solution strength. 171
B.2 Calibration curve. 172
B.3 Schematic of the binder content measurement procedure. 173

C.1 Schematic of the contact anglometer (a) preparation of the compressed powder bed; (b) and the introduction of the droplet onto the powder surface via a hypodermic syringe. 175

D.1 Schematic of the pellet press and the pellet cast both manufactured from stainless steel. Adapted from Smith (2008). 178
D.2 Schematic of the granular pellet undergoing axial compression. Adapted from Iveson et al. (2002). 178
D.3 Stress versus natural strain profiles for varying platen velocities for binder-to-solids-ratio of 0.10 and 0.14. 180
D.4 Peak flow stress versus strain rate profiles for binder-to-solids-ratio of 0.10 and 0.14. 180
D.5 Dimensionless pellet strength versus the dimensionless capillary number for binder-to-solids-ratio of 0.10 and 0.14. 181

E.1 Illustration of the locations of the six sample locations. 183

List of Tables

1.1 Typical characteristics of granulator units. 26

3.1 List of parameters used for simulations involving aggregation and consolidation. 88
3.2 List of parameters used for the nucleation simulations. 92
3.3 List of parameters used for the nucleation and spray flux simulations 100
3.4 Probability of single drops with corresponding spray flux parameters 101

4.1 Model forms of the consolidation, nucleation and aggregation kernels. 106
4.2 Summary of inputs used in mechanistic kernels. 108
4.3 Batch granulation variables 113
4.4 Adjustable parameters pertaining to sub-rate process kernels. 115
4.5 Fundamental material properties and adjustable parameters set with nominal values. 115

5.1 Summary of formulation properties. 132
5.2 Simulation parameters for consolidation, nucleation and aggregation. 132
5.3 Spreading coefficient evaluated from liquid binder surface energies. 133

B.1 Repeatability tests on working standard with a 2% solution strength. 170

E.1 Normalised GSD for binder-to-solids ratio of 0.11 and 1.5 kg of powder–Set 1. 184
E.2 Normalised GSD for binder-to-solids ratio of 0.11 and 1.5 kg of powder–Set 2. 184
E.3 Normalised GSD for binder-to-solids ratio of 0.11 and 1.5 kg of powder–Set 3. 185
E.4 Granule porosity for binder-to-solids ratio of 0.11 and 1.5 kg of powder–Set 1. 185
E.5 Granule porosity for binder-to-solids ratio of 0.11 and 1.5 kg of powder–Set 2. 185
E.6 Granule porosity for binder-to-solids ratio of 0.11 and 1.5 kg of powder–Set 3. 186

E.7 Fractional binder content of granules for target binder-to-solids ratio of 0.11 with 1.5 kg of powder–Set 1. 186
E.8 Fractional binder content of granules for target binder-to-solids ratio of 0.11 with 1.5 kg of powder–Set 2. 187
E.9 Fractional binder content of granules for target binder-to-solids ratio of 0.11 with 1.5 kg of powder–Set 3. 187
E.10 Normalised GSD for binder-to-solids ratio of 0.12 and 1.5 kg of powder. . . . 188
E.11 Granule porosity for binder-to-solids ratio of 0.12 and 1.5 kg of powder. . . . 188
E.12 Fractional binder content of granules for target binder-to-solids ratio of 0.12 with 1.5 kg of powder. 189
E.13 Normalised GSD for binder-to-solids ratio of 0.11 and 1.75 kg of powder. . . . 189
E.14 Granule porosity for binder-to-solids ratio of 0.11 and 1.75 kg of powder. . . . 190
E.15 Fractional binder content of granules for target binder-to-solids ratio of 0.11 with 1.75 kg of powder. 190
E.16 Normalised GSD for binder-to-solids ratio of 0.13 and 1.5 kg of powder. . . . 191
E.17 Normalised GSD for binder-to-solids ratio of 0.14 and 1.5 kg of powder. . . . 192
E.18 Normalised GSD for binder-to-solids ratio of 0.13 and 1.75 kg of powder. . . . 193
E.19 Normalised GSD for binder-to-solids ratio of 0.14 and 1.75 kg of powder. . . . 194

Chapter 1

Introduction

1.1 Granulation process

1.1.1 Introduction

Granulation is an example of a size enlargement process in which smaller particulate entities are brought together forming a larger semi-permanent aggregate, whilst the constituent particles that comprise the granule structure remains distinguishable from the main body of the granule matrix (Snow et al., 1997).

The granulation process has been established across a wide range of industries producing final agglomerated products to cater for many of the end-user applications, notably in the production of speciality chemicals, pharmaceutical industry, mineral ore processing and the production of fertilisers to name the least. As a result of the broad usage of this process different technologies are available for the production of granules exhibiting characteristics 'tailored' towards their final end-use application. The particular method of granulation will largely be dictated by the final application for the product since each type of granulation equipment will produce granules of varying attributes (see Table 1.1). The desired properties from granulation and the advantages conferred to the granules as opposed to their un-granulated counterparts are given below:

- *Flowability*: To improve the flow properties and in particular to reduce the tendency for particulate materials to form lumps (*e.g.* hygroscopic materials). Poor flow properties may lead to a wide weight variation in the final product originating from variable fills of tablet dies, which could be minimised or avoided altogether by improving the flow

properties in the blend.

- *Densification*: To reduce losses via handling or transport due to particulate material in their un-granulated form in addition to lower cost of storage and transportation as a result of higher bulk density.
- *Solubility*: To prevent the lumping of fine powders in fluids thus facilitating the dispersion of the powder in the fluid medium.
- *Immobilisation*: In granule form the activity of the principle component (*e.g.* catalyst/biocatalyst in fabric washing powders) is preserved whilst in this so-called carrier form, else the activity will rapidly deteriorate in solution environments.
- *Segregation*: Particle segregation is primarily due to the differences between the particle densities and sizes. It is important to achieve uniform composition of the particles with respect to multiple components to avoid segregation related problems.

In addition to the aforementioned desired properties, granulation can be used to obtain controlled release of active ingredients within the granule. The enhanced attributes of granules provides added value to the final product, in particular foodstuffs will benefit significantly where both the taste and the appearance can improve its market appeal. From a pharmaceutical perspective, controlling the granule size distribution is equally important. Despite not having segregation of multi-components, if there is a wide granule size distribution, segregation of granules with size will occur, which will lead to variations in bulk densities. This is undesirable in applications such as tablet machines, which fill according to volume and not by weight resulting in products with large weight variations, and an uneven dosage of the active pharmaceutical ingredient (API) in the final batch. This situation is undesirable where the objective is to obtain content uniformity with respect to the ingredients.

Owing to the broad usage of the granulation process across numerous industrial sectors, it is not surprising that various terminologies are adopted depending on the industry under consideration. For instance, granulation has been referred to in the past as agglomeration, pelletisation and dry granulation. Therefore in the context of this research, the primary focus will be on the study of wet granulation, *i.e.*, size enlargement by agitation with the addition of a liquid binder.

Typical examples of the various production methods employed utilising different types of equipment to achieve granulation are rotary drums (Figure 1.1), which achieve granulation

through repeating cycles of tumbling motion within the drum. Alternatively, mixer agglomeration units (high-speed flow-type mixers, Figure 1.2) which employ fast moving impeller blades to ensure good liquid dispersion accompanied by the mixing action of the impellers subsequently leading to granule formation under permitting conditions (Hoornaert et al., 1998). Fluidised-bed spray granulators (FBSG) are also commonly used, in which granules are formed through the combination of a hot gaseous fluidised-bed and a fluid spray nozzle that sprays the liquid binder directly onto the fluidised particles (Figure 1.3).

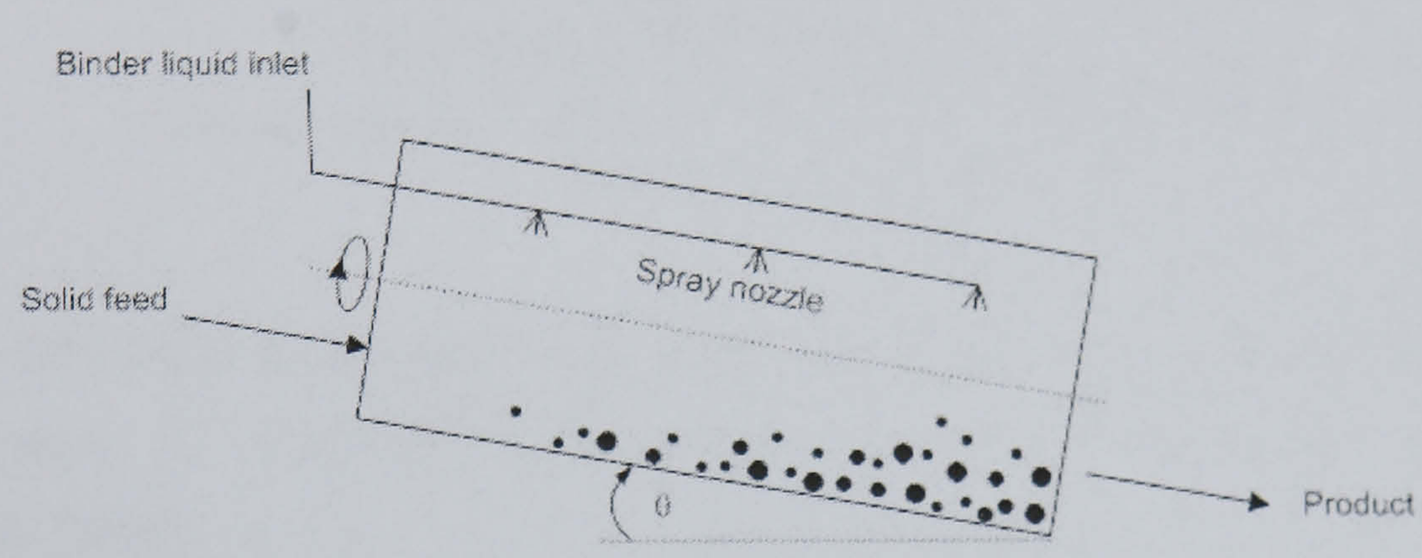

Figure 1.1: Schematic of a rotary drum granulator.

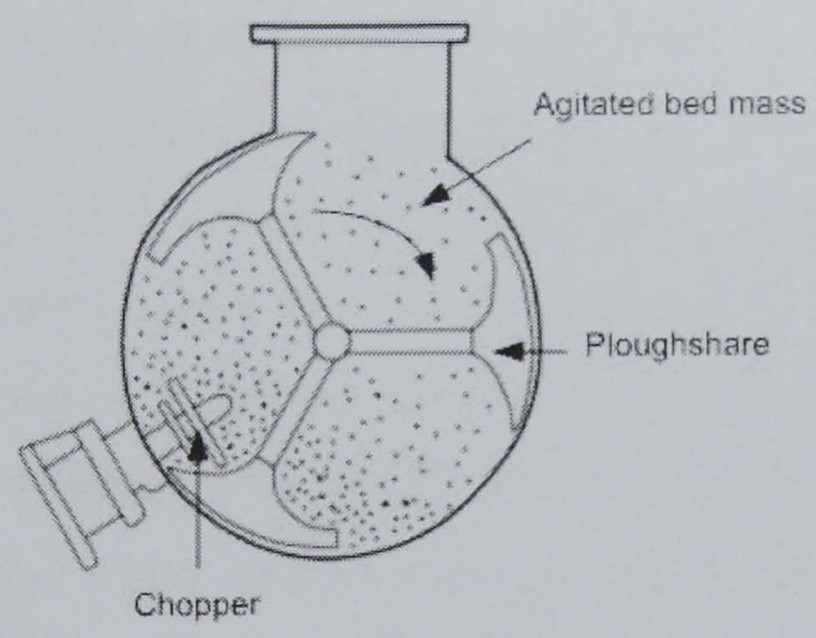

Figure 1.2: Schematic of a Lödige mixer granulator. This particular granulator unit has chopper blades to facilitate the break-up of any material build-up against the internal walls of the equipment. Adapted from Hoornaert et al. (1998).

The granules produced from each of the different granulator units will possess different physical attributes. For instance, the granules produced from either the FBSG or the high shear mixer will produce granules within size ranges typically between $0.1 - 2\,\mathrm{mm}$, which is in contrast to those produced in a low shear drum granulator which are capable of producing granules in the range of $0.5 - 20\,\mathrm{mm}$. In addition to each configuration of the granulator

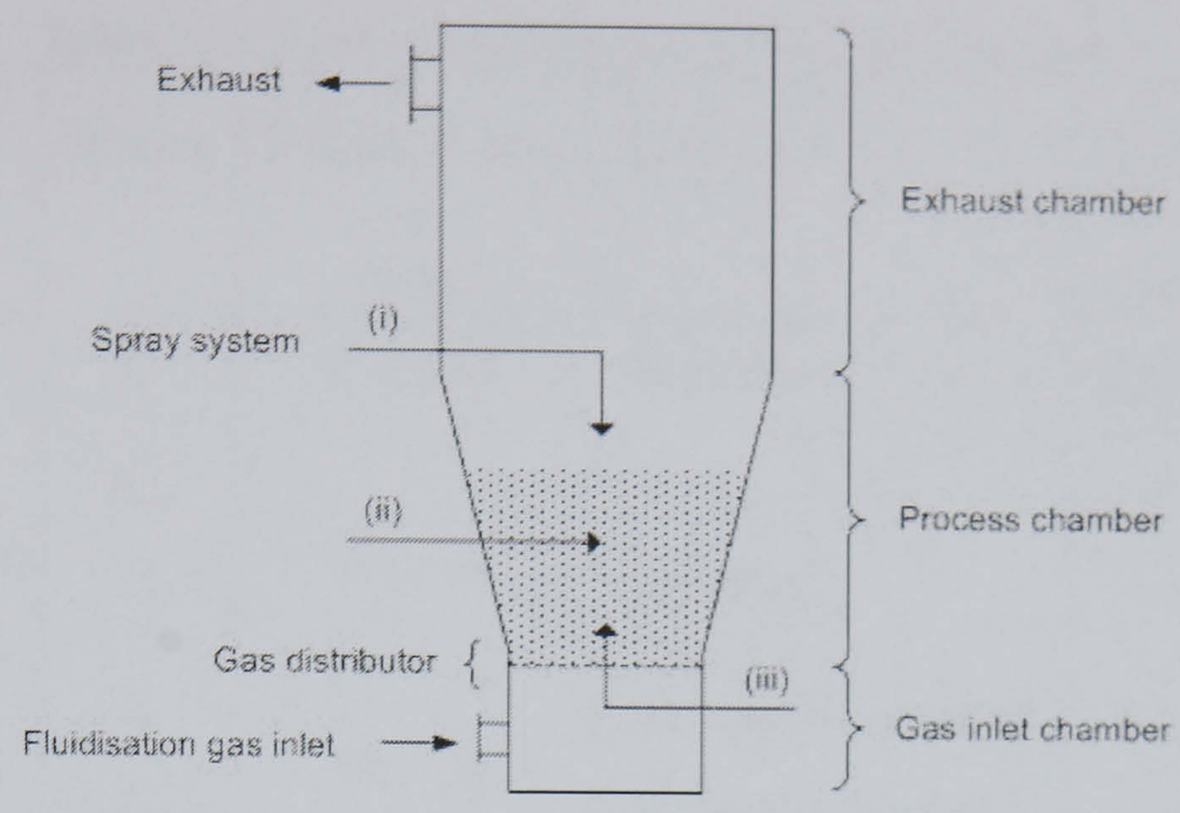

Figure 1.3: Schematic of a fluidised bed granulator with three possible configurations for the spray system: (i) top-spray, (ii) tangential-spray and (iii) bottom-spray. Adapted from Salman et al. (2007).

equipment, there are varying degrees of process operating parameters that may influence the granulation process. For instance, the drum granulator is usually inclined to the horizontal in order to promote the flow of the bed mass. Traditionally, the number and placement of the spray nozzles are fixed beforehand and manipulation of the granulation process may be effected by changing either the spray rate of the binder solution, increasing the residence time, or by changing the drum speed. For the FBSG, in addition to the binder spray rate and the droplet size (achieved through the atomising air pressure) emitted from the spray nozzle there is also the fluidising air velocity and the bed temperature since the FBSG allows for simultaneous granulation and drying to occur within the same processing volume. For the high shear granulator (high-speed flow-type mixers) the control of the bowl temperature, the impeller speed and the spray rate of the binder solution are potential control handles for influencing the granulation process. A high shear mixer of the Lödige type incorporates a chopper for prevention of the accumulation of wall build-up. Table 1.1 provides a summary of the typical granule characteristics that can be expected from a given type of granulation equipment (Snow et al., 1997; Litster and Ennis, 2004).

An example of a continuous granulation circuit is shown in Figure 1.4. At present, granulation processes operated continuously suffer from the drawbacks of experiencing high recycle ratios (3-4:1, recycle/product) (Mort et al., 2001), which indicate that the process is not

Table 1.1: Typical characteristics of granulator units.

Granulator	**Mode**	**Product size** (mm)	**Density**	**Capacity** (ton/hr)
Drum	C	0.5 – 20	Moderate	0.5 – 800
	B			< 500
High shear mixer	C	0.1 – 2	Low-high	< 50
	B		Low (agglomerated)	0.1 – 0.9
Fluidised bed	C	0.1 – 2	Moderate (layered)	50

B = Batch operation

C = Continuous operation

operating at its optimal conditions. The result is the production of off-spec product that require re-work via the recycle. This is undesirable as this can raise the operating costs (*i.e.* additional crushing of oversized particle) with more energy put into the process (*i.e.* requiring additional units: dryer, milling equipment). Process instability may also arise since the effects of the re-introduction of recycle material may cause a shift in the granulation operating regime, moving from steady growth through to rapid uncontrolled growth producing a slurry which may not be reversible leading to loss of materials and loss of production time due to plant shutdown and restart. The inefficient manner in which these processes run originate from the stringent requirements imposed on the products (*e.g.* particle size) in order to maintain the quality standards expected from the products. This is especially true for those products intended for human use such as in pharmaceutical products or in foodstuffs. These requirements in addition to the underlying nature of the complex interactions that exist between the individual granulation phenomena make this process difficult to control.

1.1.2 Granulation mechanisms

The extent of granule growth will depend on the level of liquid saturation, the amount of energy that is put into the system and the physicochemical properties of the solid and the type of liquid binder used during wet granulation. Before introducing the granulation mechanisms, the various likely states of the solid and the liquid aggregates will be discussed. Figure 1.5 illustrates the five different granule states that exists depending on their moisture

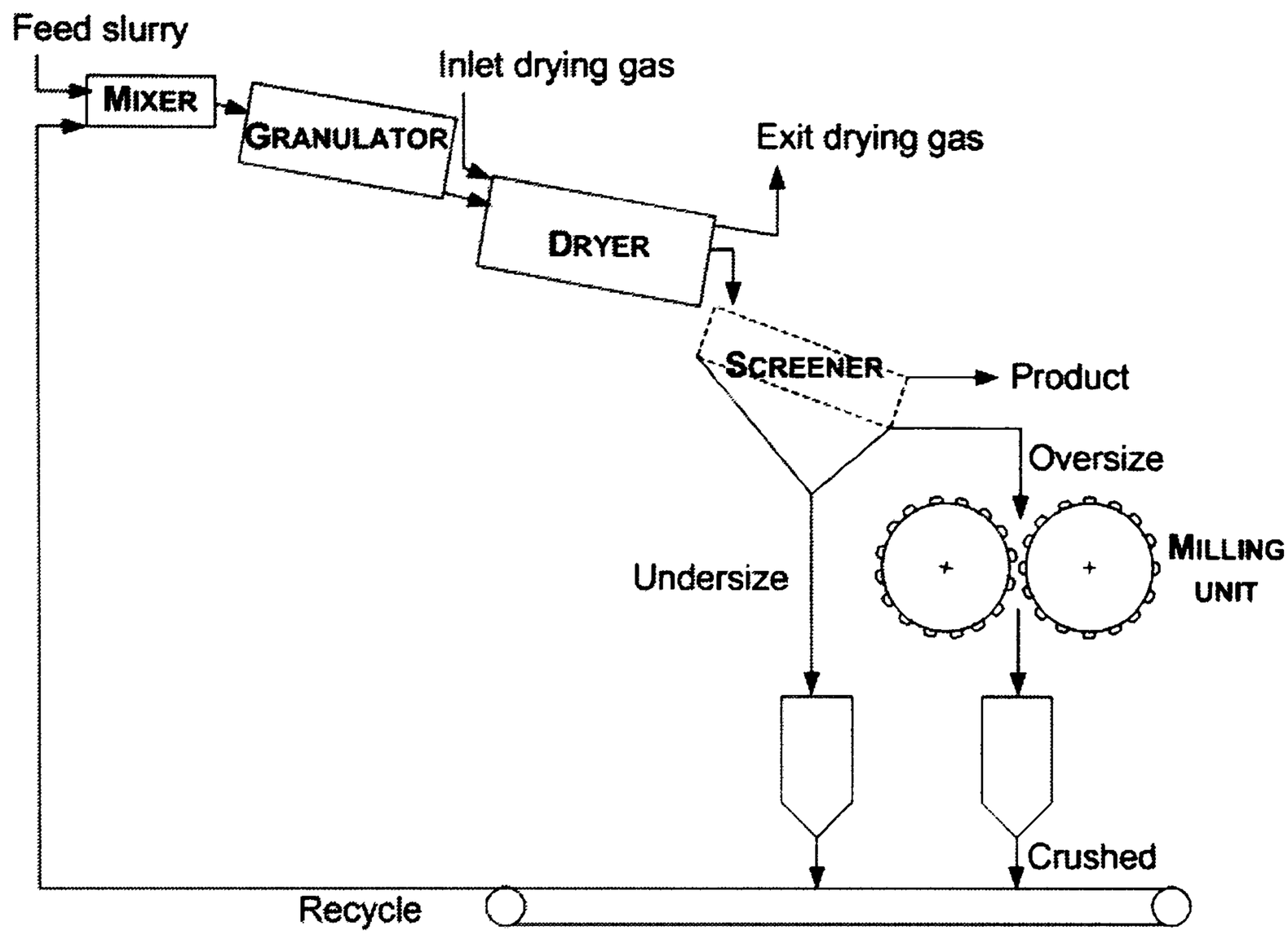

Figure 1.4: Schematic of a continuous granulation circuit employed in the fertiliser industry. Adapted from Ennis (1996).

content. Initially, as the particles and the binder solution are introduced into the system, the particles move through the pendular state whereby the particles are held together by liquid bridges forming pendular bonds at their contact points. With increasing moisture content the granule moves through to the capillary state via the funicular state in which the pores are completely saturated with liquid. Further addition of liquid incorporated into the granule leads to the droplet state where the constituent particles are held within or under the liquid droplet surface. The pseudo-droplet state is a more realistic representation of a granule state with trapped pores or macrovoids since it is likely that not all the pores will be filled with the binder solution. Thus granule growth is influenced in part by the extent of granule liquid saturation as well as the availability of surface-bound liquid that is able to contribute towards the establishment of liquid bridge links holding the particles together.

Having discussed the different states of the granules in Figure 1.5, now the mechanisms of granulation will be presented both the earlier view and the more recent views. Sastry and Fuerstenau (1973) formerly presented five principle granulation mechanisms derived from their tracer studies. These five agglomerate mechanisms were classified as: (a) nucleation, (b)coalescence, (c) breakage, (d) abrasion transfer, and (e) layering ('*snowballing*'). However,

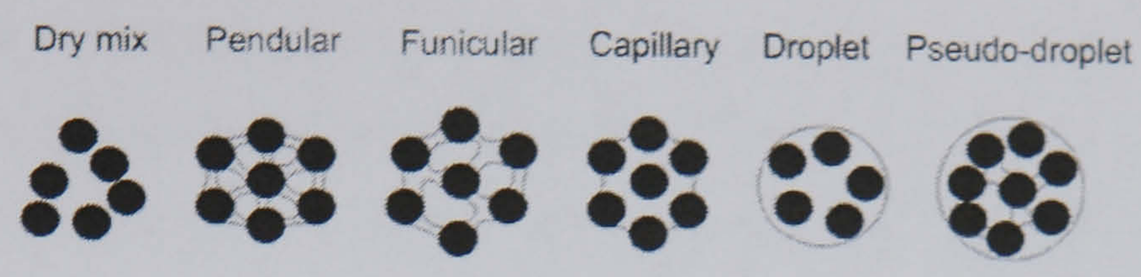

Figure 1.5: Schematic of the different liquid saturation states that exist for liquid-bound granules of varying liquid binder-to-powder ratios (Combined findings from Rhodes (1990) and York and Rowe (1994)). Adapted from Iveson et al. (2001).

a modern view of the process (Figure 1.6) states that there are three predominant rate processes instead of the five growth mechanisms that govern the granulation process (Iveson et al., 2001):

Wetting and nucleation The formation of granules is first initiated by the nucleation of the initial small particles (primary particles). This involves the distribution of a binder solution over the powder bed mass, with the subsequent penetration of the liquid droplet into the powder capturing the particles within its immediate vicinity to form the nucleus. It is quite possible that the initial formation of the nucleus will be weak, with the loosely formed liquid bridges holding the primary particles together to be easily disrupted within the agitated granulator equipment. Thus, these initial nuclei formed during *primary nucleation* are broken up and the nuclei formed during *secondary nucleation* are more likely to be stronger and continue to grow, establishing a platform for future granule growth.

Consolidation and growth The particles at this stage are constantly undergoing consolidation under the influence of the circulating motion within the granulator as well as the weight of the powder bed mass. The particles are compacted, experiencing a reduction in the porosity. A reduction in the internal pore volume forces the internalised liquid to be squeezed from the pores and onto the surface of the granules. The increased availability of surface bound liquid promotes growth via coalescence with other particles or via the layering of fines on the surface of the particles.

Attrition and breakage Granules are susceptible to fragmentation as a result of collisions made with either other particles or by direct contact with the internal surfaces of the granulator (*e.g.* impeller blades, chopper).

The previous growth mechanisms proposed by Sastry and Fuerstenau (1973) could be

considered as either coalescence and/or breakage depending on the cutoff sizes of the particles, which distinguishes one mechanism from the other (Iveson et al., 2001). The modern view is more general, and encompasses the earlier view of Sastry and Fuerstenau (1973). The modern view of the granulation process is now commonly accepted in which the three particle-level phenomena (*i.e.* wetting and nucleation, consolidation and growth, attrition and breakage) are the main driving events for the evolution of the particle population with respect to their characteristic traits (*e.g.* composition, age, size, *etc.*).

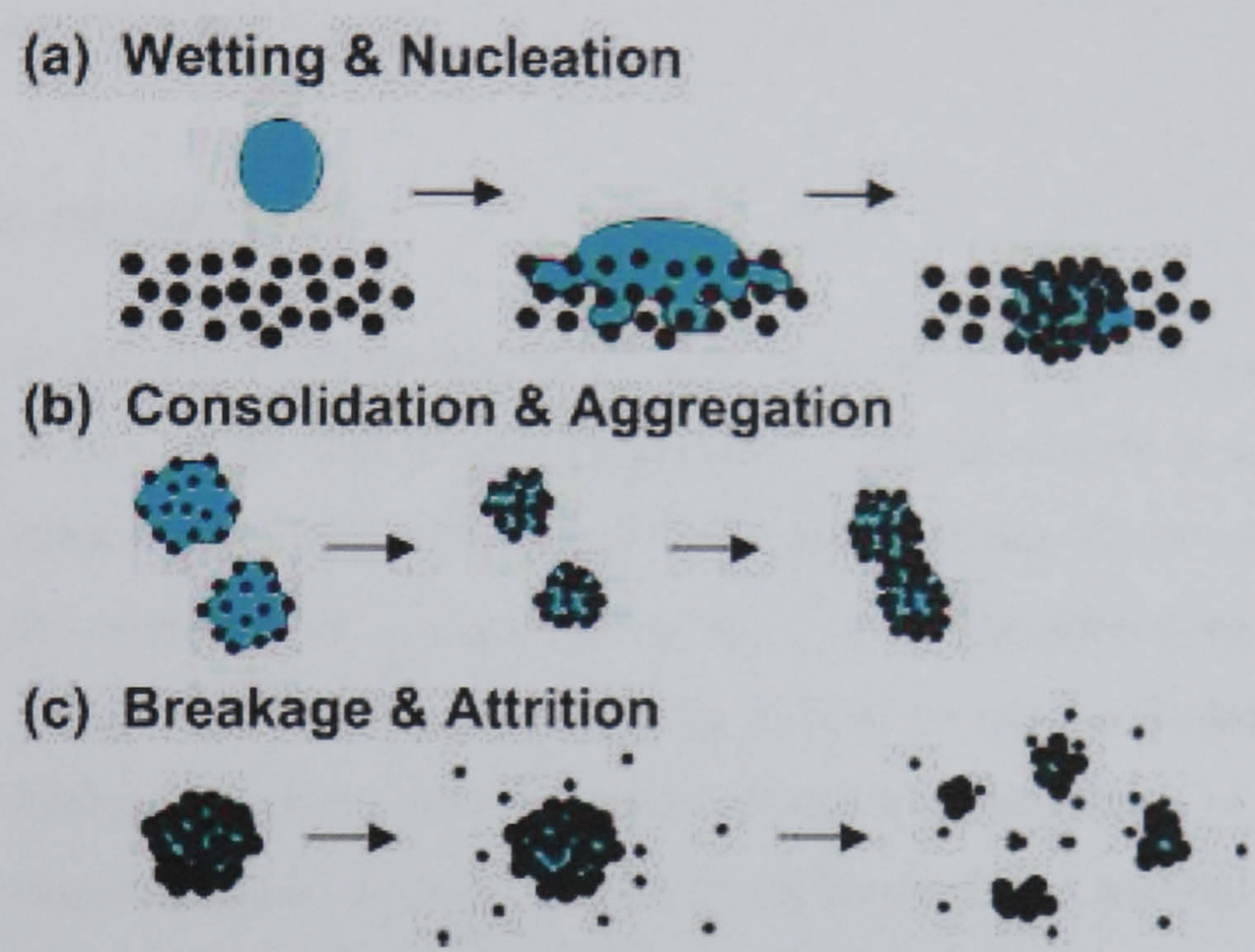

Figure 1.6: Modern view of the granulation process comprised of three predominant growth mechanisms: (a) wetting and nucleation, (b) consolidation and coalescence, and (c) attrition and breakage. Adapted from Iveson et al. (2001).

1.1.3 Concluding remarks

The establishment of the granulation process across various industries emphasises the many applications for granulation, be it the final consumer product or an intermediate within a process (*e.g.* granules used in making tablets). However, the design and scale-up is largely left to empiricism and the dependency on heuristics (Michaels, 2003). The drawback with the empirical approach are the numerous experiments that must be run, which can be a time consuming process, in addition to the amount of resources required for this experimental approach. This presents a need for the development of accurate models capable of mimicking the behaviour of real granulation processes within tolerance limits. However, the complexity

of the process arising from the myriad of interactions that exist between competing granulation phenomena in conjunction with the formulation properties and the process operating conditions, makes the development of such a model a challenging task.

The simplified view of the granulation process comprised of the three aforementioned particle level phenomena has helped in directing the development of models, but so far with reduced ability to account for the formulation properties and the process design parameters. This provides the impetus for the development of models to complement the particle design process (*i.e.* desired particle traits).

1.2 Thesis objectives

Research into granulation processes has been thorough on the mechanistic aspects (Fu et al., 2005; Hoornaert et al., 1998; Sastry and Fuerstenau, 1973; Hounslow et al., 2001; Tardos et al., 1997; Hancock et al., 1994) and equally with the modelling of the process. However, the majority of the models employ empirical kernels (*e.g.* aggregation kernel), having been optimised for a specific formulation and/or being limited to the particular scale at which the model was validated against the experimental data. The limitations of such models, in addition to the aforementioned reasons, often include kernel forms without physical meaning. It is clear that there is limited work in the area of establishing models incorporating phenomenological kernels based on the underlying physics of the process with the notable exceptions of Ennis et al. (1991) and Liu et al. (2000). There is a clear need to investigate the considerable advances on the mechanistic aspects into the multi-scale model for the granulation process, traversing from the micro-scale (particle level) to the macro-scale (equipment level) (Michaels, 2003).

In light of these issues, the aims of this thesis are to address the disconnect by:

- Development of a mechanistic nucleation kernel. The key features of this novel kernel formulation are the incorporation of the material properties for both the binder solution and the solid. Thus, this kernel is able to account for the nucleation thermodynamics and equilibria of the nucleation phenomenon.

- Formulation of a comprehensive multi-dimensional population balance model for the process, with model validation and model based controllability analyses for the granulation process.

- Using experimental measurements distributions of particle size, granule porosity and binder content for the validation of the three-dimensional population balance model incorporating mechanistic representations for the nucleation and the aggregation phenomenon with respect to the three measured particle traits.

- Incipient demonstration of the application and utility of the model for engineering purposes.

1.3 Thesis outline

An outline of the thesis providing a brief synopsis pertaining to each chapter is given below:

- Chapter 2 provides a review of the studies performed in the past on both the experimental side and on the modelling of the granulation process, and the application of numerical solution techniques for this particular type of problem.

- Chapter 3 formally introduces the population balance equation and the framework in which it is applied to the modelling of the granulation system. In particular, the chapter includes the extension of the one-dimensional population balance to a three-dimensional problem eliciting three internal state variables (*i.e.* particle size, porosity, binder content). The development of a mechanistic nucleation kernel is introduced, incorporating material properties into the nucleation dynamics. Parametric sensitivity studies on the initial distribution of primary particles and the dynamics of drop penetration into the powder bed are considered for their effects on the nucleation phenomenon.

- Chapter 4 provides an examination of the growth kinetics for a Calcite-Polyvinyl alcohol formulation using underlying phenomena commonly observed in the granulation literature for data interpretation.

  Experiments were preformed for testing the effects of the binder content and the powder bed depth, to gauge their influence on the granule growth kinetics of the system. The three-dimensional population balance model, employing mechanistic kernel representations for key particle level phenomena linking formulation properties to operating parameters, is validated against experimental results. A demonstration is made of the applicability of first principle models relating formulation properties with processing parameters for the prediction of key particle traits.

- Chapter 5 combines the theoretical analyses from chapter 3 and the experimental studies carried out in chapter 4 and discusses typical controllability issues of the granulation process.

- Chapter 6 provides a summary and concluding remarks for future work.

Chapter 2

Literature survey

2.1 Physics and mechanisms of the granulation process

In the previous chapter, the motivations for granulated products over their fine powdery counterparts were given. Despite the proliferate usage of this process, the majority of these are uneconomical owing to the generation of out-of-spec products. These unqualified products will subsequently require further rework through recycling back into the granulation process (Iveson et al., 2001). Thus, it is clear that the majority of the time has been devoted towards the development of granulation processes, based on empiricism relying on heuristics for providing guidelines to facilitate process design and scale-up. This is partly reflected in the plethora of research on the macroscale level of the process, where there have been many studies investigating the influences of various process operating parameters and the effects of formulation properties on the granulation behaviour. Many of the studies have also been performed on a variety of formulations on different types of granulator equipment and configurations, in an attempt to establish a qualitative link between observations made during the experiments to the granulation phenomena. This represents a challenging task where there are complex interactions among the individual granulation phenomena, which at present all occur within the same working volume of the granulator. Therefore, any study at the macro-level will be difficult in order to isolate the predominant effects that are attributed to a particular granulation sub-rate process. The added complexity to these studies is also due to the different types of equipments, where the contributions of particular sub-rate processes may exert varying degrees of influence on the process. For instance, drying of the granules plays a more dominant role during the granulation process using a fluidised bed granulator

compared to a rotary drum granulator.

As previously indicated, both the formulation properties and the conditions used during the operation of the granulator will influence the extent and the behaviour of the granulation process. An understanding of the extent of these influences will facilitate our ability to design and to take effective control actions, should disturbances cause conditions to deviate away from the desired operating conditions. As an example of the importance of characteristic material properties of the powder, Scott et al. (2000) found that larger granules were predominantly comprised of small primary particles compared to small granules, which were made up of coarse particles for a granulation recipe of Durcal 40 and polyethylene glycol (PEG 1500). The method of binder distribution was also investigated using either pour-in or in-situ binder melting-in. They found that although a bimodal distribution was observed for both cases, the bimodal nature of the distribution persisted throughout the experiment when melting the binder in-situ of the process. Furthermore, the weight-based mean particle size for the pour-in method of binder distribution was significantly greater than the binder melt method for binder distribution. The heterogenous binder distribution and their subsequent effects on the granule size distribution (GSD) was explained, using the Shaefer and Mathiesen's Immersion Hypothesis (SMIH) and the Shaefer and Mathiesen's Distribution Hypothesis (SMDH) (Schaefer and Mathiesen, 1996a) (see Figure 2.1).

- **Shaefer and Mathiesen's Immersion Hypothesis (SMIH)**: This mechanism refers to the primary particles that are smaller than the binder droplet size. Under these circumstances the primary particles will embed themselves onto the surface of the droplet. The resulting granule nucleus will be denser with minimal incorporation of air within the granular matrix.

- **Shaefer and Mathiesen's Distribution Hypothesis (SMDH)**: This mechanism refers to the case when the binder droplet is smaller than the primary particles, in which case the binder will coat the particles surface. These surface wet particles will aggregate forming nuclei with a higher incorporation of air compared to those formed from the SMIH mechanism.

These two hypotheses provide two possible routes for nucleation, which may help explain why some systems undergo faster growth rates, and others go through long induction growth, subjected to identical operating conditions are used but differing only in the methods of

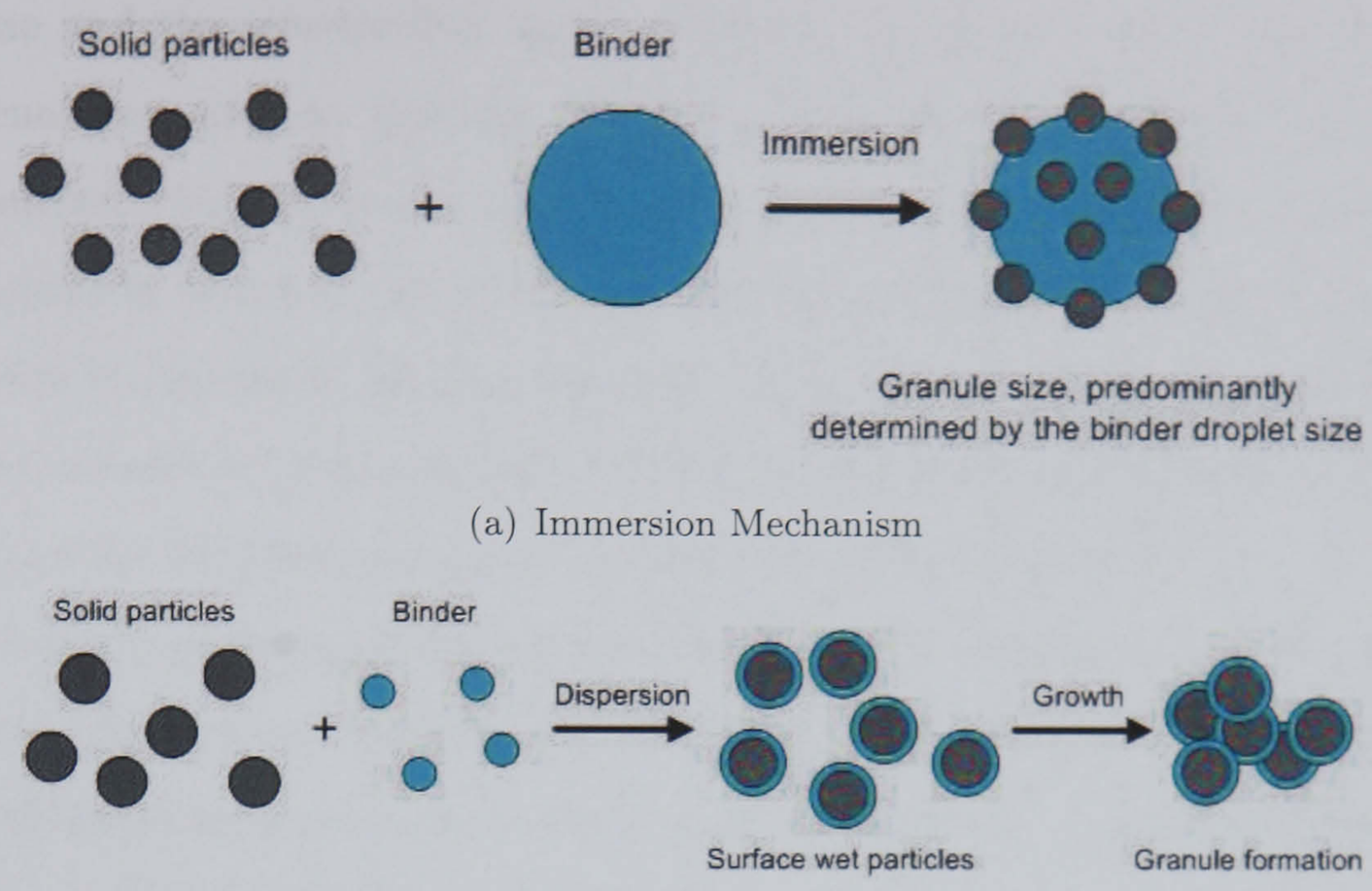

(a) Immersion Mechanism

(b) Distribution Mechanism

Figure 2.1: Schematic representation for the methods of nucleation based on the immersion (SMIH) and distribution (SMDH) hypothesis proposed by Schaefer and Mathiesen (1996a). Adapted from Schaefer and Mathiesen (1996a).

binder delivery (Iveson and Litster, 1998). Induction growth is characteristic when little or no granule growth occurs, corresponding to periods when the granules undergo consolidation and as a result become surface wet, then leading to growth. The effects of binder distribution on the mean granule size was studied by Rankell et al. (1964) and Davies and Gloor (1971), in which they varied the positioning of the binder spray nozzle with respect to the powder bed. Litster et al. (2001) demonstrated that the characteristics of the drop size distribution was reflected by the nuclei size distribution obtained. Narrower nuclei size distribution was achieved through higher nozzle pressures leading to narrower drop size distributions, whilst a broader nuclei distribution was observed owing to a broad drop size distribution.

Litster et al. (2001) established an equipment independent parameter, the dimensionless spray flux (Ψ_a) defined in Equation (2.1).

$$\Psi_a = \frac{3\dot{V}}{2\dot{A}D_d} \tag{2.1}$$

Where, $\dot{V}$ (m^3/s) is the liquid binder spray rate, $\dot{A}$ (m^2/s) is the powder flux traversing the spray zone, and D_d (m) represents the average drop size. The Ψ_a will enable a comparison to be made on a quantitative basis, in determining the quality of the liquid dispersion across granulators of different scales by comparing only the solution flow rate to the size of

the spray zone and the powder flux moving through the spray zone. Using Ψ_a, commonly observed phenomena such as 'pooling', where accumulation of the liquid binder occurs on the powder surface, may be predicted based on the operating conditions of the granulator and the penetration times of the binder on the selected solid phase. For example, a high spray flux value translates to pooling whereas a low value corresponds to well interspersed droplets. This concept of characterising the effectiveness of dispersion was incorporated into a nucleation regime map first proposed by Hapgood (2000) (Figure 2.2).

The nucleation regime map demarcates three regions termed as (a) droplet controlled regime, (b) the intermediate regime, and (c) the mechanical dispersion regime. Low spray flux values with rapid drop penetration times were characteristic of the drop controlled regime where droplet overlapping does not occur. At higher spray flux values droplets begin to overlap and the assumption that a single droplet forms a single nucleus no longer holds true. Instead droplet overlapping, resulting in non-uniform binder distribution, will require mechanical dispersion to break-up this wetted powder mass. This regime is called the mechanical dispersion regime. The regime map introduces another dimensionless group, called the dimensionless drop penetration time (τ_p) defined as $\tau_p = \frac{t_p}{t_c}$. The drop penetration time is represented by t_p whilst t_c represents the circulation time *i.e.*, the time it takes the same portion of powder that has previously passed through the nucleation zone ('spray zone') (Iveson et al., 2001) to re-enter the nucleation zone. Hapgood et al. (2003) granulated lactose powder with various binder solutions, and computed their respective τ_p and Ψ_a, plotting each binder-solid combination on the nucleation regime map. They found that for binder solutions with droplets exhibiting short penetration times and decreasing Ψ_a resulted in a narrower nuclei distribution. Similarly, high t_p lead to a broader nuclei distribution independent of the value of Ψ_a.

The onset of granulation has also been identified as a crucial period when the binder solution is sprayed onto the powder bed mass, giving rise to the formation of early granule nuclei particles. The nuclei size distribution obtained will influence the future GSD, as Venkataramana et al. (1999) found the nuclei size distribution to exert template like effect on future GSDs.

The role of the binder viscosity during granulation has an important role, exhibiting dual behaviour in contributing towards granule formation. For instance a binder with a higher viscosity will have a greater viscous contribution to the dynamic pendular liquid

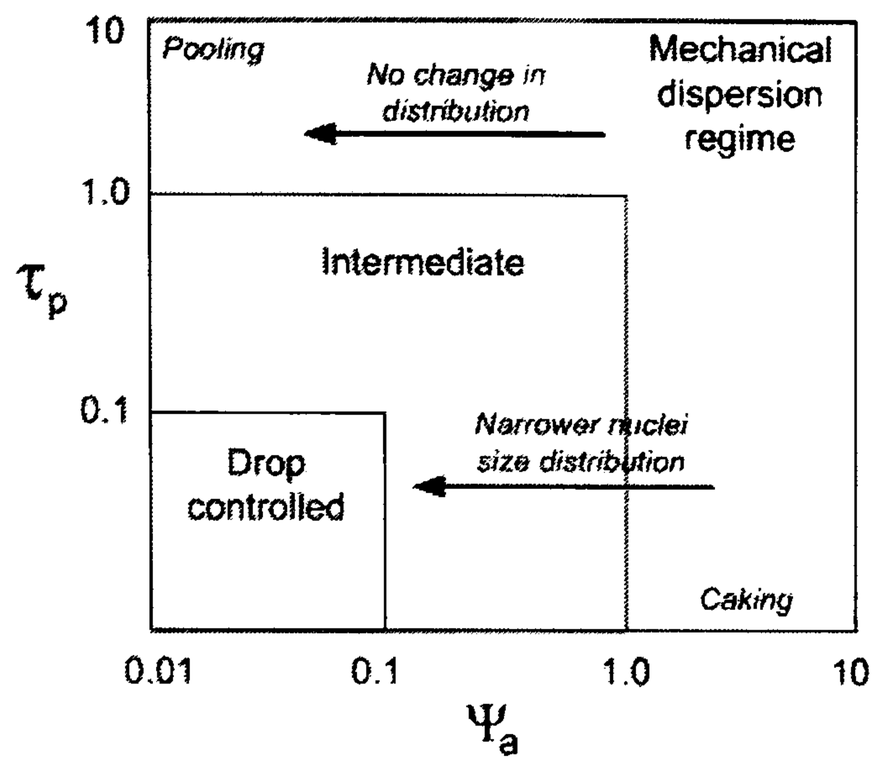

Figure 2.2: The nucleation regime map describes three regimes: (a) the droplet controlled regime, (b) the intermediate regime and (c) the mechanical dispersion regime. Different granule formation characteristics are exhibited within each type of regime domain. Adapted from Hapgood (2000).

bridge links between constituent particles incorporated into the granule. However, too high a binder viscosity may have an antagonistic effect causing the granule to be less deformable. Consequently, the contact area between two colliding particles will be lower thereby limiting the potential for granule growth (Schaefer and Mathiesen, 1996b,a). Clearly, a compromise needs to be established in order to ensure sufficient binder content to allow for granule deformation to occur and yet avoid having too high a viscosity, such that particle deformation is reduced creating a contact/bond area upon collision.

A requirement for granules to deform involves the individual particles that comprise the granule to be able to move past one another, as an external force is exerted onto the granule (*i.e.* particle-particle collision, particle-equipment surface collision), which is resisted by inter-particle friction. The liquid binder serves as a lubricant at the particle-particle contact points. Thus, increasing the binder liquid content of granules ensures a greater likelihood that the pores are filled with the binder, enabling lubrication of the particle contacts and thus facilitating the deformation of granules during collision. Associated with particle deformation is the appearance of a binder on the particle surface, as the binder is squeezed from within the granular matrix (Iveson et al., 1996). This formulation property alone has been demonstrated to play a complex role influencing the granulation behaviour of the system. Iveson and Litster (1998) observed an induction type granulation behaviour when granulating glass ballotini with

glycerol, but a steady-type growth was observed when granulating with water as the binder.

Therefore a conclusion can be drawn from both the works by Schaefer and Mathiesen (1996b) and Iveson and Litster (1998), that granules need to have sufficient binder content that will permit deformation, enabling a large contact area to be formed. Stronger bonds will be formed between the coalescing particles, which will promote a steady-growth behaviour for the system. Alternatively, a highly viscous binder will lower the granules propensity to deform, which will likely undergo an induction period. Thus, an accurate understanding of the role of the binder viscosity will provide insight into the type of granulation behaviour likely to be encountered for a specific binder-solid formulation and granulator operating conditions.

Amidst the granulation literature the granulation phenomena that has received the most attention is the aggregation phenomenon. In modelling this process, the coalescence kernel representing the probability of coalescence between two particles is a key parameter in population balance (PB) modelling. It is common to view the functional form of this coalescence kernel as two parts, first suggested by Sastry (1975) given in Equation (2.2). The first part (β_0) is dependent on the material characteristics and on the granulator operating conditions (*i.e.* drum speed, moisture content, liquid binder viscosity, *etc.*), whilst the other part of the kernel ($\beta^* (v_i, v_j)$) carries the dependencies on the size of the coalescing granules.

$$\beta_{i,j} = \beta_0 \beta^* (v_i, v_j) \tag{2.2}$$

Here, $\beta_{i,j}$ represents the coalescence kernel with an assumed functional form comprised of two parts: size-independent part, size-dependent part for two particles i and j with respective volumes of v_i and v_j. A small number of coalescence kernels are physically based, whilst in most other cases, an empirical approach has been adopted in which the kernels themselves are fitted to the experimental data through a trial and error fashion (*i.e.* macroscopic plant modelling). These previously proposed functional forms for $\beta^* (v_i, v_j)$ have been reviewed by numerous authors (Iveson, 2002; Cameron et al., 2005). Balliu (2004) formulated a coalescence kernel adopting the same functional form first proposed by Sastry (1975), but in addition incorporated key granulator operating conditions to the β_0 term accounting for the drum speed and the bed depth in addition to the moisture content of the granules.

Wauters (2001) produced a simplified view of the coalescence kernel whilst still accounting for the explicit nature of the kernel's dependency on the size of the coalescing particles and their binder content. In this kernel, the coalescence either succeeds or fails, *i.e.*, probability of 1 or 0 respectively. The particles are first classified as 'big' or 'small' based on a defined cutoff

particle volume. In a similar fashion, the particles are either 'wet' or 'dry' depending on a defined particle moisture content (set according to experimental observations). Based on the particles binder content and size (*e.g.* big/wet, big/dry, small/wet, small/dry) the particles will coalesce or not. For example, a 'small' and 'wet' particle will successfully aggregate with other particles of different size and binder content. But, a 'big' and 'dry' particle will only aggregate with 'small' and 'dry' particle (see Wauters (2001), Table 5.1).

The parameter-fitting approach for tuning the adjustable parameters pertaining to the empirical kernels is reminiscent of the black-box modelling strategy that is prone to plant-model mismatch (Wang and Cameron, 2002). Wang and Cameron (2002) attributed these model discrepancies to the lack of structure switching models (multiple models), in which the granulation process can be physically divided into several stages according to the three principle rate processes (*i.e.* wetting and nucleation, consolidation and growth , attrition and breakage). Wildeboer (2002) attributes the difficulties in controlling granulation processes to poor equipment design.

In contrast to the above kernel models, there have been some efforts to actually model the kernel based on particle-level physics. Ouchiyama and Tanaka (1975) developed a theoretical coalescence model for a rotary drum and a pan granulator, in which the granulator volume was divided into two distinct zones primarily the compression zone and the separation zone. The granules were modelled as deformable surface-dry granules. When the granules collide and form a dumbbell, comprised of the two particles in the compression zone under constant-angular-velocity, then a compressive force will act on each granule causing the granules to deform and creating a contact zone (Wauters, 2001; Iveson et al., 2001; Knight, 2004) with the cohesive strength being proportional to the area of contact. In the separation zone, Ouchiyama and Tanaka (1975) based the separation force on the bending moments and the adhesive force as the capillary force. The force balance was then used to calculate the probability of coalescence between two granules. The model assumes that the probability of coalescence will be greater if the size difference between the granules was large, compared to granules of equivalent size, which had the least probability of coalescence.

Ennis et al. (1991) provided an important contribution towards the development of such physically based kernel models. In this model, the particles are assumed to be spherical, surrounded by a thin viscous liquid binder layer uniformly distributed on the surface of the particles. During collision, successful coalescence leading to the aggregation of the particles is

considered only when the kinetic energy possessed by the colliding particles is fully dissipated via the viscous dissipation within the binder layer and through elastic losses in the particle itself. Particle deformation was not included in their studies and hence the particles were modelled as small rigid spheres. This situation can be realised in a fluidised bed granulator in which agitative forces are mild compared to other granulators *i.e.*, high-shear mixers with fast moving impeller blades, with or without chopper blades that prevent the accumulation of mass on the internal surfaces of the equipment.

The model defines an important criterion which determines whether coalescence will occur between two colliding particles, and is governed by the value of the viscous Stokes Number (St_v), which is defined in Equation (2.3). St_v is a dimensionless group that represents the ratio of the initial collision kinetic energy of the particles to the energy dissipated through viscous dissipation in the liquid binder layer.

$$St_v = \frac{4\rho_g \, U_c \, d_g}{9\mu} \tag{2.3}$$

Here, ρ_g is the density of the granule, U_c is the relative collision velocity between the two granules and is dependent on the mixing intensity within the granulator, d_g is diameter of the granule, μ is viscosity of the liquid binder. The condition for granule coalescence is the following:

$$St_v \; < \; St^* \tag{2.4}$$

The critical Stokes Number (St^*) is defined in Equation (2.5).

$$St^* = \left(1 + \frac{1}{e}\right) \ln \frac{h_b}{h_a} \tag{2.5}$$

Here, e is the coefficient of restitution of the granule, h_b is the film thickness of the liquid binder layer coating the particle and h_a is the height of the surface asperity of the particle (see Figure 2.3). Adopting this energy dissipation criteria for granule coalescence, the various collisions that occur within the granulator may be further classified into three distinct growth regimes. These growth regimes are classified as (i) the non-inertial growth regime, (ii) inertial growth regime, and (iii) the coating regime, which are summarised below:

Non-inertial growth regime, ($St_v < St^*$) In this regime, collisions between particles of all sizes will lead to successful coalescence, since all the particles will have a St_v less than the critical Stokes Number. Thus, at this stage of the process, changes in the process operating parameters will have a minimal effect on particle aggregation.

Inertial growth regime,($St_v \approx St^*$) At this stage of the process, there is an equal likelihood for coalescence and particles rebounding to occur. The dependency of particle size will play an important role, the aggregation between two large particles will have a lower probability compare to either two smaller particles or a large and small particle coalescing. The process is both sensitive to changes in the formulation and process operating parameters, which could be used to influence the process in either direction *i.e.*, non-inertial regime and the coating regime.

Coating regime, ($St_v \gg St^*$) Collision between particles will not result in coalescence. The mode of particle aggregation is restricted to layering, whereby fines are deposited onto the surface of larger particles.

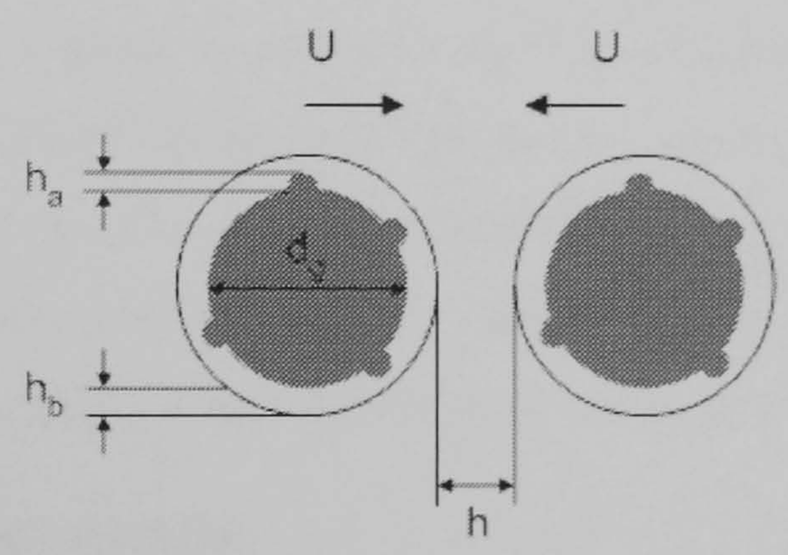

Figure 2.3: Schematic of a collinear binary collision between two granules separated by a distance h, with a representative collision velocity of U. The particles shown here have a diameter d_g, surface asperity of height h_a and are coated with a thin binder liquid layer of thickness h_b. Adapted from Ennis et al. (1991).

The model presented by Ennis et al. (1991) provides an energy dissipation based criterion for coalescence. However, the model does not account fully for the possibility of a granulating system with particles undergoing deformation. This modelling issue was addressed by Liu et al. (2000), built upon the model previously proposed by Ennis et al. (1991). A detailed model-based analysis was performed, introducing the Stokes Deformation Number (St_{def}). This dimensionless group is important since it represents the ratio of the impact kinetic energy to the plastic deformation of the granules during collision. The St_{def} is defined in Equation (2.6).

$$St_{def} = \frac{\text{impact kinetic energy}}{\text{granule plastic deformation}} = \frac{\tilde{m}u_0^2}{2\tilde{D}^3 Y_d} \tag{2.6}$$

Here, u_0 is the relative collision velocity of the two granules, Y_d is the granule yield stress, $\tilde{m}$ and $\tilde{D}$ are the corresponding reduced mass and diameter for two unequal sized particles, p_1 and p_2, which are defined as $\tilde{m} = \frac{m_1 m_2}{m_1+m_2}$ and $\tilde{D} = \frac{D_1 D_2}{D_1+D_2}$, respectively.

In this model, particle coalescence may occur via two routes classified as type I and type II coalescence. Essentially, the balancing of the kinetic/elastic energy and the viscous dissipation are used in determining the net potential driving the process of coalescence between the two particles. Further details pertaining to the net potentials, for the two types of coalescence will be given in Chapter 3. Liu et al. (2000) performed parametric sensitivity studies on the model with respect to the formulation properties (*e.g.* strength of the granules characterised by the yield stress), and various process operating parameters (*e.g.* binder content, mixing intensity of the process characterised by u_0) for their effects on the criteria for coalescence. This model was found to correspond to a rapid growth system where the granules were considered to be bounded by a thin film of liquid binder and are able to undergo deformation. Application of the model to surface-dry granules was also considered in the same study, but the authors suggested further work was required in order to clarify the transport of liquid binder to the particle-particle contacts/bonding zone where the liquid bridge links are formed.

Importance of integrated models:

Litster (2003) emphasised that granule coalescence is governed by not only the granule size but also the porosity and binder content, which necessitates the application of population balances capable of handling particle populations described by multi-dimensional distributions. The granulation is a complex process, exhibiting non-linear behaviour. The complexity of the process arises from the multitude of interactions that occur between individual granulation phenomena *i.e.*, nucleation, consolidation, aggregation and breakage. The efficient operation of granulation as a result of better controllability of the process, hinges on our level of understanding of the cumulative effects on the behaviour of the granulation process, and a means of evaluating these cumulative effects on the process is through population balances. This is reflected by recent researchers employing multi-dimensional and mechanistic coalescence kernels where, each individual particle trait is represented by the internal coordinates of the PB model (Immanuel and Doyle III, 2003).

2.2 Numerical solution techniques

The method of population balance modelling has been employed for the modelling of various industrially significant processes which include crystallisation, emulsion polymerisation, granulation and biological systems (Ma et al., 2002b; Immanuel et al., 2003; Rawlings and Ray, 1988a,b). In crystallisation processes an area that remains of primary importance is the ability to control the crystal size distribution as well as the shape of the crystals, which is of particular significance in the manufacture of crystalline products as in the pharmaceuticals. Crystals that have different polymorphs (*i.e.* crystal structures) will exhibit different physical properties (*e.g.* melting point, dissolution rates, *etc.*) (Rodríguez-Hornedo and Murphy, 1999; Fujiwara et al., 2005; Braatz, 2002). In emulsion polymerisation the influence of the particle-size distribution has been established in the past to affect many of the end-use properties including the rheological properties of the final end-use polymer (Parkinson et al., 1970; Luckham and Ukeje, 1999). In granulation, particle size is also considered an important attribute to control, however agglomerates of the same size may also differ in their final end-use properties, which may be reflected in the microstructure of the granules. For instance granules of the same size but with a higher porosity will exhibit different properties (*i.e.* friability, dispersion rates, bulk density, *etc.*) compared to higher density compact granules of equivalent size. Hence it is becoming more frequent to model the distributions of the granules with respect to their size and their binder content. In biological systems, the application of cell population balances as opposed to the treatment of an entire cell population as a continuum (lumped approach) is capable of capturing to a finer level of detail the heterogeneity of the system by incorporating information between cells that are at different stages of the cell cycle as well as the associated growth, nutrient uptake and product formation pertaining to an individual cell. Thus, a complete description of how the cell properties are distributed can be predicted by cell population balance models, which is not possible via the continuum approach in which only average properties of the population may be obtained (Mantzaris et al., 2001).

As previously indicated population balances provides a convenient mathematical framework from which to model particulate processes exhibiting heterogeneity with respect to intrinsic particle properties (*i.e.* size, composition, age, *etc.*). Particle level phenomena at the microscale such as nucleation, growth, aggregation and breakage give rise to distributions of key particle traits across the particle population. Analytical solutions to the population

balance equation (PBE) is often only available for special cases, but for the majority a numerical solution is required. Many different numerical solution techniques have been applied for solving the PBEs, which include the direct quadrature method of moments (DQMOM), the method of weighted residuals with further sub-divisions such as the orthogonal collocation on finite elements (OCFE) and Galerkin's method. In the former case the PBE is exactly satisfied at the collocation points where the residuals to the PBE are driven to zero, when the solution is approximated by a linear combination of orthogonal polynomials for each finite element.

A significant contribution towards the development of an efficient numerical algorithm for the solution of population balances was the fixed pivot technique developed by Kumar and Ramkrishna (1996a). In this method, the internal coordinate (*i.e.* particle size) is discretised into a number of finite elements or '*bins*' such that the particle population is now represented by 'x' (pivots) where $v_i < x_i < v_{i+1}$. The idea behind this method is to ensure that two general properties $\zeta_1(x)$ and $\zeta_2(x)$ are conserved. For instance the aggregation of two particles, $p(x_i)$ and $p(x_j)$ each with a property $\zeta(x_i)$ and $\zeta(x_j)$ leads to a new particle with property $\zeta(x_i) + \zeta(x_j)$. The new born particle may in some instances correspond exactly with the pivots, however when a particle formed does not correspond to a pivot then a method is required that will appropriately assign the particles to the adjacent pivots accordingly whilst ensuring that the two pre-chosen properties are preserved. A schematic of the aforementioned scenario is depicted in Figure 2.4.

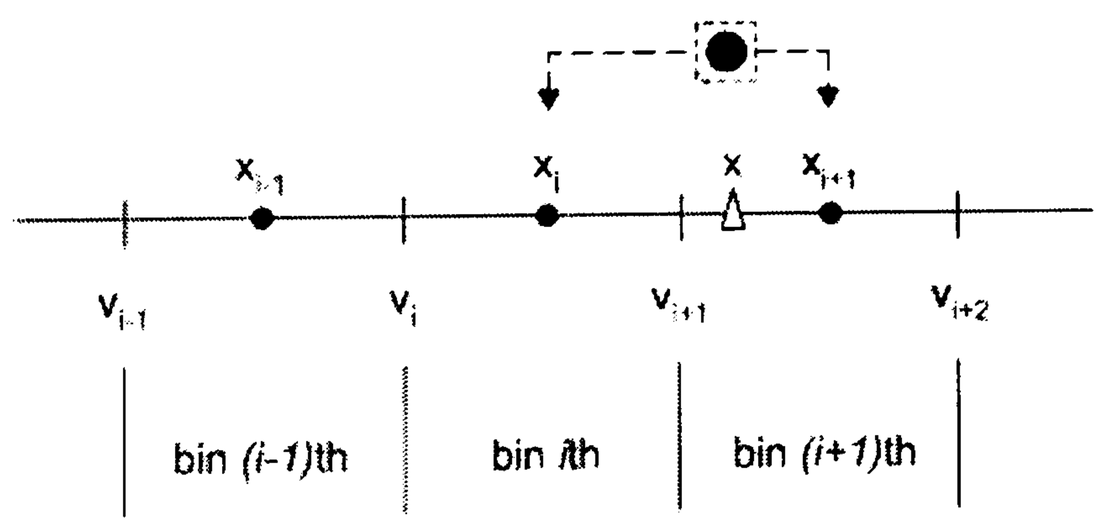

Figure 2.4: Discretised grid indicating the pivots (x_i) and a hypothetical new born particle partitioned between the two pivots such that two pre-chosen properties are conserved. The grid shown here is for illustration purposes only, and need not be linear. Instead a geometric, or arbitrarily discretised grid may be used. Adapted from Kumar and Ramkrishna (1996a).

The approach used in this technique in order to correctly assign fractions to the particle

populations represented by the pivots, must satisfy the following:

$$a(\nu, x_i)\zeta_1(x_i) + b(\nu, x_{i+1})\zeta_1(x_{i+1}) = \zeta_1(\nu) \tag{2.7a}$$

$$a(\nu, x_i)\zeta_2(x_i) + b(\nu, x_{i+1})\zeta_2(x_{i+1}) = \zeta_2(\nu) \tag{2.7b}$$

Where ν is the new born particle such that $x_i < \nu < x_{i+1}$ to be assigned appropriately to both pivots with fractions $a(\nu, x_i)$ and $b(\nu, x_{i+1})$ contributing to the particle populations at x_i and x_{i+1} respectively. $\zeta_1(\nu)$ and $\zeta_2(\nu)$ are the two pre-chosen properties to be conserved. An additional comment to this numerical technique is that the flexibility in the choice of the discretised grid along the chosen internal coordinate can allow for improved accuracy as opposed to previous studies that employed either a geometric grid (Hounslow et al., 1988) or a uniform grid. In addition, this technique is generalized so that arbitrary grids containing coarse grids over some size ranges and finer grids in others can also be used. Kumar and Ramkrishna (1996a) were able to demonstrate in the same study for an aggregation-only system that selective refinement of the discretised grid towards the larger particle sizes resulted in an improved accuracy where previously there was over-prediction due to sharp variations in the density functions spanning the large particle size range.

Kumar and Ramkrishna (1996b) presented an improvement to the fixed pivot technique, whereby previously the pivots were fixed and as a consequence resulted in the over-prediction in large particle size classes owing to the sharp variations in the density function in these size ranges. In that previous study (Kumar and Ramkrishna, 1996a), a selective refinement of the grid was adopted to correct for this over-prediction, but in the moving pivot technique the pivot is no longer fixed but is able to move thereby reflecting the changes in the number density with size in the size ranges whilst still maintaining key features of the fixed pivot technique (*i.e.* flexible grid, conservation of two pre-chosen properties, *etc.*). Kumar et al. (2006) developed a novel method which enabled a more accurate means for the assignment of particles to each size class, and is known as the cell average technique. The premise of this work is based on the previous study by (Kumar and Ramkrishna, 1996a) and (Kumar and Ramkrishna, 1996b). The essential difference between this technique and the fixed or moving pivot techniques is that the fractional assignment of particles to the adjacent pivots is based on the value of the average particle volume within the size class as shown in Equation (2.8). The average particle volume is given by

$$\overline{X}_i = \frac{M_i}{B_i} \tag{2.8}$$

where the M_i and B_i are the net volume flux and the net rate of particles contributing to the ith bin, and are given by

$$M_i = \sum_{\substack{j,k \\ x_{i-1} \leq (x_j + x_k) < x_{i+1}}}^{j \geq k} \left(1 - \frac{1}{2}\delta_{j,k}\right) \beta_{j,k} F_j F_k \left(x_j + x_k\right) \tag{2.9}$$

$$B_i = \sum_{\substack{j,k \\ x_{i-1} \leq (x_j + x_k) < x_{i+1}}}^{j \geq k} \left(1 - \frac{1}{2}\delta_{j,k}\right) \beta_{j,k} F_j F_k \tag{2.10}$$

For example a new born particle x such that $\mathrm{v}_{i+1} < \mathrm{x} < \mathrm{x}_{i+1}$ will partially contribute towards the ith bin (see Figure 2.4). Likewise, particles falling into the $(i-1)$th bin given that the particles (x) are such that $\mathrm{x}_{i-1} < \mathrm{x} < \mathrm{V}_i$ will also partially contribute to the ith bin in addition to those particles that are born directly into the ith bin.

The cell average technique still maintains the key features from the fixed pivot method in preserving any two pre-chosen properties, such as the total number of particles and mass, by solving for the pair of simultaneous equations given in Equations (2.11a) and (2.11b) for the fractions a and b given by Equations (2.11c) and (2.11d) respectively.

$$a + b = B_i \tag{2.11a}$$

$$a x_i + b x_{i+1} = B_i \overline{X}_i \tag{2.11b}$$

$$a = B_i \lambda_i^+ \left(\overline{X}_i\right) \tag{2.11c}$$

$$b = B_i \lambda_{i+1}^- \left(\overline{X}_i\right) \tag{2.11d}$$

$$\lambda_i^{\pm} = \frac{x - x_{i\pm1}}{x_i - x_{i\pm1}} \tag{2.11e}$$

Kumar et al. (2006) was able to show that when the continuous form of the population balance equation is reduced to a set of ordinary differential equations and by substituting the modified birth term based on the cell average value gives the following:

$$\frac{dF_i}{dt} = B_i - D_i \tag{2.12a}$$

$$\begin{aligned} \frac{dF_i}{dt} &= B_{i-1} \lambda_i^- \left(\overline{X}_{i-1}\right) H \left(\overline{X}_{i-1} - x_{i-1}\right) \\ &+ B_i \lambda_i^- \left(\overline{X}_i\right) H \left(x_i - \overline{X}_i\right) + B_i \lambda_i^+ \left(\overline{X}_i\right) H \left(\overline{X}_i - x_i\right) \\ &+ B_{i+1} \lambda_i^+ \left(\overline{X}_{i+1}\right) H \left(x_{i+1} - \overline{X}_{i+1}\right) \\ &- F_i \sum_{k=1}^{N} \beta_{i,k} F_k \end{aligned} \tag{2.12b}$$

In the above equations $\overline{X}_i$ is the computed average particle volume for the ith bin. F_i is the number concentration of particles in the ith bin, $H(x)$ is the Heaviside step function. β is the aggregation kernel, M_i is the net volume flux of particles and B_i is the net rate of particles contributing to the ith bin respectively.

Conventional method of moments (MOM) have proven to be computationally efficient in solving the PBE where the kth moment is given by Equation (2.13). The aim of this method is to re-formulate the PBE (Equations 2.14 and 2.15) by carrying out a moment transformation by applying the definition given in Equation (2.13) such that the following set of equations are in closed form, in which they are a function of the moments themselves (Equation 2.16). Thus, only the lower order moments of the distribution are tracked. The efficiency of this method originates from solving the equations corresponding to the moments to be tracked, arising from the moment transformation of the PBE, replacing the much larger number of differential equations one would normally solve having not applied the MOM.

$$m_k = \int_{\zeta_{min}}^{\zeta_{max}} \zeta^k F(\zeta, t) d\zeta \tag{2.13}$$

$$\frac{\partial F(r,t)}{\partial t} = B(r,t) - D(r,t) \tag{2.14}$$

$$B(r,t) = \frac{1}{2} \int_{u=r_{min}}^{r-r_{min}} \beta(u, r-u) F(u,t) F(r-u,t) du \tag{2.15a}$$

$$D(r,t) = F(r,t) \int_{u=r_{min}}^{r_{max}} \beta(u,r) F(u,t) du \tag{2.15b}$$

$$\frac{dm_k(t)}{dt} = \overline{B_k}(t) - \overline{D_k}(t) \qquad k = 0, 1, \ldots, 2N-1 \tag{2.16}$$

However, a potential drawback of this method is the closure requirement. In order to circumvent this closure requirement, the quadrature method of moments (QMOM) was developed. McGraw (1997) was the first to employ the quadrature approximation as shown in Equation (2.17), for a one-dimensional case, for modelling size-dependent growth in aerosols. The popularity with this method has grown with increased use in the modelling of particulate processes (Fan et al., 2004; Marchisio et al., 2003b; Dorao and Jakobsen, 2006). The application of this quadrature approximation was also extended to the modelling of a crystallisation

process (Marchisio et al., 2003a). Furthermore, the direct quadrature method of moments (QMOM), a variation of the QMOM, has also been extended for solving multi-dimensional population balance models (Fox, 2006; Marchisio and Fox, 2005). Extending the original formulation first proposed by McGraw (1997) to account for multi-variate-distributions (*i.e.* where there are more than one internal coordinates), then the quadrature approximation becomes:

$$f(\xi;\mathbf{x},t) = \sum_{\alpha=1}^{N} w_\alpha(\mathbf{x},t)\ \delta[\xi - \langle\xi\rangle_\alpha(\mathbf{x},t)] \tag{2.17a}$$

$$\delta[\xi - \langle\xi\rangle_\alpha] = \prod_{j=1}^{N_s} \delta(\xi_j - \langle\xi_j\rangle_\alpha) \tag{2.17b}$$

where, $f(\xi;\mathbf{x},t)$ is the distribution function, ξ is the property vector (internal coordinates), w_α is the weight at node α. The weights at their respective nodes may be regarded as equivalent to the representation of the distribution through this quadrature approximation (see Figure 2.5). The choice of moments is important, a poor selection of the moments may lead to a matrix that is singular in which case inversion will not be possible. This may arise due to identical nodes (abscissas) (see Figure 2.5). However, Fan et al. (2004) suggests alternative methods to treat such cases but the frequency of this occurrence is considered low since this would imply that the distribution is mono-dispersed, centered at a particular value, which is not commonly encountered in practice. Furthermore, the level of accuracy to which the chosen moments can be predicted accurately will also guide the selection process in determining the moments to be used in the quadrature approximation method.

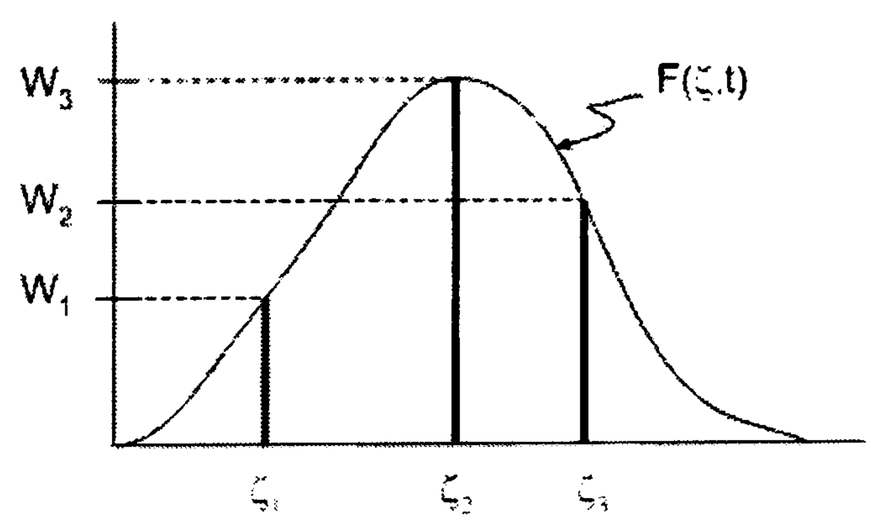

Figure 2.5: A graphical illustration with interpretation of the weights (W) and the respective nodes (the abscissas, ζ) used in the quadrature approximation to the actual distribution function.

Another discretisation based technique similar to the finite difference methods, which has also been used for solving population balance models for cases involving one and two internal

coordinates, are the high-resolution finite volume algorithms providing second-order accuracy over smooth regions of the solution without introducing numerical dispersion (LeVeque, 2002). In the class of finite volume methods, the predicted value of the distribution function within a grid cell no longer represents a single value approximation but instead an average over a specified interval as shown below:

$$F_i^n = \frac{1}{\triangle x} \int_{x_i}^{x_{i+1}} f(x, t_n)\, dx \tag{2.18}$$

where x denotes the state variable of interest, F_i^n is the approximated value of $f(x_i, t_n)$ averaged over grid cell i, $\triangle x$ is the length of the interval defined as $\triangle x = (b-a)/N$, with the limits of the system domain represented by a and b divided into N intervals.

Gunawan et al. (2004) used a high-resolution algorithm for solving the population balance model with nucleation and size-dependent growth rates for a crystallisation process employing flux limiter functions around regions of the solution with sharp discontinuities whilst obtaining second-order accuracy over smooth regions of the solution. Gunawan et al. (2004) were able to demonstrate that the high-resolution algorithm was computationally more efficient compared to other finite difference (FD) methods (the Lax-Wendroff FD method and the upwind FD method were used for comparison with the high-resolution algorithm). A direct comparison of the high-resolution algorithm with the FD methods on identical grid sizes saw a higher computation requirement owing to the higher accuracy of predictions near discontinuities.

Gantt and Gatzke (2005) used discrete element simulation (DES) for simulating a granulator, where the trajectory of a sample of particles is tracked. A physically based phenomenological kernel based on the works of Ennis et al. (1991) and Liu et al. (2000) was used for determining aggregation of particles in the event of a collision. Additional granulation phenomena were also modelled including the granule consolidation employing an empirical exponential decay relation and a criterion based on the Stokes deformation number (St_{def}) predicting the conditions under which granules will undergo breakage. In this, Tardos et al. (1997) considered granules to deform and break within a shear field when the externally applied kinetic energy exceeds a certain critical value $\left(St_{def}^*\right)$. In this study, a sample of granules were simulated in which the authors present an approach to obtain an ensemble average from this sampling size, by performing many simulations on the current computational volume domain. Their results from the simulations on various test cases were in agreement with observations made in experimental studies. In one of the test cases where they studied the effect of the impeller speeds on the particle size distribution (PSD), they found that at

BIBL. LONDON UNIV.

the highest impeller speeds there were more fines present and a tighter PSD compared to lower impeller speeds, which was also verified by the works of Oulahna et al. (2003).

Talu et al. (2000) adopted a discrete element approach to model granular flows. In their computer simulation model, the inter-particle interactions occurring within the system domain arise from interactions from either surface wet granules or from the solid cores of the particles. Results from the lubrication theory were used for computing interactions with surface wet particles involving the viscous wet binder layer and methodologies from granular flow simulations to account for the solid core interactions. An important finding from their study was that in certain cases, they were able to vary the total number of surface wet particles independently of the binder layer thickness, which is unrealistic since introducing more binder into the system will affect both the number of particles that are surface wet as well as the binder layer thickness that covers the particles. The authors attributed these results to the absence of a model that is able to accurately describe the phenomenon of binder transfer between two particles in the event of a dry particle colliding with a binder covered granule.

Gantt et al. (2006) used discrete element simulations (DEM) for computing the particle motion within the simulated granulator volume. Furthermore, the DEM simulations supply the collision frequencies and contact forces required as inputs to the coalescence model (Liu et al., 2000) in order to arrive at an overall coalescence kernel. A notable feature of the DEM simulations is that the number of particles remain constant throughout since no aggregation takes place. The purpose of the DEM simulations are solely for the determination of the collision frequencies. The coalescence kernel used in this study takes the form of the product of the aggregation efficiency ($\Psi_{i,j}$) and the collision rate ($C_{i,j}$) given in Equation (2.19) as opposed to the coalescence kernel comprised of a size-independent rate constant (β_0) and a size-dependent term ($\beta^*_{i,j}$) shown in Equation (2.20). The subscripts i and j represent particles belonging to size class i and j respectively.

$$\beta_{i,j} = C_{i,j}\Psi_{i,j}, \tag{2.19}$$

$$\beta_{i,j} = \beta_0\beta^*_{i,j}. \tag{2.20}$$

Wauters (2001) used Monte Carlo simulations (event-driven) for solving the three-dimensional population balance model with the three internal coordinates represented by the volume of solid, liquid and air. Furthermore, constant number-Monte Carlo simulations were used, wherein the particle population remains constant, and represents an accurate method pro-

vided the number of particles used is sufficiently large. During the event-driven Monte Carlo simulations, a random pair of particles are chosen during which the pair of particles are tested whether or not they will aggregate. If the chosen particles do not aggregate, then another pair of particles are chosen at random until aggregation does occur between the two randomly selected particles. In the situation where aggregation does take place, then the newly formed particle will take the place of one of the parent particles whilst a copy of a randomly chosen particle assumes the position in the array of the other parent particle. The results of the Monte Carlo simulations yielded good agreement with drum granulation experiments for a copper concentrate (chalcopyrite) and water granulation recipe. The simulation results for the time evolution (represented by the number of drum revolutions) of the average granule diameter showed a good one-to-one correspondence with the observations made in the experiments. Initially large granules possessed a higher volume of binder with the gradual depletion of smaller granules ($< 500\,\mu$m) during the induction period. The near disappearance of smaller granules lead to rapid granule growth.

In summary, various numerical techniques and model formulations exist for the modelling of particle populations, with differing potentials to handle multi-dimensional population distributions. In Chapter 3, a technique based on finite volumes adopted in this work will be presented.

2.3 Controllability of granulation processes

Inferences and direct measurements for control

In the aforementioned methods used in modelling the agglomeration process, the objective is to employ these models that are able to predict key granule properties, namely, particle size, fractional binder content and the porosity (related to product bulk density) that are often used for assessing the quality of the final agglomerated product. As previously mentioned, this can be accomplished through the modelling of multi-dimensional population balances. In addition, efficient numerical solution techniques are required. For example, the population balance equation is an example of a partial integro-differential equation that is complex and nonlinear in nature. Hence, solutions to these types of problems are often performed numerically.

Application of such models will facilitate the design of the process, which in turn will enable greater precision on the controllability of wet granulation processes. For continuous

granulation processes, several unit operations will be involved, comprising of the granulator. dryer, milling unit and a recycle conveyor belt system. Oversized granules that are produced will need to undergo a size reduction process prior to being reintroduced back into the process. As a result, granulation processes often operate at high recycle ratios due to the granules failing to conform to pre-design specifications. An example of a granulation process operating with recycle is shown in Figure 1.4. The key objective in granulation processing is to produce granules with design attributes appropriate for their end use. However. the control of the granulation process remains a difficult task due to the low availability of potentially manipulated variables. Those manipulated variables that are available mainly include the binder flow rate, the number and positioning of the spray nozzles, and the rate of mixing.

Bardin et al. (2004) studied the application of using impeller torque measurements as a means of inferring indirectly the granule size. The study showed that for the granulation of fine powders, where the effects of consolidation were more prominent compared to coarse particles, the impeller torque increases with time. This suggests that the dimensionless impeller torque can be used as a control indicator. However, after a period of time when the yield passes through a maximum (in that study, the yield was defined as the mass fraction of particles in the size range of 0.18-1.0 mm), the dimensionless impeller torque signal showed no corresponding change. Instead, the signal continued to increase. Thus, from a process control perspective, the dimensionless impeller torque may be used as a feedback signal only up until the critical period after which the yield has passed through its maximum. In the case of granulating coarse particles, an identical yield profile was obtained. However, the increase in the control signal over time was only marginal and therefore would be much less suitable as process control feedback. Bridgwater et al. (2004) explored the usage of positron emission particle tracking (PEPT) as a non-intrusive method for determining the flow fields occurring within the granulator. The effectiveness of the PEPT technique lies in the behaviour of a single tracer particle, in which the tracer particle is required to visit all regions of the working granulator volume and will provide an accurate statistical description of the flow field. However, at the onset of granulation, the process is in an unsteady state as granule nucleus and agglomerate growth are dynamically changing. Thus, the flow field within the granulator will also be changing by virtue of the transient evolution of the agglomerate particles state. Therefore, a single tracer particle will most likely be insufficient. In addition. Bridgwater et al. (2004) also state that owing to the unsteady nature of the granulation

process, PEPT will most likely be best suited to processes with transformation events on the time scale of the order of magnitude of a few minutes. This particular limitation of the PEPT technique will be an impediment to granulation processes exhibiting fast dynamics. with nucleation occurring perhaps on a much smaller time frame compared to the main growth stages (Knight et al., 1998). Hence, the PEPT technique would not be suitable for capturing the nucleation dynamics for granulation processes. Furthermore, the tracer particles must behave in the same manner as the bulk of the particles in the system (*e.g.* incorporation of the tracer particles into the granules) by ensuring that the tracer density, particle size and porosity are as similar to those of the bulk material.

Mort et al. (2001) stated that the design and implementation of effective control strategies will require the early identification of key product attributes (*e.g.* particle size, product density, *etc.*), which may be facilitated by physically separating distinct process transformation stages (*e.g.* wetting and nucleation, aggregation, *etc.*) within the process (Mort et al., 2001). This is corroborated by Wildeboer (2002) in which current equipment designs for carrying out granulation are found not optimal. Wildeboer et al. (2007) attributed this non-optimality to all contributing particle transformation processes occurring within a single working volume. Instead, Wildeboer (2002) suggests that key granulation phenomena (*e.g.* wetting and nucleation, coalescence and growth, *etc.*) be separated, thus enabling a better control over each key phenomena as opposed to lumping them together as is the current practice. Wildeboer (2002) studied the wetting and nucleation phenomena of granulation in isolation from the rest of the phenomena that would typically occur in granulation. Mort et al. (2001) also outline the problems that may be faced with in developing control strategies in that, certain feedback control schemes for controlling key product attributes may be hindered by the time delay between obtaining the output measurements and effecting the corrective measures through the actuator (*e.g.* liquid binder flow rate).

Watano (2001) applied fuzzy control to a high shear mixer granulator, using the binder flow rate as the manipulated variable for moderating granule growth. The number median diameter was used as the output. Watano (2001) developed and used a fuzzy control algorithm in this study, which was found to accurately control the median diameter within tolerance limits for their setup via the regulation of the binder flow rate. Techniques other than those mentioned here that can also be of great utility to process include non-invasive measurements using IR absorption spectra. Measurements for granule size and particle shape may be

obtained using image analysis, which is also a non-intrusive method (Watano and Miyanami, 1995).

Model-based approach for granulation control

Pottmann et al. (2000) formulated a model-based approach by using a first-order with time delay transfer function within a model predictive control scheme. The manipulated variables chosen for the process were the liquid flow rates located in three positions, and the output variables were the bulk granule density and the $90th$ percentile (d_{90}) and the $5th$ percentile (d_5). These last two outputs were required to satisfy the constraints given in Equations (2.21)-(2.22), whereby the upper and lower particle sizes are determined based on quality control considerations for the product granule.

$$d_{90} \leq d_{upper} \tag{2.21}$$

$$d_5 \geq d_{lower} \tag{2.22}$$

The d_5 and the d_{90} are however linked and cannot be controlled independent of the other. In addition, unlike the granule bulk density, there is no set-point value but instead may take up a range of values within the admissible range *i.e.*, the constraints given in Equations (2.22) and (2.21) must not be violated. Pottmann et al. (2000) performed a series of perturbation studies by varying the set tracking point of the bulk granule density. Additional studies were also performed in probing the effects of spray locations on granulation indicated by the changes in the d_5 and the d_{90} response values. Gatzke and Doyle III (2001) extended this work to include the maximisation of the number of control objectives (granule bulk density, d_{90} and d_5) that can be satisfied in a prioritised manner. Binary variables are used to indicate the status and the priority of the considered control objective. This allows the control objectives, which are considered more important to be given a higher priority. Thus, binary variables can take a value of either 1 if the control objective is satisfied or 0 if it cannot. In addition, the 'priority variables' for control objectives can be used to force control objectives to be satisfied in accordance to their precedent *i.e.* a binary variable with a value of 0 means that the corresponding control objective cannot be met and neither can the control objectives of lower priority, that is to say the binary variables associated with the lower priority control objectives are forced to 0. The binary variables indicating the status of the control objective (*i.e.* can it be satisfied?) and that of the priority for the control objective will both influence the objective constraint that requires the controlled output to remain within tolerance limits.

Zhang et al. (2000) formulated a PI controller for a fertiliser granulation circuit using the recycle size distribution as the controlled variable, in which granules were classified as either over-sized or under-sized. The water flow rate was used as the manipulated variable. Their basis for choosing the size distribution of the recycle stream as the controlled output was due to the following considerations:

- Output measurements could be carried out quickly without incurring significant time delays.
- The recycle ratio is a good performance indicator in terms of economy and the efficacy of the process.
- There is a one-to-one correspondence with the amount of recycled material and the throughput of the process (*i.e.*, reducing the recycle ratio infers that more of the granulated product are in-spec).
- The fraction of over-sized granules in the recycle is as sensitive to the moisture content as is the mean granule size. Therefore feedback from the moisture levels in the granulator can be directly observed using the size distribution in the recycle.

The results from the study concluded that the average granule size and the moisture content can be controlled indirectly by the size distribution of the recycle. A disturbance in the liquid flow rate causing decrease in the moisture level in the granulator caused the amount of under-sized particles to increase in the recycle. Corrective action of increasing the water flow rate restored the granule mean size. Implementing control strategies still remains difficult especially when large time lags and large recycles are encountered, which limits the response speed in which corrective measures can be implemented. These time lags may be attributed towards the mean residence time of the granular material residing in the granulator, in addition to the time in between obtaining measurement data.

2.4 Summary

In this chapter a brief review of the importance of macroscale modelling, emphasising the effects of the binder properties and the material characteristics on the granulation behaviour have been presented. A qualitative understanding at the macroscale and an attempt in predicting the granulation behaviour, using the nucleation regime map and the granule growth

regime map, will serve as a useful tool in helping to develop microscale level models in the form of population balances.

This is supported by early studies into the modelling of the aggregation phenomenon. Most of the literature accounts are based on coalescence kernels that were either completely empirical without incorporating the physics of the process or semi-empirical. However, in recent times it is realised that despite their simplicity and popularity these kernels will be inadequate for providing a generalised kernel representation of the process. The shortcomings of the aforementioned models (empirical/semi-empirical) will be more evident compared to physically based models, which instead rely on the physics of the process accounting for the material characteristics and on the prevalent conditions of the granulator during operation. For example, it was noted that in addition to the lack of physical insight pertaining to the empirical expressions for $\beta^*(v_i, v_j)$ and the required fitting of the parameter β_0, they would be of limited utility in predicting the granulation behaviour outside the operating range of the experimental data from which the parameter was fitted. Thus, there are considerable limitations in the potential for employing this parameter-fitting approach towards process scale-up and predicting the effects of different granulation formulations (Iveson, 2002).

The ability to numerically solve the population balance in modelling the granulation process is also important. Efficient solution techniques for solving the population balance model has been presented, with the majority of the studies considering distributions with respect to particle size as the only internal coordinate if at all they consider population balance models. However, for modelling multi-attribute particle systems in which particle size alone does not fully dictate product acceptability, it becomes necessary to employ multivariate population balances in order to model these distributions accurately. This has been recognised, in particular, that there has been important developments in moment-based multivariate population balance model simulation methods (Marchisio and Fox, 2005) notably the use of direct quadrature method of moments based on the gaussian quadrature closure methods. Finite volume approaches for multivariate population balance modelling have also been demonstrated to be advantageous in providing detailed time evolutions for different particle properties (Immanuel and Doyle III, 2005). Furthermore, the compositional tracking of granules from the agglomeration of multiple solid components, as is common in the pharmaceutical industry, could be carried out in multivariate PBE as opposed to one-dimensional PBE.

The optimisation and control of granulation processes is necessary if one is to ensure product quality is achieved consistently. Emphasis has been placed towards expending more research effort in a bid to develop models incorporating first principle knowledge of the physics of the process. The granulation process is a highly integrated process eliciting nonlinear behaviour. Whilst obtaining control at the process operating level, it does not necessarily guarantee process stability since the process may be sensitive to variations in the starting materials and the external environmental conditions (*e.g.* temperature, humidity) (Salman et al., 2007). Regime maps (Iveson and Litster, 1998) such as those specifying the formation of granule nucleus (Hapgood et al., 2003) and the dynamic granulation growth behaviour are predominantly beneficial to formulation and process scale-up. But, controlling the granulation process in order to ensure consistent product quality using metrics such as the granule size, porosity and moisture content will require accurate predictions of these aforementioned particle traits. Previously mentioned regime maps are unable to fulfill this need at present. Instead, models built into a population balance framework, incorporating phenomenological kernels describing each respective sub-rate process, will serve as a crucial aid in this regard (Litster, 2003). Nevertheless, the development of models incorporating first principle knowledge of the physics of the process remains a challenging task. In addition, independent measurements of parameters appearing in these models may pose difficulty to obtain reliably, thus, adding to the difficulty of implementing such models to real processes (Hogg, 1992). These issues will be addressed in this thesis.

An aspect concerning the control of granulation processes resides in the practicality of process measurements. Output measurements considered include, the bulk density of the granule sample, mean granule size and moisture content. As indicated by Mort et al. (2001), implementation of "fast-acting" feedback control will be limited by the time delays between obtaining the output measurements, with the actuators responsible for implementing the corrective measures to the process. Thus, sampling methods that offer rapid and accurate measurements in conjunction, with control methodologies such as those proposed by Pottmann et al. (2000) and Gatzke and Doyle III (2001), will provide a positive contribution towards providing better controllability over granulation processes.

Chapter 3

Formulation of the population balance

Part of the contents of this chapter were published in Poon et al. (2008).

3.1 Introduction

The population balance modelling framework has been described as a particle number accounting procedure, a statement of the material balance for the process at a given instance (Rhodes, 1990). This type of model framework is particularly suited for modelling particulate processes where the particle population distribution exhibits a high degree of heterogeneity. In these situations a knowledge of the distribution function for such particulate systems will be advantageous, as this will provide a full detail of the system with all the properties of interest. In the previous Section 2.2 numerical solution techniques were used on the discretised population balance equation in order to solve directly for the particle distribution function.

Furthermore, the distribution function will be subject to the influences of not only the physical conditions in which the process is operating under, but also on the formulation properties of the starting materials. Here, the applicability of population balance models to the aforementioned processes is made more apparent. Firstly, the process is interpreted into a mathematical model of the particle distribution function accounting for their spatial positioning in the physical space (external coordinates) and the intrinsic properties of the particles such as size and composition (internal coordinates). Thus, modelling of a particulate process where there are both spatial distributions, and internal distributions along the

particle's internal coordinates can be achieved within a population balance framework. Population balances have gained widespread usage in terms of modelling particulate processes such as in aerosol dynamics (Marchisio and Fox, 2005), crystallisation (Ma et al.. 2002a), to name but a few, due to its relative ease in the incorporation of additional internal coordinates necessary to model the process.

3.2 Derivation of the population balance equation

In formulating the population balance equation the number density function is used. which is a function of both the external and the internal coordinate axes, with the former referring to the spatial arrangement of particles in the physical space whilst the latter refers to the particle properties *i.e.*, size, composition, *etc.* In certain cases the external coordinate axes may be neglected if one invokes the condition of uniform mixing within the particle state space. Thus, the density distribution function will simplify to one that is dependent only on the chosen particle properties. The density function is then defined as $F(r,t)$, which represents the total number of moles of particles with property r at time t, r being the chosen particle property (internal coordinate). The evolution of the particle population with time will be subject to the influence of particle transformation processes, which include nucleation, aggregation, consolidation and breakage. These transformation processes may be collectively grouped as the source terms responsible for the evolution of the particle population.

In order to begin the derivation of the population balance equation, a schematic is provided for in Figure 3.1. The following derivation will be shown for a one-dimensional population balance equation under the assumption that the system is well mixed, enabling the external coordinates to be neglected. Later, extension to include a three-dimensional population balance will be shown in Section 3.2.1. In the schematic as depicted in Figure 3.1, the particles are convecting along the internal coordinate axis with velocity $GR_{r-\Delta r,t} = \frac{dr}{dt}|_{r-\Delta r,t}$ and $GR_{r,t} = \frac{dr}{dt}|_{r,t}$ from the LHS and RHS of the rth finite element, respectively. A material balance over this finite element can be written over a small time interval Δt, accounting for the particles entering and leaving the bin, as shown in Equation (3.1), with $S(r,t)$ representing the net rate of change of particles undergoing transformation processes (*e.g.* nucleation, aggregation and breakage).

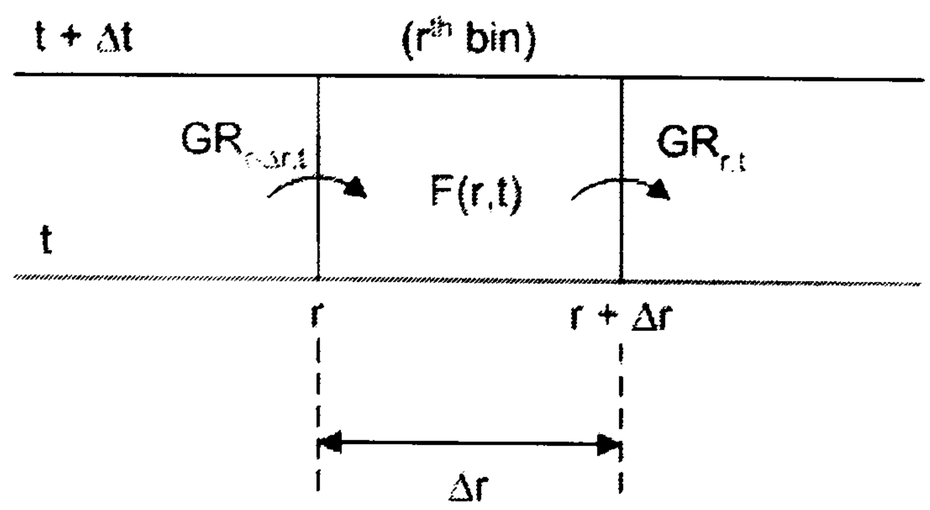

Figure 3.1: Schematic of a finite element (rth finite element) discretised along the respective internal coordinate axis. The particles are shown here convecting along the coordinate axis with a convective velocity, GR, passing across the finite element boundary interface.

$$F(r,t)\Delta r\Big|_{t+\Delta t} - F(r,t)\Delta r\Big|_{t} = F\left(\frac{dr}{dt}\right)\Delta t\Big|_{r} - F\left(\frac{dr}{dt}\right)\Delta t\Big|_{r+\Delta r} + S(r,t)\Delta t\Delta r \tag{3.1}$$

Rearranging the above equation and dividing both sides by $\Delta r\Delta t$,

$$\frac{F(r,t)\Delta r\Big|_{t+\Delta t} - F(r,t)\Delta r\Big|_{t}}{\Delta r\Delta t} + \frac{F\left(\frac{dr}{dt}\right)\Delta t\Big|_{r+\Delta r} - F\left(\frac{dr}{dt}\right)\Delta t\Big|_{r}}{\Delta r\Delta t} = \frac{S(r,t)\Delta t\Delta r}{\Delta r\Delta t} \tag{3.2}$$

Taking limits for $\Delta r \to 0$ and $\Delta t \to 0$,

$$\frac{\partial F(r,t)}{\partial t} + \frac{\partial}{\partial r}\left(F(r,t)\frac{dr}{dt}\right) = S(r,t) \tag{3.3}$$

Here, the partial derivative term with respect to r on the LHS of Equation (3.3) represents the continuous change of a particle property, and is referred to as the internal convective velocity along the particle's respective coordinate. The net rate of entry of particles is represented by $S(r,t)$, accounting for all the particle-level transformations such as nucleation, aggregation and breakage, *etc.* Elaboration for each individual sub-rate process (nucleation, consolidation, aggregation and breakage) contributing to the source term is provided in Section 3.2.2.

3.2.1 Higher-dimensional population balances

In the above derivation of the population balance equation, only one internal coordinate was considered. However, when modelling distributed systems where the particles are distributed

along several characteristic properties of the particles, the one-dimensional population balance becomes inadequate and it becomes necessary to employ higher-dimensional population balance equations in order to model the evolution of the particle population with their internal coordinates accurately. The general equation accounting for multivariate population balances is given in Equation (3.4) (Randolph and Larson, 1971).

$$\frac{\partial F(\mathbf{x},t)}{\partial t} + \sum_{j=1}^{N_c} \frac{\partial}{\partial x_j}\left[F(\mathbf{x},t)\left(\frac{dx_j}{dt}\right)\right] = S(\mathbf{x},t), \quad j \in 1,2,\ldots,N_c \tag{3.4}$$

Where, $\mathbf{x}$ is the internal coordinate property vector of length N_c. In the context of this work, three internal coordinates are required for modelling the granulation of particles for the reasons given in Chapter 2. That is, granule coalescence is dependent upon the porosity and binder content of granules in addition to, the size of the granule. Verkoeijen et al. (2002) and Iveson (2002) also arrived at the same conclusion of the importance of three-dimensional PB with the three aforementioned particle properties. The resulting three-dimensional population balance equation with the volume of solid (s), volume of liquid (l) and the volume of gas (g) as the three chosen internal coordinates is given in Equation (3.5).

$$\frac{\partial}{\partial t}F(s,l,g,t) + \underbrace{\frac{\partial}{\partial g}\left(F(s,l,g,t)\frac{dg}{dt}\right)}_{consolidation} + \underbrace{\frac{\partial}{\partial s}\left(F(s,l,g,t)\frac{ds}{dt}\right)}_{layering} + \underbrace{\frac{\partial}{\partial l}\left(F(s,l,g,t)\frac{dl}{dt}\right)}_{drying/re-wetting} = \Re_{nuc} + \Re_{aggre} + \Re_{break} \tag{3.5}$$

Here, $F(s,l,g,t)$ represents the particle density function and is defined such that the moles of granules with a value of the internal coordinate property vector between $\mathbf{x}$ and $\mathbf{x} + d\mathbf{x}$ with the coordinate property vector $\mathbf{x} \equiv (s,l,g)$ is given by $F(s,l,g,t)ds\,dl\,dg$. The partial derivative term with respect to s represents the layering of fine particles onto the surfaces of larger size particles. The partial derivative term with respect to g represents the consolidation of the granules. As the granule is compacted, the total pore volume of the granule decreases whilst the volume of the liquid binder phase and the volume of solid remain unchanged, thereby leading to an increase in the fractional liquid saturation of the granule. The drying and re-wetting of the granules is represented by the partial derivative term with respect to l. The particle-level transformation processes *i.e.*, nucleation, aggregation and breakage are represented by the source terms $\Re_{nuc}$, $\Re_{aggre}$ and $\Re_{break}$.

3.2.2 Description of sub-rate processes

The aggregation term is comprised of two terms, which account for the formation of the newly born particle and the depletion of the two particles consumed in the process in forming the new born particle. The formation and depletion terms associated with the aggregation phenomenon are defined in Equations (3.6)-(3.8) (Ramkrishna, 2000; Immanuel and Doyle III, 2005). In these equations, s_{nuc} is the solid volume of nuclei (assumed fixed), and $\beta(s_1, s_2, l_1, l_2, g_1, g_2)$ is the size-dependent aggregation kernel that signifies the rate constant for aggregation of two granules of internal coordinates (s_1, l_1, g_1) and (s_2, l_2, g_2). The internal coordinates are computed on volume basis, since this is a conserved property, as previously advocated by Verkoeijen et al. (2002).

$$\Re_{aggre} = \Re_{aggre}^{formation} - \Re_{aggre}^{depletion} \tag{3.6}$$

$$\Re_{aggre}^{formation} = \frac{1}{2}\int_{s'=s_{nuc}}^{s-s_{nuc}}\int_{l'=0}^{l}\int_{g'=0}^{g}\beta\left(s', l', g', s-s', l-l', g-g'\right)F\left(s', l', g', t\right) \times F\left(s-s', l-l', g-g', t\right)ds'\,dl'\,dg' \tag{3.7}$$

$$\Re_{aggre}^{depletion} = F\left(s, l, g, t\right)\int_{s'=s_{nuc}}^{s_{max}}\int_{l'=0}^{l_{max}}\int_{g'=0}^{g_{max}}\beta\left(s', l', g', s, l, g\right) \times F\left(s', l', g', s, l, g\right)ds'\,dl'\,dg' \tag{3.8}$$

Empirical model forms for the aggregation kernel have been proposed in the past, which require parameter tuning with experimental results. However, due to their shortcomings as outlined in Chapter 2, development of mechanistic based kernels are in demand. An example of a mechanistic aggregation kernel is presented in Section 3.4, which will be incorporated into the population balance model for the granulation process.

Granule nucleation represents an important process at the outset of granulation. Traditional methods for modelling this sub-rate process was adopted from crystallisation, employing the Dirac delta as shown in Equation (3.9). Here, k_{nuc} represents the nucleation rate constant, δ is the Dirac delta function, r is the particle size and r_0 represents the size of a nuclei. This model representation for the nucleation rate process assumes nuclei particles of a particular size is formed *i.e.*, r_0. Research has indicated that nucleation is affected by various

factors, which include process operating parameters like the liquid binder flow rate and the bed turnover rate, and are not accounted for in Equation (3.9). Later, a novel mechanistic kernel for nucleation will be shown that accounts for the possibility of nuclei of different sizes to be formed, which better represents the physical processes in reality. In addition, the model allows for the possibility to predict the behaviour of the process for different physicochemical properties of formulations.

$$\Re_{nuc}(r,t) = k_{nuc}\delta\left(r - r_0\right) \tag{3.9}$$

The consolidation phenomenon accounts for the compaction of the granules, with the effect of reducing the porosity of the granules, making them more dense and compact. The porosity of the particles is defined by Equation (3.11). An exponential decay relation was used for representing granule consolidation and is modelled using heuristic information as shown below in Equation (3.10) (Iveson et al., 1996). Here, ε_{min} is the minimum porosity of the granules and c is the compaction rate constant. The constant c has been found to be dependent upon the mixing rate or tumbling rate in the granulator, although no clear correlations have been established.

$$\begin{aligned} \frac{d\varepsilon}{dt} &= -c\left(\varepsilon - \varepsilon - min\right) \\ \frac{dg}{dt} &= -c\frac{s+l+g}{s\left(1-\varepsilon_{min}\right)}\left[l - \frac{\varepsilon_{min}s}{1-\varepsilon_{min}} + g\right] \end{aligned} \tag{3.10}$$

Additional transformation processes that also play a role in granulation include coating of fine particles, attrition, abrasion transfer and particle breakage. For particle breakage, it is possible that for different granulator configurations and setups, breakage will become more prevalent in one granulator equipment than another. For instance, granules are less prone to breakage in rotary drum granulators, as opposed to high shear mixers with fast moving impeller blades with or without choppers. The experimental work that was carried out during this research were performed in a rotary drum granulator, and under the conditions employed, granule breakage was not seen as the prevailing mechanism influencing granule growth behaviour.

By solving the three-dimensional population balance in terms of the three independent variables (s,l,g), it is possible to extract other useful information pertaining to the granule (Figure 3.2) such as the porosity of the granules (ε), pore saturation (l_{sat}), liquid-to-solid

fraction of the granules (w) and the volume of a granule (V) given in Equations (3.11)-(3.14).

$$\varepsilon = \frac{V_l + V_g}{V_s + V_l + V_g} \tag{3.11}$$

$$l_{sat} = \frac{V_l}{V_l + V_g} \tag{3.12}$$

$$w = \frac{V_l}{V_s} \tag{3.13}$$

$$V = V_s + V_l + V_g \tag{3.14}$$

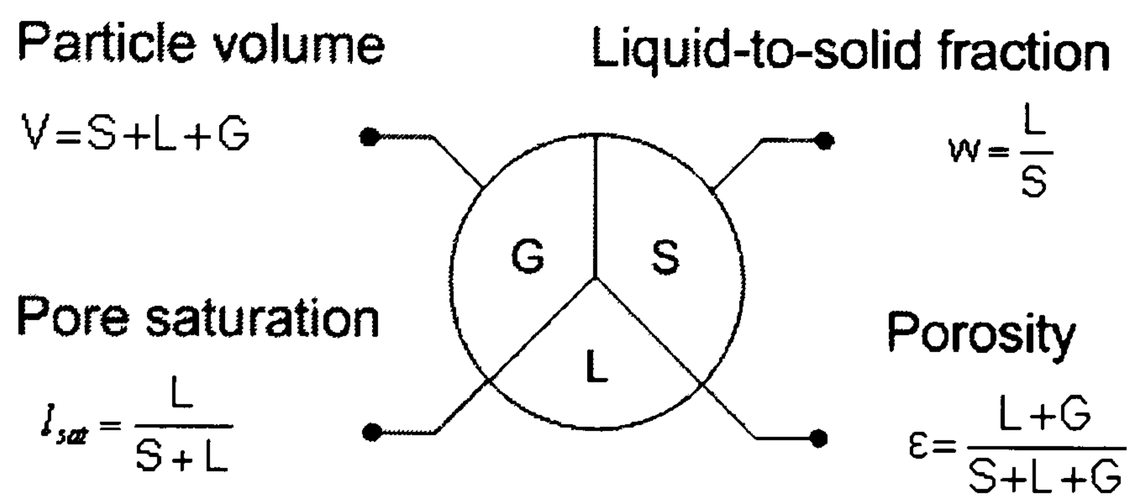

Figure 3.2: Establishing the relationships for the granule properties (l_{sat}, w, ε) from the three internal state variables of a granule: solid volume (S), liquid volume (L) and volume of air (G). Adapted from Verkoeijen et al. (2002).

3.2.3 Two-dimensional visualisation

A more meaningful aid in interpreting the behaviour of granules with respect to changes to their particle properties is to appropriately transform the three-dimensional distribution into a two-dimensional distribution, *i.e.*, taking the volume of each phase s, l and g and computing the corresponding particle size, $r = \left(\frac{3V}{4\pi}\right)^{1/3}$, and the fractional binder content. The result of the transformation from three-dimensions to two-dimensions is a 2D visualisation of the particle distribution with respect to changes in the particle size and fractional content. Transformation to two-dimensions is carried out using Equation (3.15).

$$F^{2D}(r, w) = \int_{r'=r_{min}}^{r_{max}} \int_{w'=w_{min}}^{w_{max}} F(r, w)\delta(r - r')\delta(w - w')\, dw'\, dr' \tag{3.15}$$

The methodology involves defining and discretising two new coordinate axes, each for the particle size and the fractional binder content. The fractional binder content range and the particle size range are computed for each three-dimensional grid (solid, liquid and air axes). Thus, the particles from the three-dimensional model simulation are appropriately assigned

to each finite element in the two-dimensional discretised grid (Figure 3.3). The advantages of recasting the particle distribution with coordinate axes as size and fractional binder content allows for an easier visualisation of the population evolution in response to the source terms.

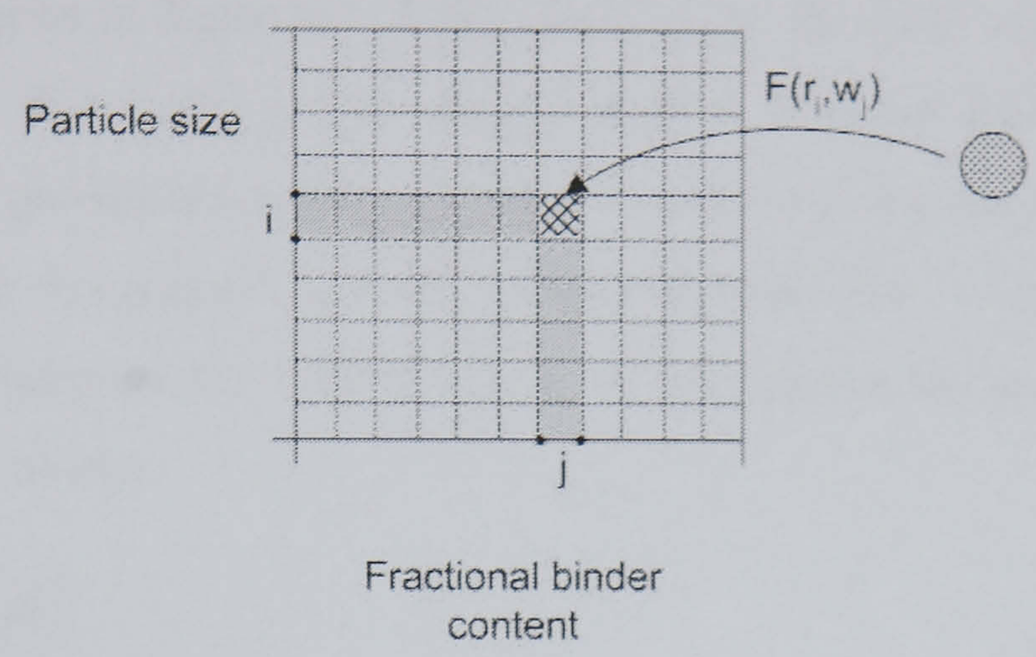

Figure 3.3: Illustration showing the assignment of particles with corresponding size and fractional binder content for a two-dimensional visualisation of the particle distribution.

3.3 Model extensions to other scenarios

The previous section introduced three-dimensional population balances where it is necessary to model the evolution of the particle population with at least three internal coordinates for granulation (volume of solid, volume of liquid and volume of gas). A general population balance equation for the three-dimensional population balance was given in Equation (3.5). In addition to specifying particle state variables as internal coordinates to be modelled in the population balance equation, extension to the model to provide a finer detail of the state of individual particles may be introduced as additional internal coordinates. To exemplify this particular model formulation of the population balance, Darelius et al. (2006) and Braumann et al. (2007) used the volume of solid and the volume of the liquid binder as internal coordinates but further categorised them. For instance, Darelius et al. (2006) further classified the liquid binder according to their location on the granule either on the surface of the granule or residing within the granule matrix occupying the granule pore spaces. Braumann et al. (2007) further differentiated the solid volume of the granule by partitioning the solids content into those derived from the constituent particles that make up the granule matrix, with further addition to the solid volume of the granule arising from reaction-induced precipitation of the binders. Further details pertaining to the rate law expressions for the reaction of the

binder and the corresponding equations for partitioning the binder (internal or external to the granule matrix) during coalescence may be found in their aforementioned studies. Thus, the vector of internal coordinates used in their model with five independent variables to describe a granule is given in Equation (3.16). Here, s_o is the solid volume attributed to the constituent particles that make up the granule matrix, s_r is the solid volume arising from the reaction-induced precipitation from the binder reaction, l_i represents the volume of liquid binder located within the granule, l_e is the volume of liquid that is located on the surface of the granule and g represents the volume of gas *i.e.*, occupying the pore spaces that are not filled with the liquid binder.

$$\mathbf{x} = [s_o \; s_r \; l_i \; l_e \; g]^{\mathrm{T}} \tag{3.16}$$

As in the previous case where Braumann et al. (2007) incorporated chemical reactions a common phenomenon in the manufacture of granules, so too is the agglomeration of multiple solid components. This is especially common in the pharmaceutical industry where in addition to the active drug ingredient, other components are added to facilitate the process of making tablets (*e.g.* excipients). Iveson (2002) formulated a four-dimensional population balance equation accounting for binary solid mixtures (solid components a and b). The following are included in the set of internal coordinates: granule solid phase mass (m), binder-to-solid mass ratio (w), granule porosity (ε), solid phase mass fraction for component a (x_a). In this case the vector of internal coordinates is given in Equation (3.17).

$$\mathbf{x} = [m \; w \; \varepsilon \; x_a]^{\mathrm{T}} \tag{3.17}$$

Particular attention to the conservation of the total mass within the system, by ensuring appropriate partitioning of the amounts of solid component a and b should be considered during numerical solution of the PBE. Where liquid binder is introduced into the system, then the change in the mass of binder should also be reflected by this liquid addition when numerically solving the population balance equation. The above mentioned model extensions involving higher-dimensional population balances can provide a greater detail in tracking the individual state of a particle (*e.g.* varying compositions of binary solids, liquid distribution in individual granules, contribution of solids volume from reaction-induced precipitation). Thus, population balance lends itself as a convenient framework towards predictive modelling tool of particulate systems with particle properties that are heterogeneously distributed across the particle population.

3.4 Introducing a mechanistic representation of the aggregation kernel

An important mechanism during granulation is the aggregation phenomenon. The aggregation term is comprised of two terms, the formation and depletion of particles as shown in Equations (3.6)-(3.8). As previously mentioned the aggregation kernel represents an important parameter for the growth phenomenon, as it is a measure of the rate at which two particles will successfully aggregate forming a single larger particulate entity. In the case of Equations (3.7) and (3.8), it is a measure of success for particles p_1 and p_2 with characteristics (s', l', g') and $(s - s', l - l', g - g')$, respectively, coalescing to form a new particle with characteristics (s, l, g).

Previous attempts to represent the aggregation kernel in the form of empirical kernels, with particle size as the main contributing factor predominating aggregation, have been used with varying degrees of success, coupled with parameter fitting to experiments. However, it has been long recognised that collision between particles resulting in successful coalescence is dependent upon other factors in addition to the sizes of the participating particles, such as the binder content of the particles, binder viscosity, the initial distribution of the seed particles (primary particles). In addition, equipment level parameters such as the rate of mixing, binder flow rate, powder flux under the spray zone and the geometry of the granulator will impart a significant influence with respect to the granule growth mechanisms. An overview of mechanistic kernel for aggregation is introduced, which is based on the previous works of Ennis et al. (1991), Liu et al. (2000). Immanuel and Doyle III (2003) applied this micro-level model for aggregation from an energy dissipation perspective, by computing the net attractive potentials (based on energies) between various particle combinations with each other. This approach was later adopted for granulation modelling in three-dimensional population balances (Immanuel and Doyle III, 2005).

The model used prescribes two conditions in which coalescence can occur and these are designated as type I and type II coalescence and is schematically depicted in Figure 3.4. In type I coalescence, the initial kinetic energy of the approaching particles are completely overcome by the viscous dissipation in the liquid layer, leading to coalescence prior to their surfaces making direct contact with each other. The relative velocity of the particles as a

function of their separation distance is defined in Equation (3.18).

$$u(h) = u_0, \quad h > h_0$$
$$u(h) = u_0 \left[1 - \frac{1}{St_v} \ln\left(\frac{h_0}{h}\right)\right], \quad h < h_0 \tag{3.18}$$

Where, u_0 is the initial approach velocity of the particles (based on the mixing intensity within the granulator), h is the separation distance between the colliding particles, u represents the relative velocity of the particles as they approach each other and is a function of the separation distance between the two particles, h_0 represents the thickness of the liquid binder layer that forms around each particle. The net attractive potential (ψ) between the particles is calculated using Equation (3.19), based on the relative velocity of the particles as determined from Equation (3.18).

$$\psi\left(p_1, p_2, h\right) = \frac{1}{2} m (2u(h))^2. \tag{3.19}$$

Type II coalescence involves two sequential stages prior to coalescence - the forward path and the reverse path (see Figure 3.4). The path with the higher energetics is taken as the rate-determining step. The forward path is represented by the approach stage, with the initial kinetic energy being dissipated by the viscous liquid layer. The elastic energy that is released upon particle deformation following collision leads to the rebound stage (reverse path). The energy lost during the impact and particle deformation may be calculated using Equation (3.20). At this particular instant, the particles will either coalesce if the elastic energy is fully dissipated by viscous dissipation, or particle separation (rebound) will occur. The velocity of the particles corresponding to the retraction phase is given in Equation (3.21) with δ'' representing the permanent plastic deformation of the particles defined in Equation (3.22). The net attractive potentials corresponding to the forward path and the reverse path are given in Equations (3.23) and (3.24), respectively.

$$E_c = \frac{1}{2} m (2u_1)^2. \tag{3.20}$$

$$u'(h) = u_2 - \frac{3\pi\mu\tilde{\mathrm{D}}^2}{16\tilde{\mathrm{m}}h^2}\left[(\delta'')^2\left(\frac{h^2}{h_a^2} - 1\right) + 2h\delta''\left(\frac{h}{h_a} - 1\right) + 2h^2 \ln\left(\frac{h}{h_a}\right)\right], \quad 0 < h < h_0$$
$$u'(h) = u'(h_0), \quad h > h_0 \tag{3.21}$$

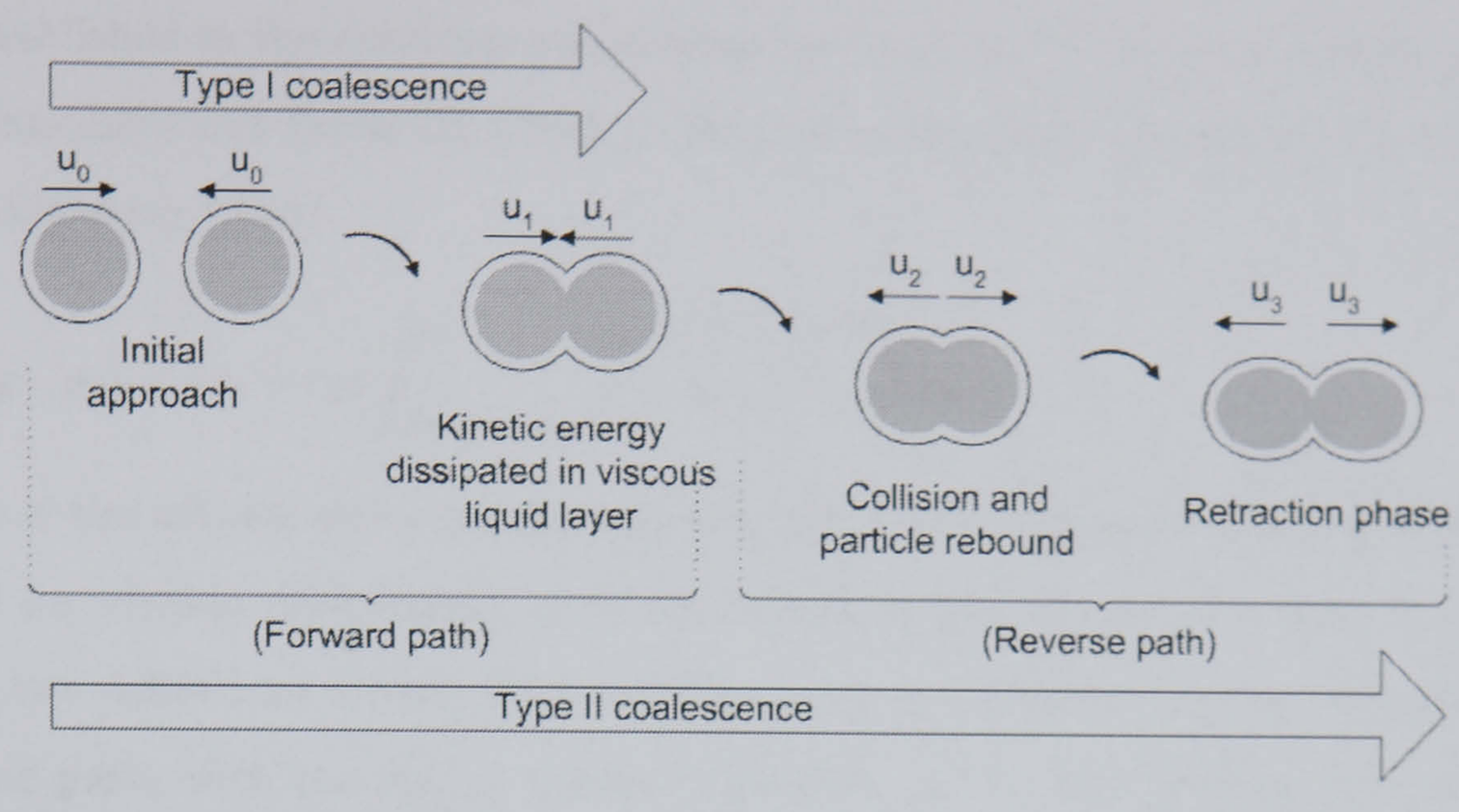

Figure 3.4: Schematic representation for type I and type II coalescence (Liu et al., 2000). The representative collision velocity between the two particles is denoted by u_0. For type I coalescence (i), the particles' initial kinetic energy is fully dissipated in the viscous binder layer ($u_1 \leq 0$). In type II coalescence, particle surfaces collide as the kinetic energy is greater than can be dissipated in the viscous binder layer (forward path). The particles begin to rebound from one another due to inherent elastic energy, which is dissipated during the retraction phase. There is again viscous losses through the binder layer, which bring the particles to rest ($u_3 \leq 0$) thereby preventing complete particle separation (reverse path). Adapted from Liu et al. (2000).

$$\delta'' = \left(\frac{8}{3\pi}\right)^{\frac{1}{2}} (St_{def})^{\frac{1}{2}} \tilde{\mathrm{D}} \left[1 - \frac{1}{St_v} \ln\left(\frac{h_0}{h_a}\right)\right] \left[1 - 7.36 \frac{Y_d}{E^*} (St_{def})^{-\frac{1}{4}} \times \left[1 - \frac{1}{St_v} \ln\left(\frac{h_0}{h_a}\right)\right]^{-\frac{1}{2}}\right] \tag{3.22}$$

$$\psi_{forward}(p_1, p_2, h) = \frac{1}{2} m \left[2u(h)\right]^2 - E_c \tag{3.23}$$

$$\psi_{reverse}(p_1, p_2, h) = -\frac{1}{2} m (2u')^2 \tag{3.24}$$

Thus, the kinetic energy of the particles, suitably corrected for viscous dissipation, constitutes the major factor in modelling the aggregation phenomenon. These steady state forces are then employed for the dynamic calculation in the Smoluchowski formulation (Immanuel and Doyle III, 2005), drawing a parallel with the DVLO theory (transition state theory that

is well established in the emulsion polymerisation literature; Coen et al. (1998); Melis et al. (2000); Immanuel and Doyle III (2003)). The Fuch's stability ratio for type I coalescence is given by Equation (3.25).

$$W(p_1, p_2) = (r_1 + r_2) \int_{D=(r_1+r_2)}^{\infty} \frac{\exp\left(\frac{\psi(p_1,p_2,D)}{kT}\right)}{D^2} d(D) \tag{3.25}$$

Where, ψ is the net attractive potential (calculated from the kinetic energies of the particles corrected for viscous dissipation), r_i is the radius of particle p_i. For type II coalescence, there are two definitions for the Fuch stability ratio, corresponding to the forward path and the reverse path, with the higher energetic pathway as the rate-limiting step, and is given in Equation (3.26). Here, the $\psi_{forward}$ is the net attractive potential driving the approach phase and $\psi_{reverse}$ is the net attractive potential driving the retraction phase.

$$\frac{W(p_1, p_2)}{r_1 + r_2} = max\left(\int_{D=(r_1+r_2)}^{\infty} \frac{\exp\left(\frac{-\psi_{forward}(p_1,p_2,D-r_1-r_2)}{kT}\right)}{D^2} d(D), \int_{D=(r_1+r_2)}^{\infty} \frac{\exp\left(\frac{-\psi_{reverse}(p_1,p_2,D-r_1-r_2)}{kT}\right)}{D^2} d(D)\right) \tag{3.26}$$

The energy dissipation calculations for type I and type II coalescence and the modelling of the steady state forces at the particle level are subsequently used in the calculation of the aggregation kernel using the Smoluchowski formulation given in Equation (3.27). Here, k is the Boltzmann constant, T is the temperature and c_1 is an adjustable constant accounting for errors arising from model lumping assumptions.

$$\beta(p_1, p_2) = c_1 \frac{4\pi u_0 (r_1 + r_2)^2}{W} \tag{3.27}$$

3.5 Mechanistic formulation of the nucleation kernel

3.5.1 Review of the nucleation phenomenon

Research in the past have predominantly focussed their attention on the particle aggregation process, with little attention given to other key phenomena involved in granulation such as nucleation or breakage. It has only been in recent times that wetting and nucleation, which occurs at the beginning of the granulation process, has been recognised to play a crucial role in the process. In addition, carrying out investigative studies into the nucleation phenomenon during granulation does not present itself to be as straightforward. This is

because the nucleation process occurs over a very short time frame. As soon as the binder makes contact with the powder, nuclei particles begin to form as the liquid binder spreads across the powder surface and penetrates the bed mass. The granulation process is usually carried out within a single working volume, there is no demarcation between nucleation, aggregation and breakage phenomena. Thus, the short time scale over which nucleation occurs and the lack of demarcation of the individual granulation phenomena pose as a challenging task to study the nucleation phenomenon.

Wildeboer (2002) addressed the issue of isolating the nucleation process from other interfering granulation phenomena, by designing a purpose built laboratory scale apparatus to study separately wetting and nucleation. Hapgood (2000) employed fast imaging techniques to study the kinetics of droplet penetration on the powder surface, and the penetration of the liquid from the droplet into the porous material for various binders and solid powder compacts.

The nucleation stage is regarded as a crucial period at the start of the granulation processes since the nuclei size distribution (NSD) obtained at these initial stages of the process will impart a large influence on future GSDs. Venkataramana et al. (1999) stated that large variations in the size distribution of the feed would have a template like effect on the GSD (Section 2.1). This argument may similarly be applied to the characteristics of the NSD and its effect on the GSD. The nucleation process may be described as a sequence of events leading up until the formation of the granule nucleus. Firstly, the liquid binder is dispersed from its source forming binder droplets, which are distributed across the powder bed mass. Depending on the prevailing operating conditions at the time (*i.e.* binder flow rate, bed turnover rate, *etc.*), the binder droplets may either coalesce in mid-air to form larger droplets before landing on a section of powder surface or, the droplets may overlap on top of each other at the surface of the powder (see Figure 3.5) or each droplet might lead to separate nuclei. The second, would correspond to low surface replenishment rate or low bed turnover rate. The droplet will spread across the powder surface and begin penetrating the powder through surface pores via capillary action. The extent as to how much the binder wets the solid powder and the time taken to completely penetrate the powder without residual binder remaining on the surface will be governed to a large extent on the formulation properties of the solid and liquid, which will also play an influential role in the wetting kinetics of the nucleation process. This consideration is likened to the nucleation thermodynamics. During the initial

stages of the granulation process, the powder is in constant motion and usually aided with mechanical internal devices to promote powder mixing. Thus, mechanical agitation provides an important means for binder dispersion. The nucleation process is also depicted in Figure 3.5 to illustrate the sequence of events involved during the process of nucleation.

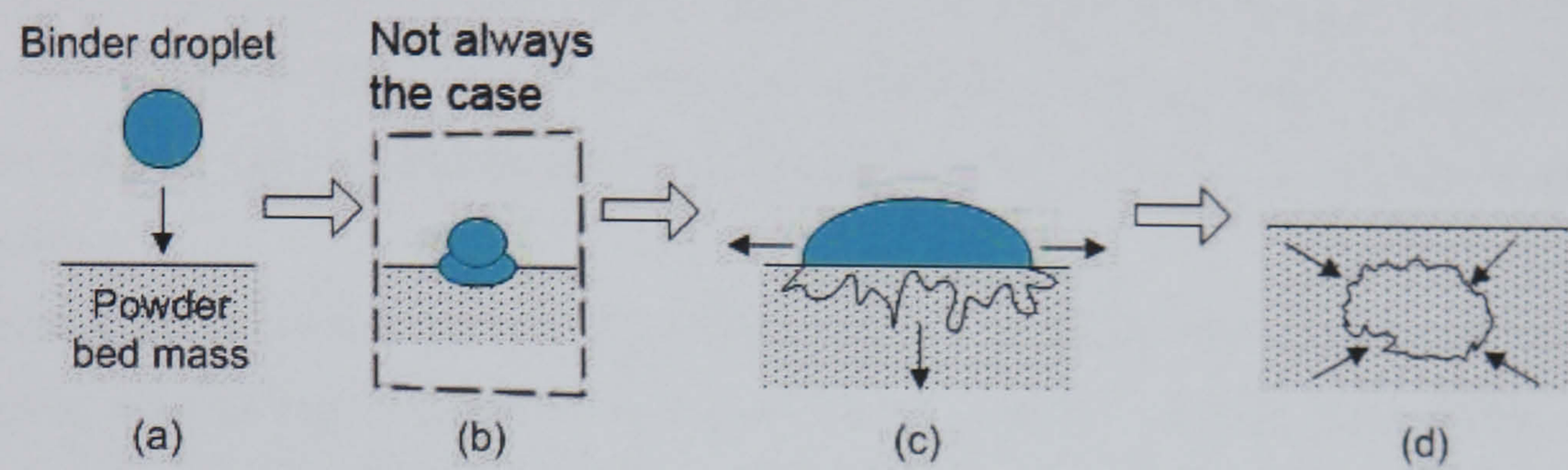

Figure 3.5: Schematic illustration of the nucleation process. (a) binder droplet formation, (b) droplet coalescence and overlap, (c) binder dispersion via wetting and capillary penetration, (d) mechanical dispersion of the binder droplet. Adapted from Litster and Ennis (2004).

In this section the primary focus is the development of a mechanistic nucleation kernel, based on the physics of the process. Providing an accurate model that will best represent the nucleation process will need to take into consideration the formulation properties that will enable a quantitative determination of the nucleation rate based on the thermodynamics of the process. This treatment will be introduced later in the following section.

3.5.2 Formulation properties

The physicochemical properties for both the solid powder and the liquid binder (*e.g.* spreading coefficient, contact angle, cohesion and adhesion energies) will play a dominant role in the agglomeration kinetics and the granule properties. It is anticipated that the effects will be most prominent at the early stages of the process during nucleation of the initial solid particles. Hemati et al. (2003) and Pont et al. (2001) both confirmed that the effect of wettability, *i.e.*, the contact angle, had a profound influence on the agglomeration kinetics, more so when the contact angle decreased, corresponding to higher adhesion tension (see below) which lead to the growth of larger granules. Malamataris and Kiortsis (1997) found that for various powders tested there were resistances to densification (granule consolidation), and this was found to be related to the work of adhesion for liquid binders of similar viscosities.

Separate studies by Krycer and Pope (1983), Zajic and Buckton (1990) and Zhang et al. (2002) found that the wetting properties of the binder and substrate (solid powder) showed a direct consequence on the granule properties such as granule friability, density, morphology and porosity. Bajdik et al. (2008) used the testing of the wetting properties as an essential step for determining the optimal binder composition and conditions needed for the formation of granules with the binder hydroxypropyl methylcellulose (HPMC) with the powder mixture comprised of $\alpha-$lactose monohydrate and microcrystalline cellulose (MCC) in a high-shear granulator.

The spreading coefficient and the contact angle made between the binder-substrate combination, both provide a quantitative measure of the extent of wetting obtained for a given binder acting on a solid. The spreading coefficient provides an important parameter from which to determine the wettability of one phase over the other. The spreading coefficient also has implications over the mode of granule formation. This coefficient is related to the interfacial works of adhesion and cohesion and is depicted in Figure 3.6. The interfacial surface free energies for different combinations of solid and liquid phases are defined in Equations (3.28)-(3.30). The work of cohesion represents the work required to separate a unit cross-sectional area of a material from itself whilst the work of adhesion represents the energy required to separate a unit cross-sectional area of an interface. The work of adhesion is defined by Equation (3.30)-(3.32).

Work of cohesion for a solid: $W_{CS} = 2\gamma^{SV}$ (3.28)

Work of cohesion for a liquid: $W_{CL} = 2\gamma^{LV}$ (3.29)

Work of adhesion for an interface: $W_A = \gamma^{SV} + \gamma^{LV} - \gamma^{SL}$ (3.30)

Substitute Young-Dupré's equation into Equation (3.30):

$$W_A = \gamma^{LV}\left(1 + \cos\theta\right) \tag{3.31}$$

The contact angle is the angle formed at the junction of the three phase contact line as shown in Figure 3.7 and is a measure of the affinity of the liquid binder for the solid particle surface.

The contact angle provides a convenient measure of the wettability of the solid by the binder. A high contact angle (hydrophobic) exemplifies the condition of poor wetting, in contrast to good wetting characteristics reflected by a low contact angle (hydrophilic) with better adhesiveness. Under ideal conditions neglecting environmental, surface roughness and

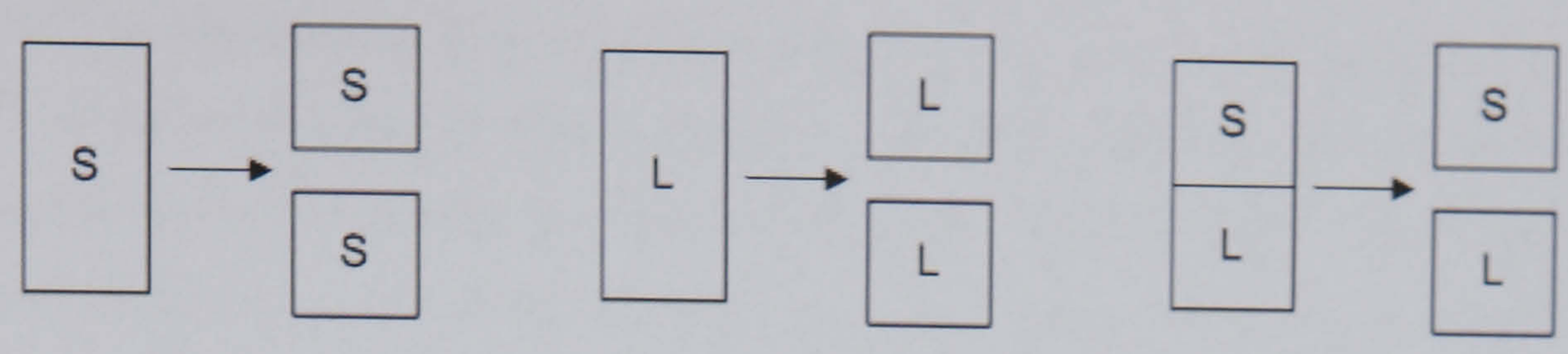

(a) Work of cohesion for a solid interface, $W_{CS} = 2\gamma^{SV}$ (b) Work of cohesion for a liquid interface, $W_{CL} = 2\gamma^{LV}$ (c) Work of adhesion for an interface, $W_A = \gamma^{SV} + \gamma^{LV} - \gamma^{SL}$

Figure 3.6: Schematic depicting the work of cohesion for homogenous phases and the work of adhesion for composite interfaces for solid and liquid systems. The solid and liquid phases are denoted by S and L respectively. Adapted from York (1995).

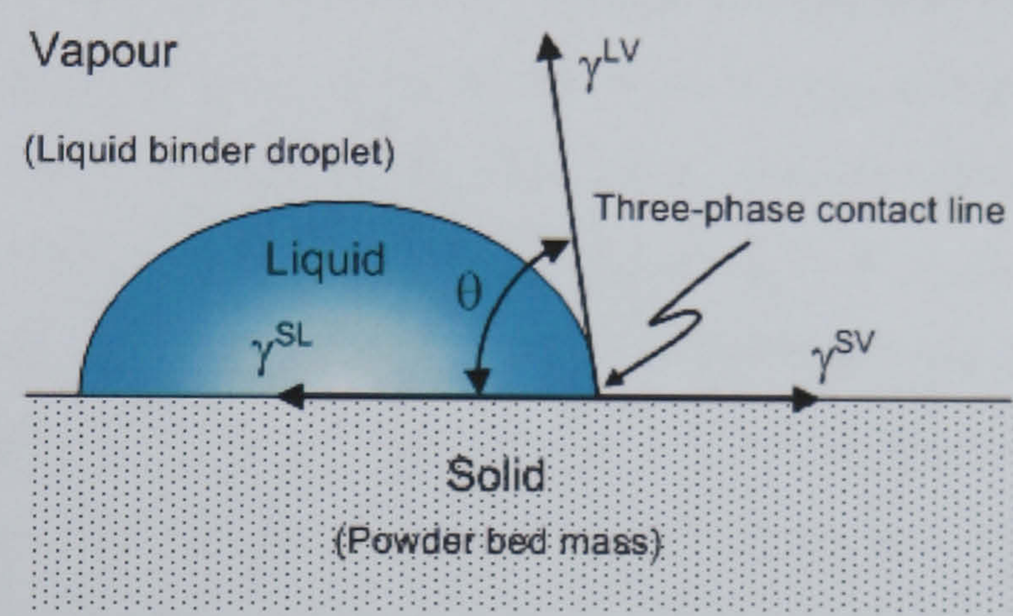

Figure 3.7: Schematic of a liquid binder droplet placed on the surface of the powder bed mass. The solid, liquid and vapour/gas phase is denoted by S, L and V respectively. The interfacial surface energies between solid-vapour, liquid-vapour and solid-liquid are denoted by γ^{SV}, γ^{LV} and γ^{SL} respectively. Adapted from Litster and Ennis (2004).

chemical heterogeneity effects, the relationship between the equilibrium contact angle[1] and the forces involved in the interaction, between cohesion and adhesion of each participating phase (solid, liquid, gas) can be described by the Young-Dupré equation given in Equation (3.32).

$$\gamma^{SV} = \gamma^{SL} + \gamma^{LV} \cos\theta, \quad \theta > 0^\circ. \tag{3.32}$$

[1]The advancing angle, receding contact angle and the contact angle hysteresis have been neglected. The underlying focus is the introduction of the relevant physicochemical properties, which will latter be used in the development of the nucleation kernel. The kinetics of the contact angle formed between the binder drop and that of the moving powder still remains unclear in the literature. Thus, use of the equilibrium contact angle is assumed to be sufficient for the present study. Hereafter, the term contact angle will refer to the equilibrium contact angle.

Where, γ^{SV} is the solid-vapour interfacial energy, γ^{LV} is the liquid-vapour interfacial energy, γ^{SL} is the solid-liquid interfacial energy and θ is the contact angle made between the binder and the substrate measured through the droplet. The *adhesion tension* represented by $(\gamma^{LV}\cos\theta)$ in the Young-Dupré equation is important in determining the wettability of the powder by the binder. From Equation (3.32), liquid binders forming low contact angles with the solid particle surface will have a higher propensity to spread resulting in better wetting. Likewise, a high contact angle indicates hydrophobicity of the binder on the solid particle surface with poor wetting. A binder will spontaneously spread over the powder if the contact angle is 0° corresponding to $(\gamma^{SV} - \gamma^{SL}) \geq \gamma^{LV}$, *i.e.*, if its spreading coefficient is positive.

Rowe (1989) found that the spreading coefficient calculated from different binder substrate pairs and with different interactions exhibited by them indicated that the formation of moist agglomerates may occur in different ways with differing end granule properties. In the case where the spreading coefficient of the binder over the solid (λ_{LS}) is positive, a strong adhering film is formed around the solid particle, with liquid bridge links formed at all points of particle-particle contact in the growing aggregate. These aggregate particles will likely be characterised as strong dense granules (low friability) with the granule strength dependent on the work of cohesion of the binder. In contrast, in a positive spreading coefficient of the solid over the binder (λ_{SL}), no film formation occurs instead the solid particles will embed or adhere to the binder, leaving only isolated patches of binder to be available to form bonds at other particle contacts. The resultant granule will be porous, with an open structure and typically weak and friable. In the third case where both the works of cohesion of the binder and the solid are high, the solid-liquid interface will be minimised. The spreading coefficient for the two aforementioned cases (λ_{LS} and λ_{SL}) can be calculated from Equations (3.33) and (3.34) (York and Rowe, 1994). Hancock et al. (1994) reaffirmed the importance of knowledge of the binder-substrate physical interactions, with particular regard to the spreading coefficient, in understanding the wet massing behaviour of granulation systems. In these expressions. D_d is the droplet diameter and D_p is the particle diameter.

$$\lambda_{LS} = W_A - W_{CL}, \quad D_d \approx D_p \tag{3.33}$$

$$\lambda_{SL} = W_A - W_{CS}, \quad D_d \gg D_p. \tag{3.34}$$

Having introduced the concepts of key physicochemical properties pertaining to the solid (powder) and the liquid (binder), it would appear that having a binder exhibiting good wetting and a low contact angle with the solid surface would be an optimal choice in formulation

for granulation. However, according to a study by Thielmann et al. (2008). particle wettability and granulation performance may not exhibit a simple relationship as previously thought. Good particle wetting is important as it contributes towards the aggregation of particles during agglomerate growth. But a compromise is required in terms of achieving complete coverage on the surface of particles by the binder, and the thickness of this binder layer on the particle surface. A localised thick layer of surface binder with only partial surface coverage will translate into stronger bonding at the particle contacts, since a lot more binder volume is able to contribute towards this bonding process. In addition, a thicker layer of binder even only as localised patches will be able to better dissipate the kinetic energy of the particles compared to a particle with complete surface coverage but only with a thin layer of binder. Iveson et al. (2004) studied the variation of contact angles in iron ore, which was shown to be dependent on the compositions of hematite and geothite, the primary constituents of the ores. The ores exhibit a hydrophobicity with increasing hematite composition and decreasing geothite content. The contact angle affects both the amount of liquid that is absorbed into the pores of the particles and the amount of liquid required to successfully granulate particles together. In cases with low contact angles, more liquid will be required to saturate the pores before being present on the surface for enabling particles to bond at these particle contact points. The liquid binder is drawn into the pores under capillary action, leaving a low fraction remaining on the surface. In cases where the binder exhibits a low contact angle with the solid surface, nucleation will begin once the pore spaces have been saturated before binder availability occurs on the surface of the particle, provided the binder droplet size is smaller or of equivalent size to the solid particles (Iveson et al., 1998; Hapgood, 2000). Thus, we may conclude from the work carried out by Thielmann et al. (2008) that better wettability does not necessarily translate into giving better granulation.

These recent findings suggest that the effects of the physicochemical properties of the formulation materials on the agglomeration behaviour and on the granule properties is complex. Clearly, an integrated system model that accounts for the various physical phenomena is crucial for engineering purposes.

3.5.3 Development of the nucleation kernel

The importance of taking into consideration both the wetting kinetics and the nucleation thermodynamics has already been mentioned. In the theoretical treatment of the nucleation

phenomenon, a droplet-controlled regime is assumed, with optimal and uniform binder distribution leading to well formed nuclei *i.e.*, individually formed nuclei particles (Hapgood et al., 2003).

In formulating the dynamic kernel, it is important to account for key process variables that influence the wetting and nucleation phenomena in an explicit manner, so as to prevent a lumping (averaging) effect. In particular, it is important to account for situations wherein

- the droplets do not wet the powder rapidly
- once wetted, the penetration rate is not fast enough relative to the bed turnover rate, resulting in partial penetration of the droplet into the powder bed

These factors are incorporated into the model developed below. The model adopts a few simplifying assumptions on certain other phenomena:

- The droplets are well spread and do not overlap. This assumption can be relaxed in later studies (Wildeboer et al., 2005).
- If primary particles (fines) are present, then the existent particles receive binder only if (a) the droplets do not wet the bed fast and hence are left on the powder surface at the time of bed turnover or (b) the droplets do not penetrate into the bed fast and part of the droplet remains on the powder bed surface at the time of bed turnover. Such surface binder is assumed to be uniformly distributed to all the existent granules by the mixing in the granulator.

Although the assumptions made are potentially limiting, they could be more easily relaxed in a refined model in the future. This is because, the assumptions pertaining to the phenomena regarding the droplet spread formation and the distribution of binder are distinct from the core wetting and nucleation phenomena.

The developed nucleation kernel accounts for the wetting kinetics and the nucleation thermodynamics as described next. The wetting kinetics is being explicitly accounted for in determining the nucleation rates whilst both the wetting kinetics and the nucleation thermodynamics account for the nuclei characteristics and the drop penetration time. The liquid penetration into the porous material is based on the studies presented by Hapgood (2000), which has been validated in Hapgood et al. (2002). The form of the nucleation kernel is derived from the collision/transition state theory as in the case of the aggregation kernel.

in which a minimum energy requirement for this rate process must be satisfied before the nucleation of solid particles is successful. The advantages with this kernel representation of the nucleation sub-rate process compared to previous attempts to model this phenomenon, is the direct inclusion of the physicochemical properties of the formulation materials *i.e.*, binder and solid powder surface free energies, through the physics of the nucleation phenomenon. The spreading coefficient is used to represent this minimum energy requirement for successful nucleation. This coefficient will determine whether the spreading of the liquid binder over the solid phase (powder) is energetically favourable, which is related to the works of cohesion and adhesion. These surface free energies and their relationship with the spreading coefficient have been defined in Equation (3.28)-(3.31) and Equation (3.33)-(3.34) respectively.

The computed net work for the wetting phase between the solid-liquid combination and the process operating variables associated with the binder distribution are incorporated into the calculation of the nucleation kernel given by Equation (3.35) for the formation of nuclei particles with characteristic traits (s, l, g).

$$k_{nuc}(s, l, g) = A_0 Q e^{\left(\frac{K\lambda}{RT}\right)} \tag{3.35}$$

Where, $\lambda = (\lambda_{LS}, \lambda_{SL})$ is the spreading coefficient, Q is the liquid binder flow rate, R is the ideal gas constant, A_0 is an adjustable parameter, and K is a parameter accounting for any errors in the model simplifications adopted in using the Young-Dupré relationship between the cohesion and adhesion forces acting on the binder-solid surface but also for the usage of the equilibrium contact angle neglecting contact angle hysteresis. Note that the dependence on the particle attribute s, l and g comes through the spreading coefficient, λ. If the tendency of the liquid is low in wetting the solid surface as characterised by the spreading coefficient, then there will be a large proportion of particles that will not be nucleated, and vice versa. Both the rate at which the binder is sprayed onto the powder, and the mixing intensity, will determine the nucleation regime in which the nuclei particles are formed (*i.e.* drop-controlled regime occurs when there is no droplet overlap and each droplet forms a nucleus).

The drop penetration into loosely packed porous beds such as those found in the granulator is expected to be complex and to be highly dependent on the bed microstructure. Hapgood (2000) proposed an alternative model for liquid drainage into loosely packed beds by introducing the concept of macrovoids. By taking into consideration the presence of macrovoids a new effective pore size radius was defined, which is in contrast to the conventional treatment employing the Kozeny approach that would lead to an incorrect prediction

of the effective pore size. In the Kozeny method, the model assumes that the powder bed is well-packed with a homogenous powder bed microstructure in estimating the pore size. However, as mentioned previously this approach is unlikely to provide a characterisation of the powder bed that truly reflects those encountered in the granulator where the powder bed is in motion. Figure 3.8 depicts a possible scenario of the difference in the microstructure of the powder bed between a well-packed and a loosely-packed bed, with the latter possessing macrovoids.

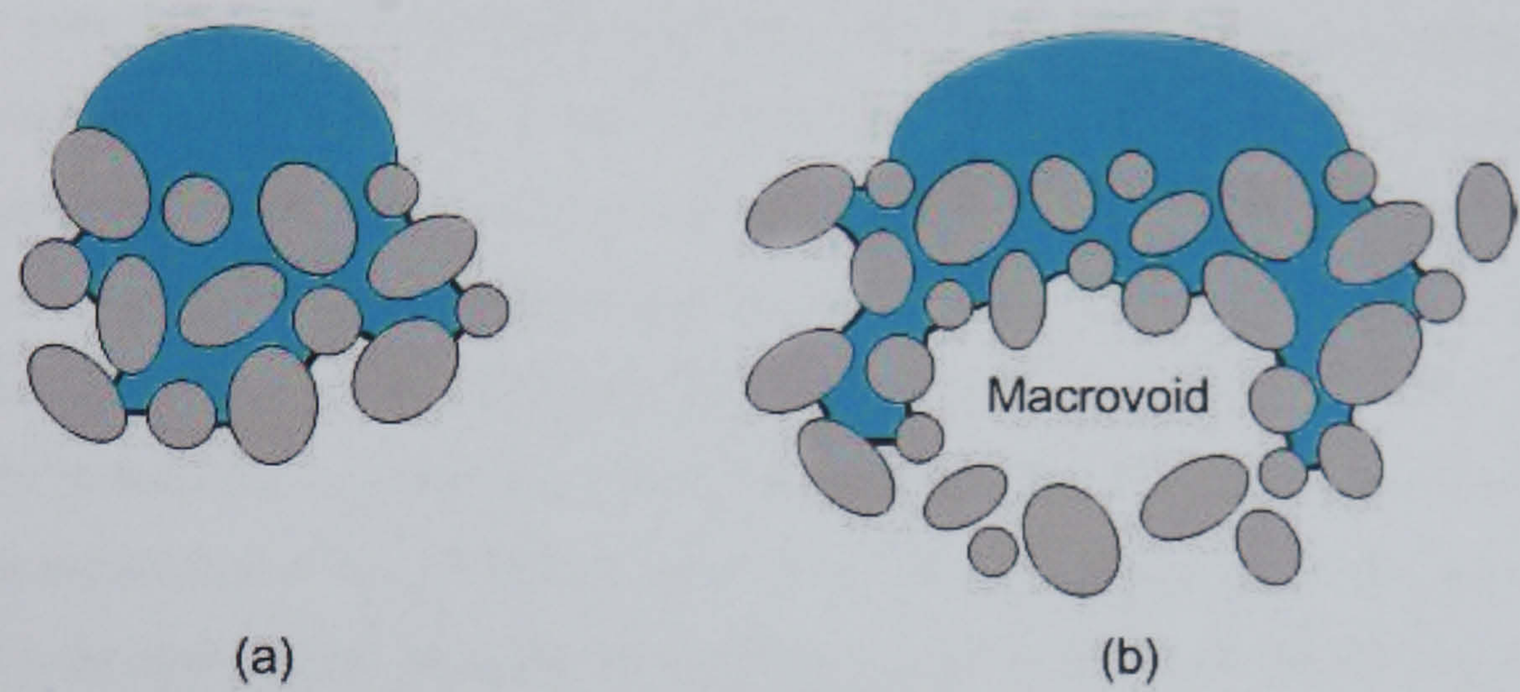

Figure 3.8: Schematic depiction illustrating the fluid flow through powder beds for (a) well-packed powder compact and (b) loosely packed powder. In loosely packed powder, the possibility of macrovoids is higher. These pockets serve to impede fluid flow whereby pores that terminate at macrovoids with a radius much greater than its own will effectively block the progression of flow beyond that point. Adapted from Hapgood et al. (2002).

Hapgood et al. (2002) assumes that no macrovoids are present when recording the tapped density (ε_{tap}), since the powder is assumed to be in its most compact form. Increasing the porosity of the powder introduces the possibility of having macrovoids *i.e.*, the powder becomes more loosely-packed. The assumption is that any additional porosity of the powder above its tapped porosity contributes exclusively towards the macrovoids Equation (3.36).

$$\varepsilon_{macrovoids} = \varepsilon - \varepsilon_{tap} \tag{3.36}$$

Where, ε is the porosity of the powder bed and ε_{tap} is the tap porosity. The new effective porosity (ε_{eff}) that will account for only those pore volume spaces that are involved in liquid drainage is given by Equation (3.37). It is assumed that the fraction of pores terminating at a macrovoid is proportional to the volume of macrovoids. The effective pore radius is

calculated based on the modified effective porosity using Equation (3.38). In this equation. ϕ is the shape factor and d_{32} is the surface mean diameter of the particle.

$$\varepsilon_{eff} = \varepsilon_{tap}\left(1 - \varepsilon_{macrovoids}\right) \tag{3.37}$$

$$R_{eff} = \frac{\phi d_{32}}{3}\frac{\varepsilon_{eff}}{1-\varepsilon_{eff}} \tag{3.38}$$

As a result of incorporating the presence of macrovoids in the imbibition of liquid through loosely packed powder beds in a granulator, drop penetration times estimated using this approach were more successful lying within the same order of magnitude, when compared to previous methods. This lies in the fact that the estimated pore size provides a better approximation of the pore volume that is involved in the liquid drainage. When the fluid flow encounters a macrovoid, the sudden widening will prevent the liquid flow from progressing any further. Previous methods include this pore volume despite the fact that it does not participate in fluid flow through the narrow pore channels of the powder bed, and hence the inaccurate estimation of the effective pore radius. The Hausner ratio of granular material is primarily a measure of the inter-particle friction condition of a moving mass of powder and is defined as the ratio of the final tapped bulk density to the aerated bulk density (Grey and Beddow, 1969; Rough et al., 2003, 2005; Mansa et al., 2008). A large Hausner ratio indicates a large inter-particle coefficient of friction. The Hausner ratio has been linked to the flowability of powders whereby a Hausner ratio > 1.40 indicates that the powder is cohesive whereas a value < 1.25 indicates a free-flowing powder. Thus, loose powders with large Hausner ratios suggests an increasing likelihood of the presence of macrovoids, and the Kozeny approach in modelling pore characteristics are unlikely to be followed, leading to inaccurate estimates of the drop penetration times.

The drop penetration model proposed by Hapgood (2000) for loosely packed powder mass is modelled using the Washburn equation (Denesuk et al., 1993) for liquid drainage into capillary pores. The Washburn equation is given by Equation (3.39), which gives the depth of liquid penetration ($h_p(t)$) into a pore as a function of time.

$$h_p(t) = \sqrt{\frac{R_{pore}\gamma^{LV}\cos\theta}{2\mu}}\sqrt{t} \tag{3.39}$$

Where, R_{pore} is the effective pore radius and is assumed to be constant for all surface pores on the powder surface, θ is the contact angle made between the solid and the liquid interface. μ is the binder viscosity and γ^{LV} is the liquid surface energy (*surface tension*). In deriving

the expression for the drop penetration time for liquid drainage into a pore, the Washburn equation is differentiated, yielding an expression for the velocity of liquid flow through the capillary pores Equation (3.40). On the powder surface, the rate at which the liquid from the binder droplet flows into the pores is given in Equation (3.41). In Equation (3.41). V represents the volume of liquid flowing into the pore, r_d is the radius of the droplet and ε_{eff} is the effective porosity of the powder accounting for macrovoids as detailed by Hapgood et al. (2002).

$$\nu = \frac{dh_p}{dt} = -\sqrt{\frac{R_{pore}\gamma^{LV}\cos\theta}{8\mu t}} \tag{3.40}$$

$$\frac{dV}{dt} = \pi r_d^2 \varepsilon_{eff}\nu \tag{3.41}$$

Substituting for ν in Equation (3.41) with Equation (3.40) and integrating through the separation of variables with the following limits:

$$V' = V_0 \quad t' = 0$$

$$V' = V \quad t' = t$$

$$\begin{aligned}
\int_{V'=V_0}^{V} dV &= -\pi r_d^2 \varepsilon_{eff}\sqrt{\frac{R_{pore}\gamma^{LV}\cos\theta}{8\mu}}\int_{t'=0}^{t}\frac{dt'}{\sqrt{t'}} \\
\therefore V(t) - V_0 &= -2\pi r_d^2 \varepsilon_{eff}\sqrt{\frac{R_{pore}\gamma^{LV}\cos\theta}{8\mu}}\sqrt{t} \\
\therefore V(t) &= V_0 - \pi r_d^2 \varepsilon_{eff}\left(\frac{R_{pore}\gamma^{LV}\cos\theta}{2\mu}t\right)^{\frac{1}{2}}
\end{aligned} \tag{3.42}$$

Upon complete drop penetration with no liquid remaining on the surface, $V = 0$. A circular footprint is assumed to be made by the droplet projected onto the powder surface, $r_d = \left(\frac{3V_0}{4\pi}\right)^{\frac{1}{3}}$. Substituting this into Equation (3.42), and re-arranging gives the expression for the drop penetration time as shown in Equation (3.43).

$$t = 1.35\frac{V_0^{\frac{2}{3}}}{\varepsilon_{eff}^2 R_{eff}}\frac{\mu}{\gamma^{LV}\cos\theta} \tag{3.43}$$

Further consideration needs to be made regarding the drop penetration into a porous bed mass. When the droplet falls onto the powder surface, a three-phase contact line is established (see Figure 3.7). During drop penetration, the contact angle may be considered to remain constant throughout the drop penetration process or to gradually decrease. These two limiting cases were identified by Marmur (1988) and are referred to as the constant drawing

area (CDA) and the decreasing drawing area (DDA) respectively, with the latter taking into account contact angle hysteresis (see Figure 3.9). In the CDA scenario, the apparent contact angle gradually decreases during the drop penetration. But, the circular footprint on the surface remains the same. Thus, the number of capillary pores available for liquid drainage remains unchanged, which is different from the DDA case in which the contact angle remains constant whilst the number of available pores decreases. Thus, the drop penetration time with respect to CDA represents the shortest time required for complete drop penetration, whilst the DDA case gives the longest drop penetration time since liquid will take longer to drain as there are fewer pores available for liquid drainage.

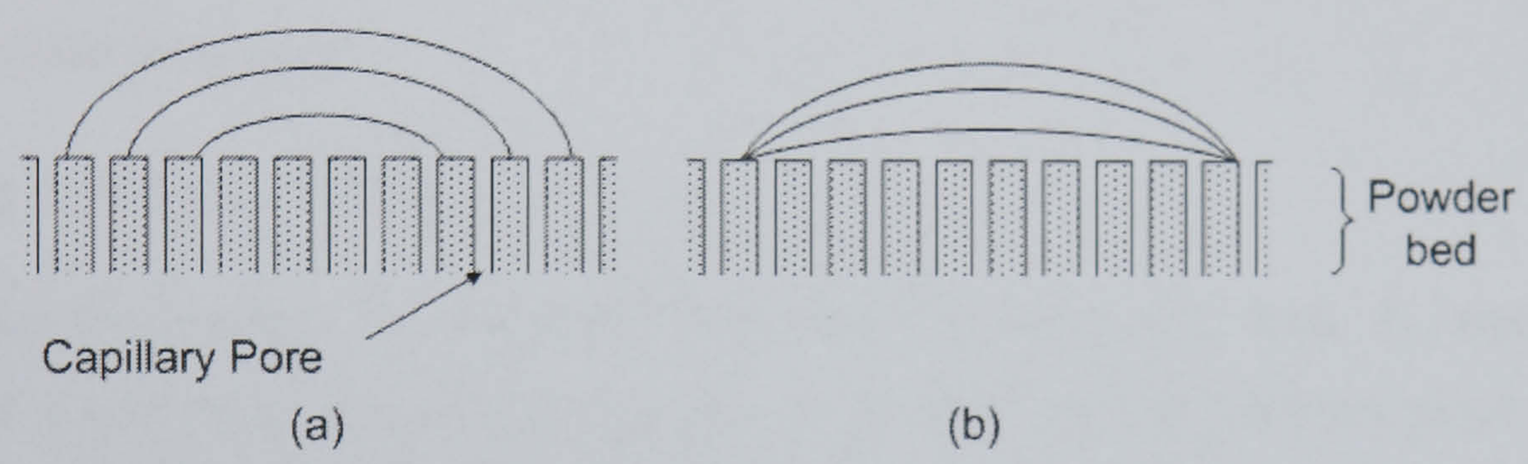

Figure 3.9: Schematic representation of (a) decreasing drawing area and (b) constant drawing area. Adapted from Marmur (1988).

The granule nucleus is formed when the binder droplet is adsorbed onto the powder surface and penetrates into the porous bed mass, capturing the constituent particles (primary particles) in the immediate vicinity of the droplet as it penetrates into the powder (see Figure 3.10). Thus, the number of constituent particles (N_p) that is incorporated into a granule nucleus may be determined based on the volume of droplet that has drained into the bed mass, which in turn depends on the bed-turnover relative to the drop penetration time. The composition of the granule nucleus *i.e.*, volume of solid, liquid and gas, may be calculated by performing a component volume balance on each of the respective phases as shown in Equations (3.44)-(3.46).

Volume of solid in nucleus:

$$V_{n,s} = V_n \left(1 - \varepsilon_{eff}\right) = N_p V_{p,s} \tag{3.44}$$

Volume of liquid in nucleus:

$$V_n l_{sat} \varepsilon_{eff} = V_0 - V(t) + N_p V_{p,l} \tag{3.45}$$

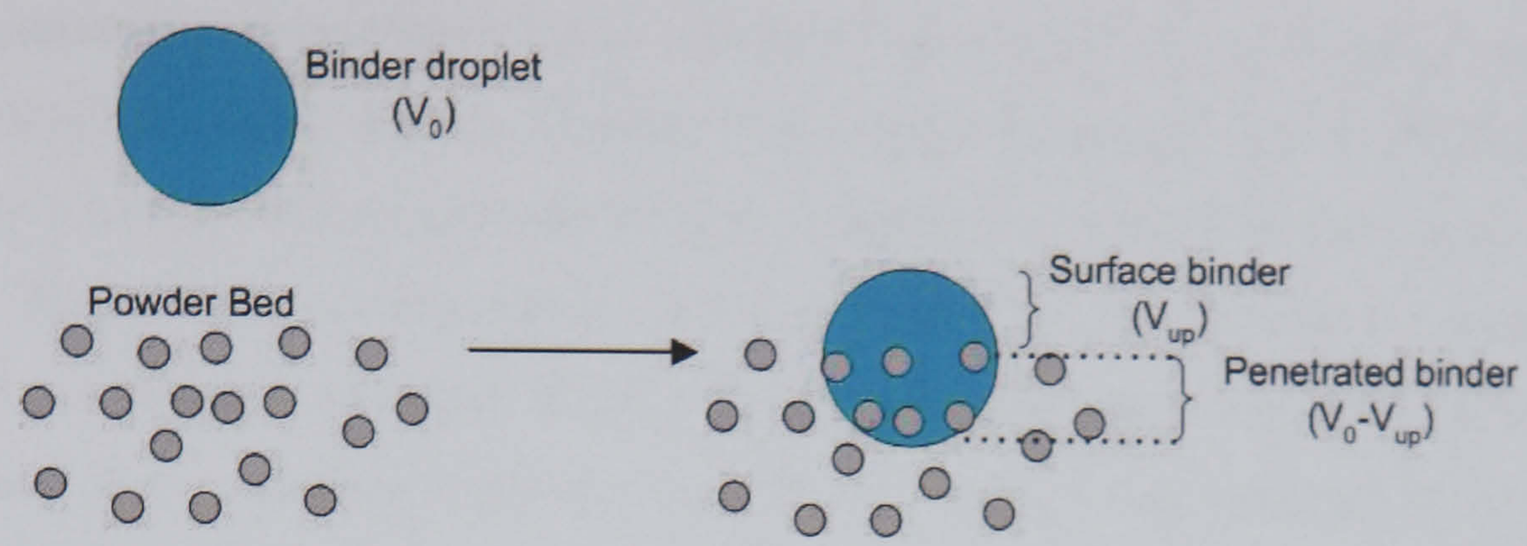

Figure 3.10: Schematic representation of the nucleation mechanism. The unpenetrated volume of droplet that remains on the powder surface is denoted by $V_{up} = V(t)$.

Volume of gas in nucleus:

$$V_{n,g} = V_n \varepsilon_{eff} \left(1 - l_{sat}\right) \tag{3.46}$$

In the above equations, V_0 represents the volume of the binder drop, V_n represents the volume of a granule nucleus, $V(t)$ is the volume of drop that has not penetrated the bed at any given time and therefore represents the volume of drop that will not contribute towards the formation of a granule nucleus at that time, $V_{n,s}$, $V_{n,l}$ and $V_{n,g}$ represents the volume of solid, liquid and gas component of the nucleus respectively, l_{sat} is the liquid saturation of the nucleus, ε_{eff} is the effective porosity of the nucleus, $V_{p,s}$ and $V_{p,l}$ are the average volumes of solid and liquid in the primary particles, and are defined in Equations (3.47)-(3.49) respectively.

$$x\left(s', l', g'\right) = \frac{F\left(s', l', g', t\right)\ ds'\ dl'\ dg'}{\int_{s'=s_{min}^{nuc}}^{s_{max}^{nuc}} \int_{l'=l_{min}^{nuc}}^{l_{max}^{nuc}} \int_{g'=g_{min}^{nuc}}^{g_{max}^{nuc}} F\left(s', l', g', t\right)\ ds'\ dl'\ dg'} \tag{3.47}$$

Average solid volume in primary particles:

$$V_{p,s} = \int_{s'=s_{min}^{nuc}}^{s_{max}^{nuc}} \int_{l'=l_{min}^{nuc}}^{l_{max}^{nuc}} \int_{g'=g_{min}^{nuc}}^{g_{max}^{nuc}} V_s\left(s'\right) x\left(s', l', g'\right)\ ds'\ dl'\ dg' \tag{3.48}$$

Average liquid volume in primary particles:

$$V_{l,s} = \int_{s'=s_{min}^{nuc}}^{s_{max}^{nuc}} \int_{l'=l_{min}^{nuc}}^{l_{max}^{nuc}} \int_{g'=g_{min}^{nuc}}^{g_{max}^{nuc}} V_l\left(l'\right) x\left(s', l', g'\right) ds'\ dl'\ dg' \tag{3.49}$$

Where $F\left(s', l', g', t\right)$ is the particle density of the primary particles and the granules, s_{min}^{nuc} and s_{max}^{nuc} are the minimum and maximum solid volume of the primary particles, l_{min}^{nuc} and l_{max}^{nuc}

are the minimum and maximum liquid volume of the primary particles, g_{min}^{nuc} and g_{max}^{nuc} are the minimum and maximum gas volume of the primary particles, $x(s', l', g')$ is the fraction of primary particles with characteristics of s', l' and g' that would be incorporated into the nucleus. The number of constituent particles that are incorporated into a single granule nucleus N_p is shown in Equation (3.50) and the corresponding volume of a nucleus is given by Equation (3.51), which is expressed explicitly in terms of the solid and liquid volumes of the constituent particles $V_{p,s}$ and $V_{p,l}$, the initial droplet volume (V_0), the volume of liquid remaining on the powder surface ($V_0 - V(t)$), the liquid saturation of the nucleus (l_{sat}) and the effective porosity (ε_{eff}).

$$N_p = \frac{V_n (1 - \varepsilon_{eff})}{V_{p,s}} \tag{3.50}$$

$$V_n = \frac{V_0 - V(t)}{l_{sat}\varepsilon_{eff} - (1 - \varepsilon_{eff}) \frac{V_{p,l}}{V_{p,s}}} \tag{3.51}$$

The rate process for both the formation of newly born nuclei particles and the corresponding rate of depletion of the primary particles given in Equations (3.52) and (3.53) respectively, are then substituted into Equation (3.5) under the assumption of a zeroth order dependency on the concentration of primary particles. The terms s_{nuc}, l_{nuc} and g_{nuc} represent the bins corresponding to the volumes of solid, liquid and gas in the nucleus (see Equations (3.44)-(3.46) respectively) along the respective discretised domain of the three internal coordinates.

$$\Re_{nuc}(s_{nuc}, l_{nuc}, g_{nuc}) = k_{nuc} \tag{3.52}$$

$$\Re_{nuc}(s, l, g) = -k_{nuc}(s, l, g)\ N_p\ x(s, l, g) \tag{3.53}$$

$$\text{for,} \quad s_{min}^{nuc} \leq s \leq s_{max}^{nuc}$$

$$l_{min}^{nuc} \leq l \leq l_{max}^{nuc}$$

$$g_{min}^{nuc} \leq g \leq g_{max}^{nuc}$$

Remember that a granule nucleus is comprised of N_p primary particles and that $x(s, l, g)$ is the fraction of primary particles with characteristics of s, l and g that contribute in making up the nucleus. In addition, the possible dependence of the nucleation rate on the binder addition rate has also been explicitly accounted for in k_{nuc} in Equation (3.35). Note that if the bed turnover rate is faster than the binder penetration rate, then $V(t)$ will be non-zero at the bed turnover. In this case, the unpenetrated liquid is assumed to be uniformly distributed into all the particles by the mixing action.

Under conditions where the nucleation rates as defined in Equations (3.52) and (3.53) is faster than the total binder spray rate, binder spray rate is rate limiting, and the rate of nucleation is given by $\Re_{nuc} = \frac{Q}{N_A V_0}$, where N_A is the Avogadro number. This condition corresponds to the perfect droplet controlled regime proposed by Hapgood et al. (2002), wherein each droplet leads to a separate nucleus. Under conditions where the wetting kinetics is rate determining, as mentioned previously under the simplifying assumptions, the unwetted and unpenetrated binder on the surface is assumed to be uniformly distributed to all the particles. This excess surface binder is given by $(Q - \Re_{nuc} N_A V_{penetrate})$. Here $V_{penetrate}$ is the actual volume of droplets that penetrate into the bed before bed turnover, which could be calculated from Equation (3.42).

3.5.4 Numerical method for multi-dimensional population balance models

A FORTRAN code was written in order to simulate the three-dimensional population balance model accounting for granule consolidation, aggregation and nucleation. The simulations were performed on a 2GHz Intel Dual Core processor desktop computer with 2GB RAM. The discretised system domain comprised of 35, 25 and 12 bins along the solid, liquid and gas internal coordinate axes, respectively. The bin width along the solid volume is $\Delta R_s = 5 \times 10^{-6}$ m, the bin width along the liquid volume ranges from $\Delta R_l = 1 \times 10^{-7}$ m to $\Delta R_l = 8 \times 10^{-6}$ m and the bin width along the gas volume is $\Delta R_g = 1.5 \times 10^{-6}$ m.

In solving the three-dimensional population balance model, a hierarchical solution strategy is employed that explicitly casts the population balance in terms of the underlying sub-rate processes *i.e.*, nucleation, aggregation and consolidation (Immanuel and Doyle III, 2005). The technique involves the discretisation of the system domain with respect to the three aforementioned internal coordinate axes followed by the recasting of the population balance into finite volumes. In this finite volume scheme, the population balance equation in Equation (3.5) may be re-written into its discrete form, as shown in Equation (3.54) for the case with

aggregation and consolidation as the granulation phenomena.

$$\frac{dF'_{i,j,k}}{dt} + \left(\frac{F'_{i,j,k}}{\triangle g_k}\right)\frac{dg}{dt}\bigg|_{g_k} - \left(\frac{F'_{i,j,k+1}}{\triangle g_{k+1}}\right)\frac{dg}{dt}\bigg|_{g_{k+1}} =$$
$$\frac{1}{2}\int_{s'=s_{nuc}}^{s-s_{nuc}}\int_{l'=0}^{l}\int_{g'=0}^{g}\beta(s',s-s',l',l-l',g',g-g')F'(s',l',g',t)$$
$$\times F'(s-s',l-l',g-g',t)ds'dl'dg'$$
$$-F'(s,l,g,t)\int_{s'=s_{nuc}}^{s_{max}}\int_{l'=0}^{l_{max}}\int_{g'=0}^{g_{max}}\beta(s',s,l',l,g',g)$$
$$\times F'(s',l',g',t)ds'dl'dg' \tag{3.54}$$

Here $F'(i,j,k) = \int_{s=s_i}^{s_{i+1}}\int_{l=l_j}^{l_{j+1}}\int_{g=g_k}^{g_{k+1}} F(s,l,g)\,ds\,dl\,dg$, s_i is the value of the solid volume at the upper end of the ith bin along the solid volume axis, l_j is the value of the liquid volume at the upper end of the jth bin along the liquid volume axis, g_k is the value of the gas volume at the upper end of the kth bin along the gas volume axis. In addition, β is the aggregation kernel and $\triangle g_k$ is the size of the kth gas bin with respect to the gas volume axis.

In the solution of the finite volume population balances, a decomposition solution framework known as the hierarchical two-tier algorithm is employed (see Figure 3.11), wherein the various rate processes of nucleation, aggregation, consolidation, *etc.*, are accounted individually at each time step while marching forward in time. Firstly, the population balance is written in terms of a number distribution by volume since the volume of the granules remain conserved during size changing mechanisms (*e.g.* aggregation) (Cryer, 1999; Verkoeijen et al., 2002). Based on the finite volume discretisation of the particle population (the particles residing in each finite volume bin may be regarded as sub-populations of the whole particle population), the particle density within each finite volume bin is assumed to be uniform, allowing for the preprocessing and a priori calculations of time independent portions of the kernels and the computation-intensive integrals in Equation (3.54) (Immanuel and Doyle III, 2003, 2005). With these simplifying model assumptions, the population balance may be reduced to a set of coupled non-linear ordinary differential equations. At each time step, the contribution of each sub-rate process, *i.e.*, nucleation, aggregation and growth are evaluated over the time interval. This step corresponds to the first tier of the two-tier algorithm. In the second tier, the cumulative effect on the PSD is calculated.

There are distinct advantages in using the hierarchical two-tier solution strategy for numerically solving the population balance, with known stiffness characteristics attributed to largely differing time constants signifying the sub-rate processes with some processes occur-

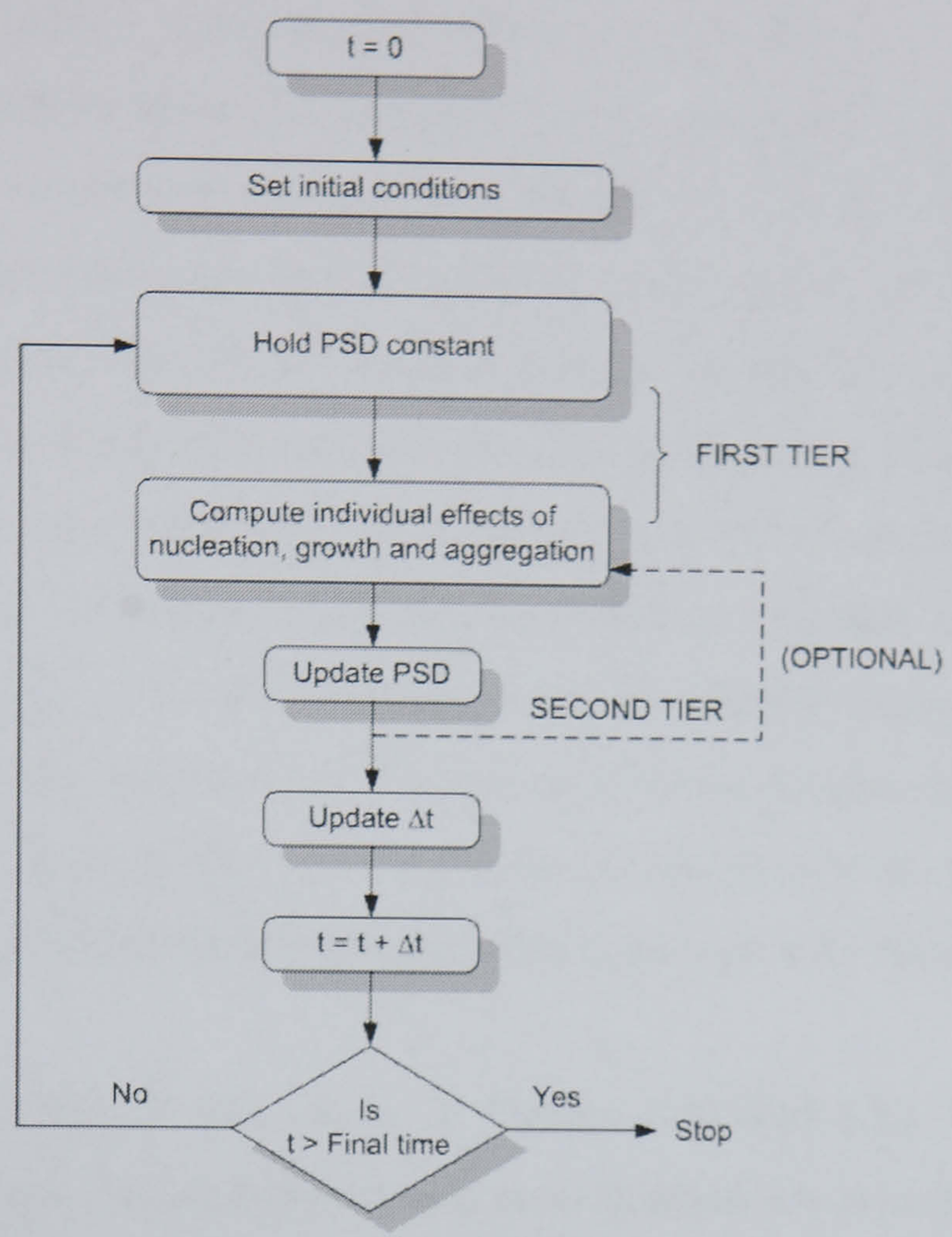

Figure 3.11: Schematic representation of the hierarchical two-tier algorithm (Immanuel and Doyle III, 2003).

ring at significantly smaller time scales relative to other rate processes. The decomposition strategy enables the tailoring of the discretisations to suit the individual accuracy requirements of the various rate processes. For instance, one could employ coarse discretisation for aggregation and fine discretisation for nucleation/consolidation (Sun and Immanuel, 2005; Pinto et al., 2007). In addition, as mentioned before, individual rates and their contributions are computed separately. This, coupled with the additional flexibility in the choice of fine or coarse grid discretisation enables this solution technique to accommodate for the stiffness characteristics of the process.

3.6 Model simulation results and discussions

3.6.1 Seeded granulation: aggregation and consolidation

A model case comprising of only granule consolidation and aggregation is considered here. The aggregation phenomenon is modelled employing the mechanistic aggregation kernel

shown in Equation (3.27). Granule consolidation is modelled according to an empirical exponential decay relation shown in Equation (3.10). Although the population balance is formulated in terms of the three internal coordinates *i.e.*, solid volume, liquid volume and the volume of gas, the results are instead presented in terms of the particle radius and the fractional binder content. This is obtained through the coordinate transformation described in Section 3.2.1 and in Figure 3.3 and also involves summing up along the third dimension corresponding to the porosity dimension, resulting in a more compact two-dimensional visual representation of the results. The two quantities are defined as follows: the particle radius is defined as $\left[\frac{3}{4\pi}(s+l+g)\right]^{\frac{1}{3}}$ and the fractional binder content is defined as $\frac{l}{s-l-g}$. As mentioned previously, representing the results in terms of these two internal coordinate properties, *viz.* the particle radius and the fractional binder content will be more physically meaningful in relating the observed behaviour of the granules with the underlying granulation phenomena.

Typical simulation results are shown in Figures 3.12 and 3.13. The parameters used in the model simulations for aggregation and consolidation are reported in Table 3.1 . The simulation is of a seeded batch granulation process. The initial seed is unimodal and narrowly distributed, with an average size of 38 μm, and a small fractional binder content of 0.02. In view of the low binder content, there is little growth at the initial times as seen in Figure 3.12. Starting from 1 min, binder liquid is being sprayed into the granulator vessel at the rate of $1 \times 10^{-6}\,\mathrm{m}^3/\mathrm{s}$ for a duration of 4 min. This binder is assumed to be uniformly distributed into the granules. Figure 3.12 records a rapid growth during this period. A reduction in the aggregation rate is observed after 5 min, when the binder addition is discontinued. There is a slight increase in the aggregation rates at about 10 min, caused by the increase in the fractional binder content due to consolidation of the granules. The final average particle size is approximately 85 μm (particle radius).

Table 3.1: List of parameters used for simulations involving aggregation and consolidation.

Parameter	
Aggregation model parameters	
c_1	$5 \times 10^6\,(-)$
Consolidation model parameter	
c	$5 \times 10^{-5}\,(-)$

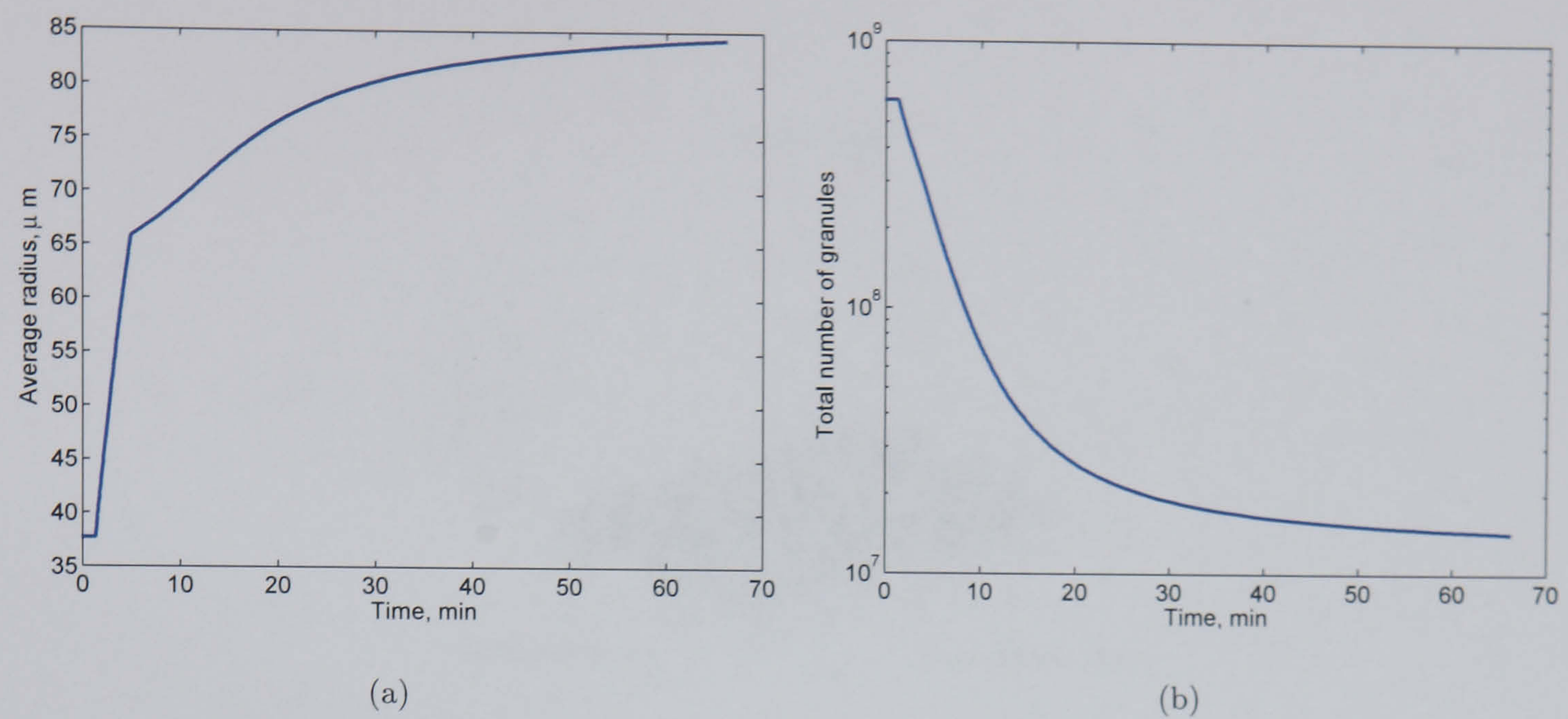

(a) (b)

Figure 3.12: Time profiles of the average particle size (a); and the total number of particles (b), due to combined aggregation and consolidation.

Figure 3.13 shows the evolution of the distribution, depicted here in two-dimensions, at different times during the batch. The initial period records an increase in both the particle size and the binder content, with an associated spreading of the distribution. Subsequently, there is a translation of part of the particles along the particle size axis, resulting in a bimodal distribution. In these plots, no interpolation is employed between the discrete points on the particle densities. Employing an interpolation between the points would lead to smoother surface plots. These simulation results, particular those of the distributed variables, prove valuable in the validation of the mechanisms and the model. Note that the aggregation mechanism used in this study for the derivation of the kernels, as depicted in Figure 3.4, is already validated by itself (Liu et al., 2000). The original model results of the three-dimensional distribution along the solid volume, liquid volume and the gas volume axes is shown in Figure 3.14 at two time instances. This shows the advantages of the two-dimensional representation of Figure 3.13, namely a more compact representation of the data in more meaningful variables (particle radius and binder content).

3.6.2 Combined nucleation, aggregation and consolidation

The model results for combined nucleation, aggregation and consolidation are presented with an initial mono-disperse seed of primary particles (fines) with an average diameter of 35.7 μm represented in Figure 3.15. The binder is being sprayed at a very rapid rate of

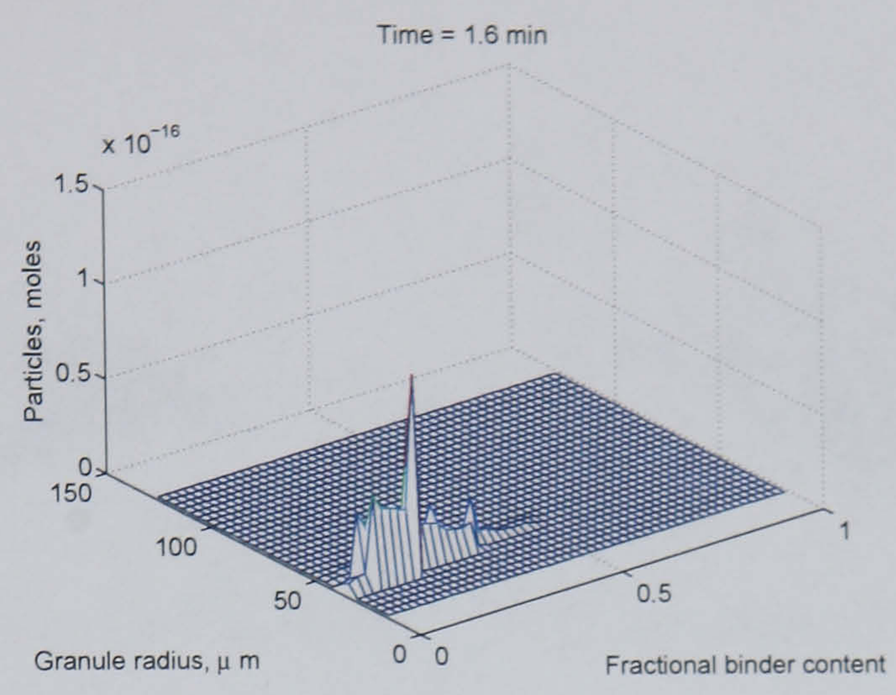

(a)

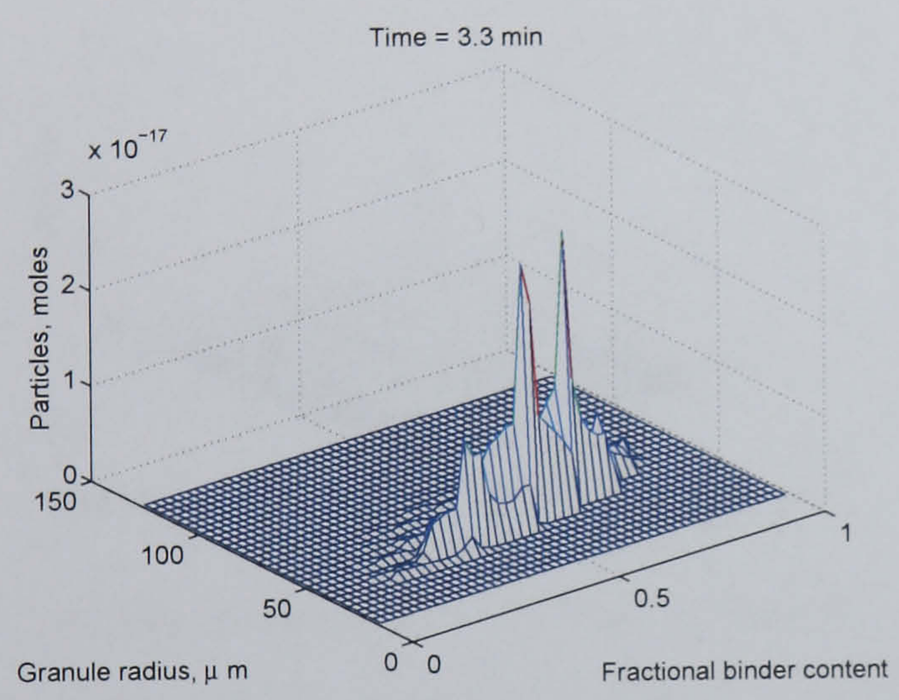

(b)

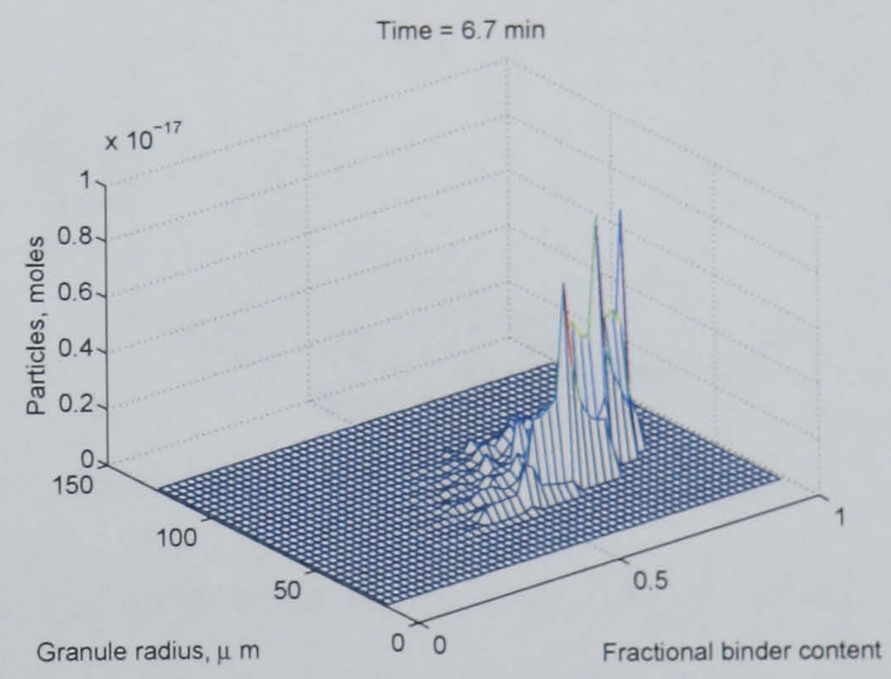

(c)

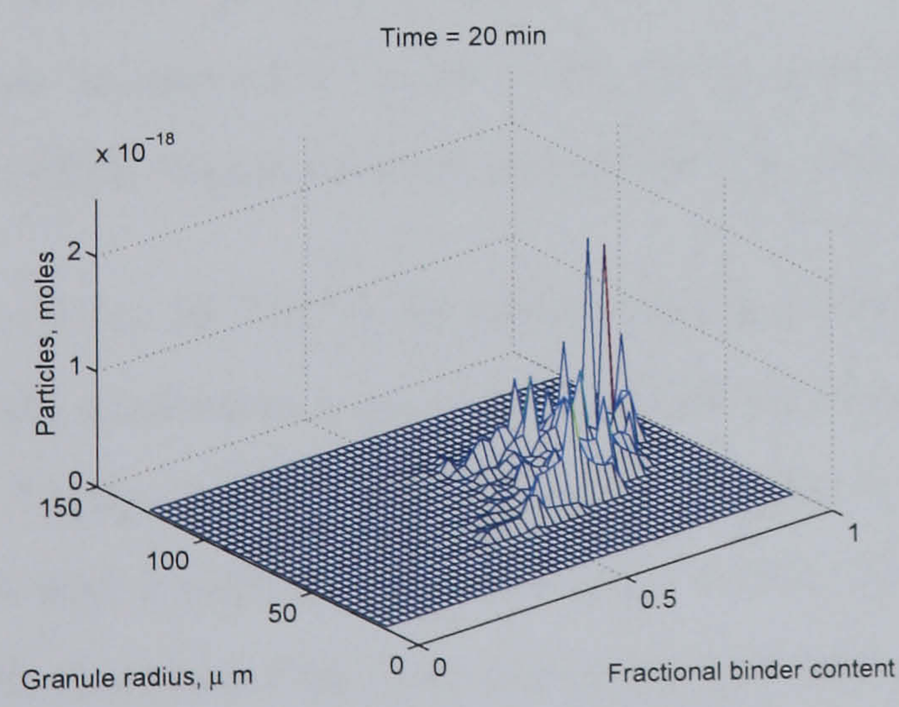

(d)

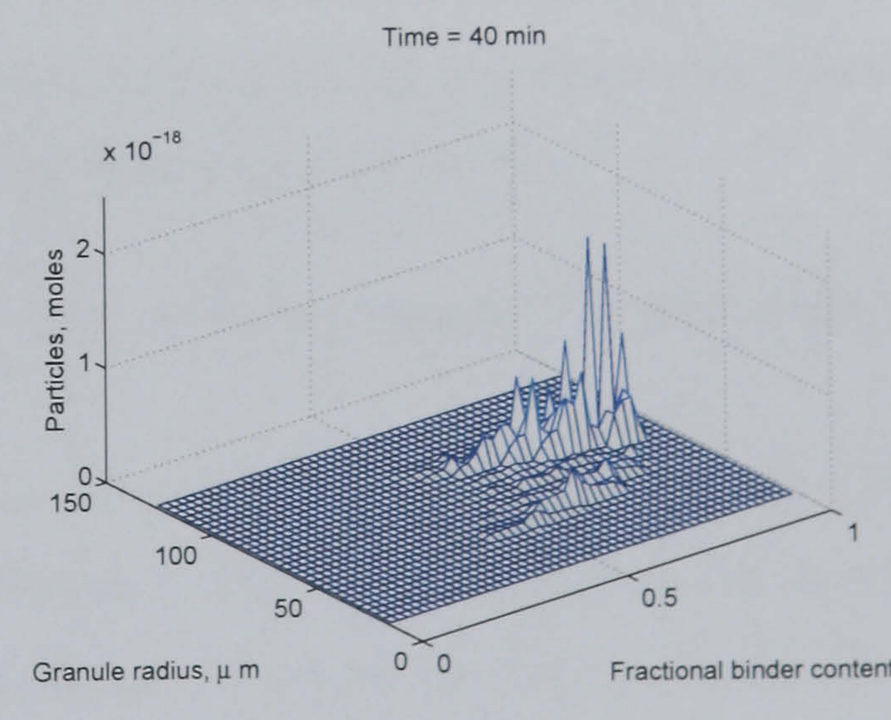

(e)

Figure 3.13: Time evolution of the granule PSD due to combined aggregation and consolidation.

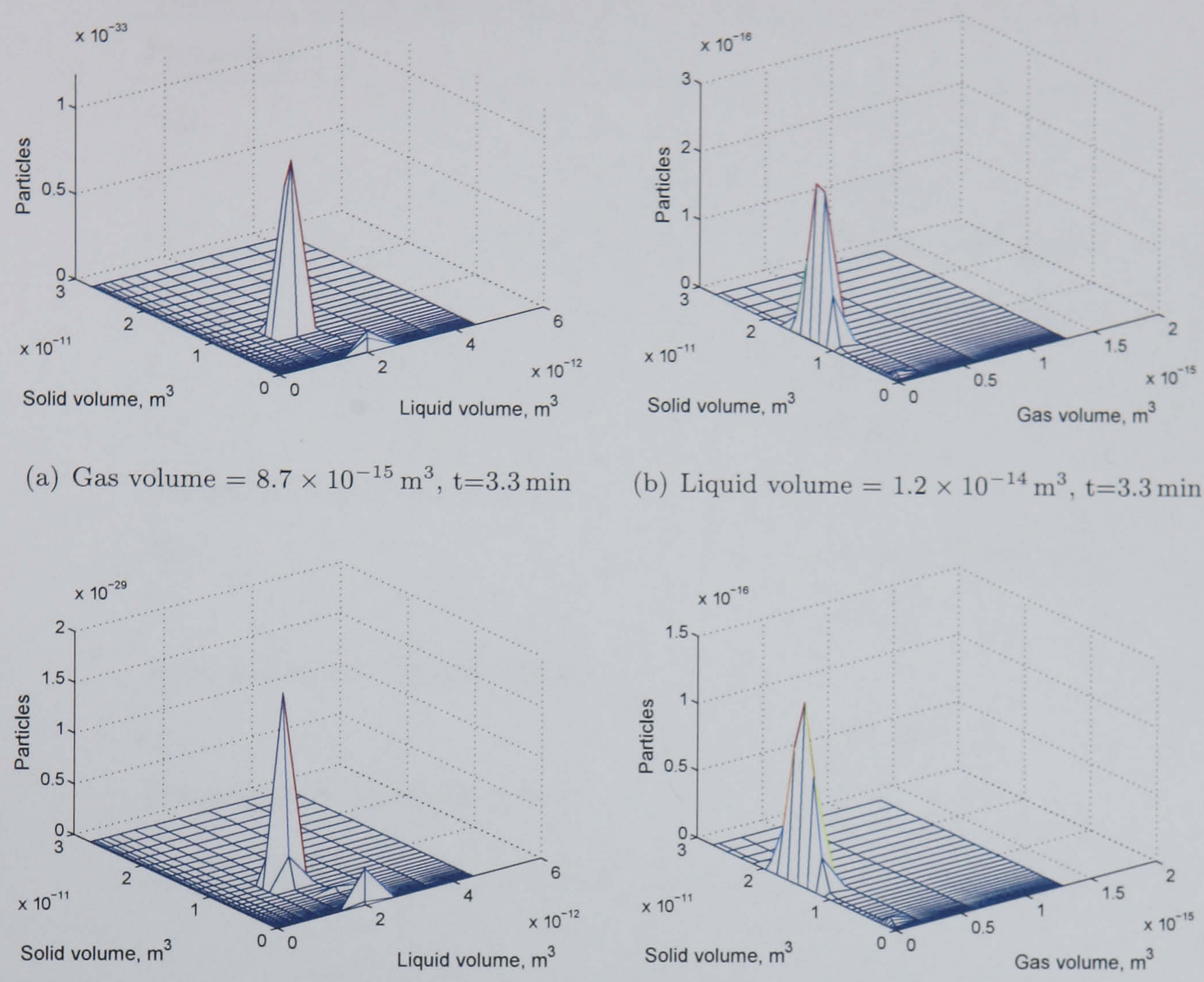

(a) Gas volume = $8.7 \times 10^{-15}\,\mathrm{m}^3$, t=3.3 min

(b) Liquid volume = $1.2 \times 10^{-14}\,\mathrm{m}^3$, t=3.3 min

(c) Gas volume = $8.7 \times 10^{-15}\,\mathrm{m}^3$, t=6.7 min

(d) Liquid volume = $1.2 \times 10^{-14}\,\mathrm{m}^3$, t=6.7 min

Figure 3.14: Three-dimensional plots at two time instances of 3.3 min and 6.7 min; (a) and (c) show the particle distributions with respect to the solid volume and the liquid volume for a gas volume of $8.7 \times 10^{-15}\,\mathrm{m}^3$; (b) and (d) show the particle distributions with respect to the solid volume and the gas volume for a liquid volume of $1.2 \times 10^{-14}\,\mathrm{m}^3$.

$Q = 2.5 \times 10^{-3}\,\mathrm{m}^3/\mathrm{s}$ for 0.6 s, with a binder droplet diameter of 93 μm. The parameters used in the nucleation model are reported in Table 3.2.

Figure 3.16(b) shows that the primary particles are depleted shortly after 0.02 s under this high binder spray rate. Figure 3.16(a) shows the change in the average granule diameter with time (starting from the initial primary particles). The first exponential increase in the granule diameter seen in Figure 3.16(a) up to about 0.02 s is attributed primarily to nucleation with some aggregation events, and the subsequent increase is attributed to aggregation alone. This is also evident from the two-dimensional distribution plots in Figure 3.17. Figure 3.17(a) indicates incipient nucleation at $t = 8 \times 10^{-3}$ s. Nucleation is well underway at $t = 2 \times 10^{-2}$ s

Table 3.2: List of parameters used for the nucleation simulations.

Parameter	
ε_{eff}	0.2 (-)
ϕ	1.0 (-)
γ^{LV}	7.28×10^{-2} N/m
γ^{SV}	4.0×10^{-2} N/m
θ	63°
l_{sat}	0.99 (-)
Nucleation model parameters	
A_0	4×10^{-12} mol/m^3
K	1.0 (-)
Aggregation model parameters	
c_1	5×10^6 (-)
Consolidation model parameter	
c	5×10^{-5} (-)

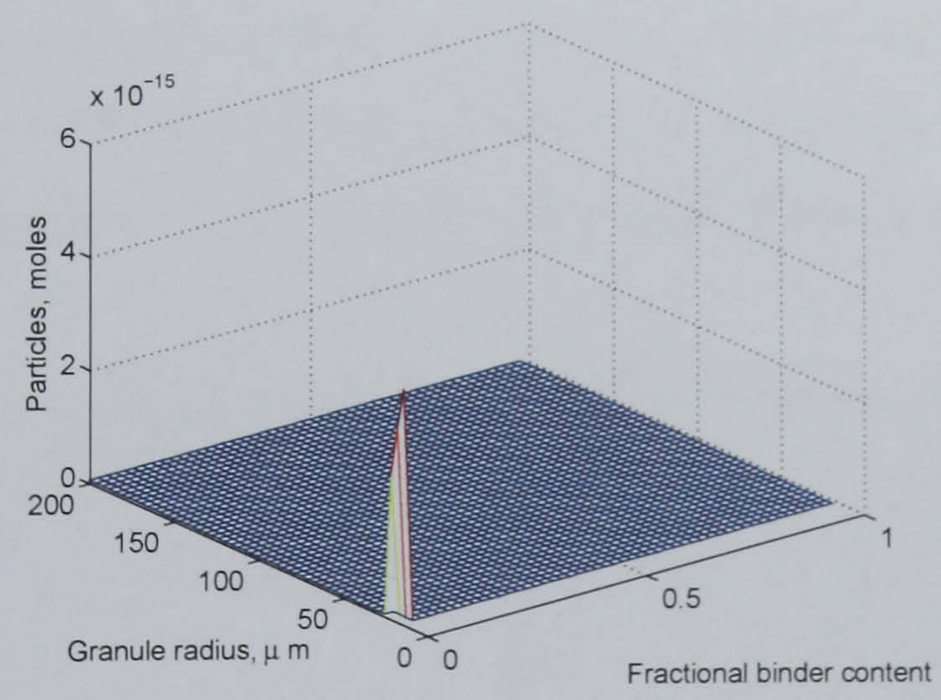

(a)

Figure 3.15: The initial seed of primary particles.

as seen in Figure 3.17(b), and is complete by $t = 5 \times 10^{-2}$ s as seen in Figure 3.17(c). Figures 3.17(d)–3.17(f) mainly indicate growth by aggregation.

3.6.3 Parametric sensitivities and perturbation studies

The results in Figure 3.18 presents model simulations depicting the effect of the primary particle distribution on the evolution of the granule size distribution. Three cases are presented. The first case considers primary particles that are monodisperse with a diameter of 35.7 μm (base case presented in Section 3.6.2), the second where the primary particles contain an equal proportion by number of two monodisperse populations of diameters 35.7 μm and 45.6 μm, and the third where the primary particles contain an equal proportion by number of four monodisperse populations of diameters 35.7 μm, 45.6 μm, 55.5 μm and 65.4 μm.

It is seen in Figure 3.18(b) that as the average size of the primary particles increases, it takes longer for the nucleation phase to end thereby delaying the subsequent aggregation phase. The average diameter of the final granules is also marginally lower for the case with larger average primary particle size. One reason for this result could be that the number of primary particles captured into a nucleus, for a fixed droplet diameter of $V_0 = 4.2 \times 10^{-13}\,\mathrm{m}^3$ (diameter of about 93 μm), decreases from 71 in the case of the mono-sized primary particles, to 46 in the case of the two-sized primary particles, to 22 in the case of the four-sized primary particles. Thus, it takes longer for all the primary particles to be nucleated. This subsequently alters the aggregation rates as seen by a comparison of the evolution of the distributions presented in Figures 3.19 and 3.20 for the cases with mono-size and four-size primary particles. Figure 3.19 shows that at comparable times, the particles in the mono-

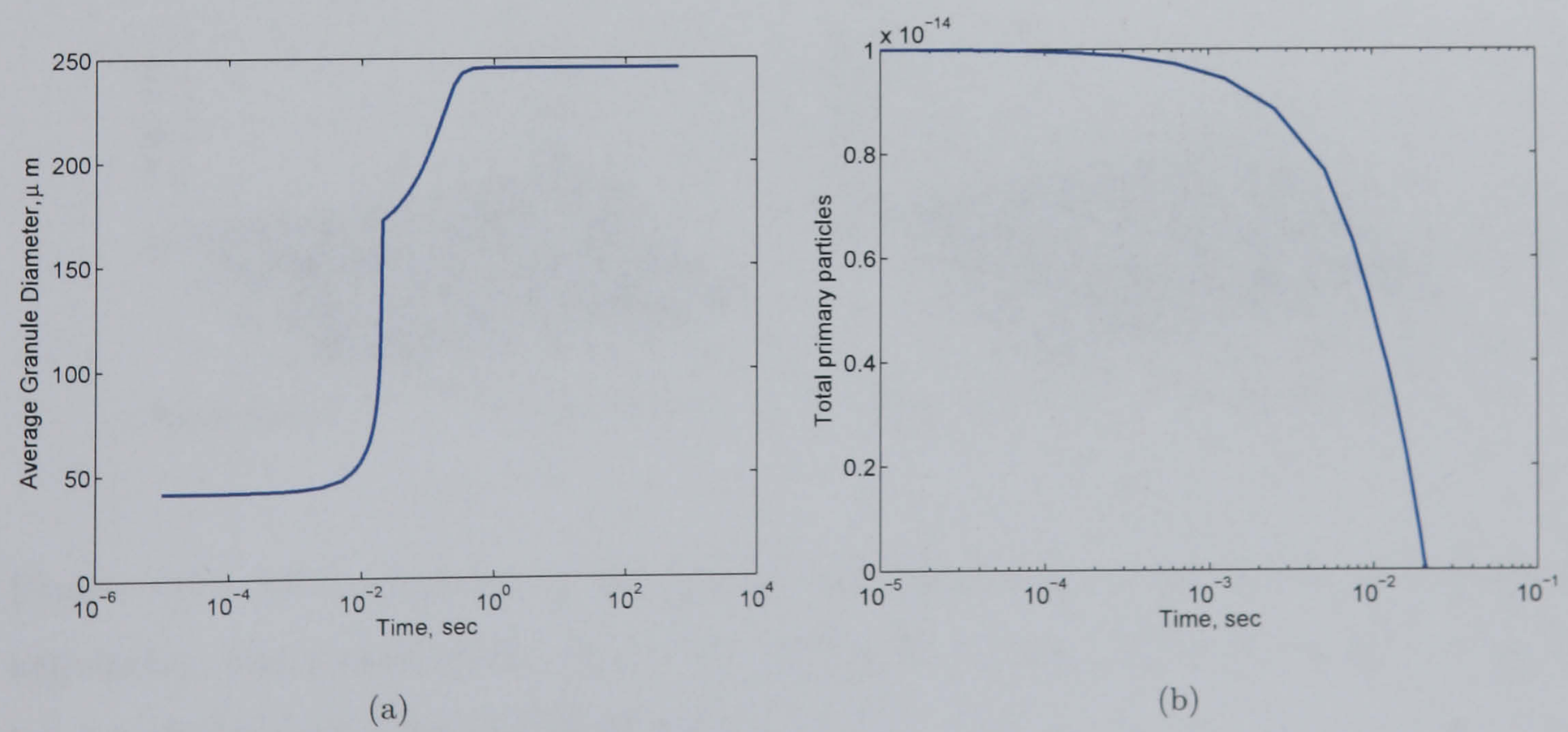

(a) (b)

Figure 3.16: Time profile of the average particle size (a); and the early time profile of primary particles (b) with progress of nucleation along with consolidation and aggregation.

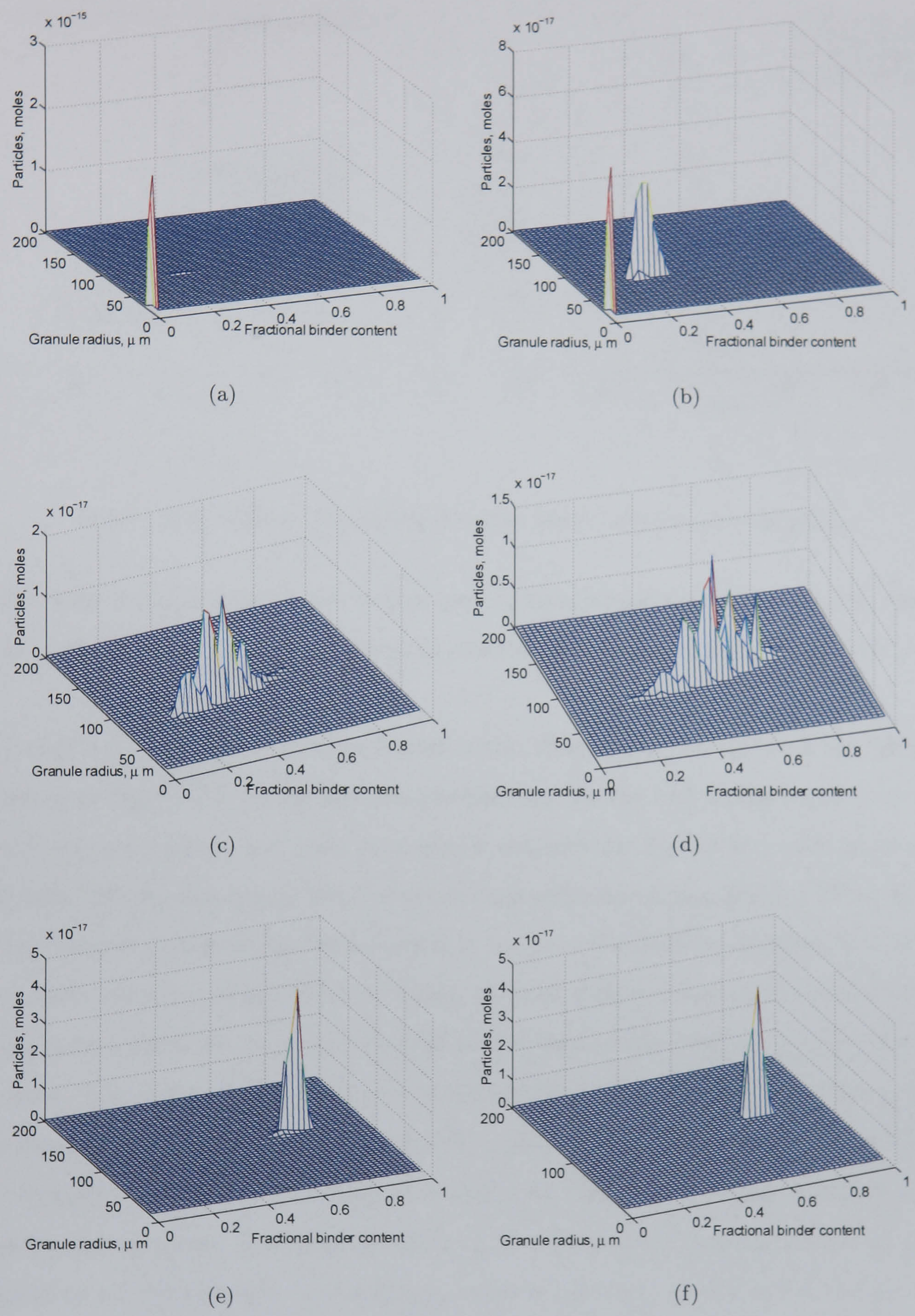

Figure 3.17: Time evolution of the granule size distribution under combined nucleation, aggregation and consolidation: (a) $t = 8 \times 10^{-3}$ s, (b) $t = 2 \times 10^{-2}$ s, (c) $t = 5 \times 10^{-2}$ s, (d) $t = 1 \times 10^{-1}$ s, (e) $t = 4 \times 10^{-1}$ s, (f) $t = 1$ s.

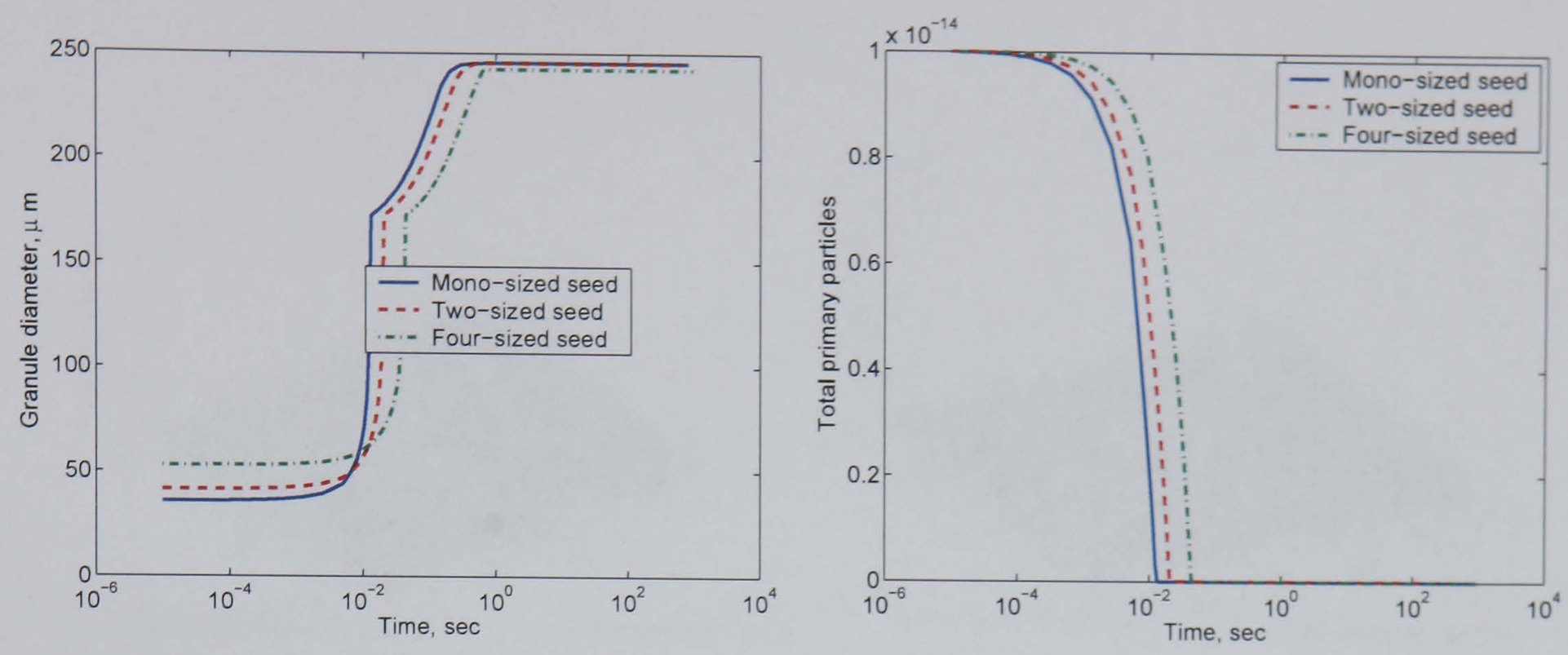

(b)

Figure 3.18: Effect of primary particle distribution on the process.

sized case have been nucleated and begun growth to a larger extent than in the case with four-sized primary particles. The end point distribution is also different, as seen in Figure 3.20.

In Figure 3.21, a comparison is presented of the effect of the bed turnover rate relative to the penetration rate of the binder into the powder bed. As the bed turnover rate decreases in relation to the penetration rate, then more time is available for the binder to wet and penetrate into the bed, thereby decreasing the amount of unpenetrated surface binder. Thus, the effect of bed turnover is conceptually characterised in terms of the fraction of unpenetrated binder droplet. Four cases are considered, one where the bed turnover rate is small relative to the penetration rate such that there is complete penetration of the droplets into the bed before bed turnover (no surface liquid; $V(t) = 0$ in Equation (3.42)). The second case corresponds to 10% unpenetrated liquid at the time of bed turnover (90% liquid penetrated into the bed before turnover). The other two cases correspond to 40% and 60% unpenetrated liquid at the time of bed turnover. The unpenetrated liquid in each case is assumed to be uniformly distributed to all the particles in the system (instead of being available for nucleation of a group of particles). A nonlinear relationship is seen in Figure 3.21(b), where there is an increase in the diameter of the nucleus between cases 1 and 2, and then a decrease for the other two cases. The relative behaviour between cases 1 and 2 is attributed to the effect of the distribution of the excess binder. The reduced amount of binder penetrated into the bed causes a decrease in the size of the nucleus. The unpenetrated binder, which is partitioned

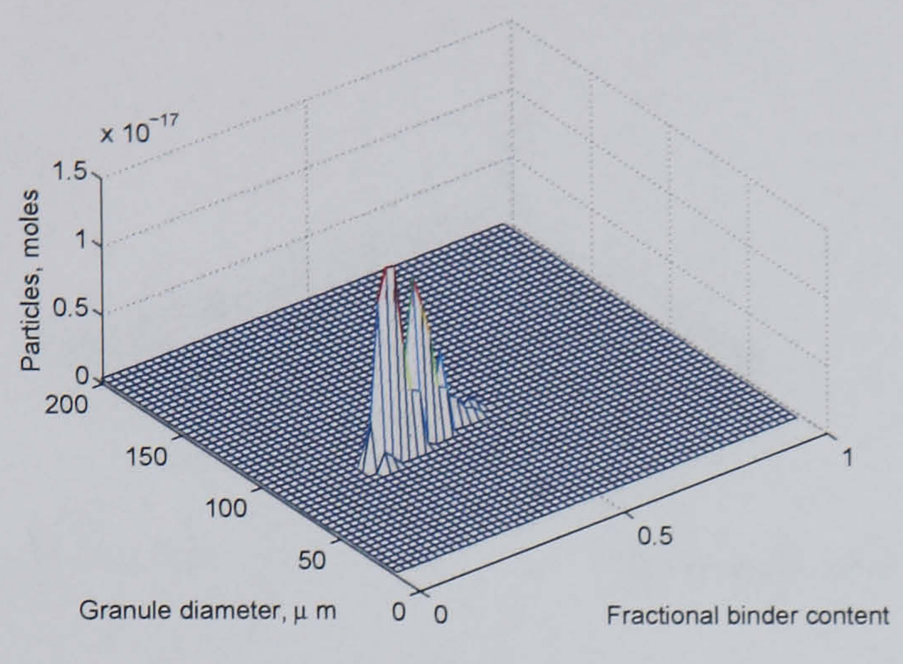

(a) mono-sized

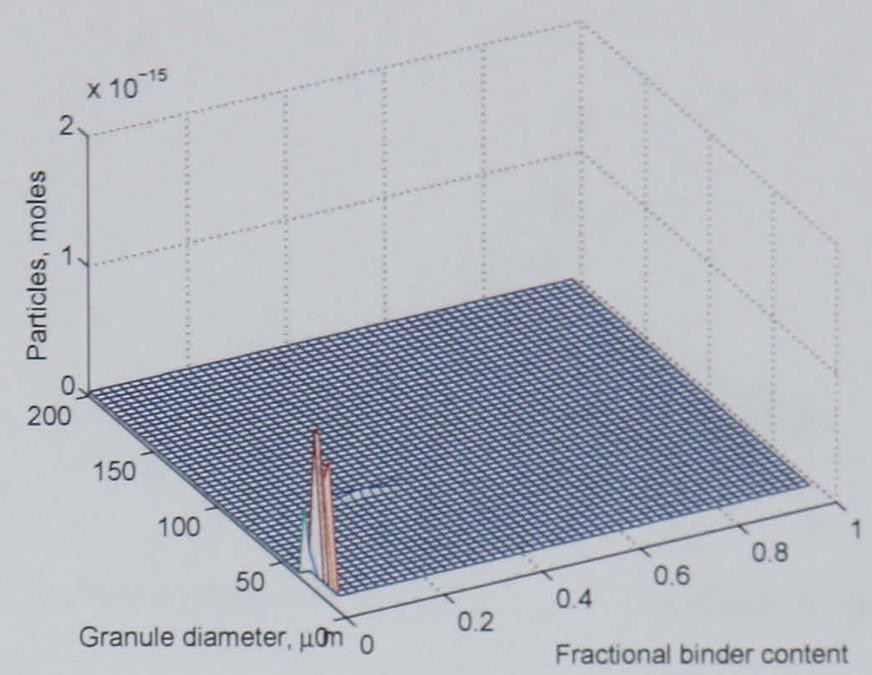

(b) four-sized

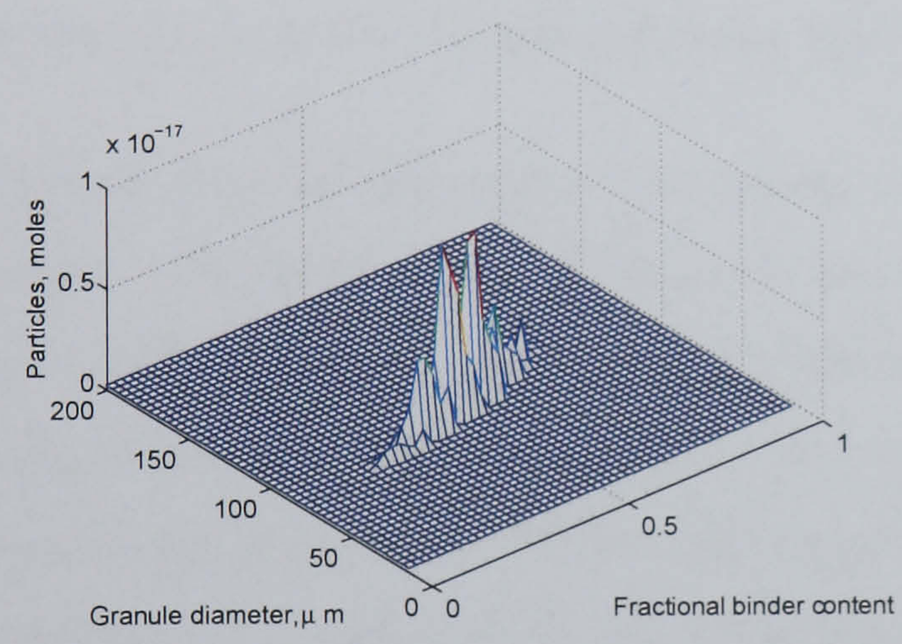

(c) mono-sized

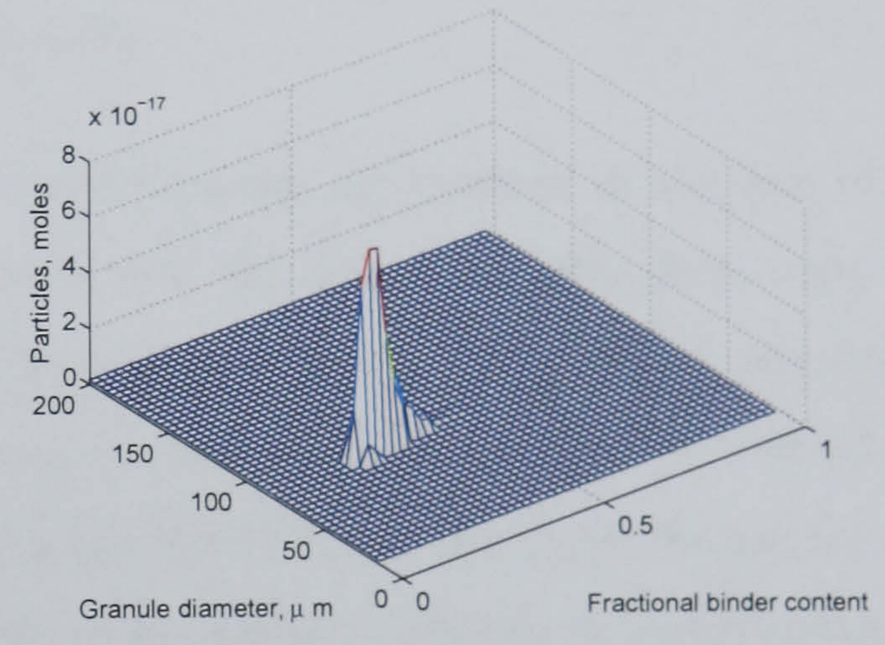

(d) four-sized

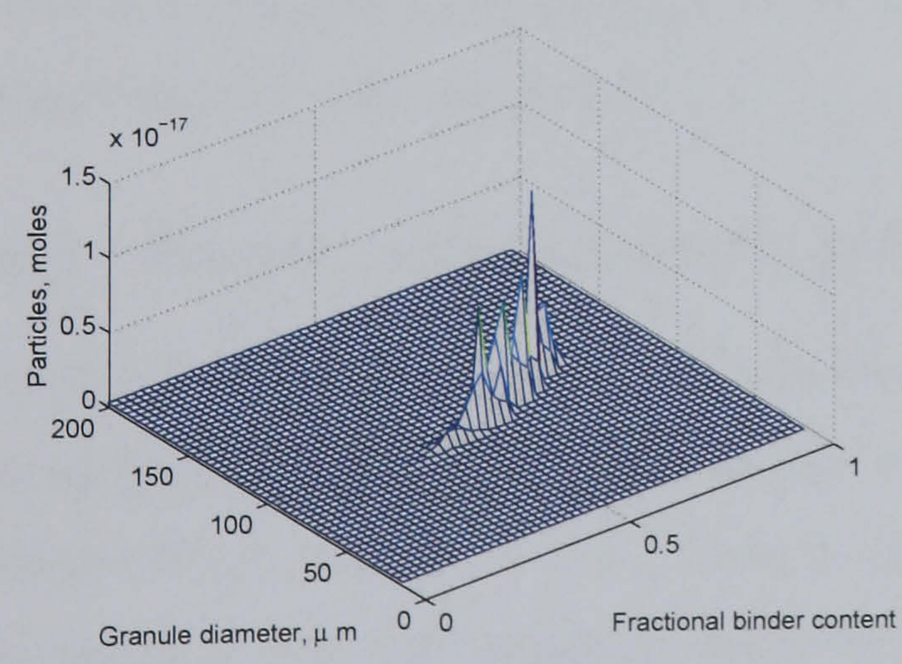

(e) mono-sized

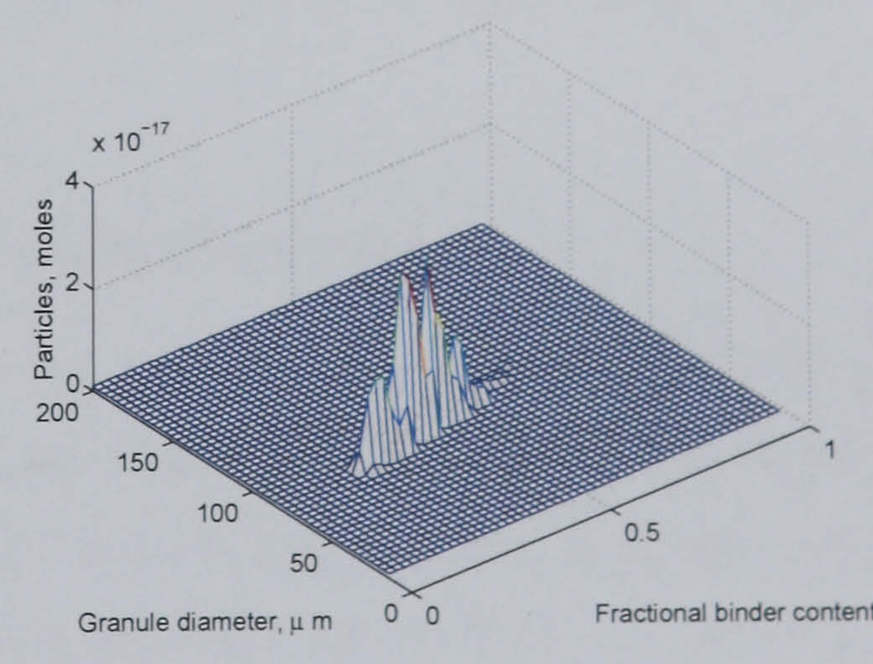

(f) four-sized

Figure 3.19: Comparison of the granule size distribution for different feed size primary particles at three different times: (a) and (b) $t = 2 \times 10^{-2}$ s; (c) and (d) $t = 5 \times 10^{-2}$ s; (e) and (f) $t = 1 \times 10^{-1}$ s.

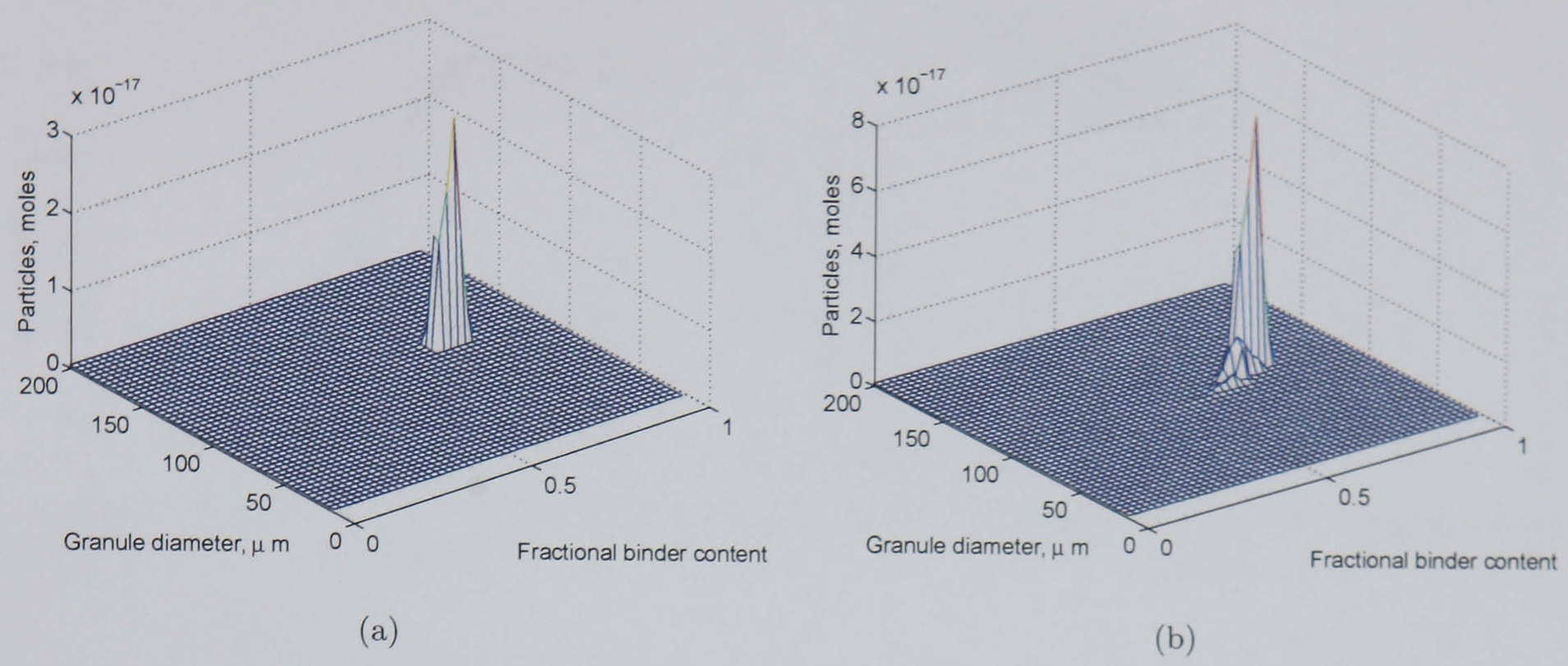

Figure 3.20: Comparison of the end-point granule size distribution for the mono-sized primary particles (a) and the four-sized primary particles (b).

uniformly into all the particles including the nuclei causes an increase in the size of the nucleus. The latter effect seems to be dominant over the former in going from case 1 to case 2 while the former effect becomes dominant in cases 3 and 4. These effects indicate the complexity of the integrated dynamics of the process. The end-point distributions obtained in cases 2-4 are presented in Figure 3.22, for comparison with the end point distribution for case 1 presented in Figure 3.17(f). The plots indicate more complex dynamic behaviour that will not be intuitively obvious, thereby showing the advantage of the comprehensive integrated model that accounts for the effects of the different rate processes, the process inputs and their interactions and inter-regulations.

3.6.4 Process sensitivities with spray flux simulations

In this section, model simulation results depicting the effect of the binder spray flux on the granulation is presented. In particular, the powder velocity is manipulated at three different values 0.33 m/s (case 1), 2.1 m/s (case 2) and 7.8 m/s (case 3), which correspond to spray flux values of 0.54, 0.09 and 0.02, respectively. The parameters used for the nucleation and spray flux simulations are reported in Table 3.3. Hapgood et al. (2003) indicated that for the granulation to be operating in the drop controlled regime the spray flux values should reside within the range of $0.01 - 0.1$ whereas, spray flux values spanning in the range of $0.1 - 1$ and $1 - 10$ characterised the nucleation process to be in the intermediate regime and the

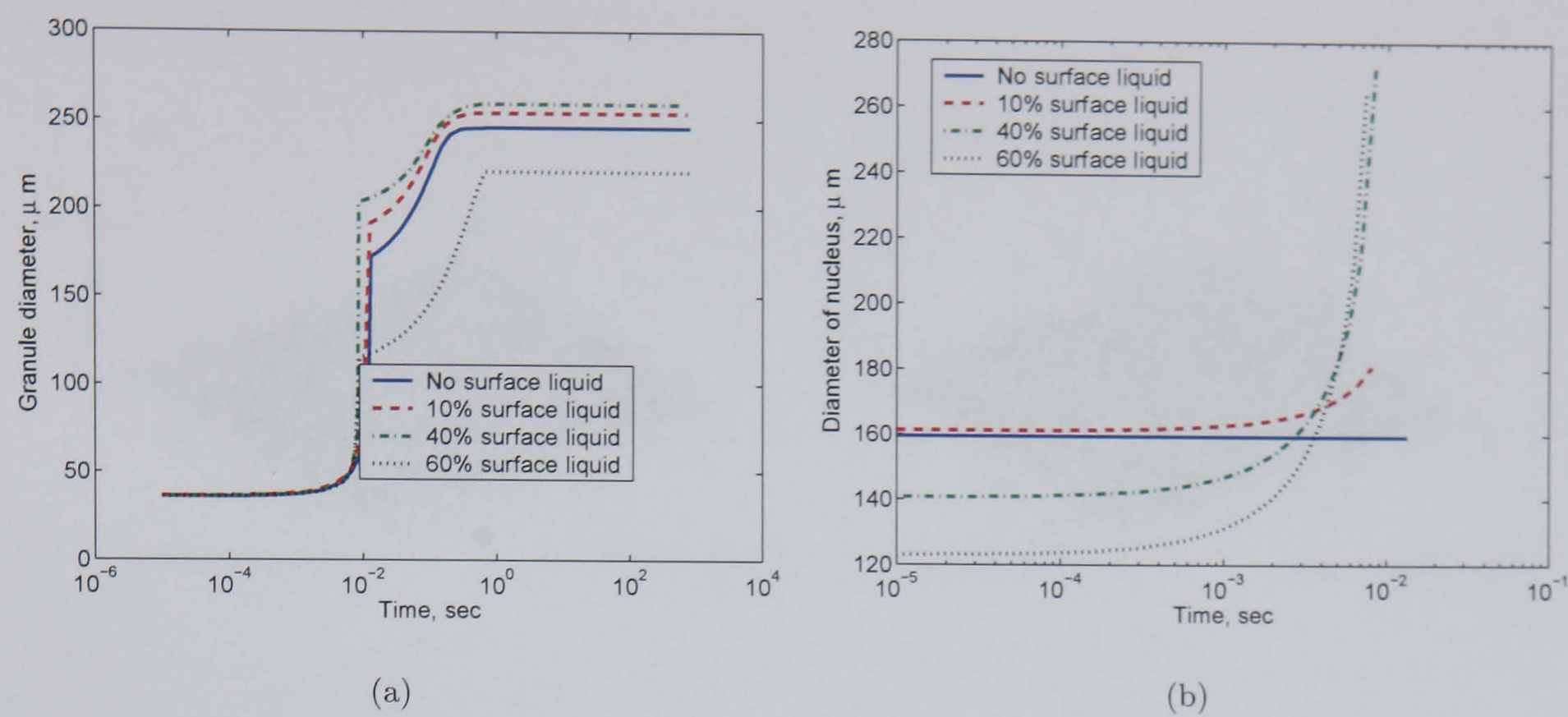

(a) (b)

Figure 3.21: Effect of bed turnover rate relative to binder penetration rate, conceptually analysed in terms of the fraction of unpenetrated binder droplet.

mechanical dispersion regime, respectively. The drop controlled regime is characterised by distinct individual droplets with minimal drop overlap. As a general rule, each droplet goes on to form a single nucleus. By comparison in the mechanical dispersion regime, there is a higher probability of droplet overlap, which will require mechanical dispersion to break up localised wetted clumps of solid mass and re-distribute through the rest of the powder bed mass.

The simulation results presented here in this section are under the combined influence of nucleation, aggregation and consolidation with a monodispersed seed of primary particles with an average particle diameter of 65.4 μm. The liquid binder flow rate is $2 \times 10^{-6}\,\mathrm{m}^3$ for a duration of 86 s with a binder droplet size of 84 μm. Figure 3.23(a) shows that at 34 s the binder spray has commenced, which causes rapid increase in the average particle size. This is observed for all three cases, and is predominantly attributed towards nucleation. After 120 s the binder flow rate has stopped, the main growth mechanisms, *i.e.*, aggregation and consolidation, begin to take a more dominant role in the evolution of the average granule size. The final average particle size for case 1 is approximately 233 μm for the first case and 238 μm for cases 2 and 3.

The observed changes to the average granule size can be related to the spray flux parameter. Cases 2 and 3 correspond to a drop controlled regime with well formed nuclei particles arising from individual droplets, whereas case 1 corresponds to the intermediate

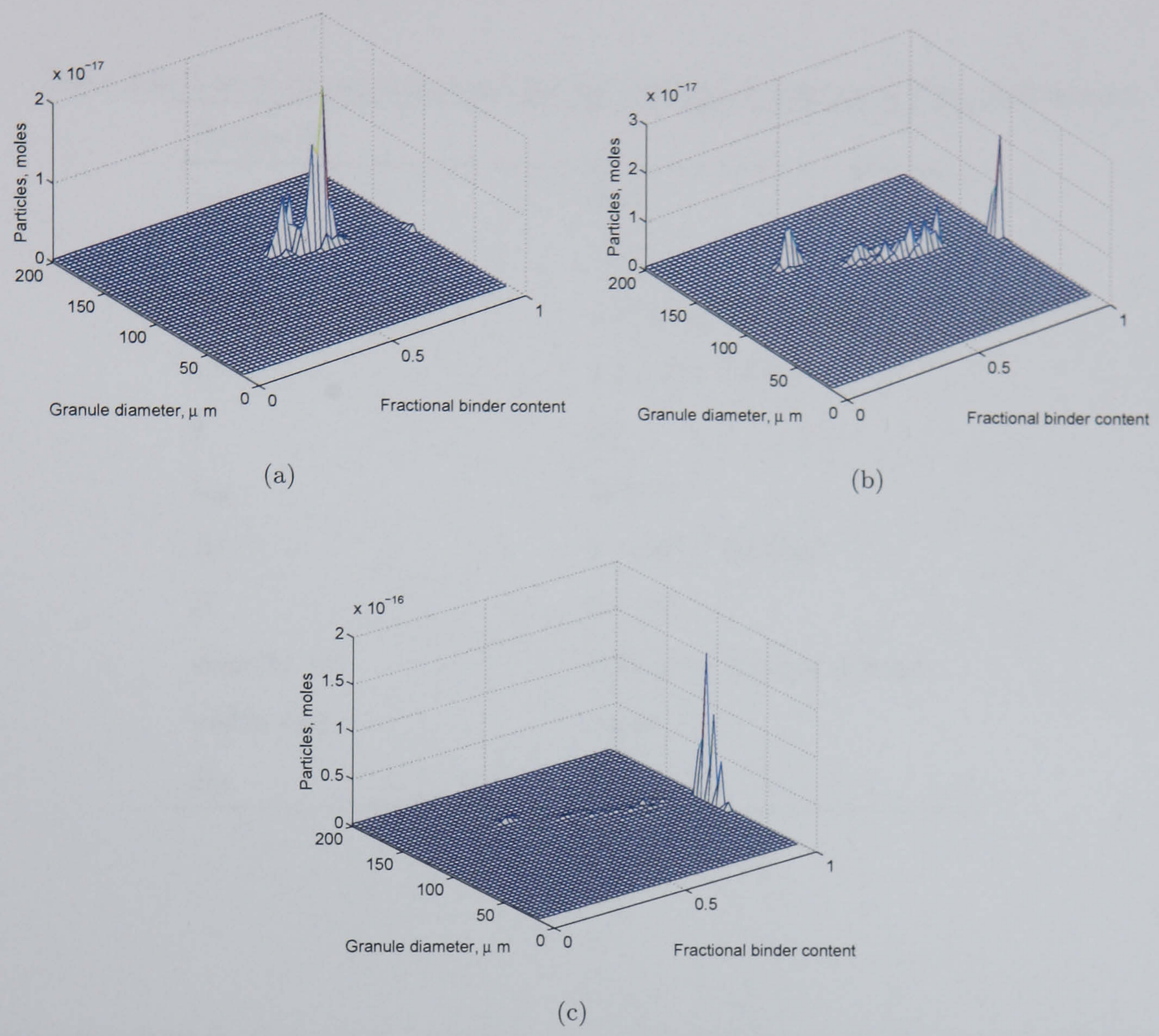

Figure 3.22: The end-point particle size distribution obtained for the cases where the bed turnover rate is larger than the binder penetration rate into the bed, thereby leaving some unpenetrated binder liquid on the surface (a) 10% unpenetrated surface liquid; (b) 40% unpenetrated surface liquid; (c) 60% unpenetrated surface liquid. The unpenetrated surface liquid is uniformly partitioned into all the particles and nuclei. Compare against Figure 3.17f for the case with complete binder penetration into the bed.

regime requiring mechanical aid to disperse the binder. The probability of a single drop without overlap can be related to the spray flux parameter as shown in Equation (3.55) (see Appendix A).

$$f_{single} = \exp(-4\Psi_a) \tag{3.55}$$

Examination of the probability of single drops with their corresponding spray flux values can further help explain why there is an observed difference exhibited between case 1 and

Table 3.3: List of parameters used for the nucleation and spray flux simulations

Parameter	
ε_{eff}	$0.2\,(-)$
ϕ	$1.0\,(-)$
γ^{LV}	$4.37 \times 10^{-2}\,\mathrm{N/m}$
γ^{SV}	$4.0 \times 10^{-2}\,\mathrm{N/m}$
θ	$65°$
l_{sat}	$0.99\,(-)$
A_0	$1 \times 10^{-15}\,\mathrm{mol/m^3}$
K	$6 \times 10^5\,(-)$
velocity (v)	$0.33\,\mathrm{m/s}$, $2.1\,\mathrm{m/s}$, $7.8\,\mathrm{m/s}$
width (w)	$0.2\,\mathrm{m}$
D_d	$84\,\mu\mathrm{m}$

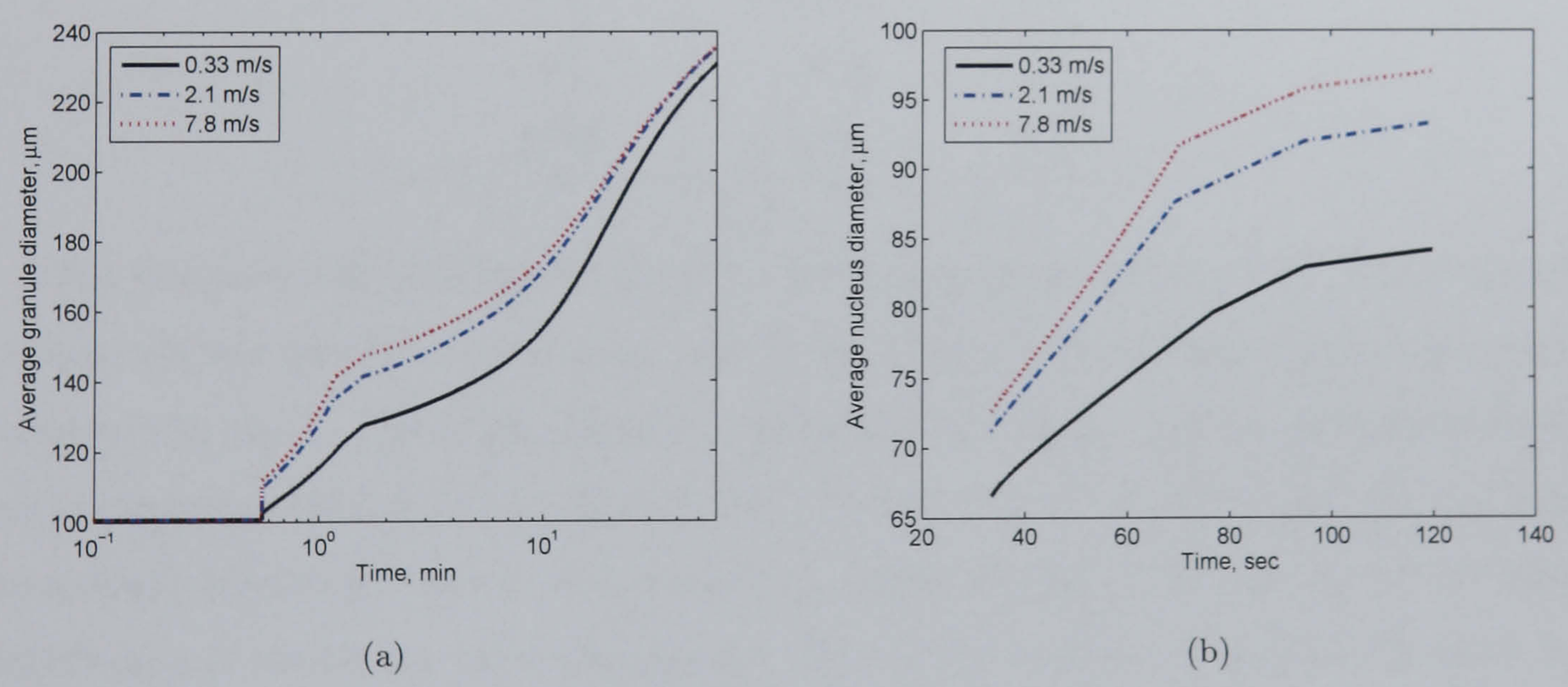

Figure 3.23: Comparison of time profiles for the evolution of the average granule size subject to the influences of nucleation with aggregation and granule consolidation (a); and the time evolution of the average nucleus diameter during early nucleation for powder velocities $0.33\,\mathrm{m/s}$ ($\Psi_a = 0.54$), $2.1\,\mathrm{m/s}$ ($\Psi_a = 0.09$) and $7.8\,\mathrm{m/s}$ ($\Psi_a = 0.02$).

cases 2 and 3. Table 3.4 reports the probability of single drops landing on the powder surface without drop overlap from their corresponding spray flux and powder velocities. The probability of single drops is considerably less for case 1 compared to either of the cases 2 and 3. Hence, a greater average diameter of the nuclei particles are formed for cases 2 and 3 (Figure 3.23b). Because there is a lower number of nuclei particles formed from a lower proportion of single droplets, the binder is distributed uniformly amongst all the particles, which is in alignment with Litster et al. (2001) that mechanical aid is required to distribute the binder when operating within the intermediate regime. Figures 3.24 (a) and (b) show that there is a much faster depletion of primary particles and similarly in the total number of granules. However, this effect could be due to the uniform binder distribution whereby each particle receives a small amount of binder facilitated by mechanical dispersion. But, the overall size of each particle upon receiving this amount of binder is still smaller than the nuclei particles formed from a single droplet. Hence, the larger value of the average granule size for cases 2 and 3 in Figure 3.23(a) compared to case 1.

Table 3.4: Probability of single drops with corresponding spray flux parameters

Powder velocity (m/s)	Ψ_a (−)	f_{single} (−)
0.33	0.54	0.11
2.1	0.09	0.71
0.33	0.02	0.91

The end-point distributions for cases $1-3$ are presented in Figure 3.25. The evolution of the particle size distribution for cases 2 and 3 are clearly more advanced when a comparison is made with case 1. The initial nuclei formation for cases 2 and 3 acts as a strong catalyst for the continued growth of future agglomerates. Significantly fewer nuclei particles are formed from single droplets for case 1, with the initial growth relying predominantly on the uniform distribution of the binder. As a consequence, the overall evolution of the particle size is much slower in comparison with the other two cases as seen in Figure 3.25.

3.7 Conclusion

The development of a realistic comprehensive model for granulation processes was addressed, albeit being subjected to a few simplifying assumptions in this first attempt. The operation

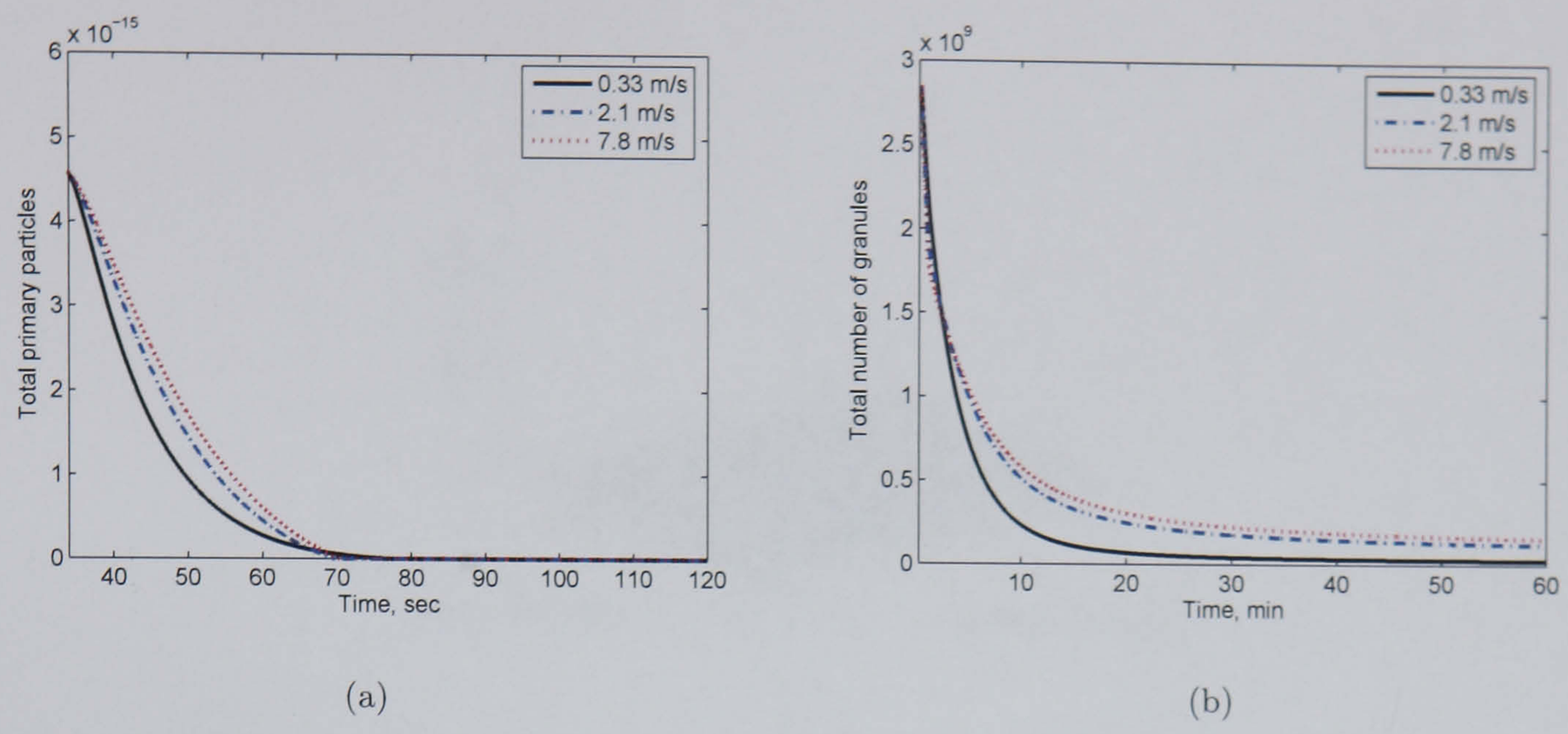

Figure 3.24: Time profiles for the depletion of primary particles during granule nucleation (a), and the overall decrease in the total number of granules in the system as a combined result of nucleation, aggregation and consolidation (b), for powder velocities 0.33 m/s ($\Psi_a = 0.54$), 2.1 m/s ($\Psi_a = 0.09$) and 7.8 m/s ($\Psi_a = 0.02$).

and control of granulation processes, like those of most solid handling processes, is currently primarily based on operator experience and is more an "art rather than a science" (Litster, 2003). Understandably, such an operation would essentially be based on a model formed in the operators mind, which will be both by-and-large linear and data-based. The granulation process is complex with intricate mechanisms, warranting a nonlinear and detailed model. With advancements and on-going developments in the understanding of the underlying science, a crucial next step is to systematise these scientific developments into an integrated mathematical model that accounts for the various phenomena, the interactions among these phenomena, and the regulations and feedback inherent in the system. Such a model will in turn find application in rigorous optimisation and control of these processes.

A population balance-based modelling approach for the granulation process has been presented. The model proposes a mechanistic framework for the aggregation and nucleation phenomena. The problem is considerably multi-scale in character, accounting for particle-level and population-level behaviour. A straightforward incorporation of details at both these levels is precluded by computational considerations. Thus, the particle-level phenomena and equations are transformed using appropriate frameworks from kinetic theory, to obtain closed form kernels. A three-dimensional population balance model is formulated at the population level, into which the particle-level kernels are embedded, in a micro-scale transformation

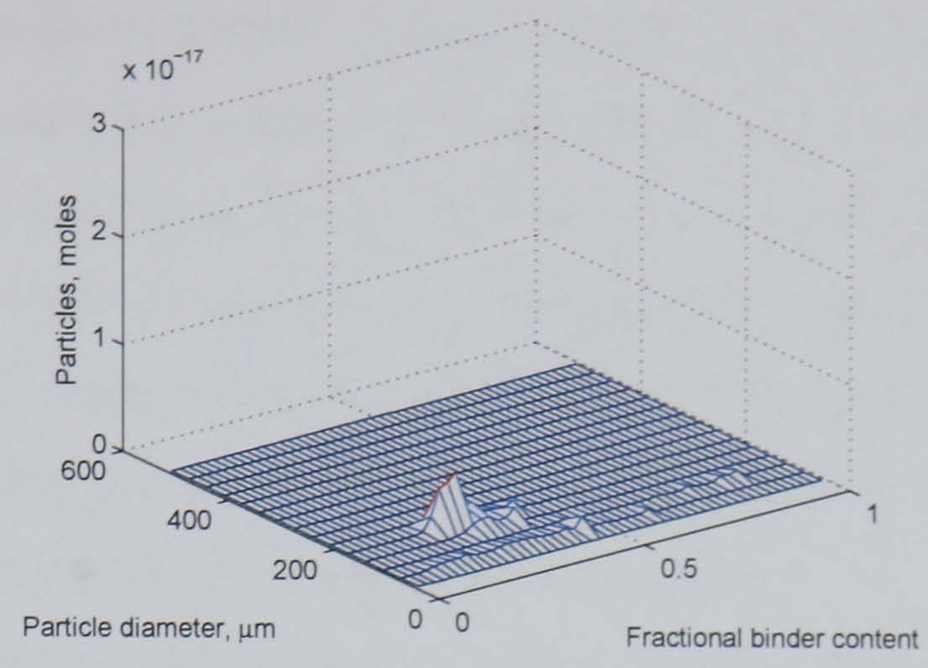

(a)

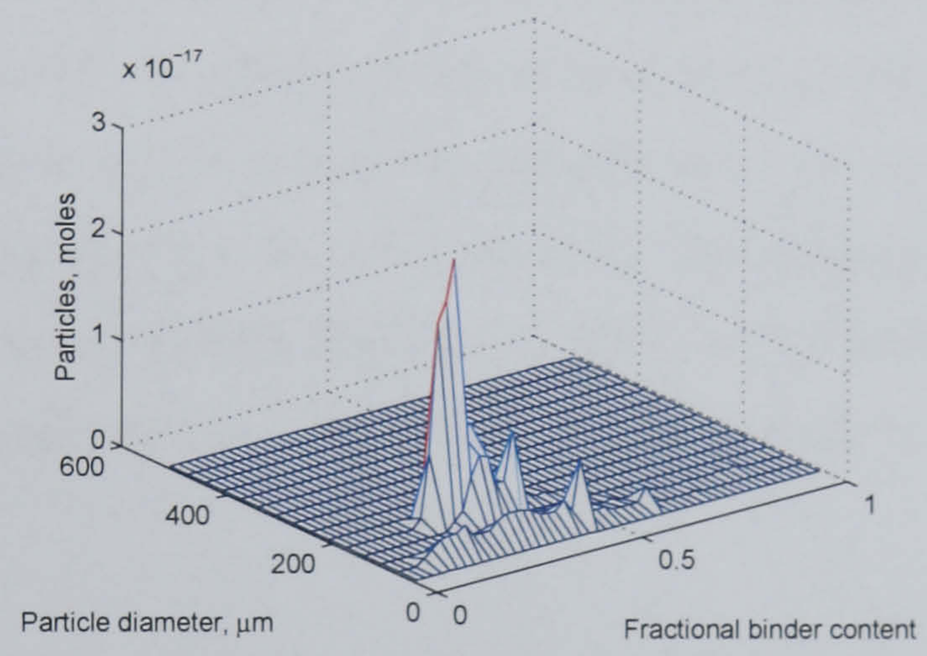

(b)

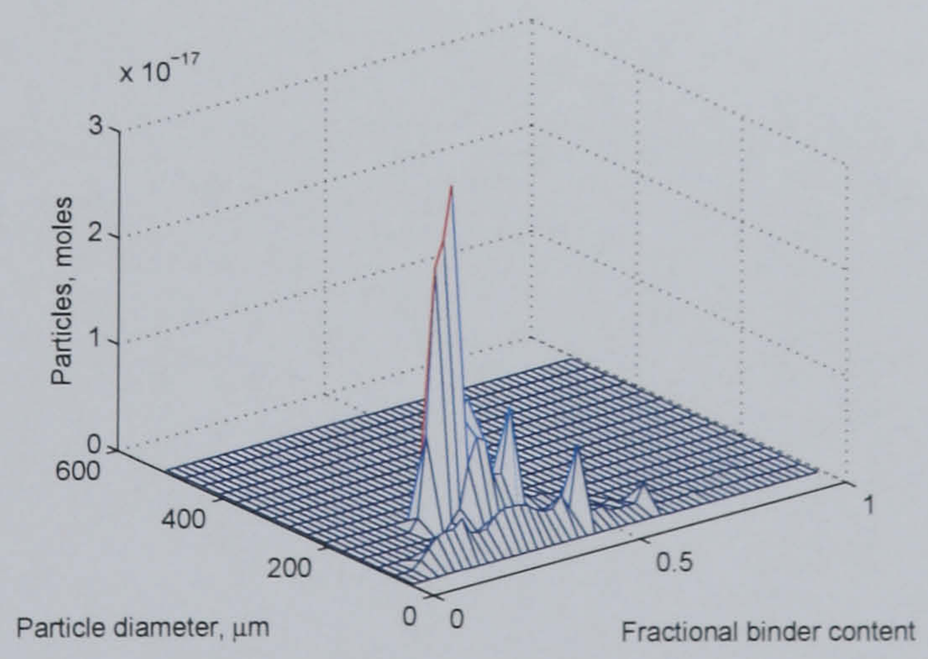

(c)

Figure 3.25: The end-point granule size distribution for three cases where the powder velocity was set to 0.33 m/s, 2.1 m/s and 7.8 m/s, which corresponds to a dimensionless spray flux of $\Psi_a = 0.54$, $\Psi_a = 0.09$ and $\Psi_a = 0.02$, respectively.

approach for this multi-scale model. This is a novel approach compared to previous models that employ empirical forms of kernels, based on macroscopic experimental observations.

The results clearly serve the purpose of confirming intuitive knowledge thereby also validating the model in a qualitative sense. Further, they reveal complex process dynamic character that is not obvious in the first place but sensible in hindsight in view of underlying theory. A sensitivity study using the present population balance model was performed, with respect to several key process operating variables in order to discern the effects of key equipment operating parameters on the granulation process.

A crucial next step in these developments is the validation of the integrated model, which is presented in Chapter 4. The kernels themselves are derived based on mechanisms of aggregation and nucleation that have been already validated at the microscale (particle) level (Liu et al., 2000; Hapgood et al., 2002). Further experimental validation of the macroscopic population PSD behaviour will constitute an important future work. A promising decomposition algorithm is employed for the solution of the multidimensional population balance model (Immanuel and Doyle III, 2005; Pinto et al., 2007), which will facilitate the formulation of such models for the analysis and study of complex multi-scale process dynamics.

Chapter 4

Batch granulation experiments and model validation

Part of the contents of this chapter was published in Ramachandran et al. (2008) and Poon et al. (Accepted). See also Ramachandran (2008).

4.1 Introduction

In this chapter, the growth kinetics for a granulation recipe consisting of calcite (also known as calcium carbonate or limestone) and polyvinyl alcohol (PVOH) are presented. The granulation of such powders is of significant importance, since it is readily employed in the pharmaceutical industries as an ingredient in the manufacture of tablets and in the production of many commodity products such as in toothpaste and in chewing gum. In the first case, it is employed as a cost-effective excipient that can be used for the manufacture of buffered aspirin. It is of particular use when compounded with hygroscopic ingredients that absorb moisture, to prevent forming powder clumps thereby causing segregation. However, despite its uses calcium carbonate exhibits poor compressibility and as such cannot be directly (dry) granulated without compromising on the physical properties of the resultant tablet *i.e.*, poor hardness that may attrite easily. Thus, by virtue of the physical properties of calcium carbonate, it is necessary to (wet) granulate them with a binder for use in tablets.

The results presented in this chapter are from the granulation experiments that were carried out on a laboratory scale rotary drum granulator, which was used in a similar study by Wauters (2001) and Wildeboer (2002) although for different granulating materials. The

facility is located in the Department of Chemical Engineering at the University of Queensland. Australia, where the author spent three months during his Ph.D. studies. The motivation for the series of experiments undertaken are summarised in the following:

- Obtain growth kinetic data for this particular granulation formulation ($CaCO_3$–PVOH) for model validation.
- Investigate sensitivities with respect to the amount of binder and the powder bed depth.
- Perform a dimensional analysis on the present granulation recipe consisting of calcite powder and PVOH for different binder-solid ratios, and couple these analyses to the granulation behaviour predicted by the integrated model and also to simultaneously ensure the richness of the data for model validation.
- Obtain measurements for important particle attributes namely, particle size, porosity and the fractional binder content. Note that the use of three-dimensional distribution evolution data is a significant improvement over typical literature reports that in most cases measure only the granule particle size distribution.

4.2 Model inputs under mechanistic kernels

In Chapter 3, a population balance model was developed incorporating mechanistic descriptions for the nucleation process and the aggregation phenomenon, whilst an empirical exponential decay relation was used for the consolidation kernel. Table 4.1 provides a reminder of the model forms of the kernels corresponding to each of the rate processes in the present integrated population balance model.

Table 4.1: Model forms of the consolidation, nucleation and aggregation kernels.

Rate process	Model representation
Consolidation kernel	$\frac{d\varepsilon}{dt} = -c\left(\varepsilon - \varepsilon - min\right)$
	$\Rightarrow \frac{dg}{dt} = -c\frac{s+l+g}{s(1-\varepsilon_{min})}\left[l - \frac{\varepsilon_{min}s}{1-\varepsilon_{min}} + g\right]$
Nucleation kernel	$k_{nuc}\left(s,l,g\right) = A_0 Q e^{\left(\frac{K\lambda}{RT}\right)}$
Aggregation kernel (size-dependent part)	$\beta(p_1,p_2) = c_1\frac{4\pi u_0(r_1+r_2)^2}{W}$

By virtue of the mechanistic description of the granulation process, the model now incorporates the material properties of the solid and binder and also the process operating conditions in an explicit manner. The incorporation of the former would not be easily possible from an empirical modelling approach. In Table 4.2, model inputs pertaining to the nucleation kernel and the aggregation kernel are specified. These model inputs are classified into (i) fundamental material properties, (ii) process manipulations and (iii) adjustable parameters.

4.3 Experimental

4.3.1 Materials

The calcite ($CaCO_3$) powder (Aglime, Landmark, Australia) used in the drum granulation experiments had a mass median diameter (d_{50}) of 130 μm and the measured skeletal density of the powder was 2743 kg/m^3, which was determined using pycnometry described later. The initial moisture content of $CaCO_3$ powder was neglected. The initial $CaCO_3$ powder was also subjected to scanning electron microscopy (SEM) as shown in Figure 4.1. Figure 4.1a shows that there is a clear indication of a broad particle size distribution in the initial $CaCO_3$ powder, which is also corroborated by the volume distribution of particles shown in Figure 4.2 obtained on the Malvern Mastersizer 2000. Using a greater magnification as seen in Figure 4.1b shows that smaller fines of $CaCO_3$ particles are adhered to the surface of a larger powder particle. From Figure 4.1, the particles are observed as non-spherical, irregular particles with rough surfaces. The initial distributions (based on volume) of three separate samples obtained from the powder stock are shown in Figure 4.2. Minimal variation between the distributions of the three samples indicated that the random sampling of the powder from the powder stock was sufficient.

The liquid binder used in this study was polyvinyl alcohol (Elvanol T66, Du Pont, USA), which was prepared in solution with concentration of 2.5% w/w (PVOH). Hereafter, 2.5% w/w concentration of polyvinyl alcohol is implicit in the notation of PVOH unless otherwise stated. The viscosity of the PVOH solution was measured using an AR-G2 magnetic bearing magnetic rheometer (TA instruments) and determined to be 5.2 mPa·s. A literature value of 52 mN/m was used for the surface tension of the PVOH binder (Bhattacharya and Ray, 2003). The measured contact angle formed between the powder and the binder droplet for this particular

Table 4.2: Summary of inputs used in mechanistic kernels.

Model Inputs
Fundamental material properties
• Binder viscosity (μ) - determined through measurements.
• Liquid binder surface tension (γ) - obtained from literature.
• Solid-liquid contact angle (θ) - determined through measurements.
• Particle density (ρ_s) - determined through measurements.
• Solid yield strength (Y_d) - determined through measurements.
• Diameter of primary particles (d) - determined through measurements.
Process manipulations
• Liquid binder spray rate (Q) - set according to experimental conditions.
• Binder droplet volume (V_0) - set according to experimental conditions.
• Initial particle size distribution - determined through measurements.
Adjustable parameters
• Consolidation frequency factor (c). See Table 4.1.
• Aggregation kernel frequency factor (c_1). See Table 4.1.
• Adjustable constant for the nucleation kernel (A_0). See Table 4.1.
• Granule size upper limit for aggregation (D_{upper}).
• *Effective porosity of the bed mass (ε_{eff}).
• *Critical liquid content for surface film formation (l_{sat}).
• *Mixing rate, which is reflected by the relative collision velocity of the particles in the granulator (u_0).
• *Volume of unpenetrated binder (V_{up}).
• *Height of particle surface asperity (h_a).

* Indicates the parameters that are less-sensitive compared to the other model adjustable parameters.

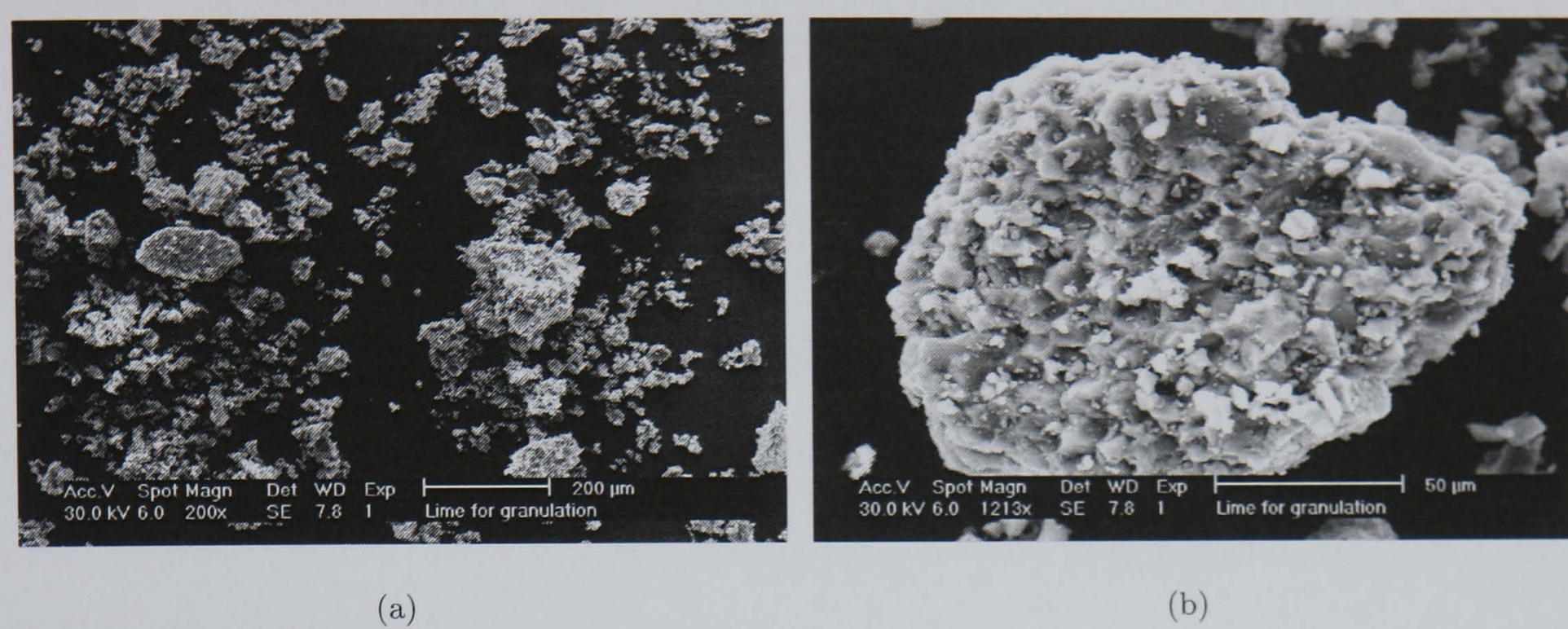

(a) (b)

Figure 4.1: Scanning electron micrograph images for primary particles of calcite powder at magnifications of ×200 (a) and ×1213 (b). Both the particle size and shape of the primary particles can be seen as non-spherical and rough.

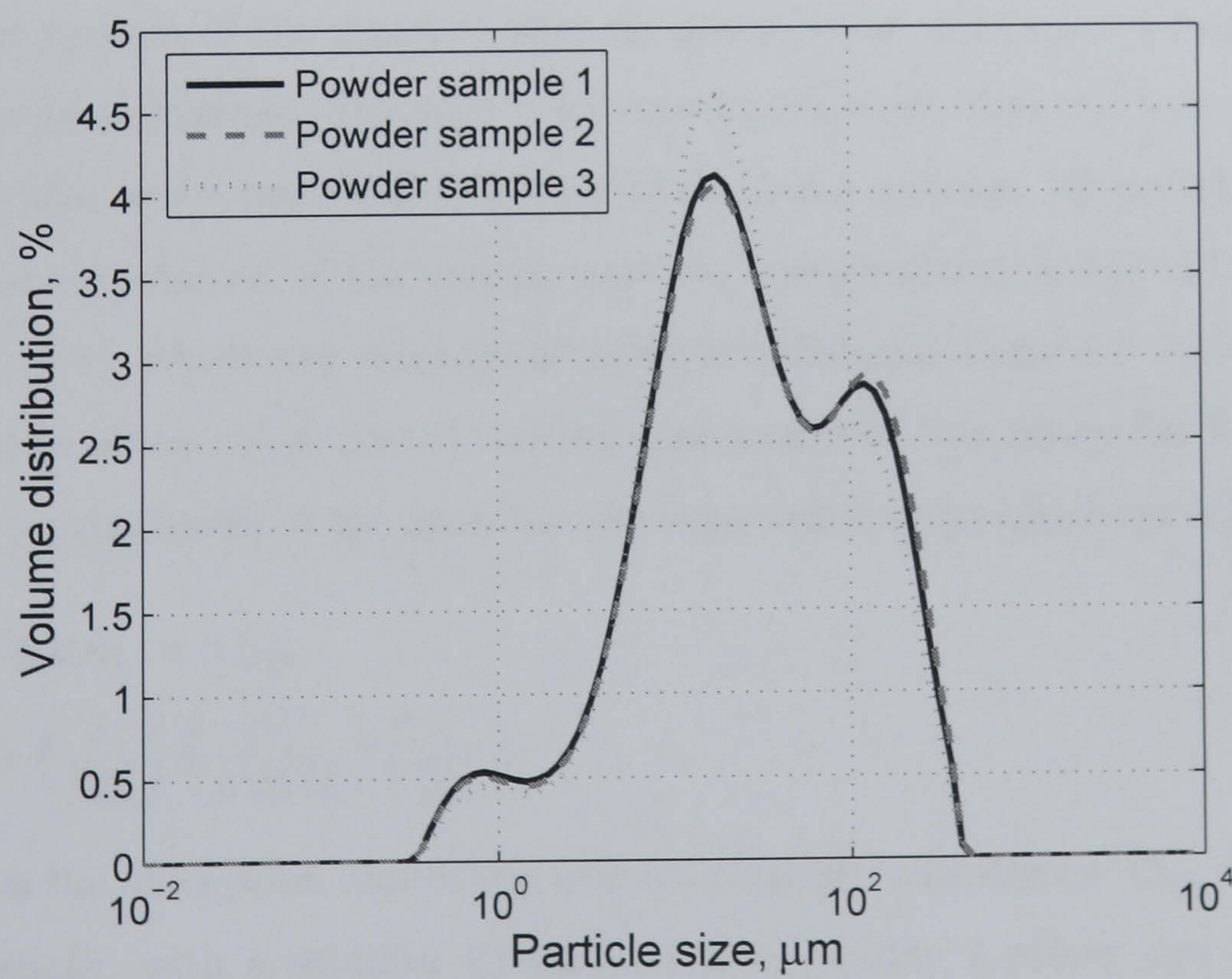

Figure 4.2: Volume distribution of primary particles from the calcite powder.

granulation recipe was found to be 43.2°, which was determined using the contact anglometer (Model 1501, Micromeritics). Further properties and procedures pertaining to PVOH. and the equipment used for determining the viscosity and the contact angle may be found in Appendix C.

4.3.2 Particle size analysis

The granule size distribution was determined by firstly drying the sampled wet granules taken from the granulator in an oven at 110°C. The dried granules were then subsequently sieved using a fourth-root-of-two progression series of sieves (Endecotts Ltd.). See Appendix B.

4.3.3 Porosimetry

The porosity of the granules from their respective size class were determined using pycnometry. The porosity of the granules required the determination of the true density of the granules, which was measured using the AccuPyc 1330 and the bulk density measured on the GeoPyc 1360 (Micromeritics) (Ramachandran et al., 2008).

4.3.4 Spectrophotometry

The moisture content of the granules were measured using spectrophotometry (Lambda 40, Perkin Elmer Instruments). The moisture content is inferred from the measured absorbance of the colour dye, which was added to the PVOH binder solution. The relationship between the measured absorbance of the sample and the concentration of the colour dye is given in Equation (4.1), which was established using a calibration curve for solutions containing known amounts of the colour dye at varying concentrations (see Appendix B). The moisture content (on a mass basis) of the granules was then found using Equation 4.2.

$$\mathrm{AU} = 0.3181 \times \mathrm{C_{dye}} \tag{4.1}$$

$$\mathrm{LS\%} = \left(\frac{1}{100}\right)\left(\frac{\mathrm{AU}}{0.3181}\right)\left(\frac{\rho_l}{\mathrm{M}_s}\right) \tag{4.2}$$

Where, AU is the absorption unit of the measured sample absorbance, $\mathrm{C_{dye}}$ is the percentage solution strength, with a solution strength of 100% having a colour dye concentration of 8.9 g/L, M_s is the sample mass (g), ρ_l is the density of PVOH and LS% is the moisture content of the granule sample.

4.3.5 Dynamic strength of moist powder compacts

A measurement technique previously employed by Iveson et al. (2002), which involved subjecting pre-formed powder compacts of known fractional binder content to axial compression tests in order to assess the dynamic strength of the powder compacts was employed in this study. Granular cylindrical pellets consisting of $CaCO_3$ and PVOH were prepared beforehand (see Appendix F). Axial compression tests were carried out on the load frame (Model 8841, Instron Dynamite^{TM}), which is capable of performing high compression velocities. The velocity of the platens used in this study ranged from 0.1 mm/s to 200 mm/s. These velocities were chosen so as to mimic the potential velocities that the particles may experience in real granulators.

Dimensional analysis is used in providing auxiliary information that can be used in the interpretation of the granulation phenomena observed in the granulation process. Specifically, the dimensionless strength of granules given by Equation (4.3) represents the ratio of the peak flow stress to the capillary force; and the capillary number given in Equation (4.4) may be interpreted as the ratio of the viscous forces to the capillary forces.

$$\mathrm{Str}^* = \frac{\sigma_D D_p}{\gamma^{LV}} \tag{4.3}$$

$$\mathrm{Ca} = \frac{\mu \dot{\varepsilon} \overline{D}_p}{\gamma^{LV}} \tag{4.4}$$

Where, σ_D is the peak flow stress, $\overline{D}_p$ is the average particle size, γ^{LV} is the surface tension of the liquid binder, μ represents the viscosity of the liquid binder and $\dot{\varepsilon}$ represents the strain rate (Litster and Ennis, 2004).

4.3.6 Granulation experiments

Batch granulation experiments were carried out on a laboratory scale rotary drum granulator, which was used in previous studies by Wauters (2001) and Wildeboer (2002). The drum granulator had dimensions of 0.3 m as the diameter and a length of 0.2 m. Notable internal features of the drum granulator were the six wedge-shaped rims equally spaced around the inner circumference of the drum. The purpose of these rims was to facilitate the tumbling motion of the granulating powder. However, it was observed that during the experiments, there was a tendency for the powder to adhere at the base of the rims, thus promoting the

gradual buildup of wall coating on the inner surfaces of the drum. The drum speed was first calibrated and then set to 25 rpm, which was used for all subsequent experiments. This drum speed setting was specifically chosen as it produced an optimal powder flow, determined by visual inspection. The following preparations were necessary prior to carrying out the granulation experiments:

- Preparation of PVOH binder solution involved weighing the appropriate mass of polyvinyl alcohol powder; adding a colour dye with a concentration of 8.9 g/L; and dissolving in deionised water at 85°C for approximately one hour. The solution was filtered to remove any suspended solids that may potentially block the spray nozzle. The final PVOH solution was left to equilibrate to ambient temperature.

- The binder delivery system used in the experiments was a pressure pot fitted with a flat-fan spray nozzle (spray angle 65°). The pressure pot was pressurised to 500 kPa ($\equiv$ 5 bar), and the flow rate calibrated. During the calibration, checks were also preformed to ensure that a smooth, continuous spray was produced.

The protocol for performing batch granulation experiments for the nominal case (*i.e.* target binder-to-solids ratio of 0.11 and a powder mass of 1.5 kg) were as follows:

1. Load 1.5 kg of the powder into the drum (stationary). The spray nozzle attached to an appendage is positioned such that the nozzle is facing above and perpendicular to the powder surface.

2. Pre-run the drum at the pre-specified drum speed (25 rpm) for a duration of 20 sec. The purpose of this pre-run is to establish a steady powder motion and a uniform distribution of the powder across the length of the drum.

3. The granulation process commences at time $t = 0$ sec, immediately after the 20 sec pre-run, and the binder spray is turned on for a predefined length of time.

4. Samples were taken out at time instances of 3 min, 5 min, 7 min, 10 min, 15 min and 30 min by scooping approximately 150 g of granule samples across the powder bed. The granulation end time was 30 min.

5. The samples were characterised with respect to their particle size, porosity and fractional binder content. The granule size distribution was determined using sieve analysis:

the porosity of the granules was determined by pycnometry; and the fractional binder content was determined via spectrophotometry. Further details pertaining to these analytical techniques may be found in Appendix B.

As stated earlier in the experimental objectives, two different binder-solid ratios are used. principally LS = 0.11 and LS = 0.12 for drum loads of 1.5 kg. Finally, a similar experiment employing a target LS = 0.11 and a drum loaded of 1.75 kg of powder into the drum granulator. Below is a summary of the experiments to be undertaken. The batch granulation variables used during the batch granulation experiments are also shown in Table 4.3. The nominal set of conditions that is referred to in these experiments corresponds to a LS = 0.11 and a drum load of 1.5 kg.

- Effects of moisture content
  - + Binder-to-solids ratio = 0.11 and 1.5 kg of calcite powder (case 1).
  - + Binder-to-solids ratio = 0.12 and 1.5 kg of calcite powder (case 2).
- Effects of powder bed-depth (mass of powder charged into the granulator)
  - + Binder-to-solids ratio = 0.11 and 1.75 kg of calcite powder (case 3).

Table 4.3: Batch granulation variables

Parameter	Case 1	Case 2	Case 3
Initial powder mass (kg)	1.5	1.5	1.75
Rate of binder spray (mL/s)	1.72	1.72	1.72
Duration of binder spray (s)	96	104	112
Volume of binder droplet (m^3)	1.15×10^{-11}	1.15×10^{-11}	1.15×10^{-11}

4.4 Results and discussions

The model simulations were carried out on a 2GHz Intel Dual Core processor desktop computer with 2GB RAM using the intel FORTRAN compiler. The total discretised domain for the simulation comprised of 50, 20 and 10 bins along the solid, liquid and gas internal coordinate axes, respectively. The width of the bin along the solid volume is $\Delta R_s = 1.07 \times 10^{-5}$ m, the width of the bin along the liquid volume ranges between $\Delta R_l = 3.35 \times 10^{-7}$ m to

$\Delta R_l = 2.68 \times 10^{-5}$ m and the width of the bin along the gas volume is $\Delta R_g = 1.5 \times 10^{-6}$ m. A first order Euler predictor-corrector method was employed for the integration of the system of ODEs. The computation time required for the simulation of the population balance model accounting for nucleation, aggregation and consolidation was approximately 1.5 hr for the nominal case (case 1). The population balance model was validated by comparing the simulated variables with experimental measurements. Granule samples were taken out from the drum granulator at the time instances of 180 s, 300 s, 420 s, 600 s and 900 s. The primary particles were mono-dispersed with a median diameter (d_{50}) of 130 μm and a standard deviation of 1.37 based on the three triplicate feed primary particle samples used earlier. Other model inputs such as the initial number/mass of seed particles, volume of the binder droplet, duration of binder addition, and binder flow rate were set as per actual experimental conditions.

A sensitivity analysis around the nominal operating regime was performed to determine the influence of the adjustable model parameters on the particle density distribution. The adjustable model parameters (see Table 4.2) pertaining to each of the sub-rate process kernels are tuned using experimental data set of the nominal case (case 1). Subsequently, the tuned model was used to predict the granule size distribution (GSD), fractional binder content and the porosity at other operating conditions (cases 2 and 3). The parameters which exhibited the most sensitivity to the process (*i.e.* c, A_0, c_3, D_{upper}) were tuned in the simulation mode, to provide an acceptable correspondence via visual inspection between model predictions and the GSD obtained from the experiments. The less-sensitive adjustable parameters (indicated by an * in Table 4.2) that remained fixed at nominal values were the height of the surface asperity of the particles (h_a), the critical binder content required prior to surface film formation (l_{sat}), the effective porosity of the powder bed mass (ϵ_{min}), relative approach velocity of the two coalescing particles (u_0), and the volume of droplet that remains unpenetrated (V_{up}). Table 4.4 lists the adjustable parameters pertaining to the kernels whilst Table 4.5 lists the fundamental material properties that were either measured or obtained from the literature in addition to the nominal values of the less-sensitive adjustable parameters.

4.4.1 Effects of moisture content and drum loading

Case 1 corresponds to a binder-to-solids ratio of 0.11 with a drum load of 1.5 kg of $CaCO_3$ powder, which is referred as the nominal case to which other experimental cases are compared.

Table 4.4: Adjustable parameters pertaining to sub-rate process kernels.

Parameter	Value
c	5×10^{-5} (-)
c_1	3×10^{7} (-)
A_0	$4 \times 10^{-20}\,\mathrm{mol/m^3}$
D_{upper}	$740\,\mu\mathrm{m}$

The total particles which was predicted by the PB model is shown in Figure 4.3a. During the first 2 min, there is a rapid depletion of particles (the combination of fine powders and granules) due to the binder spray, which promotes rapid nucleation of primary particles followed by fast agglomerate growth via coalescence. When the binder spray has stopped, the rate of depletion of particles from $2 - 15$ min is reduced significantly as this signifies the termination of the nucleation event with granules growing predominantly through particle aggregation. The steady growth of granules is also shown in Figure 4.3b with the time evolution of the mean granule size. The fractional binder content and the average granule

Table 4.5: Fundamental material properties and adjustable parameters set with nominal values.

No.	Property	Value
1	μ	5.20×10^{-3} mPa·s
2	ρ_s	$2743\,\mathrm{kg/m^3}$
3	Y_d	1.591×10^{-4} Pa
4	E	8.20×10^{6} Pa
5	h_a	5.0×10^{-5} m
6	l_{sat}	0.20 (-)
7	d_{50}	$130\,\mu\mathrm{m}$
8	γ_{LV}	5.2×10^{-2} N/m
9	γ_{SV}	4.0×10^{-2} N/m
10	θ	$43.2°$
11	ε_{eff}	0.20 (-)
12	u_0	5.0×10^{-3} m/s
13	V_{up}	$0\,\mathrm{m^3}$

porosity is shown in Figure 4.4 (a) and (b), respectively. The model predictions for the average granule diameter, the fractional binder content and the average porosity of the granules show a close agreement with the experimental measured data.

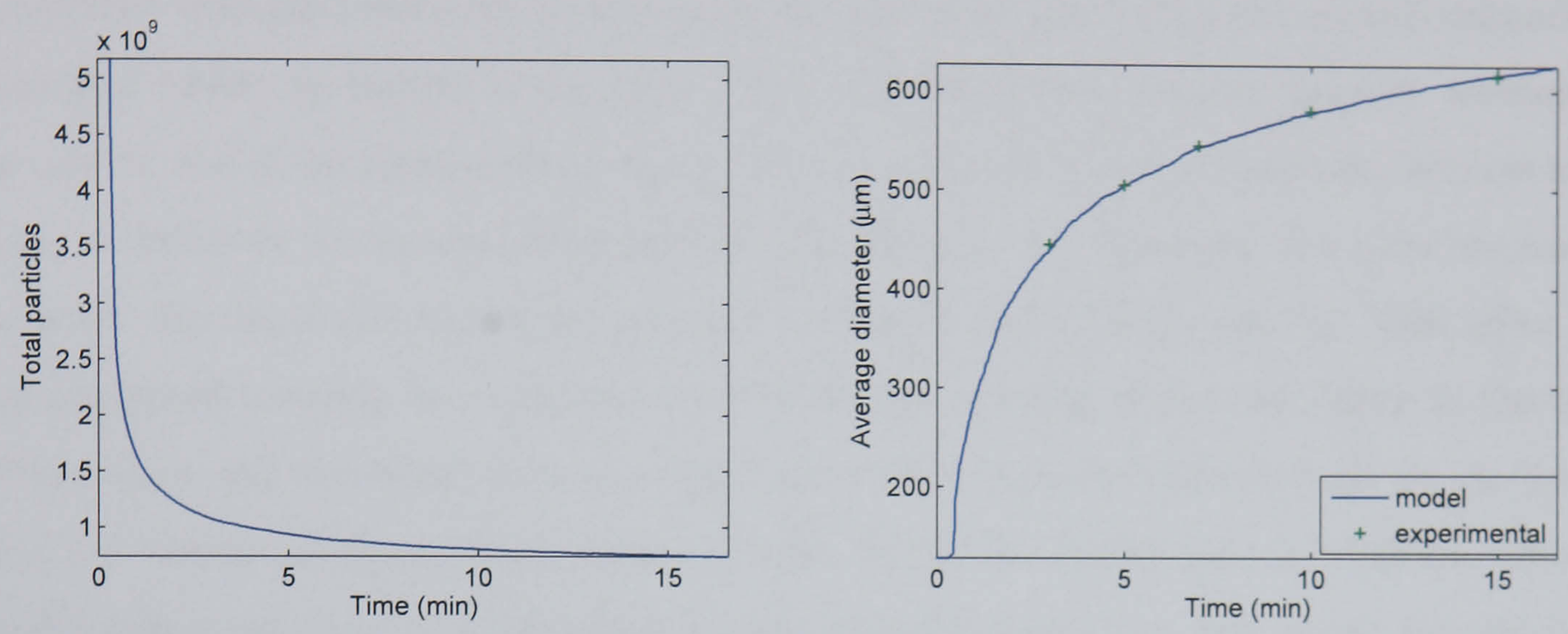

(a) (b)

Figure 4.3: Model prediction for the total number of particles (a) and a comparison between model predictions and batch granulation experiments for the evolution of the average granule diameter (b) for the case with a binder-to-solids ratio of 0.11 and a drum load of 1.5 kg of $CaCO_3$ powder (case 1).

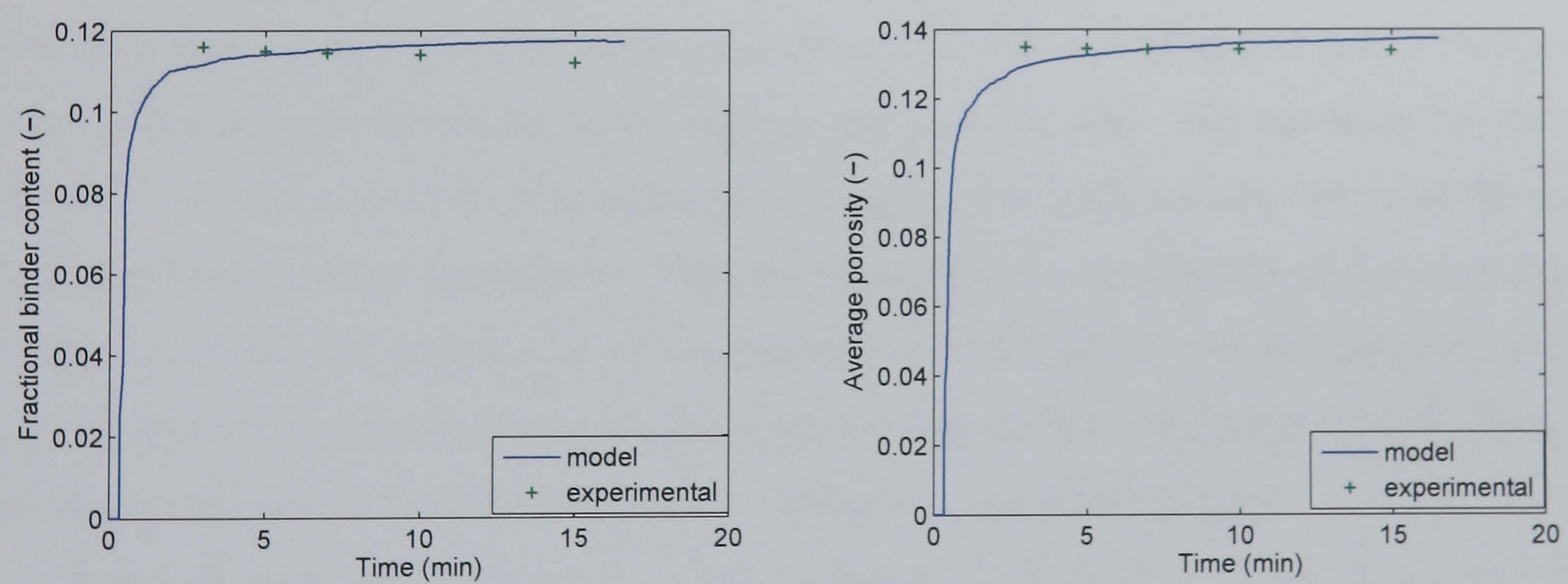

(a) (b)

Figure 4.4: Comparison between model predictions and batch granulation experiments for time profiles of the average fractional binder content (a), and the average granule porosity of the granules (b) for the case where the binder-to-solids ratio is 0.11 and a drum load of 1.5 kg of $CaCO_3$ powder (case 1).

The measured liquid binder distribution profiles across the granule size spectrum is shown in Figure 4.5 for cases 1 to 3. There is an underlying trend featured in all three cases larger sized granules tend to have a higher moisture content (*i.e.* fractional binder content), which is consistent with the theory that more liquid that is available for granulation will enhance the granules' ability to deform under stress, thus exhibiting faster growth rates by coalescence. In cases 1 and 2, progressing from 5 min, 10 min to 15 min, there is a notable decrease in the level of moisture across the entire particle size domain. Furthermore, the moisture content is below the respective target values (0.11 for case 1 and 0.12 for case 2). This effect may be attributed towards the evaporation of the binder and due to the variability in the spray, where there will inevitably be some liquid spray that does not entirely land on the powder bed but instead along the inner walls on either end of the granulator. In addition, although wall buildup was kept to a minimum, it was observed that there were minor powder build-ups along the six wedge-shaped rims whose function was to promote the tumbling motion of the powder in the granulator. Thus, binder contribution towards these minor wall buildups would also contribute to the lower moisture levels obtained in the granule samples.

In Figure 4.6, GSD profiles for intermittent sampling times (*i.e.* 3 min, 5 min, 10 min and 15 min) during the batch granulation determined from sieving are shown (indicated by the dashed lines). A normalised number frequency is used to represent the granules with respect to their particle size class. Granules are seen to gradually grow into larger agglomerates as the main peak spanning $0 - 250\,\mu$m is depleted, with a corresponding increase in the peak at $700 - 1000\,\mu$m (note the change in the range of the ordinate axis). This experimental data set (case 1) was used to tune the PB model, specifically for the GSD, and the results of the tuning is also indicated in the same figure. The model provides a clear capture of the predominant peaks in the bimodal distribution of the granules. The PB model was also shown to provide a good prediction with respect to the distribution of granule porosity presented in Figure 4.7, showing larger granules to be less porous compared to smaller granules.

A two-dimensional visualisation of the evolution of the GSD is shown in Figure 4.8(a)-(f). Initial mono-sized primary particles is represented at $t = 0$ sec. As soon as the binder is commenced into the granulator, granulation commences, immediately after $t = 20$ sec, where the initial primary particles are nucleated on a very short time scale as depicted in Figures 4.8(b)-(d) with a broadening of the initial peak. The newly formed nuclei particles during the onset of binder spray show that the particles have increased in their fractional

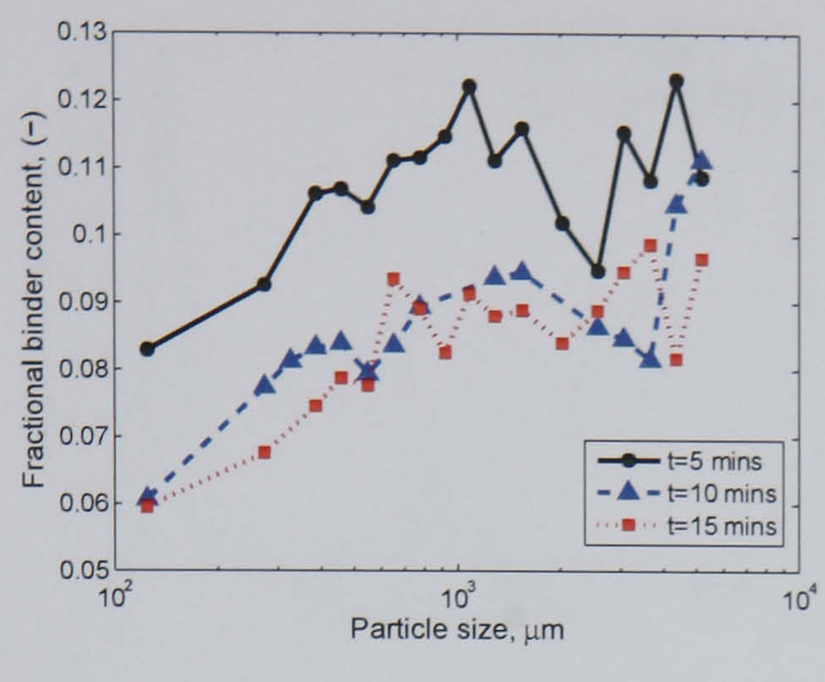

(a) $LS = 0.11$ (1.5 kg)

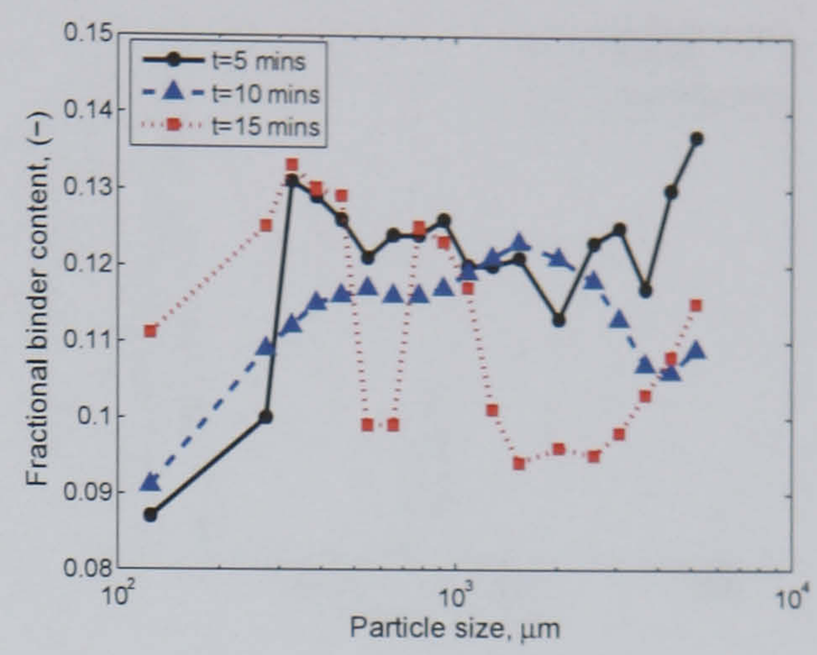

(b) $LS = 0.12$ (1.5 kg)

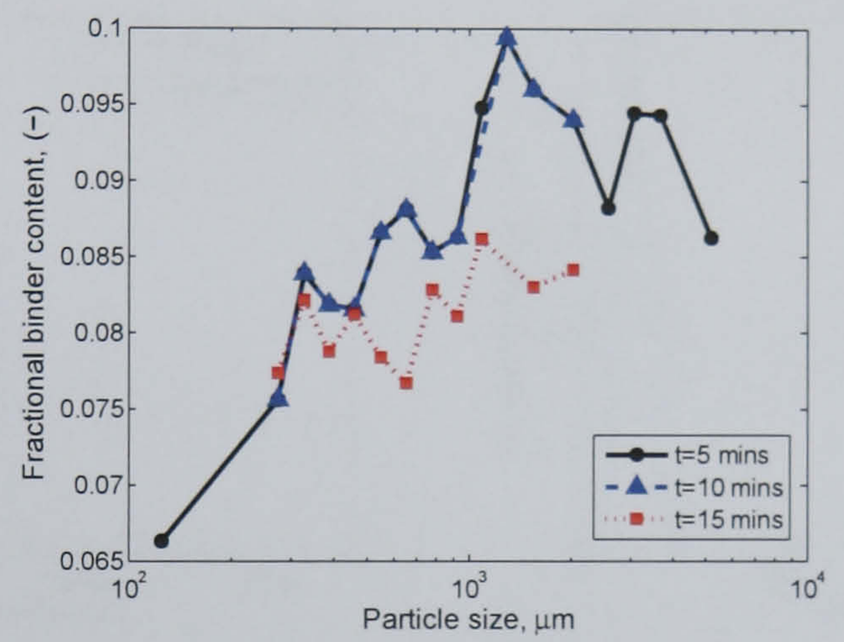

(c) $LS = 0.11$ (1.75 kg)

Figure 4.5: Distribution profile for the fractional binder content across the granule size range. Three cases are shown for target binder-to-solid ratio (LS) of 0.11 and 0.12 for initial powder loading of 1.5 kg, the third case corresponds to a LS = 0.11 with a drum loading of 1.75 kg.

binder content and the growth of larger sized particles, that is consistent with the granulation theory. The emergence of the second mode of larger size particles is the cumulative effect of both nucleation and aggregation. At $t = 180$ sec, there is steady agglomerate growth under the influences of consolidation and aggregation and the GSD is bi-modal. This observation has also been made in numerous studies by Butensky and Hyman (1971); Knight et al. (1998); Scott et al. (2000); Reynolds et al. (2004).

The PB model is now validated for the second case where the binder-to-solids ratio is 0.12, whilst maintaining an identical drum load of 1.5 kg of powder. The predictive capabilities of the PB model is now demonstrated having previously tuned the model parameters using the first set of data. These tuned parameters will remain fixed during the validation of the

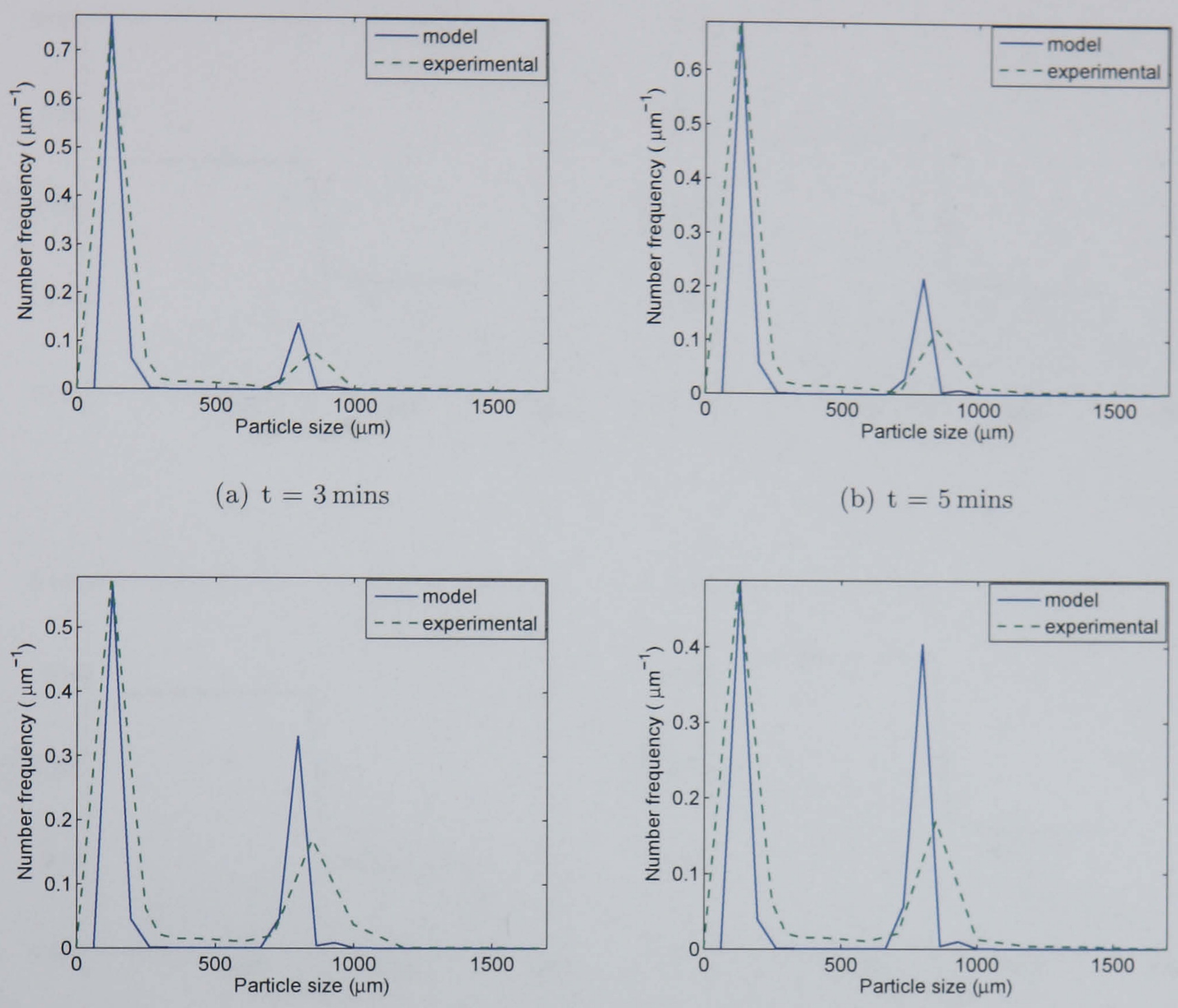

(a) t = 3 mins

(b) t = 5 mins

(c) t = 10 mins

(d) t = 15 mins

Figure 4.6: Comparison between model predictions on the granule size distribution at various time instances with data derived from batch granulation experiments for the case where the binder-to-solids ratio of 0.11 and a drum load of 1.5 kg of $CaCO_3$ powder (case 1).

model for the remaining cases 2 and 3. By increasing the amount of PVOH, we expect the granules to reach their liquid saturation faster in order for the liquid available for granulation to appear on the particle surface. Thus, it is anticipated that the average granule size and the fractional binder content would be higher in comparison with case 1, which was operating at a lower binder-to-solids ratio. Figure 4.9(a)-(d) corroborates this with a much broader size distribution in the second peak compared to case 1 in Figure 4.6, indicating a larger proportion of larger sized granules being formed. Figure 4.10 also shows a good comparison between the model predictions for the porosity distribution and those measured from the sieved granules derived from the experiment.

Model validation of the GSD profiles as shown in Figure 4.11 for case 3, which corresponds

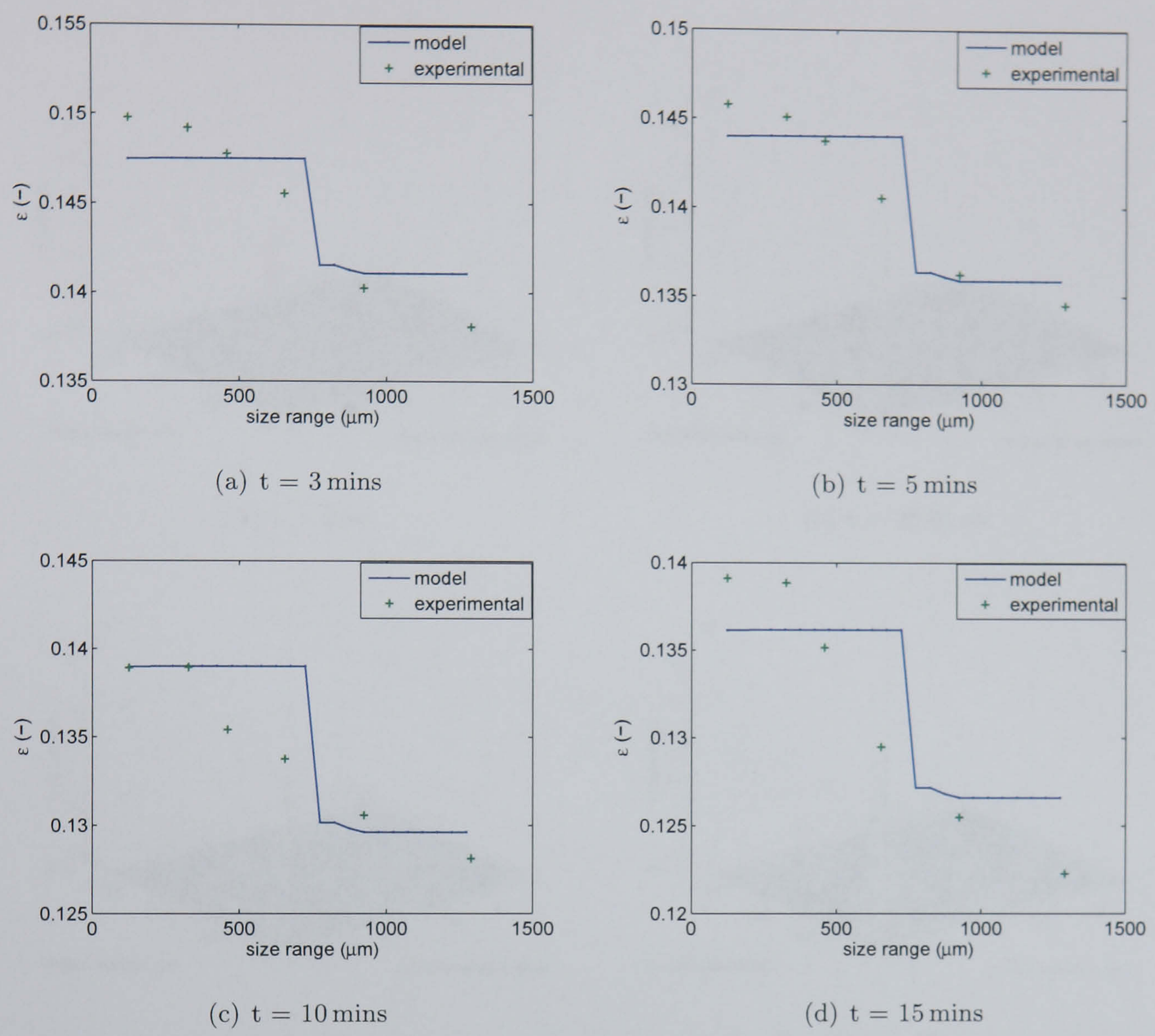

(a) t = 3 mins

(b) t = 5 mins

(c) t = 10 mins

(d) t = 15 mins

Figure 4.7: Comparison between model predictions on the distribution of granule porosity at various time instances with data derived from batch granulation experiments for the case where the binder-to-solids ratio of 0.11 and a drum load of 1.5 kg of $CaCO_3$ powder (case 1).

to an increased drum loading of 1.75 kg and an identical target binder-to-solids ratio of 0.11 as in case 1, showed good agreement with measurements from the experiment. However, a comparison between the GSD profiles for case 3 (Figure 4.11) and those with case 1 (Figure 4.6) showed no significant effects. This was also observed by Butensky and Hyman (1971), having noted that variation in the drum loading did not exhibit any significant effect on the granulation process *i.e.*, no change in the average granule size. Granulation experiments performed by Butensky and Hyman (1971) were also performed on a rotary drum granulator of similar dimensions to the one used in this study. Interestingly, the present PB model also displayed a reduced sensitivity towards the drum loading also seen in Figure 4.11, in addition to ensuring validation of the GSD profiles.

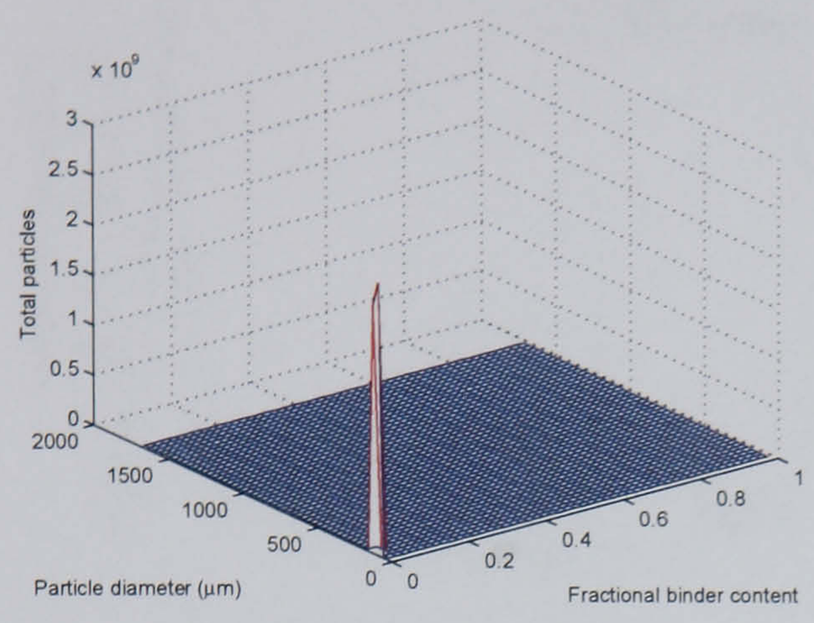

(a) t = 0 sec

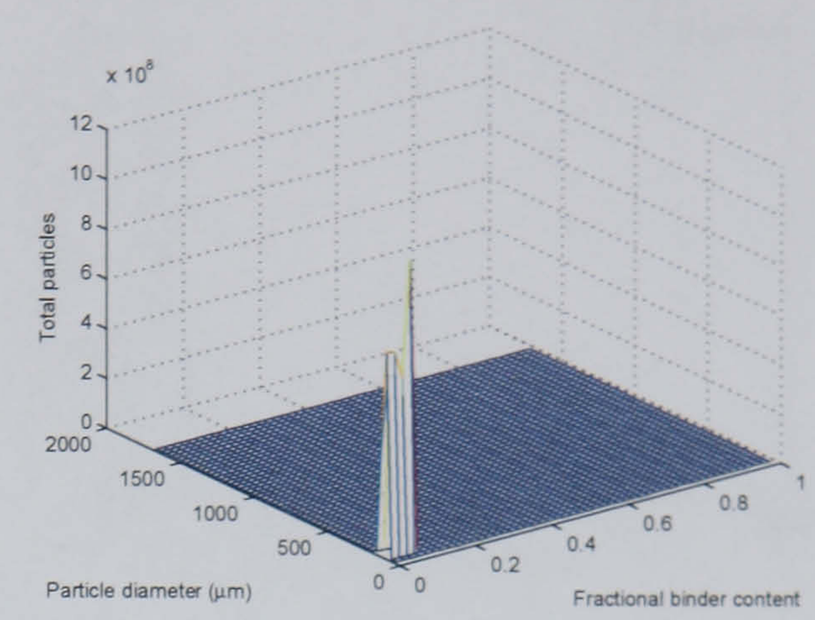

(b) t = 20.01 sec

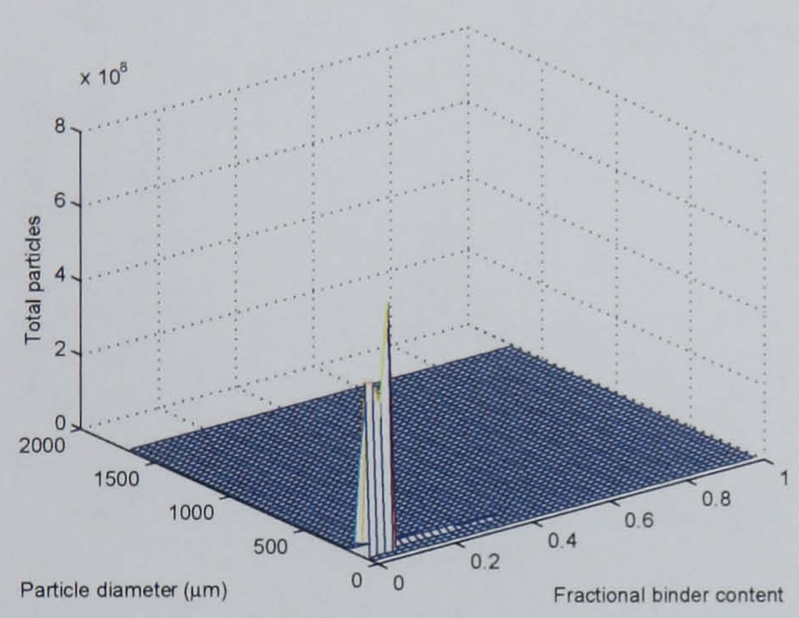

(c) t = 25 sec

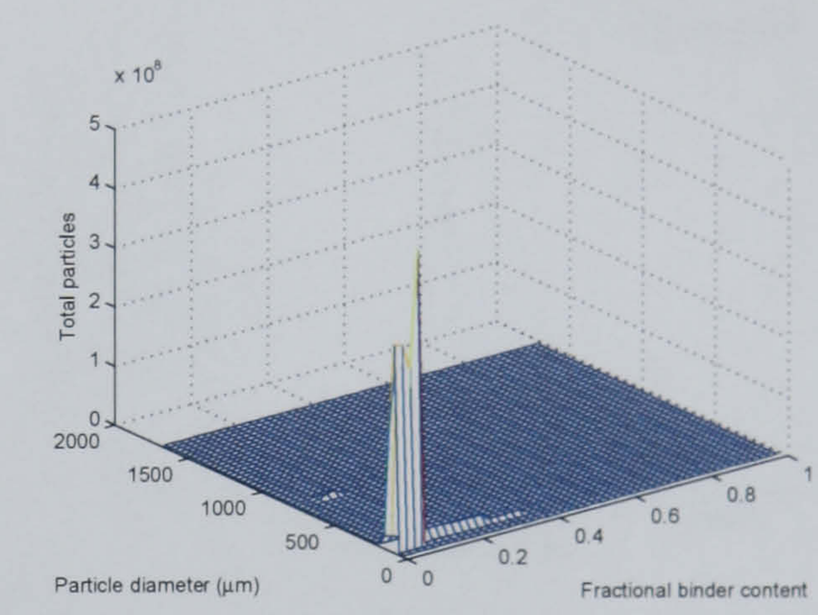

(d) t = 30 sec

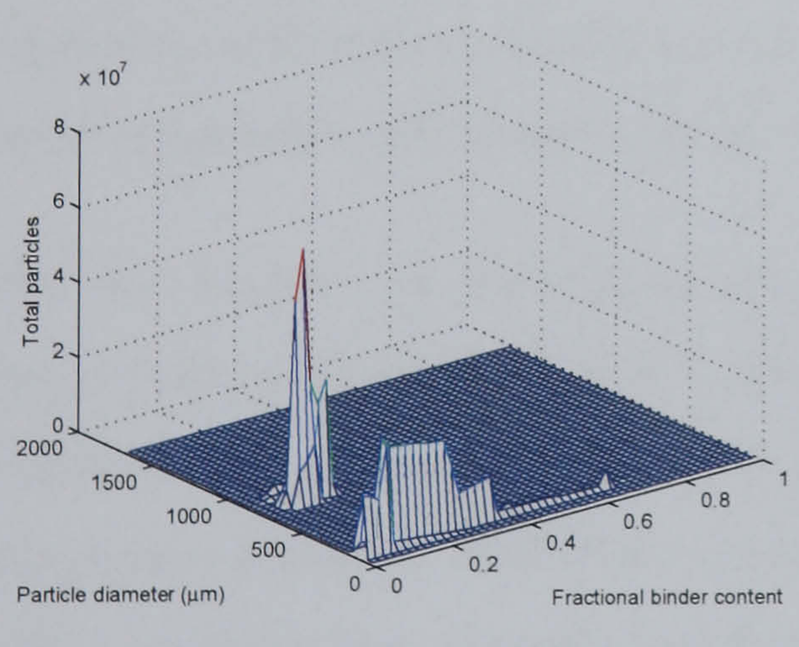

(e) t = 180 sec

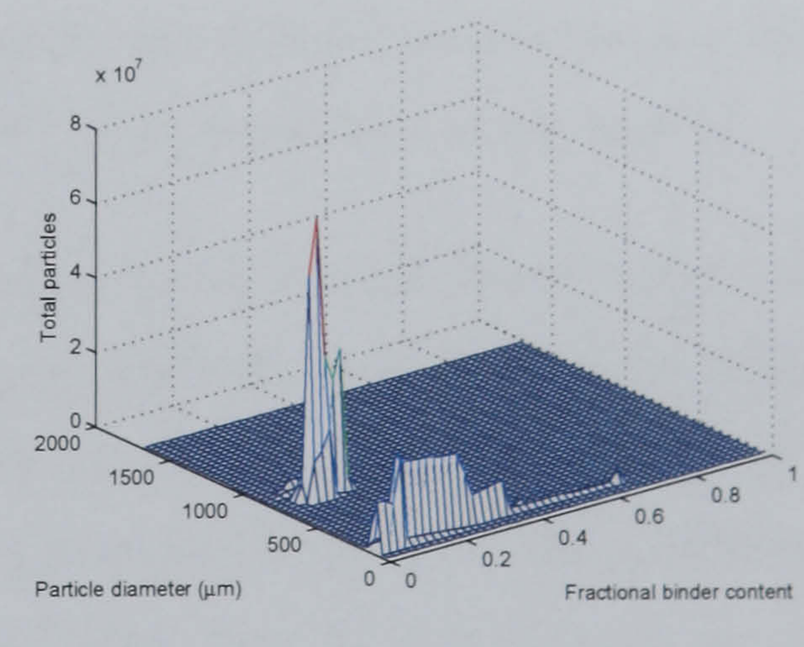

(f) t = 900 sec

Figure 4.8: Two-dimensional visualisation for the evolution of the granule size distribution at varying time instances, where the particle size and the fractional binder content are shown along each coordinate axes. The results correspond to a binder-to-solids ratio of 0.11 and a drum load of 1.5 kg of $CaCO_3$ powder (case 1).

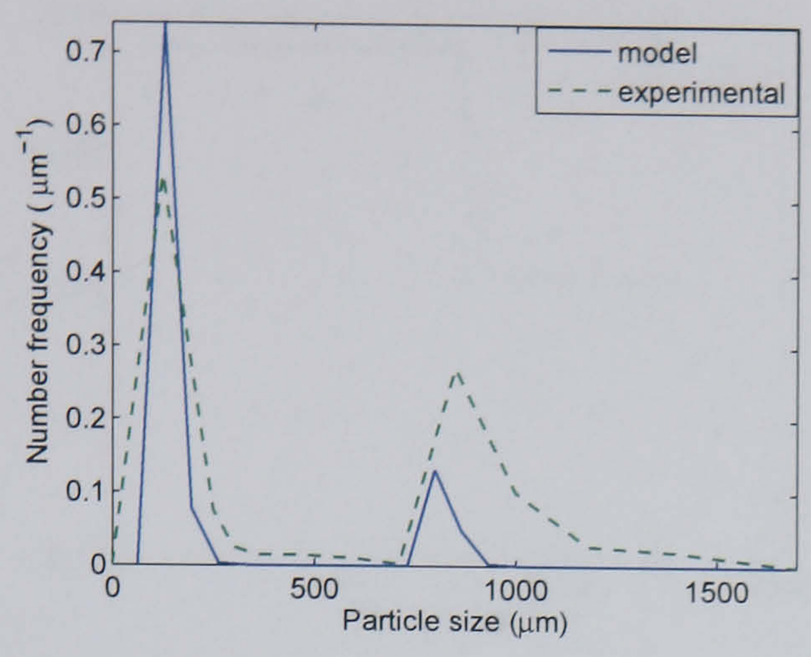

(a) t = 3 min

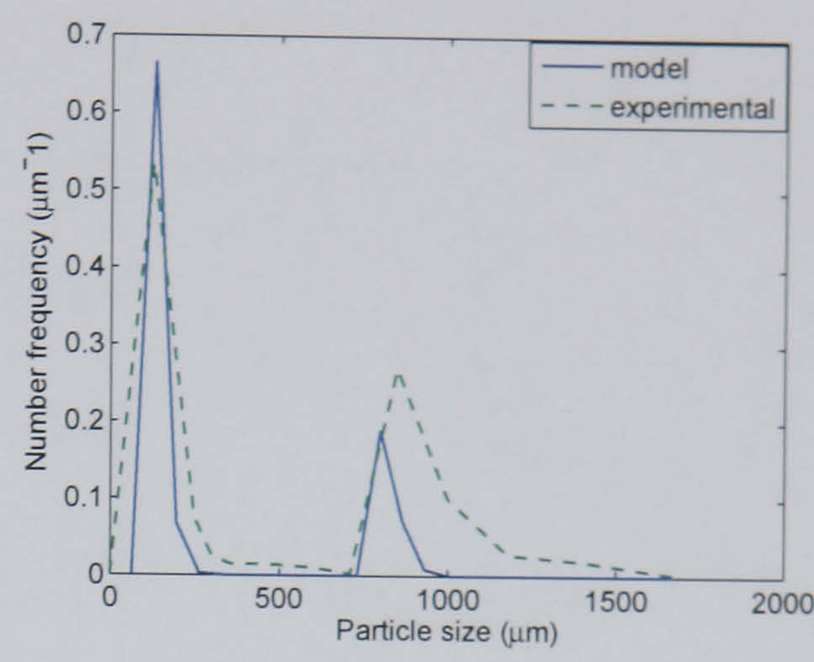

(b) t = 5 min

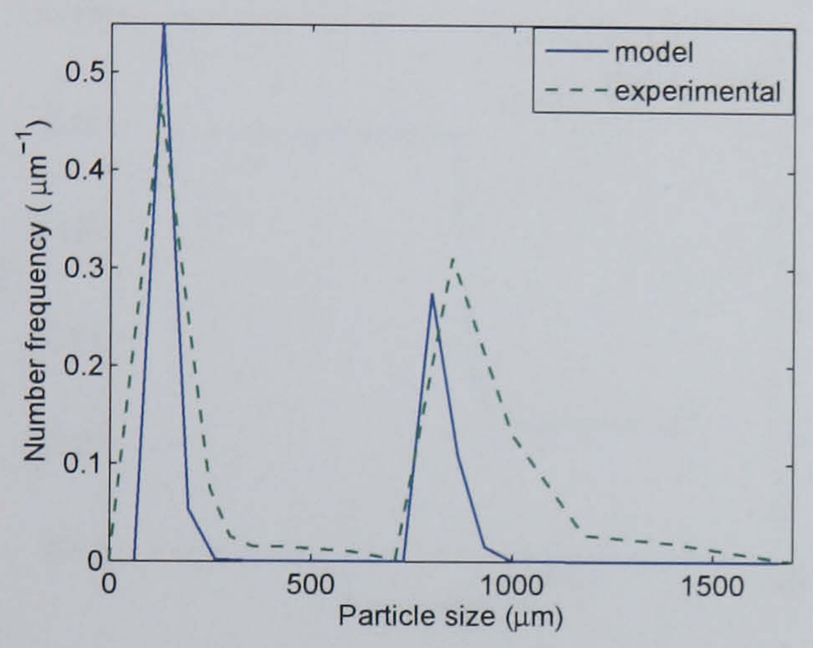

(c) t = 10 min

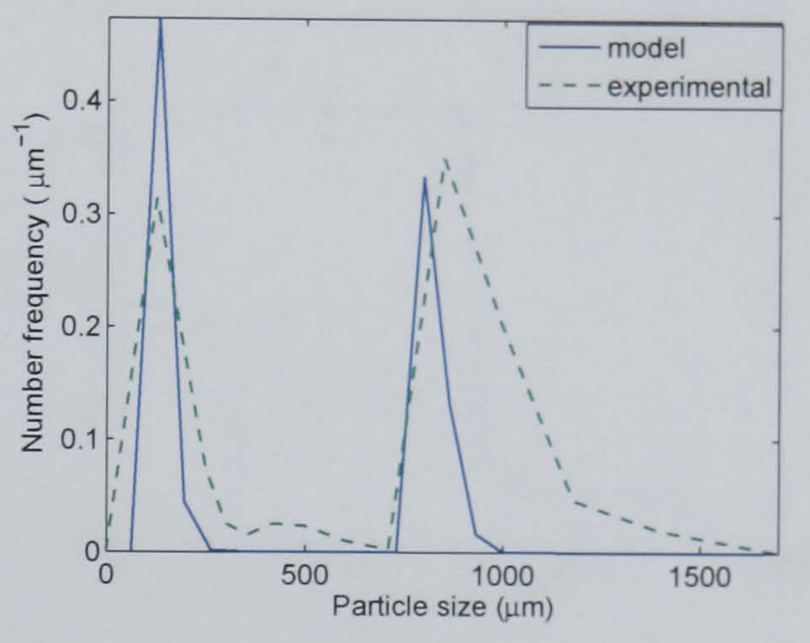

(d) t = 15 min

Figure 4.9: Comparison between model predictions on the granule size distribution at various time instances with data derived from batch granulation experiments for the case where the binder-to-solids ratio of 0.12 and a drum load of 1.5 kg of $CaCO_3$ powder (case 2).

The time profiles for the average granule diameter, fractional binder content and the average porosity is shown in Figures 4.12(a)-(c), respectively, for both model predictions and experimental measurements. Whilst the granule size was given particular emphasis as it is an important variable in the industry employing granulation processes, the validation of the secondary variables (*i.e.* porosity and fractional binder content) is also necessary to ensure that the model is capable of capturing experimentally-observed trends caused by changes in the process operation conditions. This will ensure the predictive capability of the PB model under wide operating conditions.

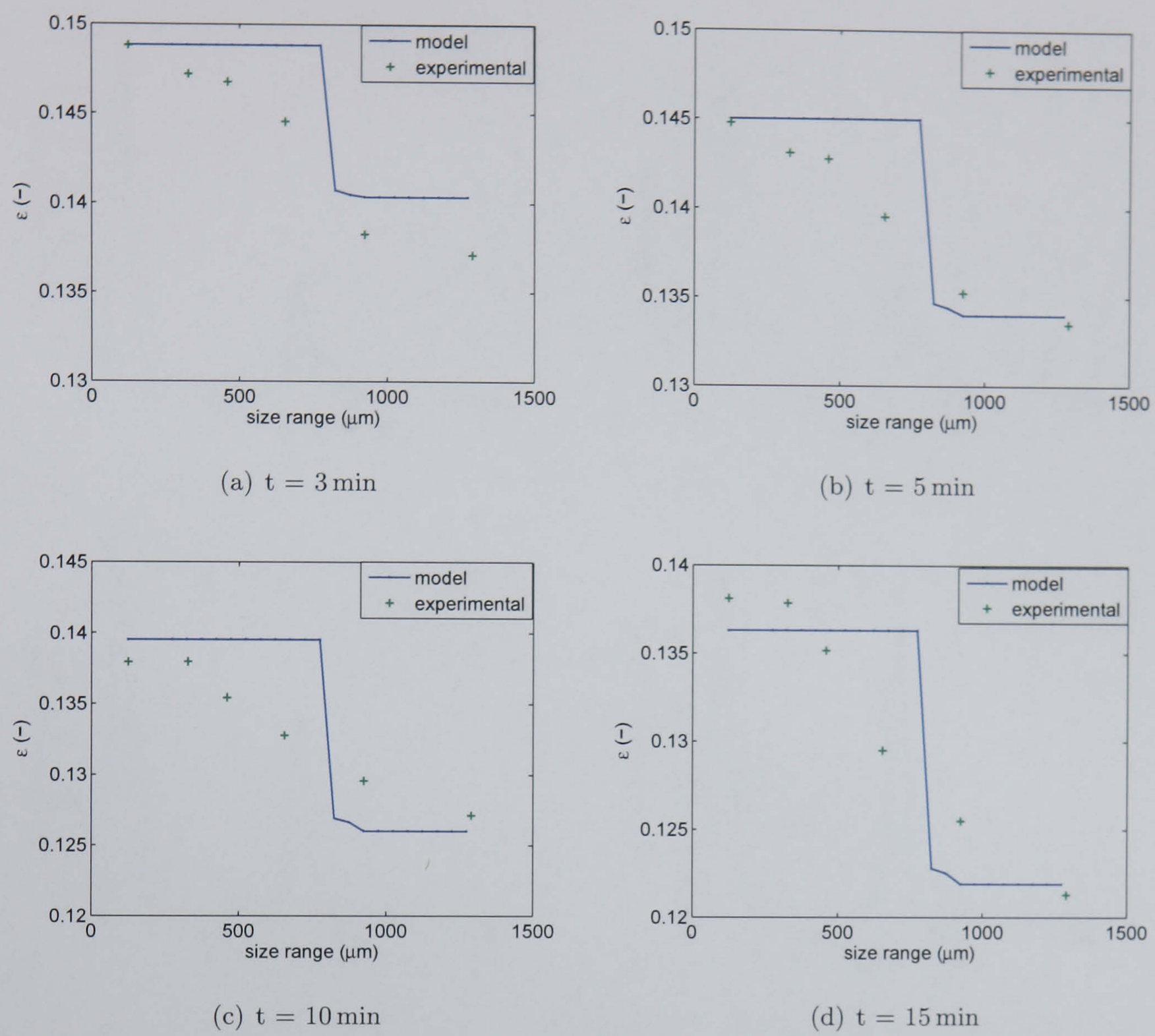

(a) t = 3 min (b) t = 5 min

(c) t = 10 min (d) t = 15 min

Figure 4.10: Comparison between model predictions on the distribution of granule porosity at various time instances with data derived from batch granulation experiments for the case where the binder-to-solids ratio of 0.12 and a drum load of 1.5 kg of $CaCO_3$ powder (case 1).

4.4.2 Dimensional analysis

The mechanical properties of $CaCO_3$ pellets were measured in order to relate the strength of granules at different strain rates *i.e.*, granules within the granulator will be subjected to a range of strain rates by virtue of the fact that not all granules will be moving with the same velocity. The two dimensionless groups used during this analysis were given in Equations (4.3) and (4.4), the dimensionless strength (Str^*) and the capillary number (Ca), respectively. In this section, the dimensionless analysis is used for two purposes, (i) to characterise the mode of breakage by relating the dynamic yield stress to the corresponding strain rates and (ii) use these findings to explain the observations made during the granulation experiments.

In Figure 4.13(a), the stress applied to the pellet is plotted against the natural strain,

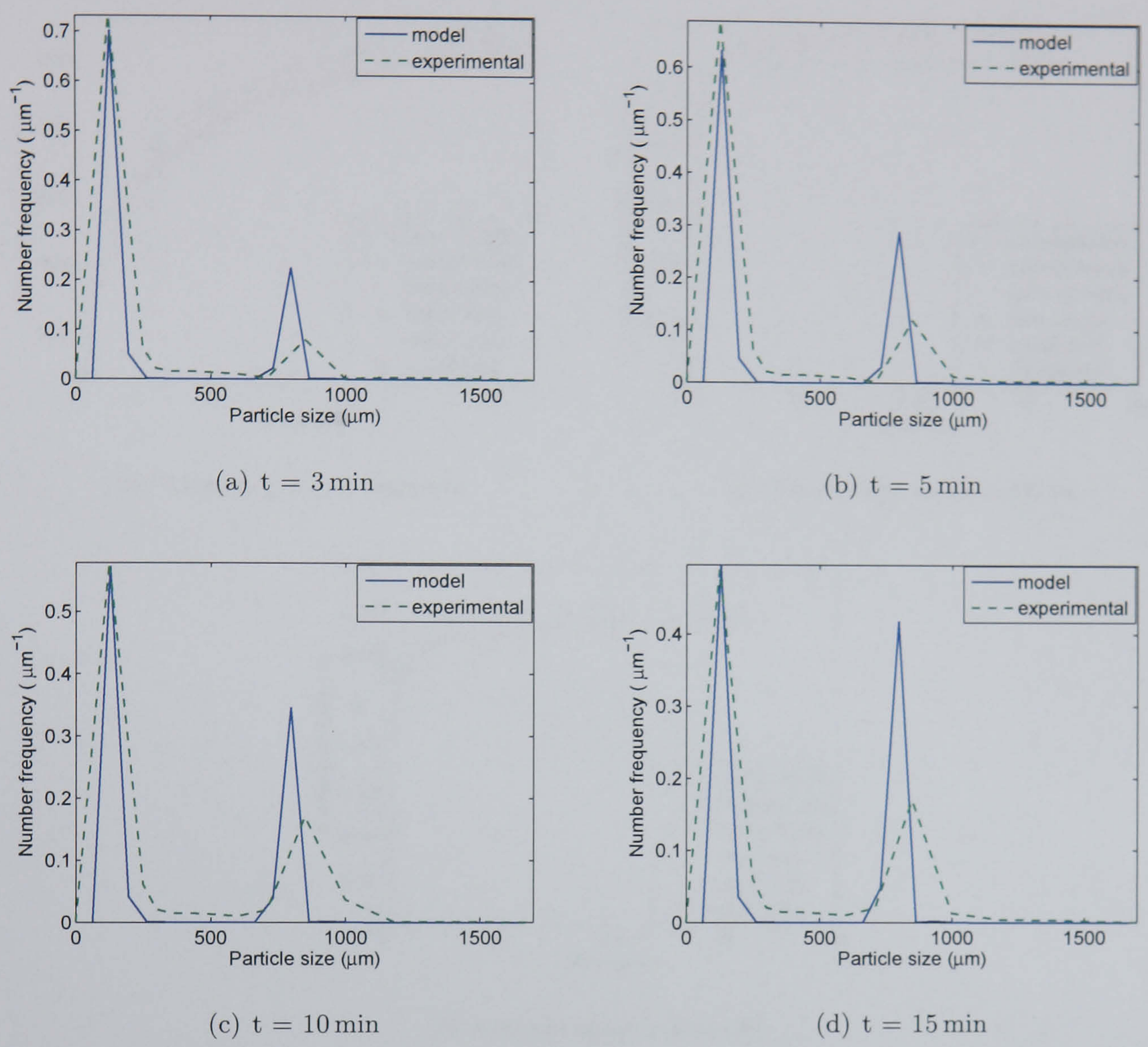

(a) t = 3 min (b) t = 5 min

(c) t = 10 min (d) t = 15 min

Figure 4.11: Comparison between model predictions on the granule size distribution at various time instances with data derived from batch granulation experiments for the case where the binder-to-solids ratio of 0.11 and a drum load of 1.75 kg of $CaCO_3$ powder (case 3).

which is a measure of the extent of deformation of the pellet based on the change in the pellet height as it is compressed. It can be seen for a particular strain rate used during pellet compression tests, the peak flow stress passes through a maximum then taken as the yield stress. Figure 4.13(b) is then obtained by re-plotting the yield stresses at different strain rates. The peak flow stress and the strain rates are both normalised by the adhesion tension ($\gamma^{LV} \cos\theta$) to generate Figure 4.14.

Figure 4.14 reveals the importance of the need to consider strain rates in granulators for a particular setting. At low strain rates indicated by a low Ca (Region I), Ca$< 10^{-4}$ the dimensionless strength (Str*) of the granules is insensitive to the low strain rates in the granulator. Low Ca means that inter-particle friction and capillary forces are dominant over

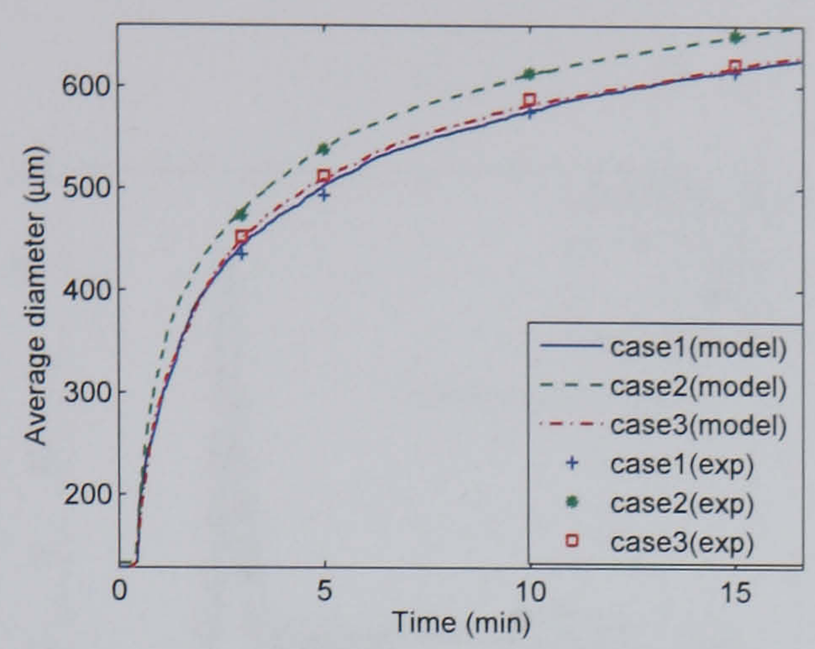

(a) Average granule diameter.

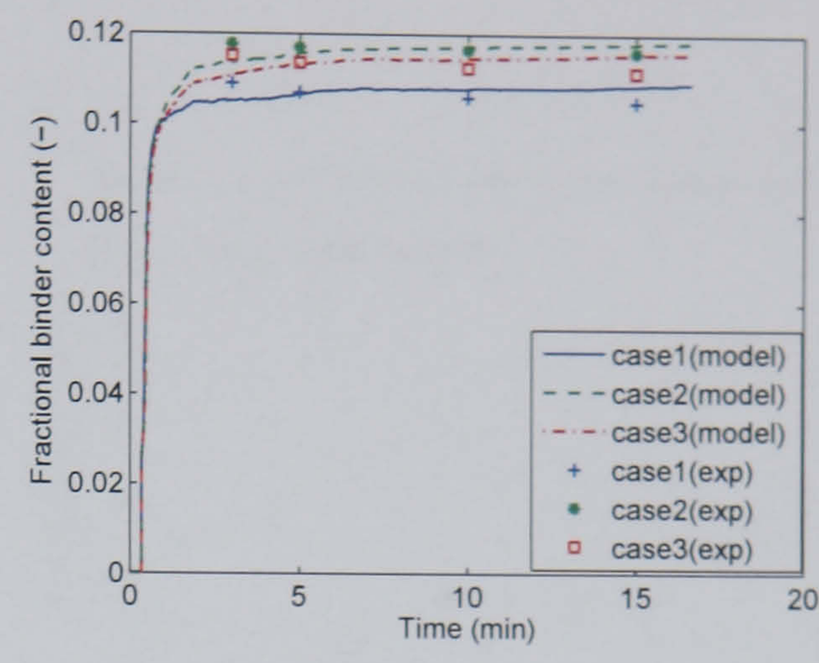

(b) Fractional binder content.

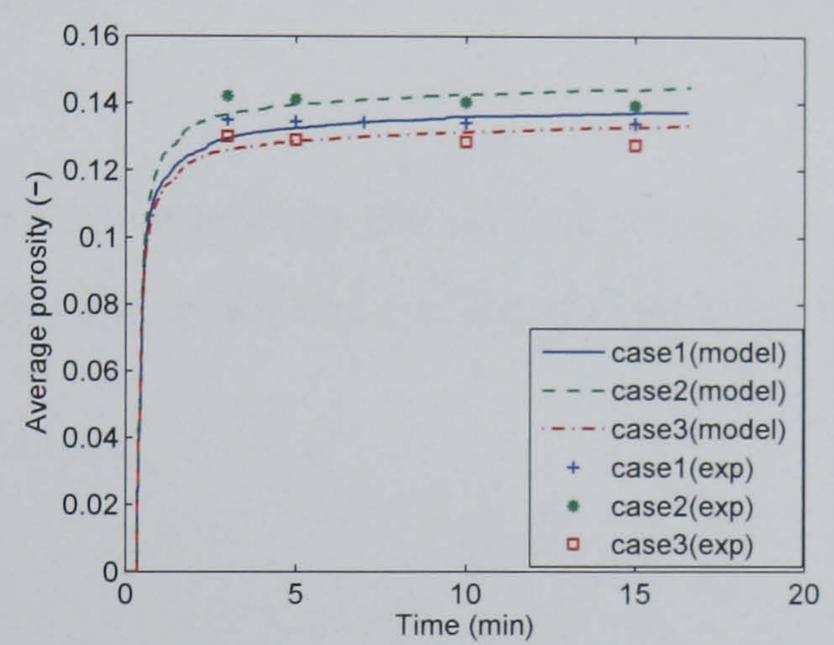

(c) Average granule porosity.

Figure 4.12: Evolution of the average granule diameter, fractional binder content and the average granule porosity for cases 1, 2 and 3 with comparisons made between model predictions and data derived from batch granulation experiments. Cases 1 and 2 correspond to a binder-to-solids ratio of 0.11 and 0.12, respectively, and an initial drum load of 1.5 kg with $CaCO_3$ powder. Case 3 corresponds to a target binder-to-solids ratio of 0.11 with an initial drum load of 1.75 kg with $CaCO_3$ powder.

the viscous effects of the binder. Granules in Region I will tend to break via micro-fractures through crack propagation (cracking/brittle) since the granules have a lower propensity to deform under applied stresses. In contrast, granules in Region II Ca$> 10^{-4}$, are able to deform much more with granule failure exhibiting plastic flow prior to breakage. In Region II, Str* is a strong function of the operating strain rate. Thus, in order to predict the granulation behaviour, say, for different combinations of powder and liquid binder, one must ensure that the granulator is operating at high strain rates (velocities) in order to probe a mean-

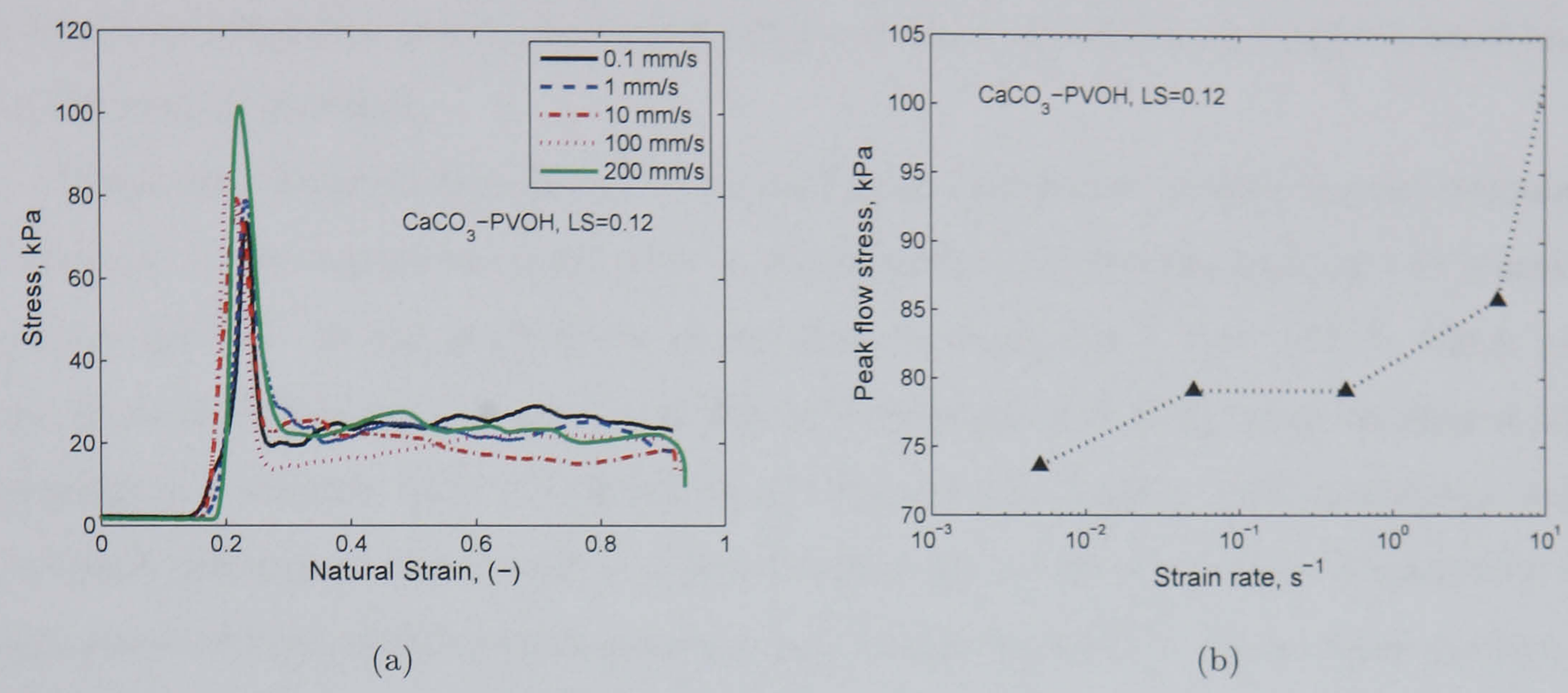

(a) (b)

Figure 4.13: Profile of the stress against the natural strain (a) and (b) the peak flow stress against varying strain rates for preformed $CaCO_3$ pellets with a fractional binder content of 0.12.

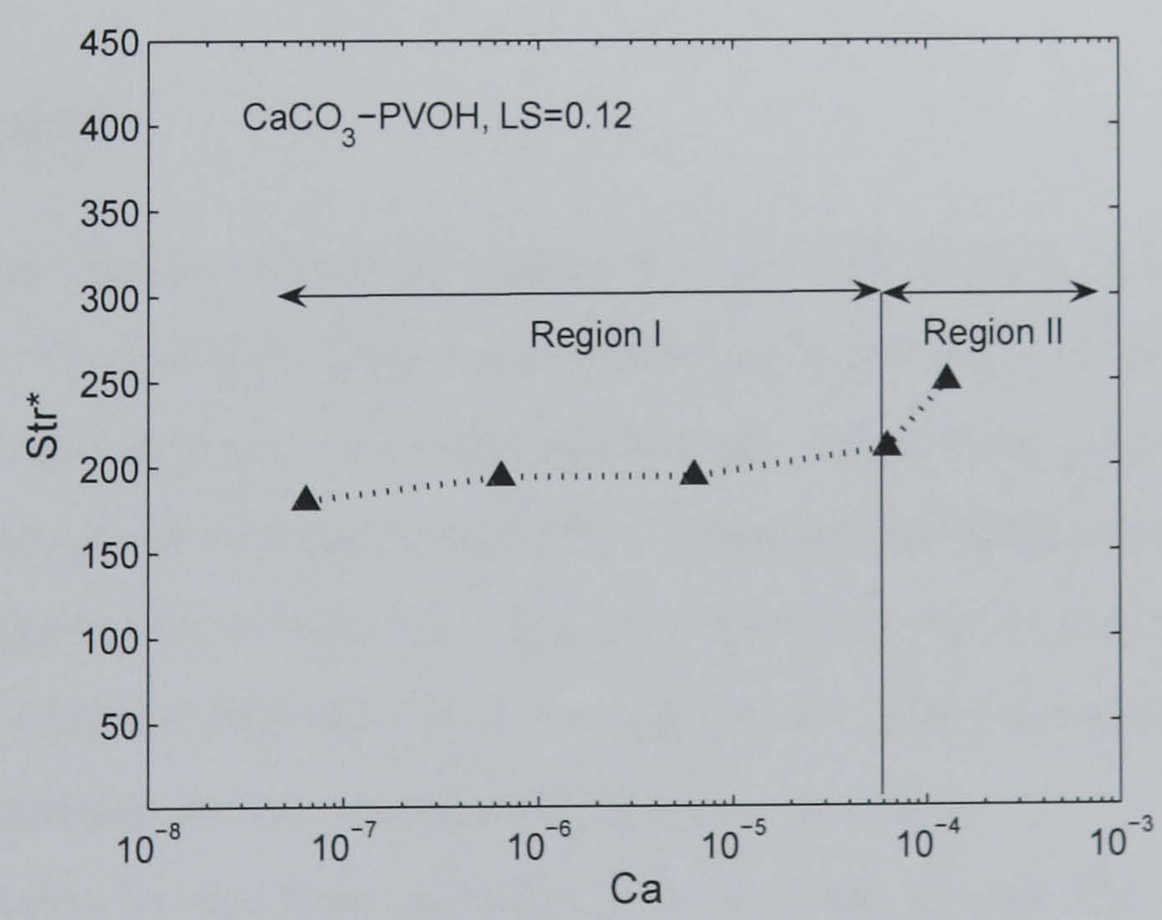

Figure 4.14: Profile of the dimensionless strength (Str*) against the capillary number (Ca) for $CaCO_3$ pellets with fractional binder content of 0.12.

ingful comparison between different granulating materials, because, it is only in Region II that granule strength is most sensitive to the strain rate. Little information governing the granulation behaviour can be drawn from Region I since the binder viscosity has little impact on the granule strength.

Using the interpretations from the dimensionless analysis with the observed granulation behaviour in the experiments can yield a more qualitative understanding of the kinetics of granule growth. In the granulation experiments of Section 4.4, Ca $\approx 10^{-4}$, which places our granulating system in Region II of Figure 4.14 where the $CaCO_3$ granules have a higher propensity to deform. Hence, agglomerate growth via consolidation and coalescence was the prevalent mechanism over breakage. From the granulation theory, particle deformation is an important criterion facilitating coalescence as it enables particles to form a large contact area as well as to dissipate some of the initial kinetic energy of the particle via plastic and elastic losses. Adetayo and Ennis (1997) also iterated the fact that the critical size for successful coalescence is strongly affected by the granules ability to deform. Kristensen et al. (1985) also noted that the strain behaviour of granules was primarily controlled by the extent of liquid saturation of the granules, which in turn affected the ability of granules to deform. Thus, granules with a higher liquid saturation will exhibit faster growth rates due to aggregation as a direct consequence of the granules ability to deform.

4.5 Summary

In this chapter the kinetics of granule growth for a granulating mixture consisting of calcite powder and a polyvinyl alcohol binder was studied on a laboratory scale rotary drum granulator. Three particle traits were measured, namely the granules size, fractional binder content and porosity. These measurements revealed the heterogenous distribution of these properties across the entire particle size spectrum. The population balance model incorporating mechanistic descriptions for the nucleation and the aggregation phenomena was validated with the granulation experiments for the aforementioned particle traits.

Model predictions for the time evolution of the average granule size, the average granule porosity and the average fractional binder content of granules yielded good correspondence with the experimentally measured data. In particular, the model was able to track the GSD and the distribution of the granule porosity across the particle size range. The effects of variation in the liquid-to-solid ratio in the recipe was validated. In addition, the drum loading

was modified to probe the effects of this process variable on the granulation behaviour. The results suggested that the granulation behaviour was insensitive to the drum loading (related to the powder bed depth) with respect to the measured GSD, which was coincident with the observations made by Butensky and Hyman (1971).

Thus, these are valuable albeit early studies that have provided a demonstration of the validity of the population balance model as a predictive tool and as a suitable framework for the modelling of systems with multiple internal coordinate properties distributed across the particle population. In this present study, only a portion of process variables were probed in the design of experiments, the model nonetheless has shown that by incorporating the physicochemical properties of the binder solution (*e.g.* surface tension, viscosity, contact angle and the spreading coefficient) and the material properties of the powder (*e.g.* density, average size, size distribution, height of surface asperities, and the effective porosity of the powder) explicitly into the kernels of the underlying granulation phenomena (*e.g.* nucleation and aggregation) will provide an integrated PB model with the potential to aid scale up, and the possibility of predicting the effects of formulation changes or the effects of new granulation recipes on the granulator operation, with a significant reduction in the number of carefully considered experiments. The use of dimensional analysis to correlate the dynamic mechanical properties of the granules represented by Str* with the granulator operating conditions has provided a separate means to ensure the richness and suitability of the data used for model validation, thereby providing greater fidelity (Iveson et al., 2002).

In conclusion, the proposed PB model, which attempts to address the issue of bridging the link between different length scales in traversing from the microscale to the macroscale, by appropriately transforming the particle-level model to a form which can then be *embedded* into the process-level model, has been addressed with encouraging preliminary results. The process level behaviour of the granulation process is exemplified by the GSD, which is described by the PB model. The microscale phenomena comprise of the underlying granulation phenomena such as nucleation and aggregation, and the physics that describe the phenomena.

Chapter 5

Studies of granulation variables on process inferences

5.1 Introduction

In previous chapters, the granulation process has been shown to be markedly affected by the formulation properties of the agglomerating material feed (solid and binder), and the conditions applied during the granulation process. Their effect on the outcome of the resultant granule properties (*e.g.* size and morphology) has been analysed. Studies involving the effects of formulation properties in tandem with influences from the process operating parameters will be necessary in discerning the complex interactions amongst the myriad of variables affecting the process. This is feasible with the present model based on mechanistic kernels that explicitly account for the properties of the materials as well as the process operating conditions.

During scale up of new formulations, it becomes important to rapidly analyse process alterations that would be necessary for the new materials in order to obtain the desired granulation. For example, given the fundamental properties of the new formulation materials (surface energies, contact angle, densities, *etc.*), it is necessary to determine the operating variables (binder spray, mixing rate, equipment type) that will ensure the attainment of target granule properties. The present model will be a crucial aid in this regard, to complement and minimise experiments.

There are a number of equipment types available for carrying out granulation, which include fluidised bed granulators, high shear mixers, and drum granulators. The number of

process control handles will therefore depend on the equipment type. For instance, the air flow rate controls the extent of bed fluidity and is applicable to fluidised bed granulators but not for high shear mixers. However, there are a few potential manipulatable variables that are common to most granulators, with some playing a more dominant role than others, and include the liquid flow rate, mixing rate, the temperature at which granulation is performed and the granulation processing time. In addition, for the continuous granulation process, the powder feed rate and the recycle ratio may also be used as process manipulating variables.

In granulation, a good dispersion of the binder is essential if a wide particle size distribution is to be avoided. If the initial powder has a wide particle size distribution (*e.g.* bimodal granule size distribution), it may need a long granulation time to obtain the desired narrow granule size distribution. This scenario may arise as a consequence of maldistribution of the binder coupled with poor mixing (Knight et al., 1998). The factors that can influence binder dispersion include the *delivery method* adopted (*e.g.* pouring, melting and spraying) and the mixing rate. Thus, for the purpose of achieving optimal binder distributions, spraying of *binder droplets* of small diameter are commonly employed in order to ensure that there is maximum coverage of the powder surface, thereby avoiding over wetting and causing preferential areas of the powder bed to undergo faster growth than other drier areas of powder (Holm et al., 1983, 1984). The *mixing rate* ensures that the whole powder bed receives an equal amount of binder by ensuring a new patch of previously unwetted powder passes through the spray zone. Therefore, the controllability of the granulation process may be effected by strategically manipulating the control handles (*e.g.* liquid flow rate). Given that there is a qualitative understanding of the effects of each manipulative variable on the process outputs, there still remains the need to formulate a control strategy that will enable a more precise tuning of the manipulated variables during the process.

A number of studies have addressed this issue by developing a control strategy in the form of an optimisation problem (model predictive control) (Pottmann et al., 2000; Gatzke and Doyle III, 2001). In these problem statements, the objective may be to maximise the plant throughput; minimise the amount of recycle containing off-spec product granules (*i.e.* granules that do not conform to a predefined granule size range); to achieve the desired granule size distribution in the shortest time. The decision variables are the optimal moisture content, mixing rate, and the material loading.

The aim of this chapter is to use the population balance (PB) model that was introduced

in Chapter 3, with the proposed mechanistic descriptions for the nucleation phenomenon and the aggregation phenomenon, for providing model predictions on the influences of the granulation process. In order for this study to be fully beneficial, a range of conditions were simulated that would be encountered in real processes, to elucidate the effects of changes in the material formulation to be granulated or the equipment characteristics (*e.g.* effects of spray droplet sizes) on the granules. This undertaking is different from other studies in that a mechanistic model is now used to complement previous studies that were based purely on experimental trials. Effects due to different formulation properties pertaining to the liquid binder and the powder in conjunction with particular equipment characteristics are investigated. A summary of the case studies considered are given below:

- Effects of different design *formulation properties* for the granulation recipe. This is a marked improvement of current population balance models, which enables the prediction of the possible effects attributed to material property differences.
- The effects of the operational *powder properties*, which have often been seen as contributory factors influencing the growth behaviour of certain granulation recipes: powder porosity, feed size distribution, and the sizes of the constituent feed particles (primary particles).
- Changes to the operation conditions has been represented in this study by varying the liquid binder droplet size, which has been recognised as one of the key operating variables in granulation.

5.2 Formulation properties and process conditions

5.2.1 Effects of formulation properties

The effects of the fundamental material properties on the behaviour of the granulation process is now investigated. In particular key material properties pertaining to the liquid binder and the powder solid that are investigated include the liquid surface tension, the contact angle, and the effective porosity of the powder bed. The binder liquids considered here include hydroxypropyl cellulose (HPC), polyethylene glycol (PEG 200), sodium dodecylbenzene sulphonate (NDBS) and water. Two powder substrates were considered and these were glass ballotini and lactose. The specific powder-binder combinations used for each granulation formulation

is given in Table 5.1 showing the relevant physicochemical properties. The simulation parameters pertaining to the nucleation model, consolidation model, and the aggregation model are shown in Table 5.2. The following granulation conditions are used in carrying out the investigative studies into the sensitivity of the process to different formulations:

- Sufficient time is allowed for complete drop penetration into the porous powder bed mass *i.e.*, the bed turnover rate relative to the drop penetration time. Thus, the volume of binder from the droplet that remains on the powder surface is zero, *i.e.*. $V(t) = 0$ in Equation (3.42) (see Section 3.5.3).
- The granulator is operating within the droplet controlled regime whereby each granule nucleus is formed from a single binder droplet that lands on the powder bed, which corresponds to a spray flux of $\Psi_a = 0.085$ (Equation 2.1).
- Binder distribution is considered optimal, *i.e.*, liquid binder is uniformly distributed amongst all the particles.

Table 5.1: Summary of formulation properties.

Powder	ε_{eff}	Binder fluid	θ (°)	Surface tension (γ^{LV}) (mN/m)
Lactose	0.61	HPC	35	42.5
Lactose	0.2	PEG 200	56	43.7
Lactose	0.2	NDBS	52	31.0
Glass ballotini	0.2	Water	52	72.1

θ is the contact angle.

Table 5.2: Simulation parameters for consolidation, nucleation and aggregation.

Parameter		Value
A_0	(nucleation model)	1×10^{15} mol/m^3
K	(nucleation model)	6×10^5 (-)
c_1	(aggregation model)	5×10^6 (-)
c	(consolidation model)	5×10^{-5} (-)

In Figure 5.1(a), the evolution of the average granule diameter for the four granulation recipes are shown. A common trend is observed using the lactose-NDBS formulation as a

reference for the following discussion, a rapid increase in the particle size corresponding to the formation of nuclei as binder is sprayed into the granulator at a flow rate of $2 \times 10^{-6}\,m^3/s$ for 86 sec. Soon after the formation of the initial granule nucleus, these nuclei particles continue to grow in size by aggregation, aided by consolidation. As they consolidate reducing their size, there is an increase in the particles liquid saturation such that the binder is squeezed from within the particles and onto the surface of the particles. This process serves to promote coalescence, which is indicated by the continued increase in the average particle diameter. At approximately 1 min into the process, larger and more stable granules are formed which compact further through consolidation, repeating the process of becoming surface wet and growing via aggregation. Beyond 10 min the process is well underway and a steady increase in granule size is observed as the granules grow, also predominantly by aggregation with consolidation. As the particles undergo nucleation and aggregation, there is also an associated reduction in the number of particles, which is shown in the corresponding Figure 5.1(b).

As mentioned at the beginning, the aim of this study is to determine the extent of the influence that different granulating formulations have on the overall behaviour of the process. In Figure 5.1(a) different binders have been used on glass ballotini and on a lactose powder substrate, in which a clear effect is seen with different binders causing different rates of granule growth, as reflected in the average granule size. A similar effect is also translated in the rate at which the total particles decrease as seen in Figure 5.1(b). These observed effects can be interpreted using the physicochemical properties as outlined in Table 5.1. Ignore for the time being the lactose-HPC formulation as it will be discussed later. The lactose-NDBS recipe shows that better granulation is achieved (based on a particular granule size being achievable in a shorter granulation time), followed by lactose-PEG 200 and lastly glass ballotini-water. The order of the granulation performance can be explained using the spreading coefficient corresponding to each solid-liquid combination, as shown in Table 5.3.

Table 5.3: Spreading coefficient evaluated from liquid binder surface energies.

ID	Formulation	Spreading coefficient (λ) (N/m)
case 1	Lactose-NDBS	-1.7×10^{-2}
case 2	Lactose-PEG 200	-1.9×10^{-2}
case 3	Glass ballotini-Water	-2.8×10^{-2}

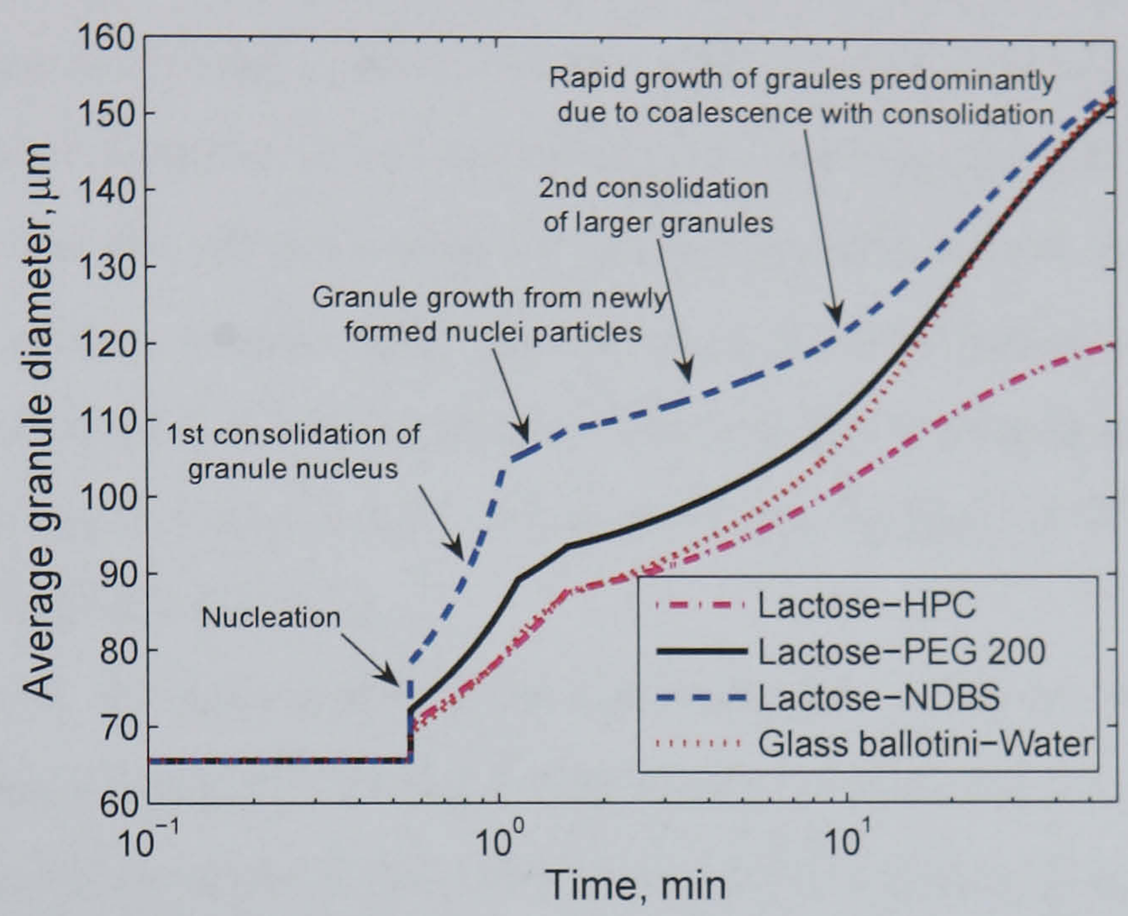

(a)

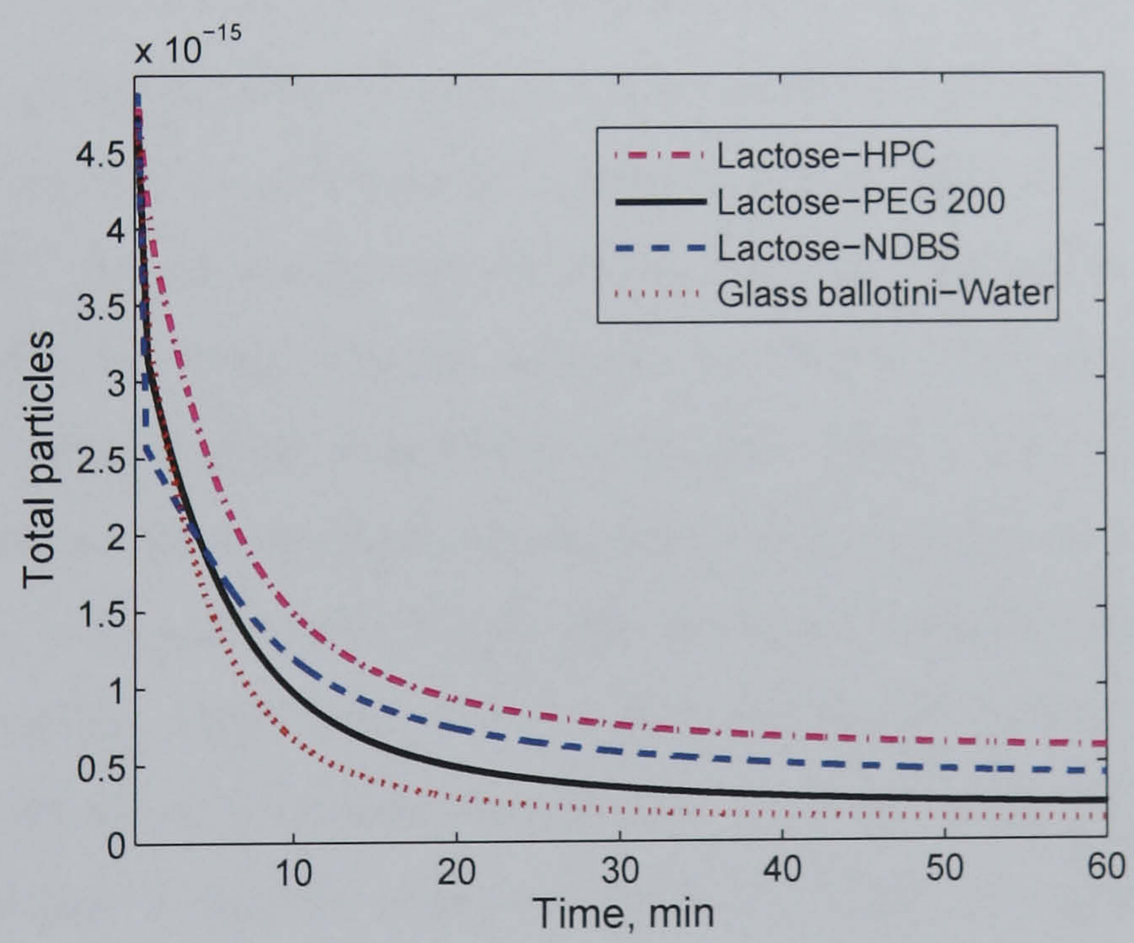

(b)

Figure 5.1: Profile of the average granule diameter (a) and the total number of particles (b) over the course of a one hour simulated granulation process for different granulation recipes.

Recall that the spreading coefficient (λ) need not always be positive. But a positive λ indicates spontaneous spreading of the liquid over the solid substrate. In this case, $\lambda_3 < \lambda_2 < \lambda_1$. Thus, the binder NDBS provides better wetting of the powder when compared to either cases 2 or 3. This is already a known contributory factor in promoting better granulation (Iveson et al., 2001). Better wetting of the powder by the binder enables a higher proportion of powder particles to be coated with a liquid film allowing them to coalesce more easily. Note also that the contact angles for each of the binders in cases 1-3 are similar. This implies that low contact angles, although necessary, is by no means sufficient in predicting the granulation performance. Other indicators such as the spreading coefficient must also be used. This result clearly corroborated the experimental findings of Thielmann et al. (2008), which was described in Section 3.5.2.

In Figure 5.2(a), the time profile of the mean diameter of nuclei particles is shown, with supporting information that the lactose-NDBS recipe is indeed the better candidate for granulation, as nucleation occurs at a much faster rate with corresponding larger nuclei particles being formed with a diameter of 109.7 μm. In contrast, in case 3 with the lowest spreading coefficient, smaller sized nuclei particles are formed (88.7 μm), with an associated rate of depletion of primary particles being the least *i.e.*, fewer primary particles are participating in the creation of a granule nucleus and thereby it takes longer to deplete all the primary particles (see Figure 5.2(b)). A consequential implication of an inappropriate choice for granulation recipes, for example the selection of an inappropriate binder with a particular powder, will have the effect of increasing the granulation end time. This is better exemplified in Figure 5.1(a), which shows for the attainment of a particular average granule size different binder solutions granulated with lactose will exhibit different endpoint times. Considering for the case of lactose-NDBS recipe, which takes 2 min of granulation before achieving a mean granule size of 110 μm. Comparing this to the formulations whereby lactose is granulated with PEG 200, a granulation time of 9 min is needed in order to obtain an equivalent average granule size of 110 μm. Similarly, for the case of granulating glass ballotini with water, a longer time of 11 min is required. The end-point granule size distribution is shown in Figure 5.3 for the four different granule formulations. The end-point GSD is the same for cases 1-3, indicating that the path does not affect the end result. Nevertheless, these findings show the effects of formulation properties on the transient behaviour of granulation, and that there is scope for the addition of binder additives to the binder formulation that will enable granulation times

to be reduced.

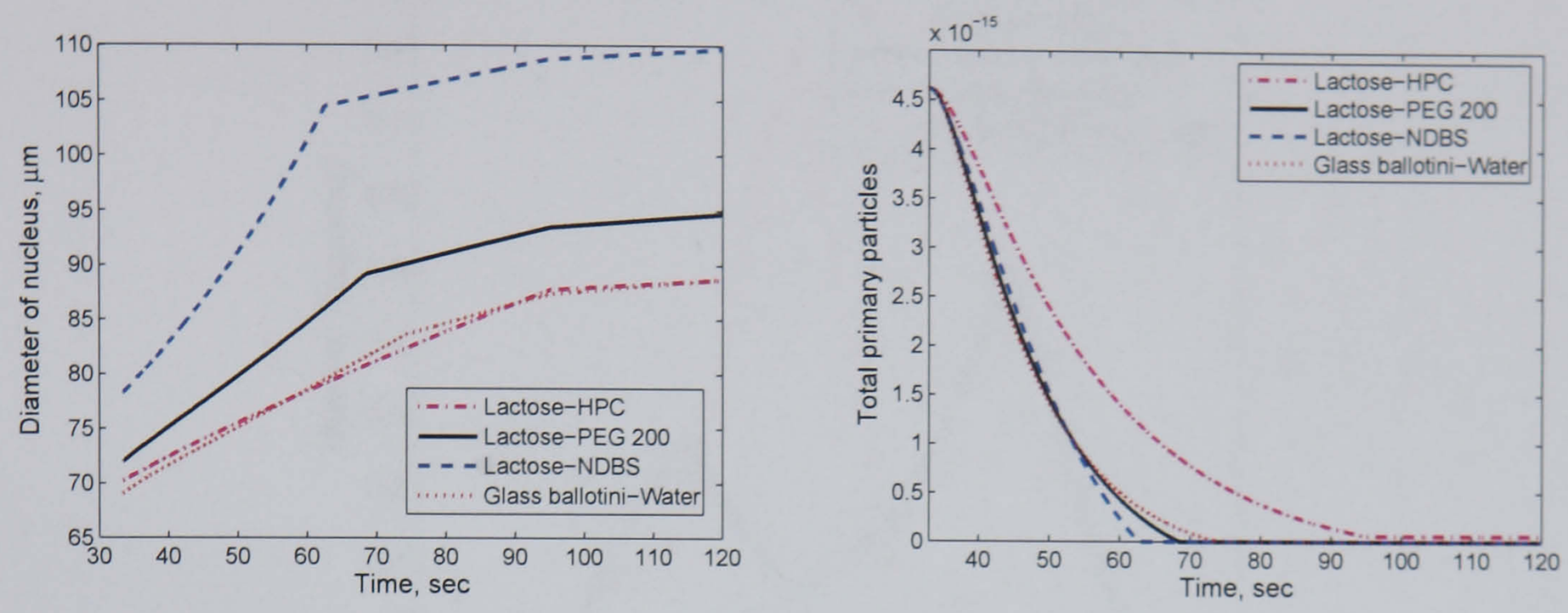

(a) (b)

Figure 5.2: Profile of the average nucleus diameter (a) and the total primary particles (b) for different granulation recipes.

The effect of the powder bed porosity was also considered as an important factor governing the behaviour of granule growth. Litster and Waters (1988) studied different iron ore blends with varying moisture holding capacities, and concluded that obtaining granule particles of a particular size was largely determined by the amount of liquid absorbed by the feed material. In light of this, the porosity of the powder was also used as a controlling parameter for the granulation process, determined by the feed material used for granulation. Figure 5.1(a) showed results of granulating a lactose-HPC formulation with an effective porosity of $\varepsilon_{eff} = 0.61$ (see Table 5.1), which is significantly higher than the other lactose formulations used. In the lactose-HPC recipe, a significantly reduced mean granule size is evident. The results are in alignment with the finding made by Litster and Waters (1988), in that a much higher amount of liquid is needed for reaching liquid saturation of the feed before liquid is available for granulation (*i.e.* liquid appearing on the surface of the particles in the form of a liquid film).

In order to isolate the effects of the powder bed porosity on the granulation behaviour, a glass ballotini-PEG 200 recipe was simulated with prescribed values of $\varepsilon_{eff} = 0.07$ and $\varepsilon_{eff} = 0.2$ with a starting primary particle size of $85.3\,\mu$m. In addition, a case whereby for the same granulating recipe, an $\varepsilon_{eff} = 0.07$ and a smaller initial primary particle size of $65.4\,\mu$m was used, to see if the size of the constituent particles have any effect on the resultant granule size. In Figure 5.4(b), larger nuclei particles are formed over the course of

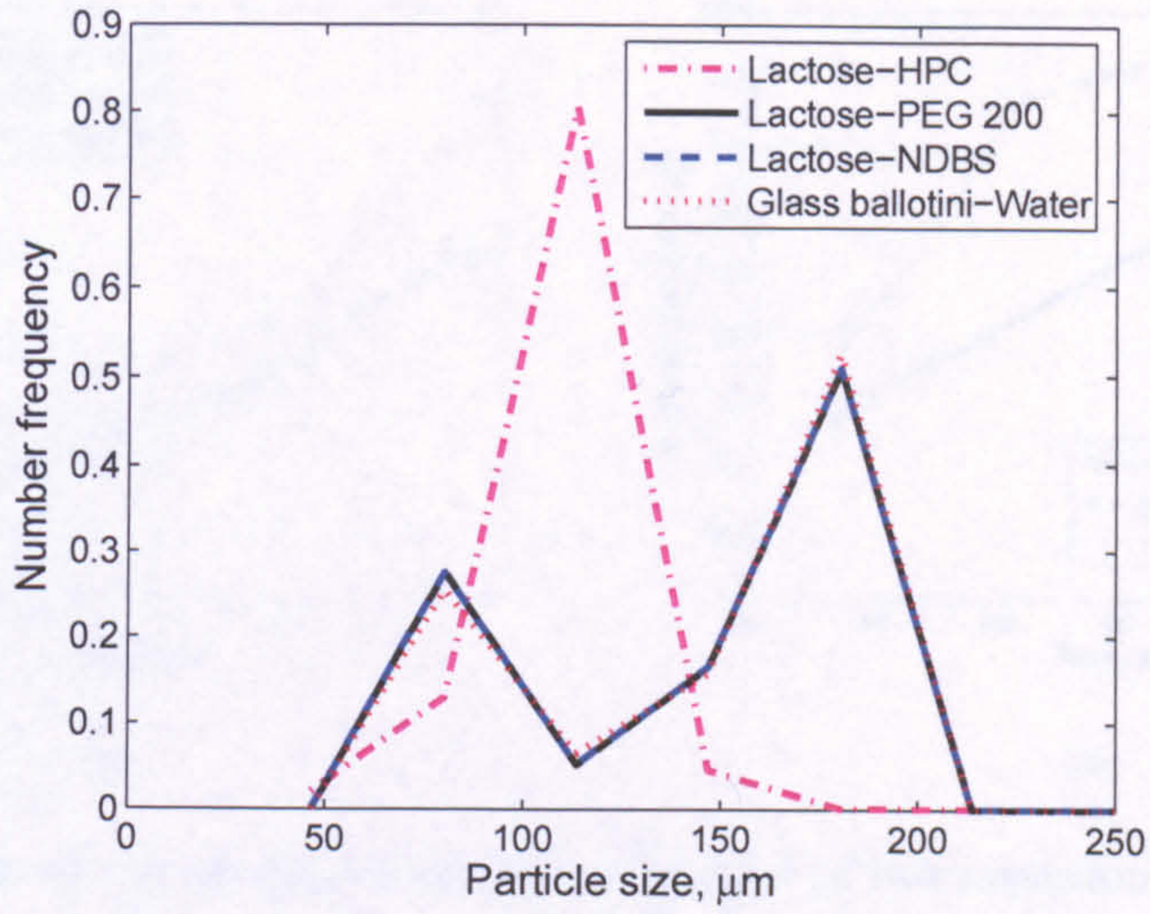

Figure 5.3: Comparison of the end-point granule size distribution for different formulations used as the granulation recipe for a one hour batch processing time.

the nucleation period with a lower effective powder bed porosity ($\varepsilon_{eff} = 0.07$) compared to a more porous powder ($\varepsilon_{eff} = 0.2$).

The maximum granule nucleus formed were 119 μm and 104 μm for the corresponding cases where the powder bed had an effective porosity of 0.07 and 0.2, respectively. The effects on the development of the nuclei particles, due to the different amounts of liquid that can be absorbed by the powder feed, is translated into the average granule size (shown in Figure 5.4(a)) attainable within the one hour granulation period. For the case where the porosity of the powder was maintained at 0.07 but with smaller primary particles of size 65.4 μm, Figure 5.4(b) shows that there is a significantly faster rate of nucleation as reflected by the rapid increase in the size of the nuclei particles when compared to the case with $\varepsilon_{eff} = 0.07$ and 85.3 μm primary particles. The results from this study on the effect of the powder bed porosity on the granulation behaviour are in agreement with the findings made by Litster and Waters (1988). In their study, Litster and Waters (1988) observed that the granulation effectiveness was significantly higher for a sinter feed with a lower porosity compared to sinter feed comprised of various ore blends with higher moisture absorbing capacities.

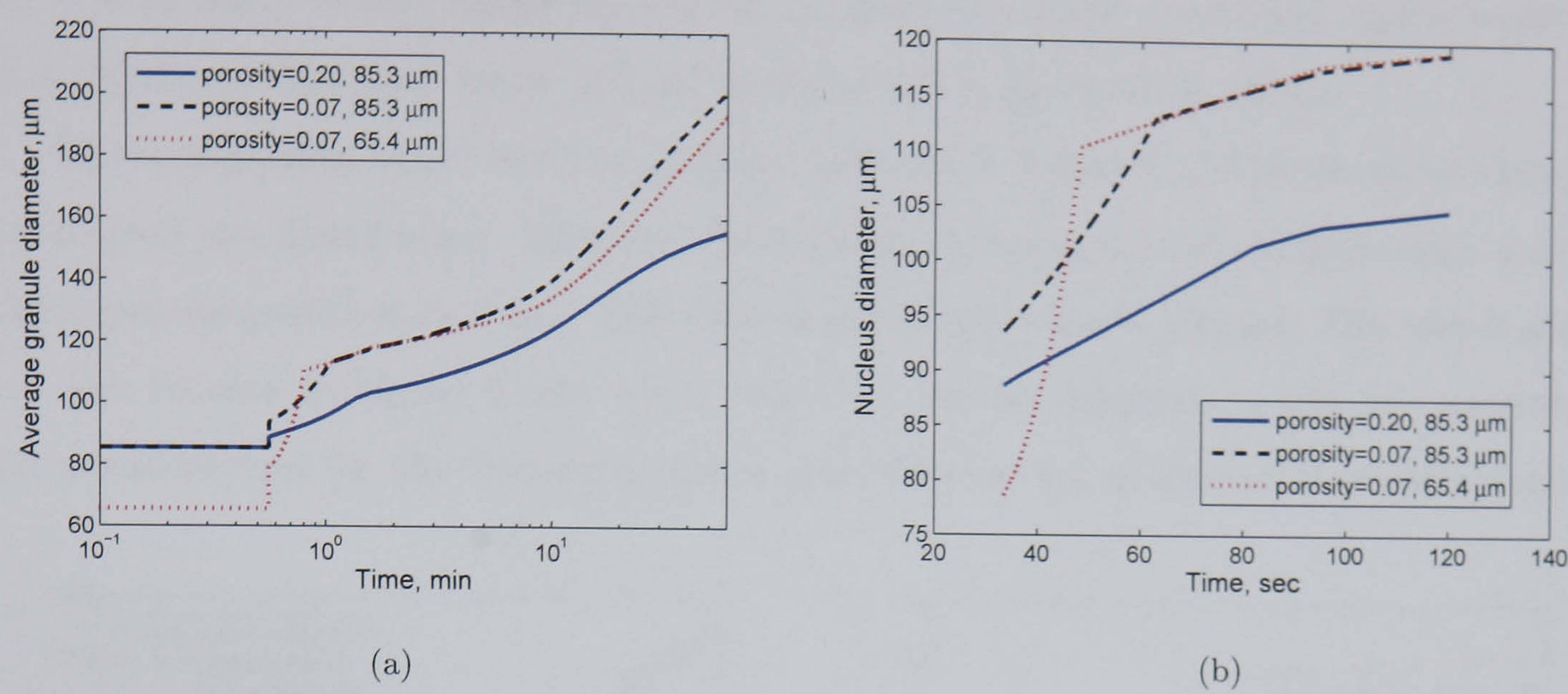

(a) (b)

Figure 5.4: Profile of the average granule size (a) and of the evolution of the average granule nucleus (b) for a granulation formulation of glass ballotini-PEG 200. Effective powder porosities of $\varepsilon_{eff} = 0.2$ and $\varepsilon_{eff} = 0.07$ were used, where in both cases, the initial primary particle size was 85.3 μm. A further case was studied where, for the same granulation recipe, smaller constituent particles were used with a size of 65.4 μm and with $\varepsilon_{eff} = 0.07$.

5.2.2 Effects of feed size distribution

The initial feed size distribution is investigated in order to determine its effects on the growth of granules and providing comparison with the observations made by experimentalists in carrying out similar studies (Litster and Waters, 1988; Adetayo et al., 1995; Scott et al., 2000). The granulation recipe used for this study consists of water as the acting binder and glass ballotini as the powder substrate with a bed porosity of 0.2. Three variations of the feed size distribution was studied: monosized particles, 85.3 μm; two-sized particles that are equally distributed, concentrated at 85.3 μm and 95.3 μm; four-sized particles that are equally distributed, with particle sizes of 65.4 μm, 75.3 μm, 85.3 μm and 95.3 μm; in all three cases, the amount of granulating material used was the same, 1 kg. The binder flow rate used in the simulations was set at $2 \times 10^{-6}\,\mathrm{m}^3/\mathrm{s}$, and the duration of binder spray for cases 1, 2 and 3 were 96 sec, 104 sec and 112 sec, respectively. In addition, the process condition in which the granulator is operating in assumes that the bed turnover relative to the drop penetration is adequate for complete drop penetration *i.e.*, the size of the entire droplet volume will contribute towards the size of a single granule nucleus. Under these circumstances the powder bed is moving with a velocity of 2.1 m/s with a corresponding spray flux value of

$\Psi_a = 0.08$, which in part fulfills the criteria for ensuring droplet controlled regime within the granulator and that each liquid droplet constitutes a single granule nucleus.

The time profiles for the mean granule size is shown in Figure 5.5(a) for the three variations in the feed size distribution. The feed distribution consisting of four particle sizes indicates rapid granule growth at ≈ 2 min, with the average granule size of 130 μm. The rate of growth can also be seen in Figure 5.5(b) where there is a steeper gradient for the size evolution of the nuclei particle for the four-sized particle size distribution in the initial material feed.

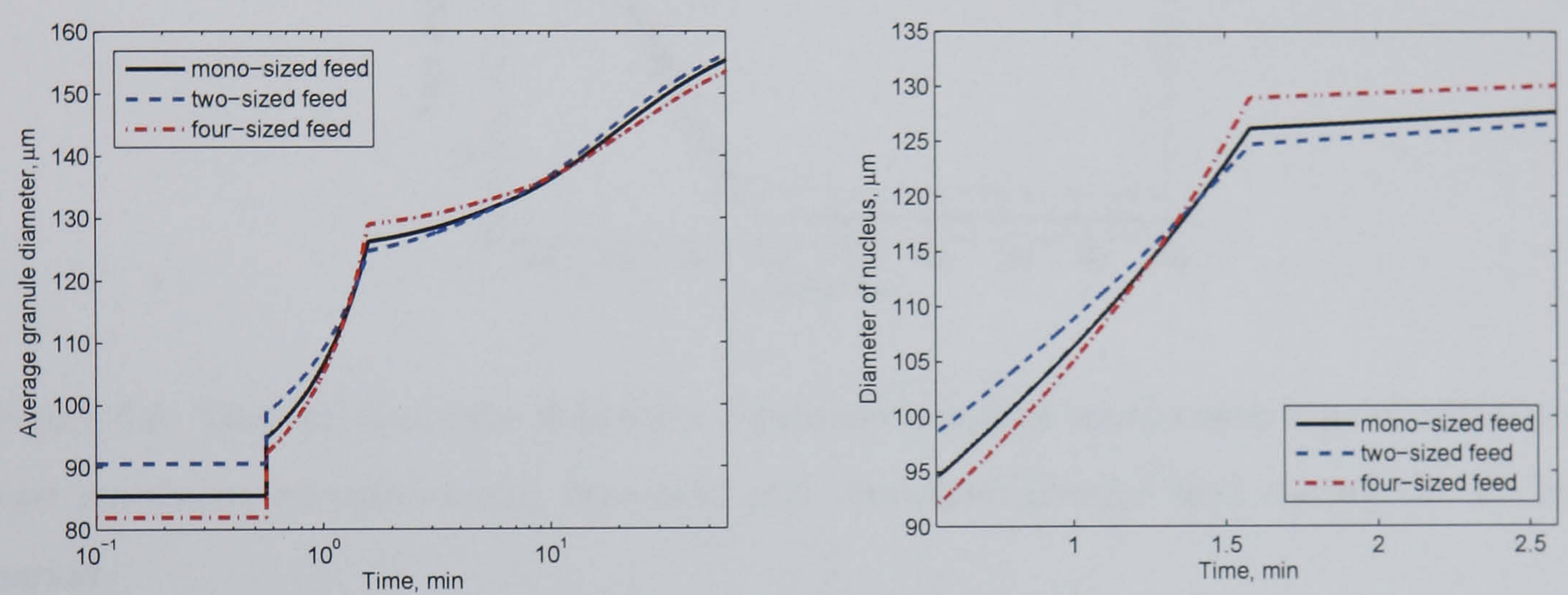

(a) (b)

Figure 5.5: Time profiles for the evolution of the average granule size (a) and the nuclei particle size (b) for a glass ballotini-NDBS formulation.

The mean primary particle size within each of the initial feeds are 80.3 μm, 90.3 μm and 85.3 μm for the four-sized, two-sized and mono-sized particle distributions. With this knowledge a plausible explanation for the faster growth rate exhibited by the feed containing four particle sizes can be made.

In the powder feed consisting of four-sized primary particles, the presence of dissimilar sized particles, the powder bed will have a more compact bed as the smaller sized particles will be able to pack in between the gaps of larger particles. Thus, during the nucleation process as the droplet lands on the powder bed, it is able to capture a higher proportion of primary particles into the formation of a nuclei particle. Thus, the primary particles within the four-sized feed are rapidly depleted compared to either of the two different sized feeds as seen in Figure 5.6. However, an unexpected result for the two-sized feed is seen, in which the depletion of the two-sized primary particles is lower than the mono-sized particles, which is also reflected in the nucleus diameter. This could be because, for the particular choices of

the two sizes, there is in fact an increase in the packing porosity compared to the mono-sized feed, than a decrease is seen for the four-sized feed. This is also borne out by the larger nuclei diameter of

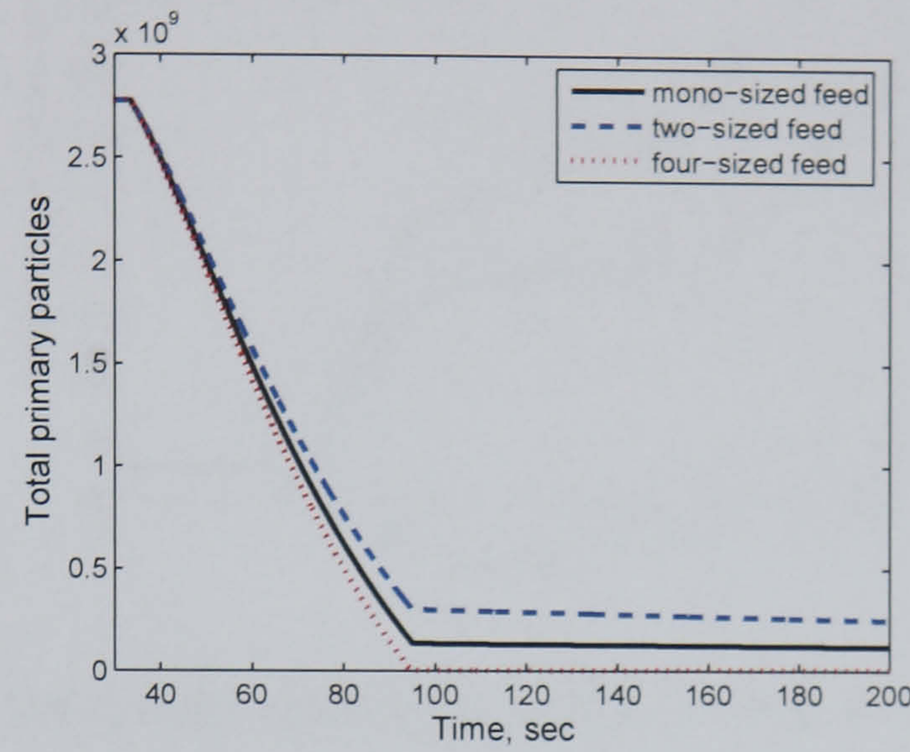

Figure 5.6: Time profile of the depletion of primary particles within each type of initial powder feed consisting of mono-sized, two-sized and four-sized powder feed during the nucleation period.

5.2.3 Manipulation of process conditions

The droplet size have been studied to probe their effects on the granulation process. In particular, this case study will demonstrate that the present PB model should be able to capture these process changes and their effects on the mean granule size attainable.

As mentioned earlier in the chapter outline of objectives, the droplet size represents a key operation parameter for granulation process. The droplet size is considered an important parameter as a number of researchers have observed that the initial size of a newly formed nucleus is dependent on the droplet size (Butensky and Hyman, 1971; Waldie et al., 1987; Waldie, 1991). The simulation results were based on a glass ballotini-water formulation and an effective porosity of 0.2 for the powder bed.

Intuitively, one would expect that as the droplet size increases, the granule nucleus would be larger as the droplet is able to capture a larger number of constituent particles. Figure 5.7 shows that indeed a larger droplet size will facilitate the formation of larger granules, which is initiated by the creation of larger nuclei particles as seen in Figure 5.8(a). Figure 5.8(b) reveals that as the droplet size increases, the depletion of primary particles is faster than the

case of smaller droplets.

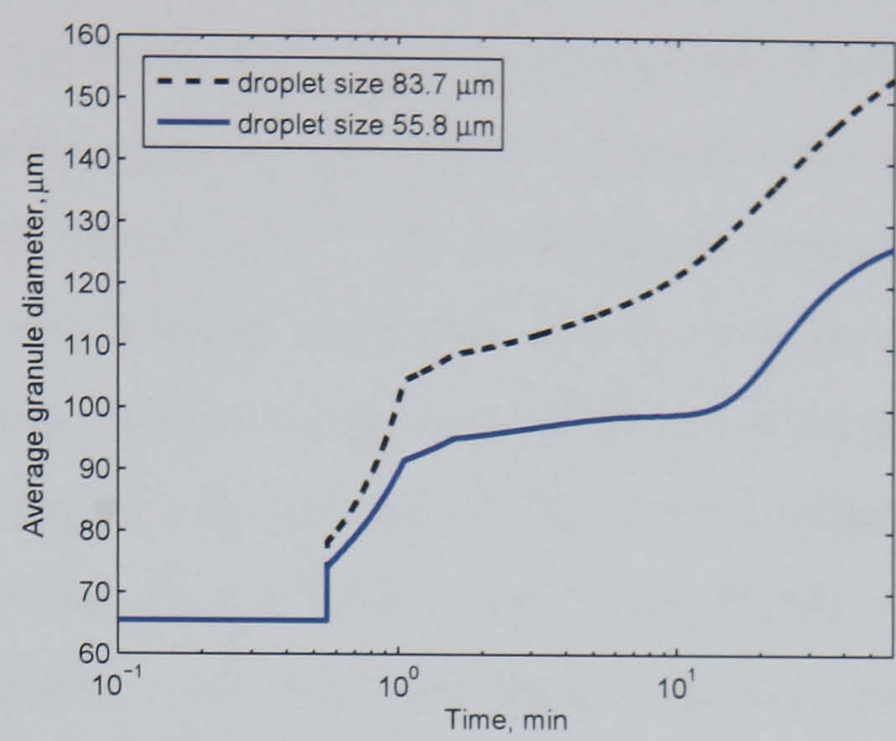

Figure 5.7: Profile of the average granule size under the influence of varying droplet sizes.

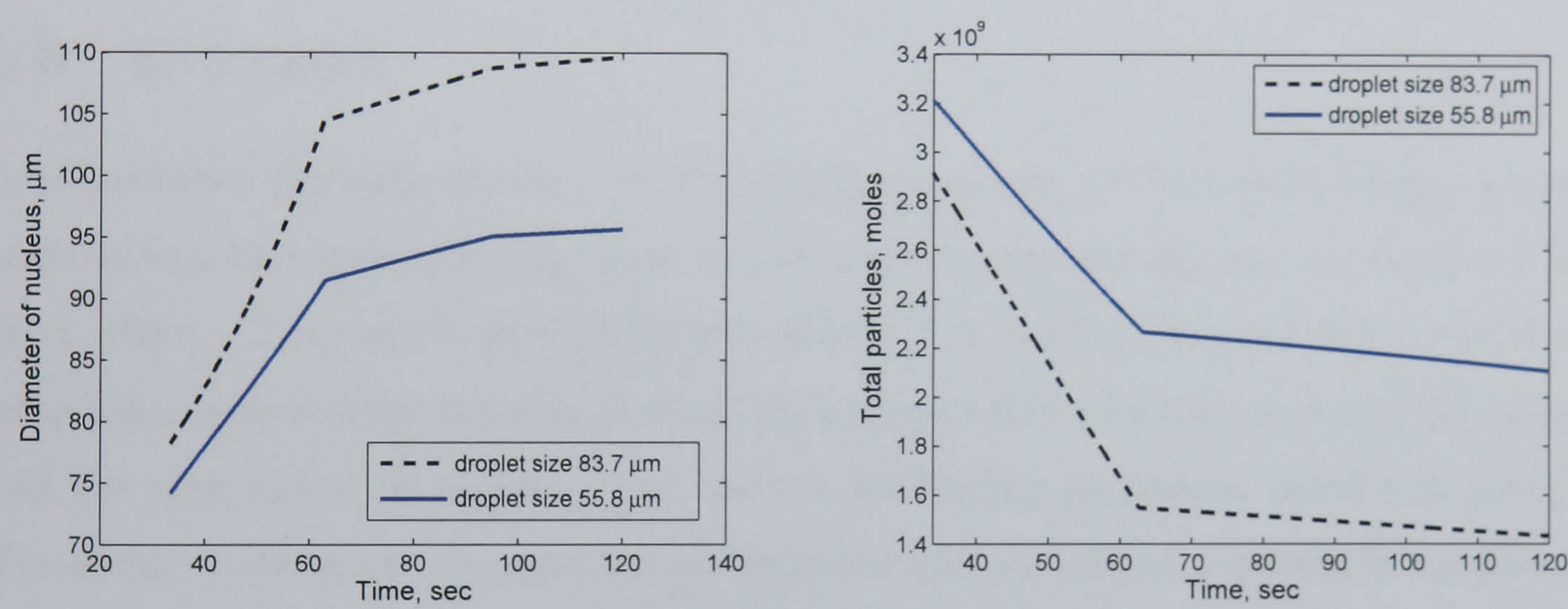

(a) (b)

Figure 5.8: Evolution of the granule nucleus size (a) and the total number of particles (b) under varying droplet sizes.

The evolution of the granule size distribution for varying time instances is presented in Figure 5.9(a)-(e). At 0.6 min a bimodal distribution is already occurring for the case corresponding to the larger droplet size of 83.7 μm, indicating that larger droplets constitute towards the formation of larger nuclei particles, which in turn are responsible for the rapid growth of larger granules as seen by the early appearance of the second peak in the size range 110 μm-180 μm. In contrast, for the droplet size of 55.8 μm, a small shoulder begins to appear only by 2 min into the operation. For the larger 83.7 μm droplet case, the GSD remains clearly bimodal with the large size peak increasing in magnitude. In contrast, the

55.8 μm droplet indicates that the distribution has only undergone a minor growth compared to the feed particle. Figure 5.10 shows a comparison of the end-point granule size distribution in the two-dimensional representation. A higher proportion of smaller sized particles remains ungranulated in the initial peak for the 55.8 μm droplet case, whereas a lower proportion remains for the 83.7 μm droplet case. This analysis has demonstrated that binder droplet size used in granulation will have an impact on both the granule trait and on the operation of the process (Gluba, 2003), such as an increase in the granulation time. Gluba (2003) found in their study that, changes in the droplet binder size will affect both the granule size and prolonged granulation time. In the former case Gluba (2003) established a relationship in the form of a power function for determining the granulation time as a function of the mean droplet size and the average particle size of the feed particles. The present model will serve to complement such empirical relationships by providing a predictive tool.

5.3 Summary

In this chapter, the controllability of the granulation process was assessed drawing supporting observations that were similarly made in past experimental studies (for examples see Holm et al. (1983), Litster and Waters (1988) and Waldie et al. (1987)). In particular, a model of the granulation process incorporating mechanistic representations for the nucleation phenomenon and the aggregation phenomenon was used in performing simulation based case scenarios. The ability of the model to reproduce the dependencies and effects, reported in the literature based on experimental studies, was analysed.

The series of case scenarios undertaken in this chapter has shown that the population balance model, whilst it has predominantly been used as a tool for furthering our understanding of the process, has now taken the next step towards being applied to engineering purposes. A number of realistic process conditions, which have been known to directly influence the granulation behaviour, have been tested using the present population balance model. These can be categorised as those relating to the fundamental material properties of the granulating mixture and those pertaining to the granulation process. Model predictions were made with population balance model using the surface tension and the contact angles of different binder liquids on various powder substrates. A small collection of process handles, which included varying the droplet size of the binder, the feed particle size distribution, and powders of varying moisture absorbing capacities (porosities) were considered in this study. The results

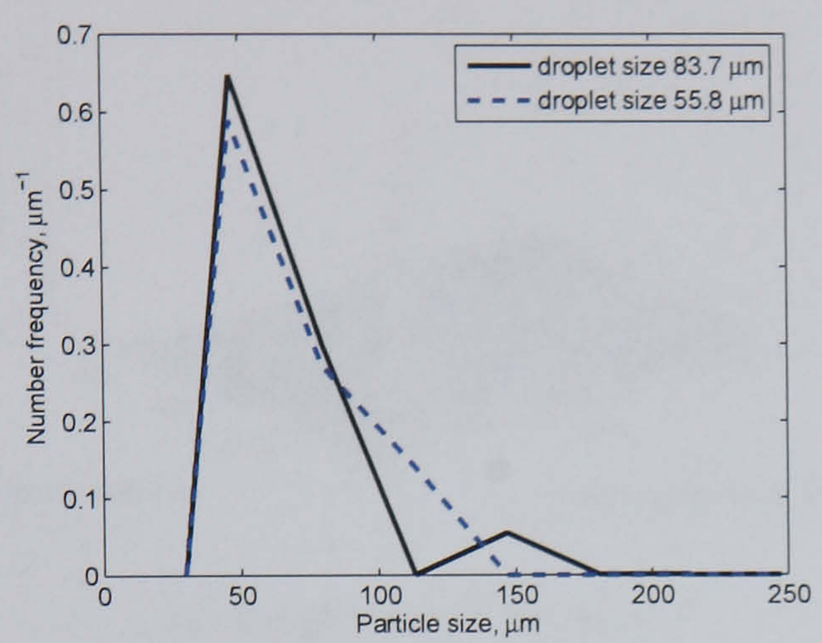

(a) t = 0.6 min

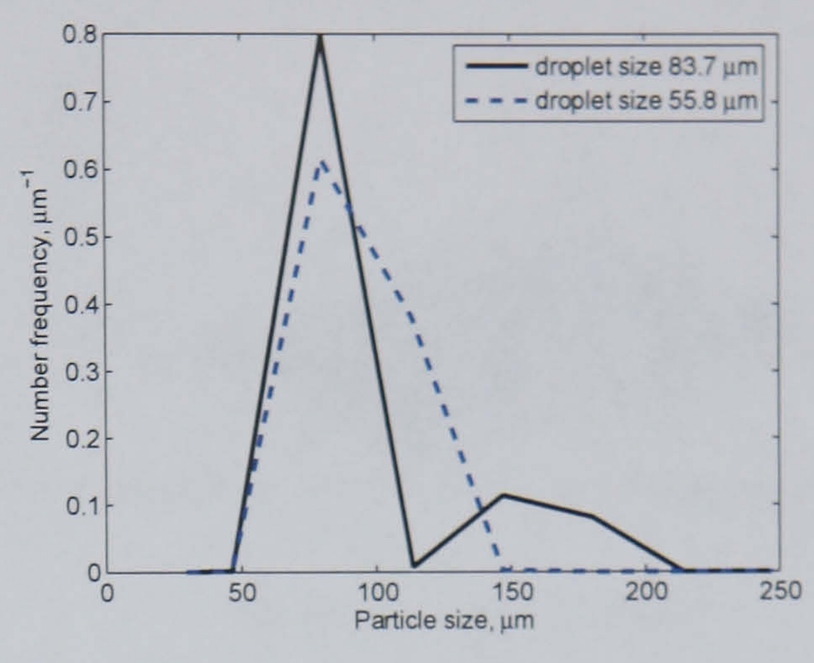

(b) t = 1.3 min

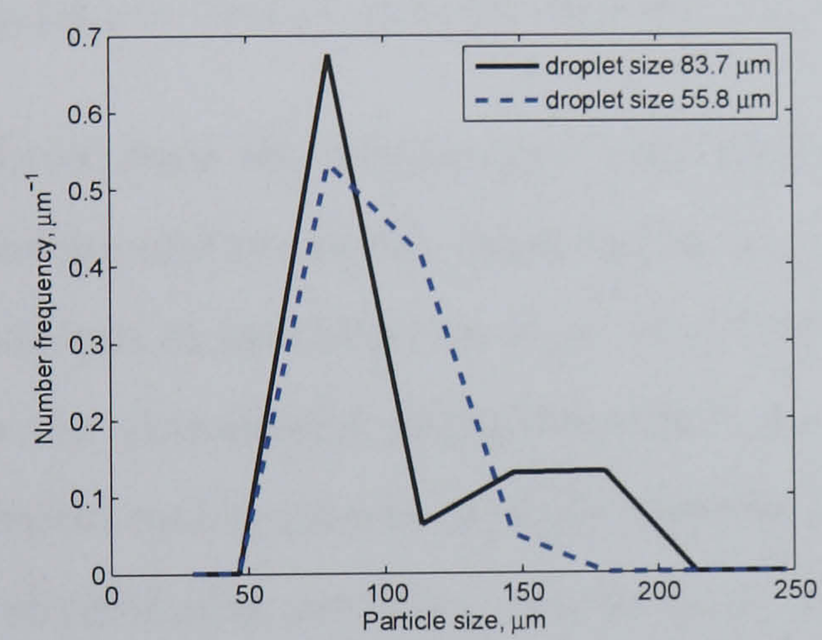

(c) t = 2 min

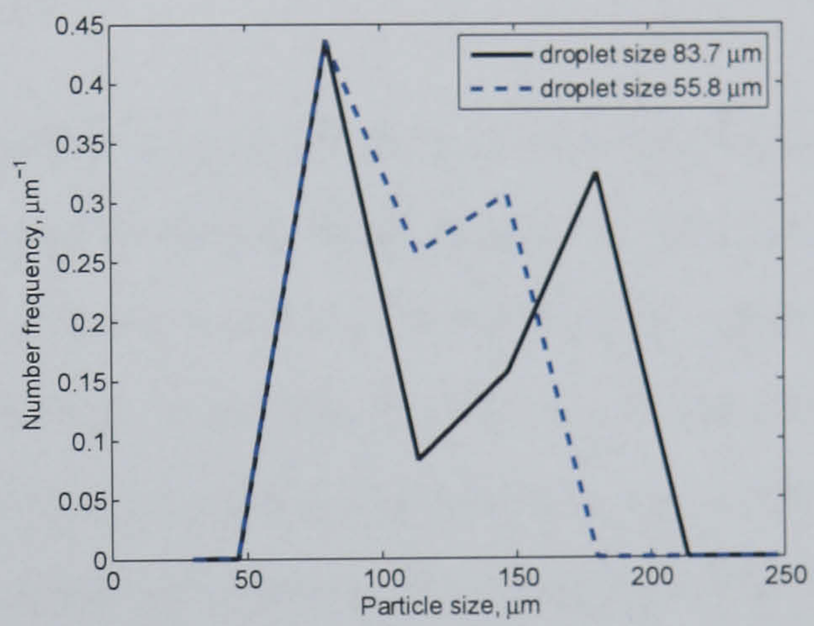

(d) t = 25 min

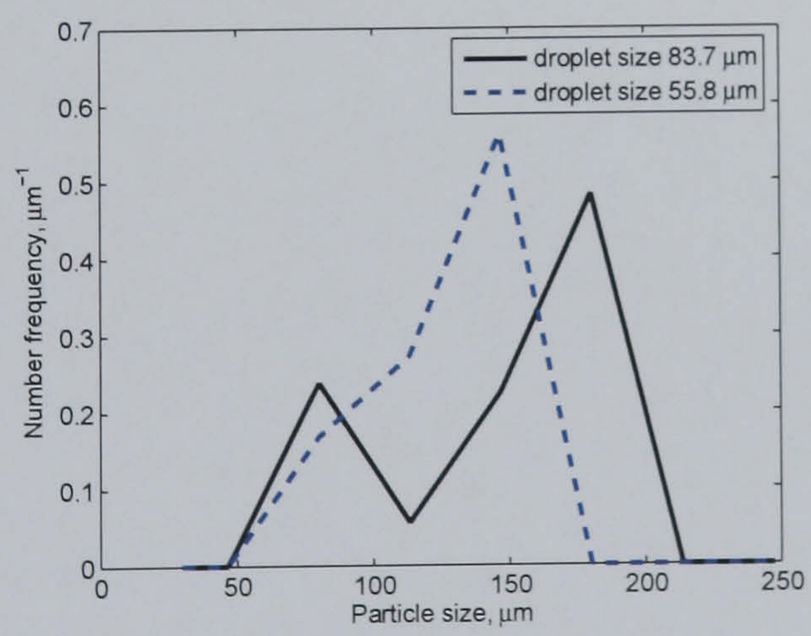

(e) t = 60 min

Figure 5.9: Simulated granule size distributions at varying time instances using a granulation recipe consisting of glass ballotini-NDBS for droplet sizes of 83.7 μm and 55.8 μm.

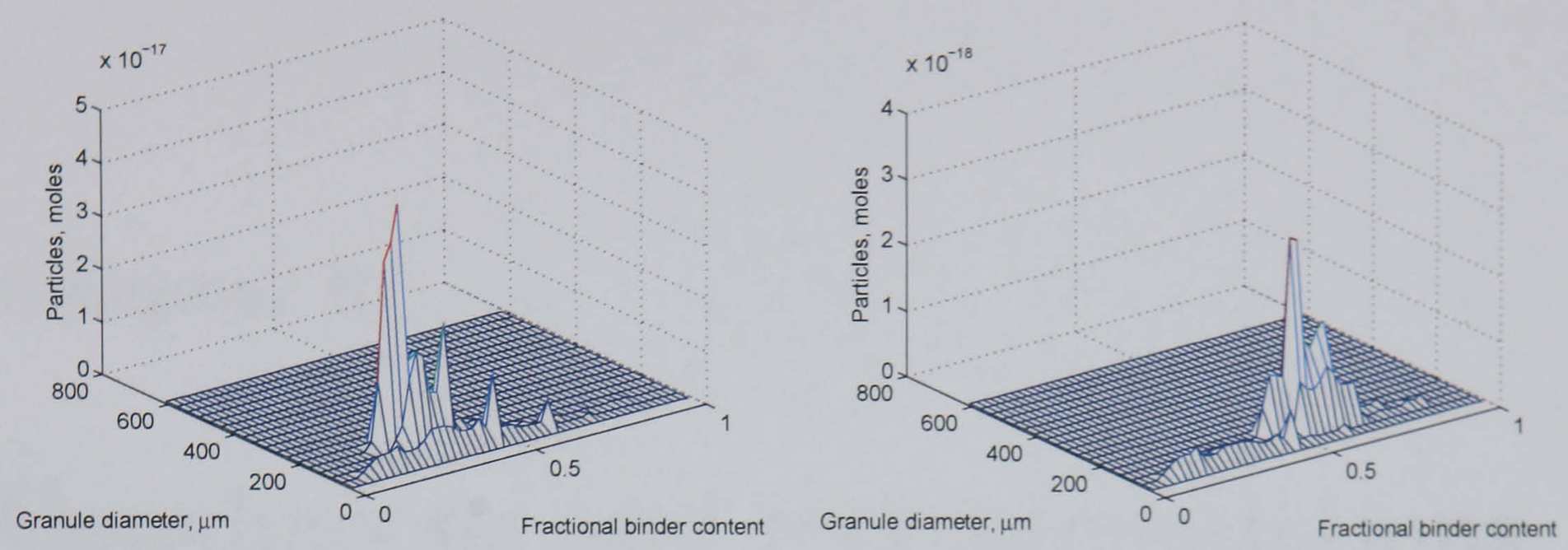

(a) Droplet size = 83.7 μm (b) Droplet size = 55.8 μm

Figure 5.10: Comparison of the end-point particle size distributions for the two cases corresponding to droplet sizes of: 83.7 μm and 55.8 μm.

gathered from the simulation studies indicate that it is possible to feed into this mechanistic based population model, the formulation properties as well as some aspects of the granulating conditions in providing an *a priori* prediction of the granulation behaviour. Further insight into the granulation mechanisms and the influences upon the granulation mechanisms are revealed, and comparisons made between the PB model and experiments to ensure the validity of particular modelling assumptions. The model will serve as a valuable tool enabling: *a priori* predictions of the granulation behaviour for new formulations; reduction in the number of trial experiments; and providing a useful tool for scale-up.

Chapter 6

Conclusions and recommendations

In this thesis, a mechanistic description for the modelling of the nucleation phenomenon has been presented within a three-dimensional population balance framework. A summary of the main findings from this work is given, with recommendations for possible directions that warrant further investigation. The population balance modelling approach, whilst serving as an invaluable tool for improving our understanding of the granulation process, a future goal is to evolve this model to the extent that it may prove useful for making *a priori* predictions for new formulations and to facilitate scale up for granulation processes.

6.1 Conclusions

Dynamic model development:

In the current state of the field of granulation, there is still the need to be able to predict the granulation behaviour for new formulations based on the materials' fundamental properties with the granulation process operating conditions. Numerous experimental studies have been carried out in the past, elucidating the potential granulation variables and their associated impacts on the process. From these experiments, the various influences upon the granulation process have been identified, and their effects on the process have been elucidated on a qualitative basis. However, at the core of granulation research, there still remains the question of exactly how to manipulate these granulation variables on a quantitative basis such that the effects on the granulation behaviour can then be translated into the end product granules with the desired attributes. The emergence of mechanistic based descriptions for the underlying granulation phenomena (*e.g.* nucleation and aggregation) have provided a

starting point from which to make quantitative predictions based on the underlying physics of the granulation phenomena, the formulation properties and the effects imparted by the granulation conditions.

Mechanistic kernels:

A novel mechanistic description for the nucleation phenomenon accounting for the physical process of liquid binder droplets landing on an area of the powder bed surface, and the subsequent penetration of the droplet into the powder resulting in the formation of the granule nucleus has been presented. The process of nucleation has been recognised as being dependent on both the wetting kinetics and the nucleation thermodynamics (Hapgood, 2000). The introduction of key physicochemical properties pertaining to the liquid binder and the powder into the nucleation kernel allows for the possibility of discerning the granulation behaviour for different granulation formulations, which would not have been possible if adopting other traditional approaches to model the kernel, such as empirical correlations. The process conditions that are known to influence nucleation have been explicitly accounted for in the model form of the nucleation kernel. This will allow for the effects influenced at the process level and at the formulation stage to be captured by the model, thereby providing a more accurate representation of the physics involved during the nucleation of fine powders.

Experimental validation:

An important next step in the model development cycle is to ensure that the assumptions made in the model are valid. Thus, laboratory scale batch granulation experiments were performed under different moisture levels and varying amounts of powder charged into the drum granulator for a calcite and polyvinyl alcohol formulation. The model was able to provide partial validation for the granule properties with regards to the average granule porosity, size and fractional binder content. In addition, the population balance modelling has proved itself suitable for granulation processes with heterogeneous distributions of the granule properties (*e.g.* size, porosity and fractional binder content) across the particle population. These preliminary results are promising for mechanism based population balances, for the prediction of the granulation behaviour. Simulations were also performed on the population balance model in order to assess the controllability of the process by varying granulation conditions. The results show that for the cases considered the feed particle size distribution, droplet size, powder bed porosity and different feed formulations the model was able to replicate

the qualitative trends as seen in the literature experimental studies. Thus, the model could potentially be used to predict the granulation effectiveness for new formulations but to also tailor different operating conditions to determine the best operating policy to implement. A concise schematic representation of the interactions between important granulation phenomena with process influences and the effects of the fundamental material properties on the end granule properties is depicted in Figure 6.1. See also Ramachandran et al. (2008).

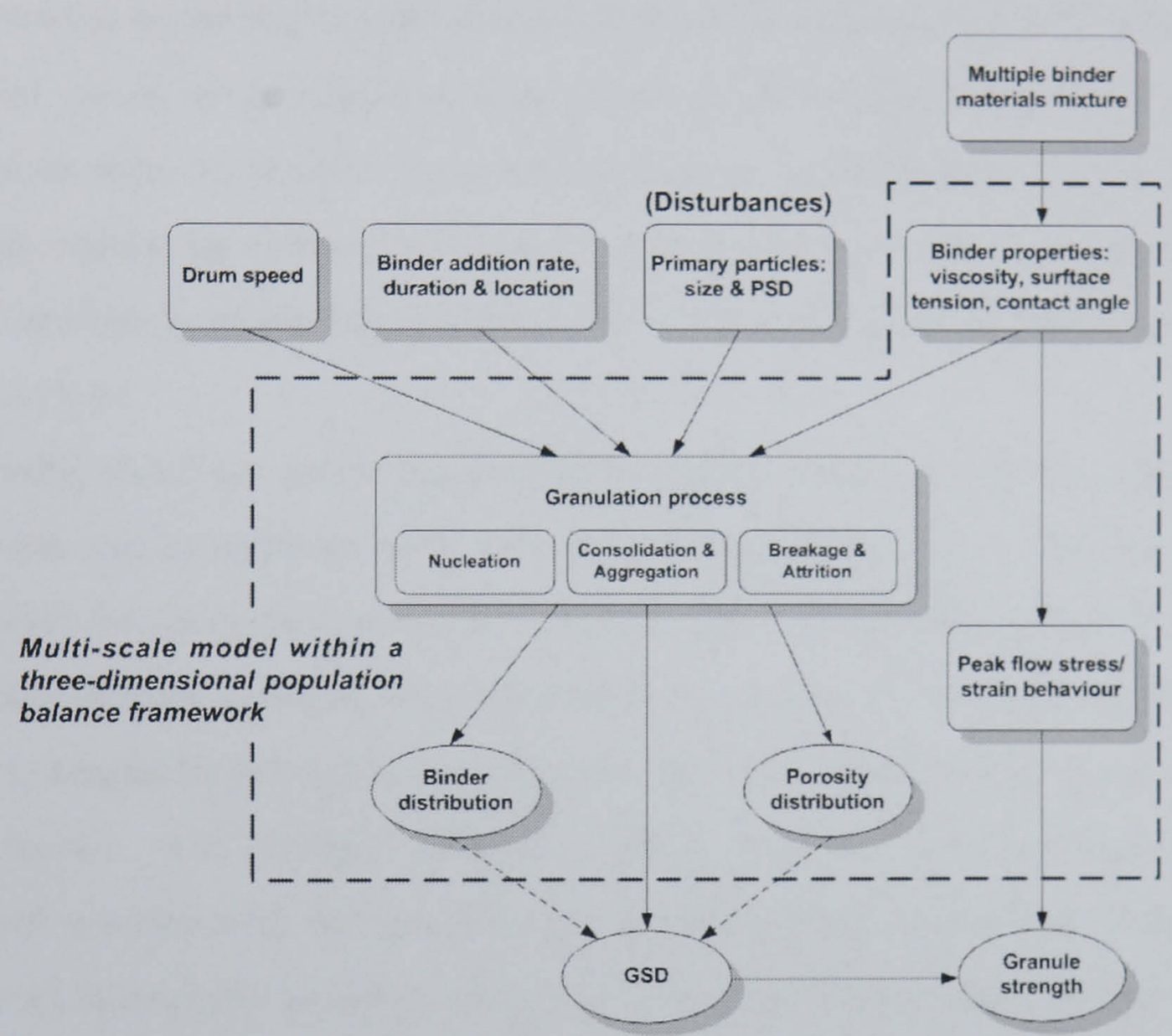

Figure 6.1: Schematic illustration of the multi-scale links in the granulation process, with important granulation interactions linked to process operations and formulation properties to the end granule properties (Ramachandran et al., 2008).

6.2 Recommendations

The mechanistic description for the nucleation phenomenon has incorporated sound knowledge of the drop penetration mechanism, which has been thoroughly studied. However, there is further scope for model improvements that will enable a better tracking of certain distributed granule properties. This includes the incorporation of the droplet size distribution, which will affect the size of nuclei formed, with subsequent influences imparted on the granule

size distribution owing to the template behaviour it has on future granule growth.

In this thesis, the granule strength has been shown to be strain rate dependent. Thus. an attempt to determine the relevant strain rates under the prevalent conditions in the granulator will facilitate prediction of the granulation behaviour for different formulations (Iveson et al., 2002). This additional piece of information will prove valuable for model validation in particular for particle coalescence used in the population balance model.

Further studies exploiting the properties of new formulations should be undertaken. Primarily, further use of the present model by testing more powder-liquid combinations should be performed in order to elucidate granulation behaviour of different granulating materials, under process conditions relevant to those frequently encountered in practice. The objective of these studies is to provide validation that will encompass a larger spectrum of feed granulation recipes.

Undoubtedly, there are some aspects of the model where simplifying assumptions have been made that can be replaced with a more rigorous description. For example, a rigorous model is needed for the partition of the liquid binder in an attempt to account for possible binder transfer between particles that encounter one another yet without aggregating,

Another potential improvement to the model is a more rigorous capturing of the droplet-powder interaction. For example, Hapgood (2000) observed that the drop release height, droplet impact velocity with the powder surface, and angled-drop impacts with the powder surface were all important in determining the drop penetration time into the powder bed, although no firm conclusions could be made due to data scattering. Developing models ascribing to each of the observed effects on the droplet penetration time, and incorporation into the PB model, may enable the elucidation of the droplet penetration mechanism in greater detail in tandem with the influences imparted by the granulator operating conditions.

A further avenue that warrants additional research effort given the widespread use of multi-dimensional population balances is the inclusion of modelling the composition of granules that consist of multiple solid components, as is typical in the pharmaceutical industries. This will mean developing kernels that can accommodate these additional internal coordinates in the principal size changing mechanisms (*e.g.* aggregation). Iveson et al. (2002) presented a population balance model, which included two solid components as internal coordinates. But, this study alone represents a deficit in the granulation field into the extension of PB models that track the evolution of the distribution of multiple components across the granule

size distribution. The incorporation of at least some of the indicated points raised above would further lend support to the current mechanistic based PB model and its modelling of the physics used for the underlying granulation phenomena. In particular, the integrated PB model would facilitate scale up of granulation processes through accurate predictions made at the small scale, and facilitate the reduction of labour-intensive and costly trial experiments.

List of Publications and Conference Contributions

Refereed journal publications:

Poon, J.M.-H., Immanuel, C.D., Doyle III, F.J. and Litster, J.D. (2008) "A Three-Dimensional Population Balance Model of Granulation with a Mechanistic Representation of the Nucleation and Aggregation Phenomena," *Chemical Engineering Science*, 63, 1315-1329.

Ramachandran, R., Poon, J.M.-H., Sanders, C.F.W., Glaser, T., Immanuel, C.D., Doyle III, F.J., Litster, J.D., Stepanek, F., Wang, F.Y. and Cameron, I.T. "Experimental Studies on Distributions of Granule Size, binder Content and Porosity in Batch Drum Granulation: Inferences on process modelling requirements and process sensitivities," *Powder Technology*, (In press).

Poon, J.M.-H., Ramachandran, R., Sanders, C.F.W., Glaser, T., Immanuel, C.D., Doyle III, F.J. and Litster, J.D., Stepanek, F., Wang, F.Y. and Cameron, I.T. "Experimental Validation Studies on a Multi-Dimensional and Multi-Scale Population Balance Model of Batch Granulation," *Chemical Engineering Science*, (Accepted).

Glaser, T., Sanders, C.F.W., Wang, F.Y., Cameron, I.T., Litster, J.D., Poon, J.M.-H., Ramachandran, R., Immanuel, C.D. and Doyle III, F.J. "Model Predictive Control of Continuous Drum Granulation of Limestone," *Journal of Process Control*, (Accepted).

Refereed conference proceedings/presentations:

Immanuel, C.D., Ramachandran, R., Poon, J.M.-H., Doyle III, F.J. and Stepanek, F., "A Mechanistic Description of the Aggregation Phenomenon in Population Balance Models of Granulation," ECI (Engineering Conferences International) Control of Particulate Processes VII, November 2006, British Columbia, Canada.

Ramachandran, R., Poon, J.M.-H., Doyle III, F.J., Litster, J.D., Stepanek, F. and Immanuel, C.D., "Batch Characterisation Studies on Drum Granulation: Formulation Properties and Growth Kinetics," Third International Granulation Workshop, June 2007, Sheffield, UK.

Poon, J.M.-H., Ramachandran, R., Doyle III, F.J., Litster, J.D., Stepanek, F. and Immanuel, C.D., "A Mechanistic Model for Nucleation and Aggregation Phenomena in Population Balances of Granulation," Coimbatore Institute of Technology International Conference on Modelling and Simulation, August 2007, Coimbatore, India.

Poon, J.M.-H., Ramachandran, R., Sanders, C.F.W., Glaser, T., Doyle III, F.J., Litster, J.D., Stepanek, F. and Immanuel, C.D., "A Three-Dimensional Population Balance Model of Granulation Employing Mechanistic Kernels," ECCE (European Congress of Chemical Engineering)-6, September 2007, Copenhagen, Denmark.

Ramachandran, R., Poon, J.M.-H., Sanders, C.F.W., Glaser, T., Immanuel, C.D., Doyle III, F.J., Litster, J.D., Stepanek, F. and Cameron, I.T., "A Three-Dimensional Population Balance Model of Granulation with Mechanistic and Phenomenological Kernels," Third International Conference on The Population Balance Modelling, Québec, Canada.

Glaser, T., Sanders, C.F.W., Wang, F.Y., Cameron, I.T., Litster, J.D., Poon, J.M.-H., Ramachandran, R., Immanuel, C.D. and Doyle III, F.J., "Model Predictive Control of Continuous Drum Granulation of Limestone," AIChE (American Institute of Chemical Engineers) Annual Meeting, November 2007, Salt Lake City, Utah, USA.

Poon, J.M.-H., Ramachandran, R., Sanders, C.F.W., Glaser, T., Doyle III, F.J., Litster, J.D., Stepanek, F., Wang, F.W., Cameron, I.T., and Immanuel, C.D., "A Mechanistic Model for Nucleation and Aggregation in Population Balances of Granulation: Batch Characterisation Studies and Experimental Validation," AIChE (American Institute of Chemical Engineers) Annual Meeting, November 2007, Salt Lake City, Utah, USA.

Bibliography

Adetayo, A. A., Ennis, B. J., 1997. Unifying Approach to Modelling Granule Coalescence Mechanisms. AIChE Journal 43, 927–934.

Adetayo, A. A., Litster, J. D., Pratsinis, S. E., Ennis, B. J., 1995. Population balance modelling of drum granulation of materials with wide size distribution. Powder Technology 82, 37–49.

Bajdik, J., Baki, G., Kelemen, A., Pintye-Hódi, K., 2008. The effect of wetting of powder mixture on the preparation of hydrophilic matrix granules with high-shear granulator. Chemical Engineering Research and Design 86, 1–7.

Balliu, N., 2004. An object oriented approach to the modelling and dynamics of granulation circuits. Ph.D. dissertation, Department of Chemical Engineering and University of Queensland.

Bardin, M., Knight, P. C., Seville, J. P. K., 2004. On control of particle size distribution in granulation using high-shear mixers. Powder Technology 140, 169–175.

Bhattacharya, A., Ray, R., 2003. Studies on surface tension of Poly(Vinyl Alcohol): Effect of concentration, temperature, and addition of chaotropic agents. Journal of Applied Polymer Science 93, 122–130.

Braatz, R. D., 2002. Advanced control of crystallization processes. Annual Reviews in Control 26, 87–99.

Braumann, A., Goodson, M. J., Kraft, M., Mort, P. R., 2007. Modelling and validation of granulation with heterogeneous binder dispersion and chemical reaction. Chemical Engineering Science 62, 4717–4728.

Bridgwater, J., Forrest, S., Parker, D. J., 2004. PEPT for agglomeration? Powder Technology 140, 187–193.

Butensky, M., Hyman, D., 1971. Rotary Drum Granulation. An Experimental Study of the Factors Affecting Granule Size. Industrial and Engineering Chemistry Fundamentals 10, 212–219.

Cameron, I. T., Wang, F. Y., Immanuel, C. D., Štěpánek, F., 2005. Process systems modelling and applications in granulation: A review. Chemical Engineering Science 60, 3723–3750.

Coen, E. M., Gilbert, R. G., Morrison, B. R., Leube, H., Peach, S., 1998. Modeling particle size distributions and secondary particle formation in emulsion polymerisation. Polymer 39, 7099–7112.

Cryer, S. A., 1999. Modeling Agglomeration Processes in Fluid-Bed Granulation. AIChE Journal 45, 2069–2078.

Darelius, A., Brage, H., Rasmuson, A., Björn, I. N., Folestad, S., 2006. A volume-based multi-dimensional population balance approach for modelling high shear granulation. Chemical Engineering Science 61, 2482–2493.

Davies, W. L., Gloor, W. T., 1971. Batch production of pharmaceutical granualtions in a fluidized bed I: Effects of process variables on phyisical properties of final granulation. Journal of Pharmaceutical Sciences 60, 1869–1874.

Denesuk, M., Smith, G. L., Zelinski, B. J. J., Kreidl, N. J., Uhlmann, D. R., 1993. Capillary Penetration of Liquid Droplets into Porous Materials. Journal of Colloid and Interface Science 158, 114–120.

Diggle, P. J., 1983. Statistical analysis of spatial point patterns. Academic Press, London.

Dorao, C. A., Jakobsen, H. A., 2006. Numerical calculation of the moments of the population balance equation. Journl of Computational and Applied Mathematics 196, 619–633.

Ennis, B. J., 1996. Agglomeration and size enlargement Session summary paper. Powder Technology 88, 203–225.

Ennis, B. J., Tardos, G., Pfeffer, R., 1991. A microlevel-based characterization of granulation phenomena. Powder Technology 65, 257–272.

Fan, R., Marchisio, D. L., Fox, R. O., 2004. Application of the direct quadrature method of moments to polydisperse gas-solid fluidized beds. Powder Technology 139, 7–20.

Fox, R. O., 2006. Bivariate direct quadrature method of meoments for coagulation and sintering of particle populations. Journal of Aerosol Science 37, 1562–1580.

Fu, J. S., Reynolds, G. K., Adams, M. J., Hounslow, M. J., Salman, A. D., 2005. An experimental study of the impact breakage of wet granules. Chemical Engineering Science 60, 4005–4018.

Fujiwara, M., Nagy, Z. K., Chew, J. W., Braatz, R. D., 2005. First-principles and direct design approaches for the control of pharmaceutical crystallization. Journal of Process Control 15, 493–504.

Gantt, J. A., Cameron, I. T., Litster, J. D., Gatzke, E. P., 2006. Determination of coalescence kernels for high-shear granualtion using DEM simulations. Powder Technology 170, 53–63.

Gantt, J. A., Gatzke, E. P., 2005. High-shear granualtion modeling using a discrete element simulation approach. Powder Technology 156, 195–212.

Gatzke, E. P., Doyle III, F. J., 2001. Model predictive control of a granulation system using soft output constraints and prioritized control objectives. Powder Technology 121, 149–158.

Gluba, T., 2003. The effect of wetting liquid droplet size on the growth of agglomerates during wet granulation. Powder Technology 130, 219–224.

Grey, R. O., Beddow, J. K., 1969. On the Hausner Ratio and its Relationship to Some Properties of Metal Powders. Powder Technology 2, 323–326.

Gunawan, R., Fusman, I., Braatz, R. D., 2004. High Resolution Algorithms for Multidimensional Popualtion Balance Equations. AIChE Journal 50, 2738–2749.

Hancock, B. C., York, P., Rowe, R. C., 1994. An assessment of substrate-binder interactions in model wet masses. 1: Mixer torque rheometry. International Journal of Pharmaceutics 102, 167–176.

Hapgood, K., 2000. Nucleation and binder dispersion in wet granulation. Ph.D. dissertation, Department of Chemical Engineering and University of Queensland.

Hapgood, K. P., Litster, J. D., Biggs, S. R., Howes, T., 2002. Drop Penetration into Porous Beds. Journal of Colloid and Interface Science 253, 353–366.

Hapgood, K. P., Litster, J. D., Smith, R., 2003. Nucleation Regime Map for Liquid Bound Granules. AIChE Journal 49, 350–361.

Hemati, M., Cherif, R., Saleh, K., Pont, V., 2003. Fluidized bed coating and granulation: influence of process-related variables and physicochemical properties on the growth kinetics. Powder Technology 130, 18–34.

Hogg, R., 1992. Agglomeration models for process design and control. Powder Technology 69, 69–76.

Holm, P., Jungersen, O., Schaefer, T., Kristensen, H. G., 1983. Granulation in high speed mixers: Part 1. Effects of process variables during kneading. Parmaceutical Industry 45, 806–811.

Holm, P., Jungersen, O., Schaefer, T., Kristensen, H. G., 1984. Granulation in high speed mixers: Part 2. Effects of process variables during kneading. Parmaceutical Industry 46, 97–101.

Hoornaert, F., Wauters, P. A. L., Meesters, G. M. H., Pratsinis, S. E., 1998. Agglomeration behaviour of powders in a Lödige mixer granulator. Powder Technology 96, 116–128.

Hounslow, M. J., Pearson, J. M. K., Instone, T., 2001. Tracer Studies of High-Shear Granulation: II. Population balance Modelling. AIChE Journal 47, 1984–1999.

Hounslow, M. J., Ryall, R. L., Marshall, V. R., 1988. A Discretized Population Balance for Nucleation, Growth, and Aggregation. AIChE Journal 34, 1821–1832.

Immanuel, C. D., Doyle III, F. J., 2003. Computationally-efficient solution of population balance models incorporating nucleation growth and coagulation. Chemical Engineering Science 58, 3681–3698.

Immanuel, C. D., Doyle III, F. J., 2005. Solution technique for a multi-dimensional population balance model describing granulation proceses. Powder Technology 156, 213–225.

Immanuel, C. D., Doyle III, F. J., Cordeiro, C. F., Sundaram, S. S., 2003. Population Balance PSD Model for Emulsion Polymerization with Steric Stabilizers. AIChE Journal 49, 1392–1404.

Iveson, S. M., 2002. Limitations of one-dimensional population balance models of wet granulation processes. Powder Technology 124, 219–229.

Iveson, S. M., Beathe, J. A., Page, N. W., 2002. The dynamic strength of partially saturated powder compacts: the effect of liquid properties. Powder Technology 127, 149–161.

Iveson, S. M., Holt, S., Biggs, S., 2004. Advancing contact angle of iron ores as a function of their hematite and goethite content: implications for pelletising and sintering. International Journal of Mineral Processing 74, 281–287.

Iveson, S. M., Holt, S., Rapmond, S., Loo, C. E., Biggs, S. R., 1998. The effect of solid-liquid contact angle on the granulation of porous materials: a case study on iron ore granulation. Advanced Particle Technologies for Particle Processing, Particle Technology Forum, Miami Beach, USA.

Iveson, S. M., Litster, J. D., 1998. Growth Regime Map for Liquid-Bound Granules. AIChE Journal 44, 1510–1518.

Iveson, S. M., Litster, J. D., Ennis, B. J., 1996. Fundamental studies of granule consolidation Part 1: Effects of binder content and binder viscosity. Powder Technology 88, 15–20.

Iveson, S. M., Litster, J. D., Hapgood, K., Ennis, B. J., 2001. Nucleation, growth and breakage phenomena in agitated wet granulation processes: a review. Powder Technology 117, 3–39.

Knight, P., 2004. Challenges in granulation technology. Powder Technology 140, 156–162.

Knight, P. C., Instone, T., Pearson, J. M. K., Hounslow, M. J., 1998. An investigation into the kinetics of liquid distribution and growth in high shear mixer agglomeration. Powder Technology 97, 246–257.

Kristensen, H. G., Holm, P., Schaefer, T., 1985. Mechanical properties of moist agglomerates in relation to granulation mechanisms part II. Effects of particle size distribution. Powder Technology 44, 239–247.

Krycer, I., Pope, D. G., 1983. An Evaluation of Tablet Binding Agents Part I. Solution Binders. Powder Technology 34, 39–51.

Kumar, J., Peglow, M., Warnecke, G., Heinrich, S., Mörl, L., 2006. Improved accuracy and convergence of discretized population balance for aggregation: The cell average technique. Chenmical Engineering Science 61, 3327–3342.

Kumar, S., Ramkrishna, D., 1996a. On the solution of population balance equations by discretization–I. a fixed pivot technique. Chenmical Engineering Science 51, 1311–1332.

Kumar, S., Ramkrishna, D., 1996b. On the solution of population balance equations by discretization–II. a moving pivot technique. Chenmical Engineering Science 51, 1333–1342.

LeVeque, R., 2002. Finite volume methods for hyperbolic problems. Cambridge University Press, New York.

Litster, J., Ennis, B., 2004. The Science and Engineering of Granulation Processes. Kluwer Academic Publishers, The Netherlands.

Litster, J. D., 2003. Scaleup of wet granulation processes: science not art. Powder Technology 130, 35–40.

Litster, J. D., Hapgood, K. P., Michaels, J. N., Sims, A., Roberts, M., Kameneni, S. K., Hsu, T., 2001. Liquid distribution in wet granualtion: dimensionless spray flux. Powder Technology 114, 32–39.

Litster, J. D., Waters, A. G., 1988. Influence of the material properties of iron ore sinter feed on granulation effectiveness. Powder Technology 55, 141–151.

Liu, L. X., Litster, J. D., Iveson, A. M., Ennis, B. J., 2000. Coalescence of Deformable Granules in Wet Granulation Processes. AIChE Journal 46, 529–539.

Luckham, P. F., Ukeje, M. A., 1999. Effect of Particle Size Distribution on the Rheology of Dispersed Systems. Journal of Colloid Interface Science 220, 347–356.

Ma, D. L., Tafti, D. K., Braatz, R. D., 2002a. High-Resolution Simulation of Multidimensional Crystal Growth. Industrial and Engineering Chemistry Research 41, 6217–6223.

Ma, D. L., Tafti, D. K., Braatz, R. D., 2002b. Optimal control and simualtion of multidimensional crystallization processes. Computers and Chemical Engineering 26, 1103–1116.

Malamataris, S., Kiortsis, S., 1997. Wettability parameters and deformational behaviour of powder-liquid mixes in the funicular agglomeration phase. International Journal of Pharmaceutics 154, 9–17.

Mansa, R. F., Bridson, R. H., Greenwood, R. W., Barker, H., Seville, J. P. K.. 2008. Using intelligent software to predict the effects of formulation and processing parameters on roller compaction. Powder Technology 181, 217–225.

Mantzaris, N. V., Daoutidis, P., Srienc, F., 2001. Numerical solution of multi-variable cell popuatlion balance models: I. Finite difference methods. Computers and Chemcial Engineering 25, 1411–1440.

Marchisio, D. L., Fox, R. O., 2005. Solution of population balance equations using the direct quadrature method of moments. Journal of Aerosol Science 36, 43–73.

Marchisio, D. L., Pikturna, J. T., Fox, R. O., Vigil, R. D., Barresi, A.. 2003a. Quadrature Method of Moments for Population-Balance Equations. AIChE Journal 49. 1266–1276.

Marchisio, D. L., Vigil, R. D., Fox, R. O., 2003b. Implementation of the quadrature method of moments in CFD codes for aggregation-breakage problems. Chemical Engineering Science 58, 3337–3351.

Marmur, A., 1988. The radial capillary. Journal of Colloid and Interface Science 124, 301–308.

McGraw, R., 1997. Aerosol Dynamics by the Quadrature Method of Moments. Aerosol Science and Technology 27, 255–265.

Melis, S., Kemmere, M., Meuldijk, J., Storti, G., Morbidelli, M., 2000. A model for the coagulation of polyvinyl acetate particles in emulsion. Chemical Engineering Science 55, 3101–3111.

Michaels, J. N., 2003. Toward rational design of powder processes. Powder Technology 138, 1–6.

Mort, P. R., Capeci, S. W., Holder, J. W., 2001. Control of agglomerate attributes in a continuous binder-agglomeration process. Powder Technology 117, 173–176.

Ouchiyama, N., Tanaka, T., 1975. The probability of coalescence in granulation kinetics. Industrial and Engineering Chemistry: Process Design and Development 14, 286–289.

Oulahna, D., Cordier, F., Galet, L., Dodds, J. A., 2003. Wet granulation: the effect of shear on granule properties. Powder Technology 130, 238–246.

Parkinson, C., Matsumoto, S., Sherman, P., 1970. The influence of particle-size distribution on the apparent viscosity of non-newtonian dispersed systems. Journal of Colloid and Interface Science 33, 1–195.

Pinto, M. A., Immanuel, C. D., Doyle III, F. J., 2007. A Feasible Solution Technique for Higher-Dimensional Population Balance Models. Computers and Chemcial Engineering 31, 1242–1256.

Pont, V., Saleh, K., Steinmetz, D., Hémati, M., 2001. Influence of the physicochemical properties on the growth of solid particles by granulation in fluidized bed. Powder Technology 120, 97–104.

Poon, J. M.-H., Immanuel, C. D., Doyle III, F. J., Litster, J. D., 2008. A three-dimensional population balance model of granulation with a mechanistic representation of the nucleation and aggregation phenomena. Chemical Engineering Science 63, 1315–1329.

Poon, J. M.-H., Ramachandran, R., Sanders, C. F. W., Immanuel, C. D., Doyle III, F. J., Litster, J. D., Stepanek, F., Wang, F. Y., Cameron, I. T., Accepted. Experimental Validation Studies on a Multi-Dimensional and Multi-Scale Population Balance Model of Batch Granulation. Chemical Engineering Science.

Pottmann, M., Ogunnaike, B. A., Adetayo, A. A., Ennis, B. J., 2000. Model-based control of a granualtion system. Powder Technology 108, 192–201.

Ramachandran, R., 2008. Multi-scale population balance modelling and controllability of granulation processes. Ph.D. dissertation, Department of Chemical Engineering and Chemical Technology, Imperial College London.

Ramachandran, R., Poon, J. M.-H., Sanders, C. F. W., Glaser, T., Immanuel, C. D., Doyle III, F. J., Litster, J. D., Stepanek, F., Wang, F. Y., Cameron, I. T., 2008. Experimental studies on the distributions of granule size, binder content and porosity in drum granulation: Inferences on process modelling requirements and process sensitivities. Powder Technology. To appear.

Ramkrishna, D., 2000. Population Balances. Academic Press, San Diego.

Randolph, A. D., Larson, M. A., 1971. Theory of particulate processes: annlysis and techniques of continuous crystallization. Academic Press, New York.

Rankell, A. S., Scott, M. W., Lieberman, H. A., Chow, F. S., Battista, J. V., 1964. Continuous production of tablet granulations in a fluidized bed II. Operation and performance of equipment. Journal of Pharmaceutical Sciences 53, 320–324.

Rawlings, J. B., Ray, W. H., 1988a. The modeling of batch and continuous emulsion polymerization reactors. Part I: Model formulation and sensitivity to parameters. Polymer Engineering and Science 28, 237–256.

Rawlings, J. B., Ray, W. H., 1988b. The modeling of batch and continuous emulsion polymerization reactors. Part II: Comparison with experimental data from continuous stirred tank reactors. Polymer Engineering and Science 28, 257–274.

Reynolds, G. K., Biggs, C. A., Salman, A. D., Hounslow, M. J., 2004. Non-uniformity of binder distribution in high-shear granulation. Powder Technology 140, 203–208.

Rhodes, M., 1990. Principles of powder technology. John Wiley & Sons, United Kingdom.

Rodríguez-Hornedo, N., Murphy, D., 1999. Significance of Controlling Crystallization Mechanisms and Kinetics in Pharmaceutical Systems. Journal of Pharmaceutical Sciences 88, 651–660.

Rough, S. L., Wilson, D. I., Bayly, A., York, D., 2003. Tapping characterisation of high shear mixer agglomerates made with ultra-high viscosity binders. Powder Technology 132, 249–266.

Rough, S. L., Wilson, D. I., Bayly, A. E., York, D. W., 2005. Influence of Process Parameters on The Tapping Characteristics of High Shear Mixer Agglomerates Made with Ultra-High Viscosity Binders. Chemical Engineering Research and Design 83, 7–23.

Rowe, R. C., 1989. Binder-substrate interactions in granulation: a theoretical approach based on surface free energy and polarity. International Journal of Pharmaceutics 52, 149–154.

Salman, A. D., Hounslow, M. J., Seville, J. P. K., 2007. Granulation (Handbook of Powder Technology). Elsevier, The Netherlands.

Sastry, K. V. S., 1975. Similarity size distribution of agglomerates during their growth by coalescence in granulation or green pelletization. International Journal of Mineral Processing 2, 187–203.

Sastry, K. V. S., Fuerstenau, D. W., 1973. Mechanisms of Agglomerate Growth in Green Pelletization. Powder Technology 7, 97–105.

Schaafsma, S. H., Kossen, N. W. F., Mos, M. T., Blauw, L., Hoffman, A. C.. 1999. Effects and control of hunidity and particle mixing in fluid-bed granulation. AIChE Journal 45. 1202–1210.

Schaefer, T., Mathiesen, C., 1996a. Melt pelletization in a high shear mixer. IX. Effects of binder particle size. International Journal of Pharmaceutics 139, 139–148.

Schaefer, T., Mathiesen, C., 1996b. Melt pelletization in a high shear mixer. VIII. Effects of binder viscosity. International Journal of Pharmaceutics 139, 125–138.

Scott, A. C., Hounslow, M. J., Instone, T., 2000. Direct evidence of heterogenity during high-shear granulation. Powder Technology 113, 205–213.

Smith, R., 2008. Wet granule breakage in high shear mixer granulators. Ph.D. dissertation, Department of Chemical Engineering and University of Queensland.

Snow, R. L., Allen, T., Ennis, B. J., Litster, J. D., 1997. Perry's Chemical Engineers' Handbook, 7th Edition. McGraw-Hill, New York, pp. 20–56 – 20–89.

Sun, N., Immanuel, C. D., 2005. Efficient solution of population balance models employing a hierarchical solution strategy based on a multi-level discretisation. Transactions of the Institute of Measurement and Control 27, 347–366.

Talu, I., Tardos, G. I., Khan, M. I., 2000. Computer simulation of wet granualtion. Powder Technology 110, 59–75.

Tardos, G. I., Khan, M. I., Mort, P. R., 1997. Critical parameters and limiting conditions in binder granulation of fine powders. Powder Technology 94, 245–258.

Thielmann, F., Naderi, M., Ansari, M. A., Stepanek, F., 2008. The effect of primary particle surface energy on agglomeration rate in fluidised bed wet granulation. Powder Technology 181, 160–168.

Venkataramana, R., Gupta, S. S., Kapur, P. C., 1999. A combined model for granule size distribution and cold permeability in the wet stage of iron ore sintering process. International Journal of Mineral Processing 57, 43–58.

Verkoeijen, D., Pouw, G. A., Meesters, G. M. H., Scarlett, B., 2002. Population balances for particulate processes – a volume approach. Chemical Engineering Science 57, 2287–2303.

Waldie, B., 1991. Growth mechanism and the dependence of granule size on drop size in fluidised bed granulation. Chemical Engineering Science 46, 2781–2785.

Waldie, B., Wilkinson, D., Zachra, L., 1987. Kinetics and mechanism of growth in batch and continuous fluidised bed granulation. Chemical Engineering Science 42, 653–665.

Wang, F. Y., Cameron, I. T., 2002. Review and future directions in the modelling and control of continuous drum granulation. Powder Technology 124, 238–253.

Watano, S., 2001. Direct control of wet agglomeration processes by image processing system. Powder Technology 117, 163–172.

Watano, S., Miyanami, K., 1995. Image processing for on-line monitoring of granule size distribution and shape in fluidized bed granulation. Powder Technology 83, 55–60.

Wauters, P., 2001. Modelling and mechanisms of granulation. Ph.D. dissertation, Delft University of Technology, The Netherlands.

Wildeboer, W. J., 2002. Design and operation of regime separated granulators. Ph.D. dissertation, Department of Chemical Engineering and University of Queensland.

Wildeboer, W. J., Koppendraaier, E., Litster, J. D., Howes, T., Meesters, G., 2007. A novel nucleation apparatus for regime separated granulation. Powder Technology 171, 96–105.

Wildeboer, W. J., Litster, J. D., Cameron, I. T., 2005. Modelling nucleation in wet granulation. Chemical Engineering Science 60, 3751–3761.

York, P., 1995. Granulation using Mechanical Agitation. International fine particle research institute first year annual report, International Fine Particle Research Institute, Bradford.

York, P., Rowe, R. C., 1994. Monitoring granulation size enlargement processes using mixer torque rheometry. First International Particle Technology Forum, Denver, USA.

Zajic, L., Buckton, G., 1990. The use of surface energy values to predict optimum binder selection for granulations. International Journal of Pharmaceutics 59, 155–164.

Zhang, D., Flory, J. H., Panmai, S., Batra, U., Kaufman, M. J., 2002. Wettability of pharmaceutical solids: its measurement and influence on wet granulation. Colloids and Surfaces A: Physicochemical and Engineering Aspects 206, 547–554.

Zhang, J., Litster, J. D., Wang, F. Y., Cameron, I. T., 2000. Evaluation of control strategies for fertiliser granulation circuits using dynamic simulation. Powder Technology 108, 122–129.

Appendix A

Dimensionless spray flux derivation

A.1 Dimensionless spray flux

The spray flux (Ψ_a) is an equipment-independent dimensionless group based on the process operating parameters. The spray flux provides a quantitative indication of the preferential mode for nucleation given the set of equipment operating conditions employed at the time of granulation. There are many influences that will affect the particle size distribution of nuclei particles. These can be broadly categorised as the physicochemical properties of both the liquid binder and the powder solid substrate (*i.e.* interfacial surface tension, solid-liquid contact angle, *etc.*), which predominantly affects the kinetics of nuclei formation as this is concerned with the penetration of the drop into the powder bed (Litster et al., 2001). The other category is related to the process variables such as the spray characteristics (*i.e.* droplet size, wide or narrow droplet size distribution and spray location), the powder flux passing through the nucleation zone also referred to as the '*wetting zone*' (Schaafsma et al., 1999) and the flux of drops landing on the exposed powder surface as it passes through the spray zone, which are determined by the equipment level parameters.

In summary, the spray flux represents the ratio of the wetted area covered by the droplets delivered by the spray nozzle onto the surface of the powder to the powder area flux ($\dot{A}$), which is defined in Equation (A.1)

$$\dot{A} = v \times w \tag{A.1}$$

Where, v is the velocity of the powder bed passing through the spray zone and w is the width of the powder bed (see Figure A.1). Thus, one may consider the spray flux as a measure of

the density of droplets landing on the exposed powder area as it passes beneath the binder spray. A high Ψ_a indicates that there will be a large portion of the droplets that will land on top of each other thereby increasing the likelihood of droplet overlap. Similarly, a low Ψ_a value indicates that each droplet that lands on the powder surface are likely to be separated from each other with minimal droplet overlap.

The implications of the extent of droplet overlap is an important consideration to taken into account during nucleation since, this will affect the nuclei characteristics. By having distinct droplets that are well-spaced without overlap on the powder surface will increase the probability of a single droplet forming an individual nucleus, provided that the bed turnover is sufficient such that complete drop penetration into the powder bed is permitted without residual unpenetrated droplet volume still remaining on the powder surface.

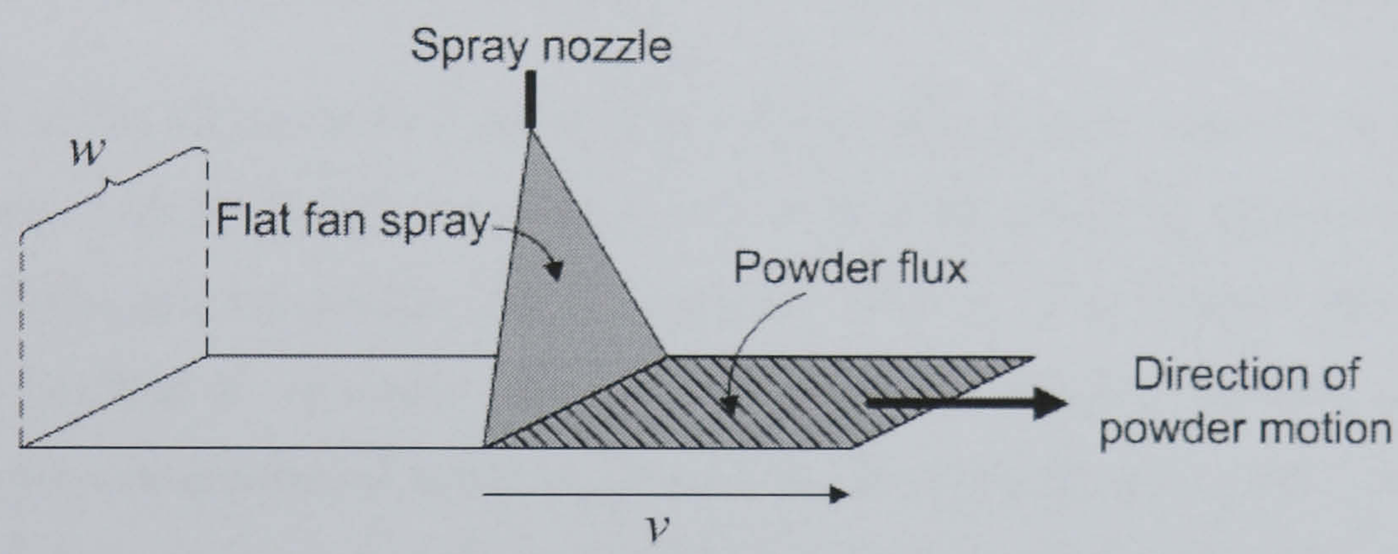

Figure A.1: Illustration of the powder surface passing through the spray zone. The shape of the spray is depicted as line spray, which can be carried out using a flat fan nozzle configuration. The width of the powder bed is w moving through the spray zone with velocity v. The powder flux is defined as $\dot{A} = v \times w$ (m^2/s).

In deriving the spray flux, and bearing in mind that the spray flux is the ratio of the projected area of droplets to the powder flux, the number of droplets ($\dot{n}_d$) produced from the spray nozzle with a liquid flow rate Q is given by Equation (A.2) with the assumption that the droplets are spherical.

$$\dot{n}_d = \frac{Q}{\left(\frac{\pi}{6} D_d^3\right)} \tag{A.2}$$

The projected area of a single droplet onto the powder surface is given by Equation (A.3) *i.e.*, the cross-sectional area of a spherical drop. Thus, the total projected area of all the

droplets onto the powder surface is given in Equation (A.4).

$$a_d = \frac{\pi}{4} D_p^2 \tag{A.3}$$

$$\dot{a}_{dT} = \dot{n}_d \times a_d$$

$$\therefore \dot{a}_{dT} = \frac{3Q}{2D_d} \tag{A.4}$$

The spray flux is then formally defined in Equation (A.5).

$$\Psi_a = \frac{\text{wetted area projected by droplets}}{\text{powder flux}}$$

$$\therefore \Psi_a = \frac{3Q}{2\dot{A}D_p} \tag{A.5}$$

A.2 Model extension of the dimensionless spray flux

The concept of the dimensionless spray flux may be extended, to determine the fraction of droplets that are sprayed onto the powder surface that will result in single droplets given as a function of the process parameters *i.e.*, powder velocity. This is done using the Poisson distribution function to represent the random pattern of droplets landing on the powder surface and the assumption of complete spatial randomness (Diggle, 1983), which proposes that the a random event is independent of all previous occurrences within the same subregion. In the context of this study, a droplet is likely to land on a region of the powder surface irrespective of previous droplets that may have landed on the same subregion of powder. Thus, the number of events (*i.e.* occurrences of droplet landing on the powder) on an area of powder (A) will follow a Poisson distribution with the mean number of events occurring on the area of powder A being given by Equation (A.7). Here, Φ represents the mean number of events (N) per unit area and is defined by Equation (A.6) and is also known as the intensity of the distribution.

$$\Phi = \frac{N}{A'} \tag{A.6}$$

$$P_n(A) = \exp(-\Phi A)\left(\frac{(\Phi A)^n}{n!}\right) \tag{A.7}$$

The probability of a single droplet landing on the powder surface without overlapping with other neighbouring droplets can be expressed as shown in Equation (A.8) by using Equation (A.7), setting $n = 0$ *i.e.*, zero droplet overlapping and specifying that the minimum center-to-center distance between droplets be D_d from other neighbouring droplets. The area

A in Equation (A.7) will be a circular area, $A = \pi D_d^2$ with radius D_d (Hapgood, 2000).

$$\text{Probability of single drop} = f_{single} = \exp(-\Phi \pi D_d^2) \tag{A.8}$$

Relating the intensity of the distribution to the dimensionless spray flux using Equation (A.9) enables us to define a relationship specifying the probability of a single droplet landing on the powder surface as function of the equipment operating parameters. Substituting Equation (A.9) into Equation (A.8) with $2r_d = D_d$ results in Equation (A.10) (Hapgood, 2000).

$$\Psi_a = \frac{n_d \times a_d}{\dot{A}} = \Phi \pi r_d^2 \tag{A.9}$$

$$f_{single} = \exp(-4\Psi_a) \tag{A.10}$$

Appendix B

Analytical techniques

B.1 Particle size analysis

The product granules produced from batch granulation experiments were dried in an oven at 110°C, which resulted in the removal of the liquid binder without any reduction in the mass of calcite granules. The granule size distribution was subsequently obtained through the use of sieves using a fourth-root-of-two progression series of sieves (Endecotts Ltd). The Retsch sieve shaker was set for 5 mins at 30% amplitude.

B.2 Porosimetry

The granule porosity was determined for each size fraction corresponding to the sieve trays previously employed for determining the granule size distribution. The porosity of the sample was determined via pycnometry by firstly measuring the true density (ρ_{abs}) of the granule sample and then the bulk density (ρ_{bulk}) of the sample. The true density and bulk density were measured using the Accupyc 1330 and the GeoPyc 1360, both by Micromeritics. The porosity is then found by using Equation (B.1).

$$\varepsilon = 1 - \frac{\rho_{bulk}}{\rho_{abs}} \tag{B.1}$$

B.3 Fractional binder content determination

An outline of the procedure used in determining the fractional binder content in granules is provided below. beginning with the preparation of the binder solution to which a colour dye

is added in order to quantify the binder content, inferred from the amount of coloured dye present in the granules.

During the formulation stage of the binder solution in preparation for the granulation experiments, a blue coloured dye was mixed into the binder solution of polyvinyl alcohol 2.5% w/w (PVOH). The final solution was well mixed with a final colour dye concentration of 8.9 g/L. During the granulation experiments, the binder along with the colour dye will be incorporated into the agglomerate. The addition of the colour dye into the binder solution did not appear to modify the binder surface tension when compared to the binder solution of polyvinyl alcohol (2.5% by mass) without the colour dye, based on contact angle comparisons.

B.3.1 Calibration curve

A preliminary scan was performed over the absorption spectrum between 300 nm to 1000 nm for various solution strength of the working standard. The results of the preliminary scan is shown in Figure B.1 with the optimum wavelength corresponding to the maximum peak absorption, which occurs at 630 nm. Repeatability tests were carried out on five separate working standards of 2% solution strength with a relative standard deviation (RSD%) of 0.7 (see Table B.1).

Table B.1: Repeatability tests on working standard with a 2% solution strength.

Sample ID	AU
1	0.6560
2	0.6615
3	0.6694
4	0.6637
5	0.6600
Average	0.6621
RSD%	0.7

*AU = absorption unit

Prior to the determination of the fractional binder content within the granules, it is necessary to first establish a linear range between the concentration of the dye and the measured absorbance corresponding to the dye component by means of a calibration curve. Firstly, a working standard containing the colour dye was prepared with a concentration of

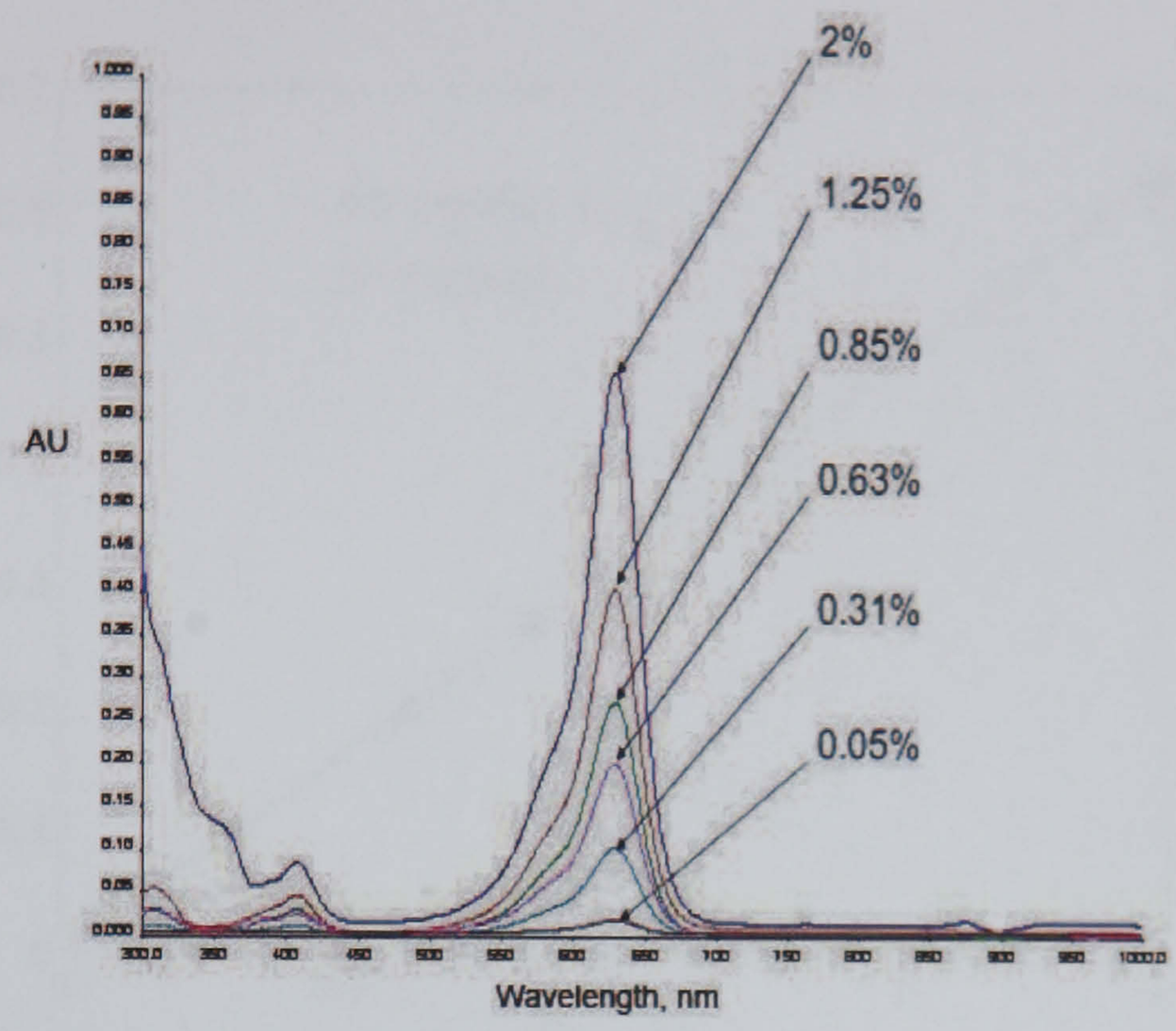

Figure B.1: Absorption spectrum for the blue dye component for solution strengths varying from 0.05%-2%. The optimum peak absorption for the dye occurs at a wavelength of 630 nm. A standard solution of dye with a concentration of 8.9 g/L represents 100% solution strength.

8.9 g/L. Having prepared 1 L of this working standard serving as the stock solution, standard solutions of different concentrations were also prepared by dilution from the stock solution. The various solution strengths with concentrations of the colour dye ranged from 0.3% to 2%. The working standard with a dye concentration of 8.9 g/L represents a solution strength of 100%. Deionised water was used as the diluent for all cases when preparing the solutions. The working standards containing the dye with solution strengths ranging from 0.3% to 2% were transferred into a cuvette for measurement on the spectrophotometer (Lambda 40, Perkin Elmer Instruments). The generated calibration curve is shown in Figure B.2. The regression curve is given in Equation (B.2) with a correlation coefficient ($R^2 = 0.9998$).

$$\mathrm{AU} = 0.3181 \times C_{dye} \tag{B.2}$$

Where, AU is the absorption unit and relates to the amount of colour dye present in the granule sample, C_{dye} can be interpreted as the concentration of colour dye related to the solution strength of the working standard.

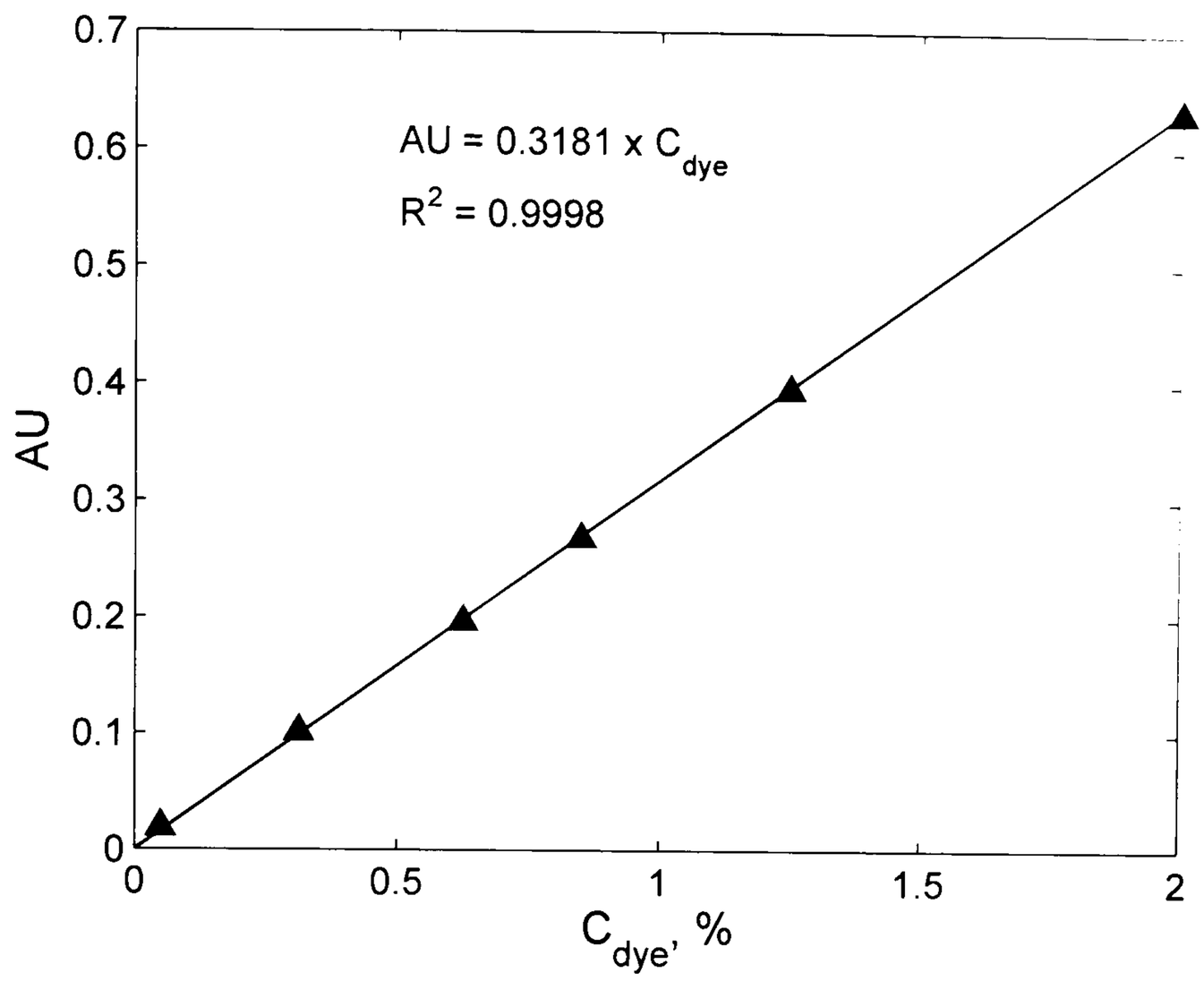

Figure B.2: Calibration curve.

B.3.2 Procedure for binder content determination

The procedure used in determining the fractional binder content of the granule sample is detailed in the following and also shown in Figure B.3.

1. Sample approximately 1 gram of sample and dissolve in 10 mL of deionised water into a centrifuge tube. Shake well to ensure that the colour dye is leached out of the granules and into the surrounding fluid medium.

2. The resultant solution prepared in the previous step is centrifuged (accuSpin^{TM}400. Fisher Scientific) for 5 mins at 5000 rpm.

3. The Supernatant is carefully extracted (dispersed particles will interfere with the absorption readings) and transferred into cuvettes for absorption measurement using the spectrophotometer (lambda 40. Perkin Elmer Instruments). The samples are diluted where necessary with deionised water in order to obtain absorption measurements within the pre-established linear range. Equations (B.2) and (B.3) are then used to determine the binder content of the granule sample.

$$LS\% = \left(\frac{1}{100}\right)\left(\frac{\mathrm{AU}}{0.3181}\right)\left(\frac{\rho_l}{M_s}\right) \tag{B.3}$$

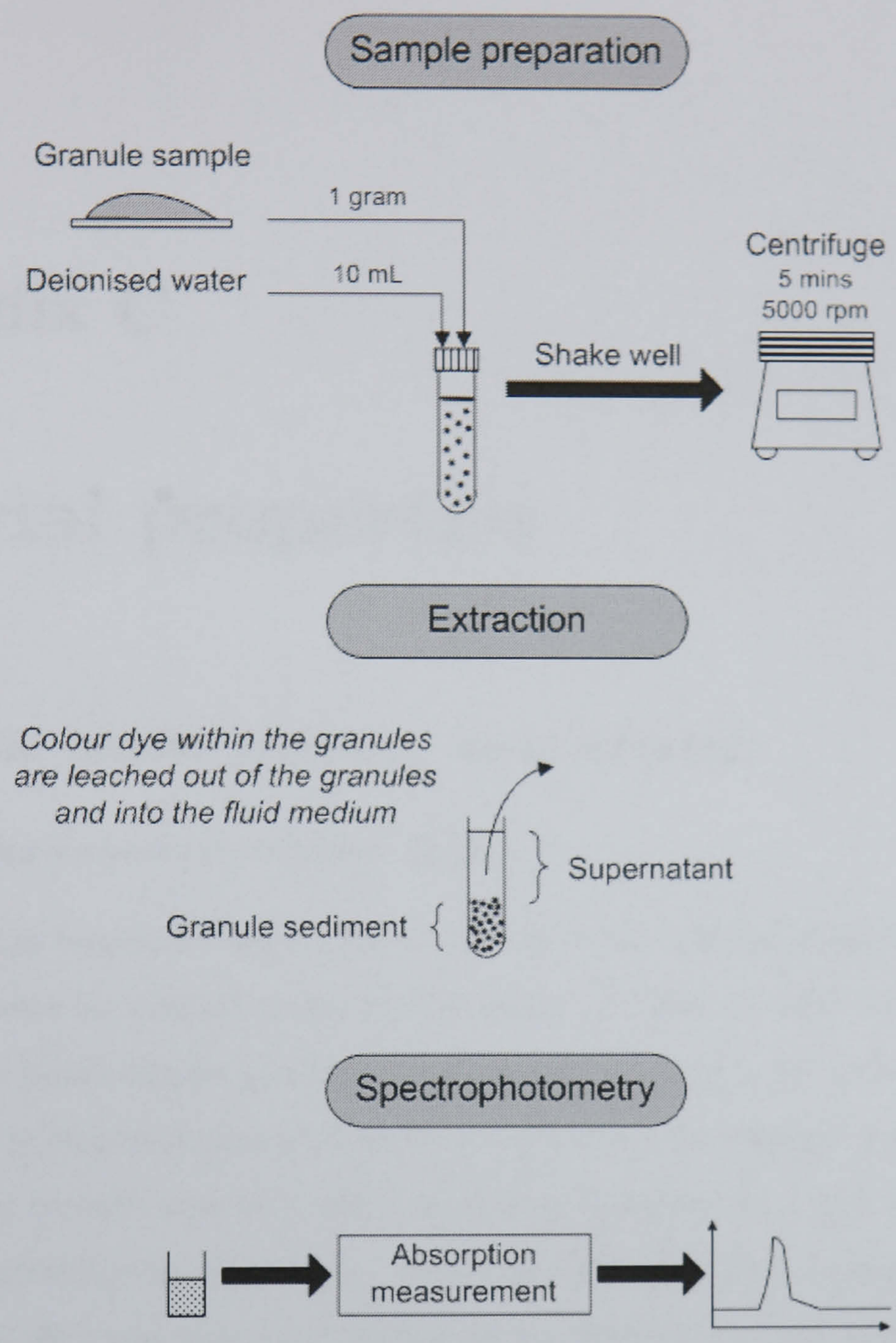

Figure B.3: Schematic of the binder content measurement procedure.

Appendix C

Material properties

C.1 Liquid binder property measurements

C.1.1 Binder-substrate contact angle

The contact angle formed between a liquid and the solid at the solid-liquid interface provides a useful parameter for characterising the behaviour of different solid-liquid interactions. In general, when a liquid droplet exhibits a high contact angle ($\theta > 90°$) then it is said that the liquid exhibits hydrophobic characteristics towards the solid surface. The droplet attempts to minimise the contact area with the solid surface, resulting in a high contact angle being formed. The wettability is poor for that particular solid-liquid pair. In contrast, a low contact angle ($0° \leq \theta < 90°$) provides good wetting of the solid with a high work of adhesion. The liquid exhibits hydrophilic characteristics when placed on the solid surface.

The measurement technique used for determining the contact angle between the liquid binder (polyvinyl alcohol 2.5% w/w. Elvanol T-66. DuPont) and the solid substrate (limestone, UQ) was carried out using a contact anglometer (Model 1501, Micromeritics). This technique is based on measuring the maximum height attainable by the liquid droplet that is deposited onto the horizontal powder surface. The maximum height is indicated by the use of a precision micrometer. Firstly, a powder cake is formed using the supplied base plate, guide and plunger. Secondly, the mass of the cake is determined (*i.e.* mass difference between the base plate containing the formed powder cake and the empty base plate prior to the preparation of the powder cake). Finally, the cover is screwed into the base plate forming an enclosure over the cake. The precision micrometer is attached to the centre of the cover in a fixed position above the cake, a side hole in the cover permits sessile drops of liquid to

be deposited gently onto the cake surface using a hypodermic syringe. A schematic set up of the contact anglometer is shown in Figure C.1. Measurement with the precision micrometer in determining the height corresponding to the flat surface is taken as the reference mark, which will later be used for determining the maximum height of droplet at the end of the procedure. Successive liquid droplets are deposited onto the cake surface in increments with the use of a hypodermic syringe. At each instance after depositing a drop, the height of the drop is carefully measured.

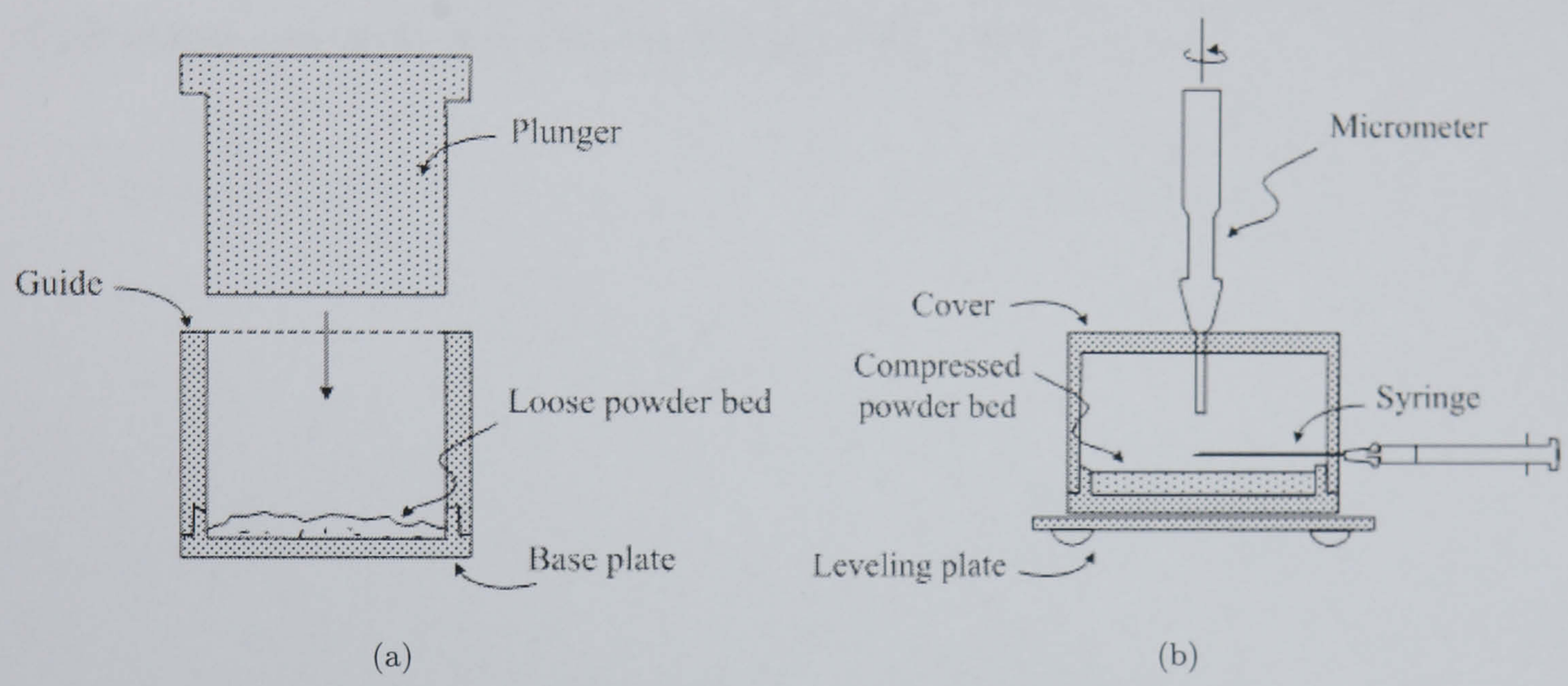

Figure C.1: Schematic of the contact anglometer (a) preparation of the compressed powder bed; (b) and the introduction of the droplet onto the powder surface via a hypodermic syringe.

The contact angle is determined using Equations (C.1)-(C.3), which is valid for contact angles measured between 0° and 90° (Micromeritics, Instruction manual, Catalogue No. 150/00000/00).

$$\cos\theta = 1 - \sqrt{\frac{Bh_m^2}{3\left(1-\varepsilon_c\right)\left(1-\frac{Bh_m^2}{2}\right)}} \tag{C.1}$$

$$B = \left(\frac{\rho_l \cdot g}{2\gamma^{LV}}\right) \tag{C.2}$$

$$\varepsilon_{cake} = \frac{\text{overall volume} - \text{actual volume}}{\text{overall volume}} = \frac{\left(D_c^2 \pi H_c\right)/4 - W_c/\rho_s}{\left(D_c^2 \pi H_c\right)/4} \tag{C.3}$$

Where, θ is the contact angle measured in degrees, h_m is the measured maximum height of the droplet, ρ_l is the liquid density, g is the acceleration due to gravity ($\equiv 9.8\,\mathrm{m/s^2}$), γ^{LV} is the liquid surface tension, ε_{cake} is the cake porosity, D_c is the cake diameter ($\equiv 5.080\,\mathrm{cm}$), H_c is the cake thickness, W_c is the mass of the powder composing the cake, ρ_s is the particle density of the powder ($\equiv 2743\,\mathrm{kg/m^3}$).

C.1.2 Binder viscosity

The viscosity of the liquid binder for a solution of polyvinyl alcohol with a concentration of 2.5% w/w (PVOH) was measured using an AR-G2 magnetic bearing rheometer (TA Instruments) with a reported value for the viscosity of 5.2 mPa·s. The measuring device comprised of two parallel stainless steel plates with the PVOH solution poured into the spacing separating the two plates (approximately 1000 μm). The equipment setting was configured with a strain sweep set in the range of 0.01% to 10% strain at a frequency of 1 Hz. The measurement of the sample was performed at a room temperature of 22°C.

Appendix D

Dynamic strength - axial compression test methodology

D.1 Preparation for axial compression

The methodology outlined in this section was adopted from Smith (2008) at the University of Queensland. Prior to the formation of the granular pellets, the $CaCO_3$ powder and PVOH binder solution were hand-kneaded together in a sealed plastic bag until a uniform consistency of the mixture was achieved through visual inspection (Iveson et al., 2002). Demonstrational results are shown for binder-to-solids ratios of 0.10 and 0.14. Approximately 100 g of powder was used for each binder-to-solid case, during the hand-kneading stage where the liquid binder was mixed with the powder. The amount of liquid used for each case was approximately 10 g and 14 g corresponding to binder-solid ratios of 0.10 and 0.14, respectively. The cylindrical pellets were formed using the pellet press and the pellet cast as shown in Figure D.1. A stainless steel spacer bar was fitted between the pellet press and the pellet cast, allowing for pellets with dimensions of 25 mm (height) and 20 mm (diameter) to be formed correctly.

Axial compression tests on the granular pellets were carried out on a load frame (Model 8841, Instron Dynamite^{TM}) capable of performing high compression velocities. Platen velocities used in this study were 0.1 mm/s, 1 mm/s, 10 mm/s, 100 mm/s and 200 mm/s. The platens were Teflon coated, which were also smeared with a thin layer ($\approx$ 0.5 mm) of lubricant (molybdenum disulphide grease, Castrol, LMM Grade) in order to minimise lateral friction. Figure D.2 shows a schematic of the arrangement for pellet compression tests.

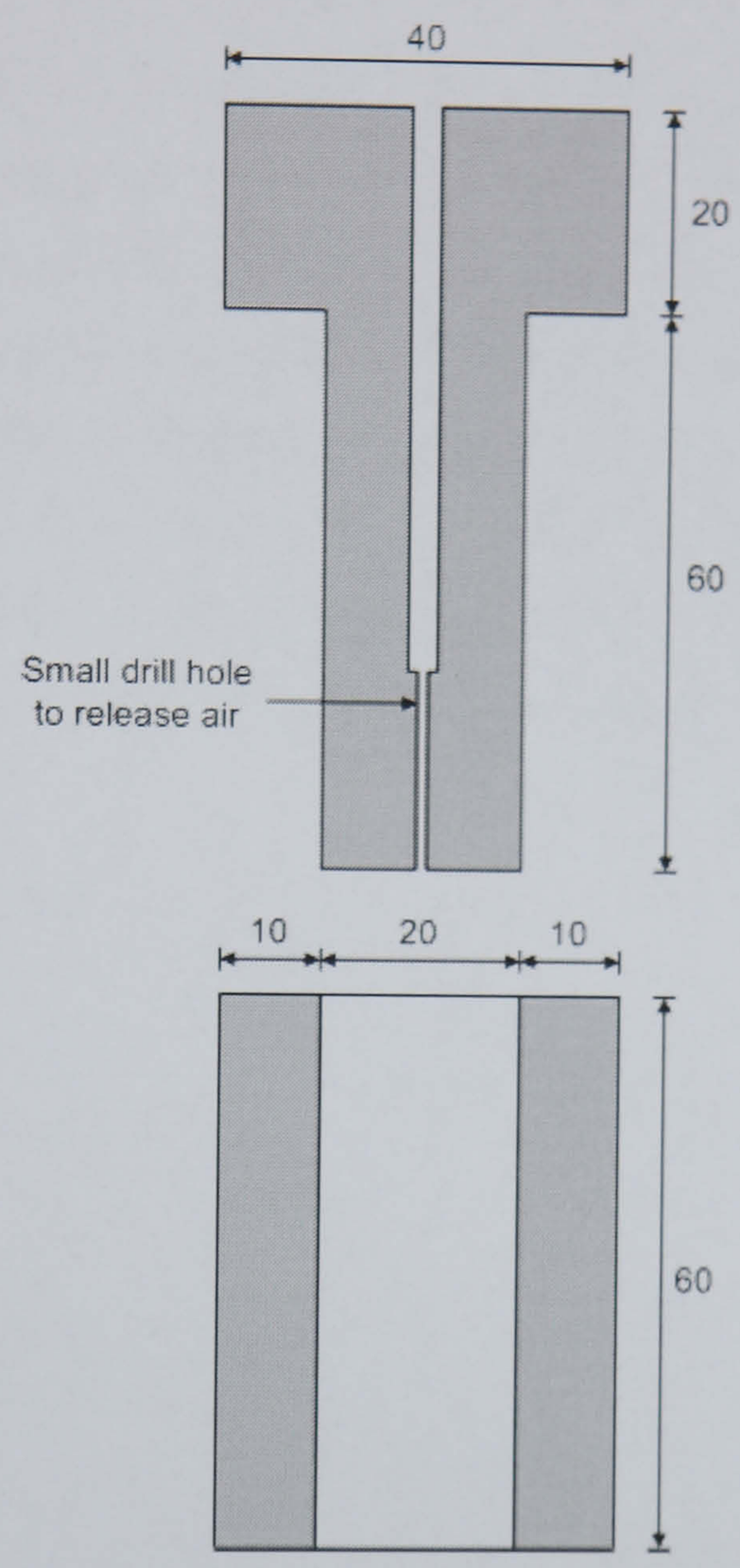

Figure D.1: Schematic of the pellet press and the pellet cast both manufactured from stainless steel. Adapted from Smith (2008).

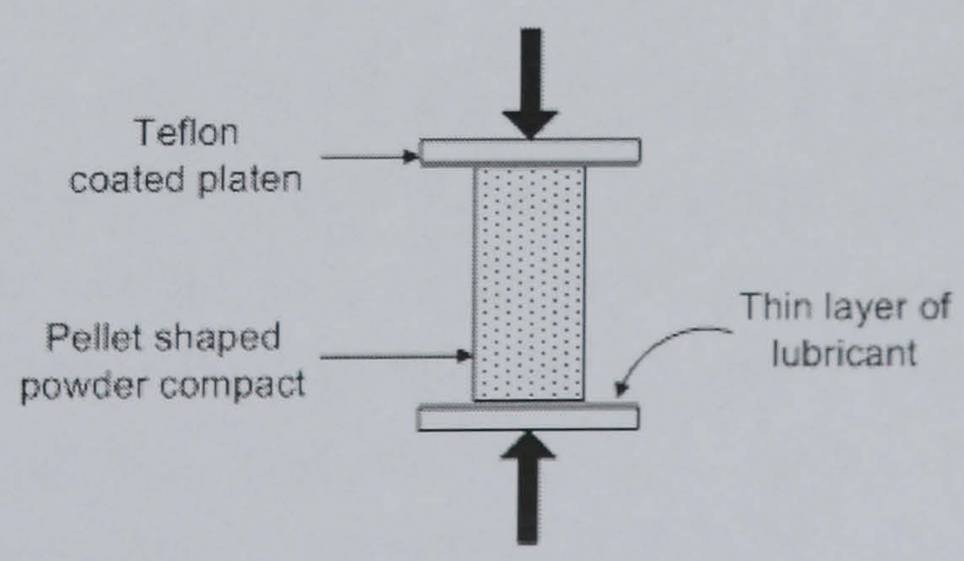

Figure D.2: Schematic of the granular pellet undergoing axial compression. Adapted from Iveson et al. (2002).

D.2 Dimensional analysis with Str* and Ca

The data obtained from the axial compression tests on the granular pellets of varying fractional binder content are reported in the form of pellet height at the corresponding load. conducted at a given platen velocity. These measurements are then used to compute the natural strain (ζ) given in Equation (D.1); the applied stress (σ) corresponding to the amount of compression that the pellet has undergone, which is related to the reduced pellet height determined by Equation (D.2) the volume of the pellet is conserved with each pellet deforming as a perfect cylinder. Thus, the cross-sectional area (A) of the pellet at any compression height of the pellet is given by Equation (D.3); and the strain rate ($\dot{\varepsilon}$) is given by Equation (D.4).

$$\zeta = \ln \frac{H_0}{H} \tag{D.1}$$

$$\sigma = \frac{F_{\text{load}}}{A} \tag{D.2}$$

$$A = \frac{H_0}{H} \frac{\pi D_{op}^2}{4} \tag{D.3}$$

$$\dot{\varepsilon} = -\frac{1}{H} \frac{dH}{dt} = \frac{v_{platen}}{H} \tag{D.4}$$

Where, D_{op} is the original pellet diameter, H_0 is the initial height of the granular pellet, H is the pellet height (mm) at a particular time instance after the pellet has undergone some axial compression, F^{load} is the applied force on the pellet at the corresponding time instance and v_{platen} is the velocity of the platen (mm/s). Results for pellets with a binder-to-solids ratio of 0.10 and 0.14 for stress versus natural strain profiles at varying platen velocities and profiles for the peak flow stress versus strain rate are shown in the Figures D.3 and D.4, respectively. The peak flow stress (σ_p) (determined as the maximum stress corresponding to a particular platen velocity obtained from Figure D.3) and the strain rate (Figure D.4) are made dimensionless using Equation (D.5) and Equation (D.6), respectively. The profiles of the Str^* versus Ca is shown in Figure D.5.

$$Str^* = \frac{\sigma_p \bar{D}_p}{\gamma^{LV} \cos\theta} \tag{D.5}$$

$$Ca = \frac{\mu \dot{\varepsilon} \bar{D}_p}{\gamma^{LV} \cos\theta} \tag{D.6}$$

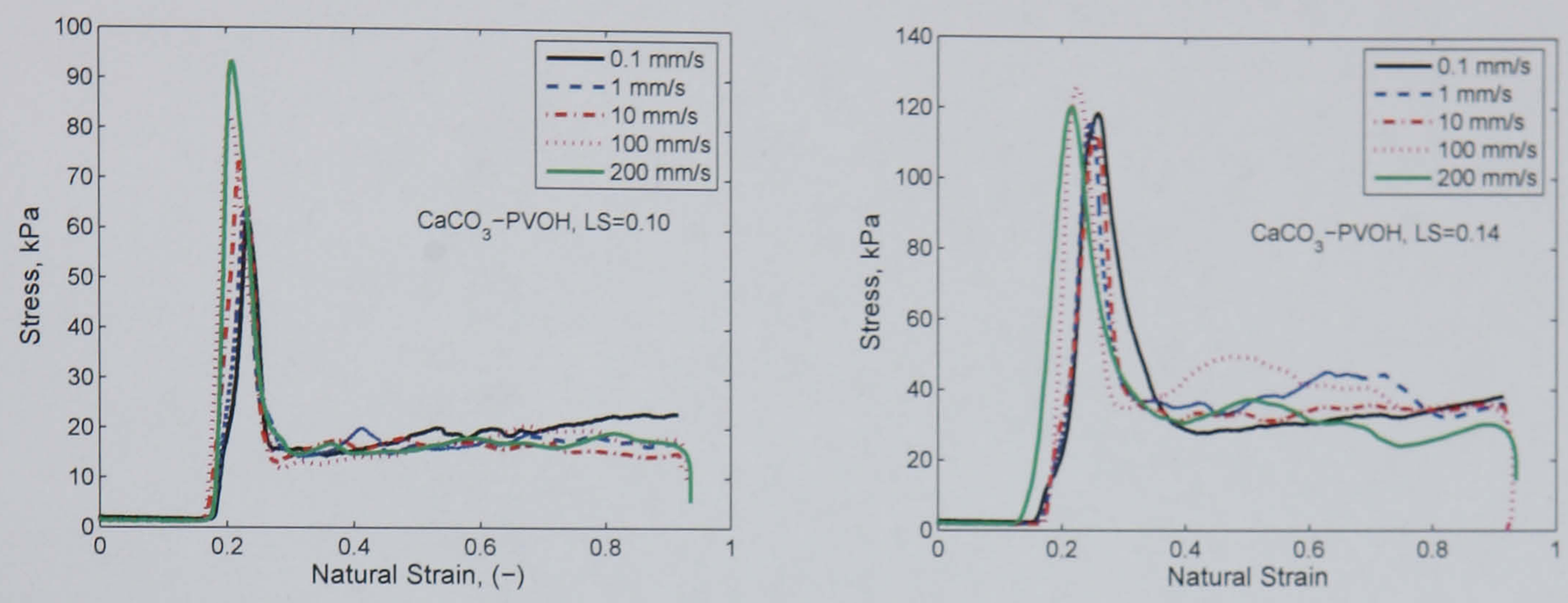

(a) Binder-to-solids ratio = 0.10 (b) Binder-to-solids ratio = 0.14

Figure D.3: Stress versus natural strain profiles for varying platen velocities for binder-to-solids-ratio of 0.10 and 0.14.

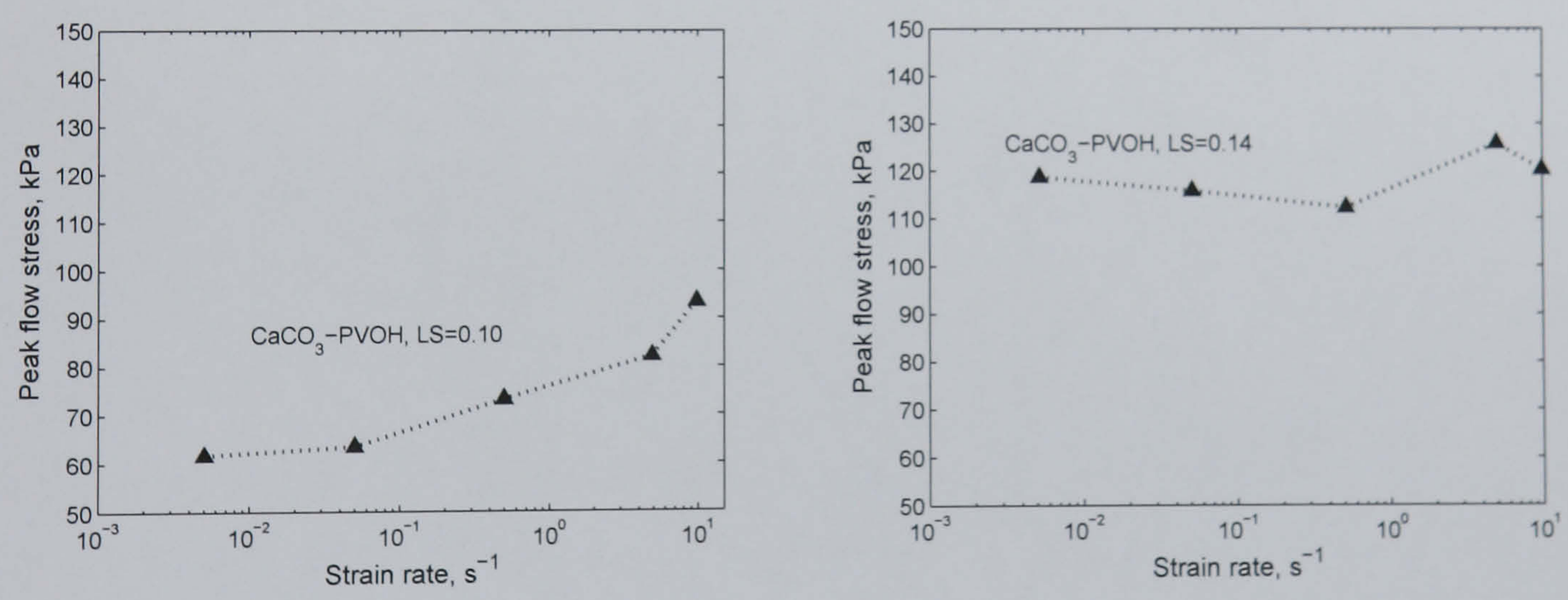

(a) Binder-to-solids ratio = 0.10 (b) Binder-to-solids ratio = 0.14

Figure D.4: Peak flow stress versus strain rate profiles for binder-to-solids-ratio of 0.10 and 0.14.

$$Ca = \frac{\mu \dot{\varepsilon} \bar{D}_p}{\gamma^{LV} \cos\theta} \tag{D.6}$$

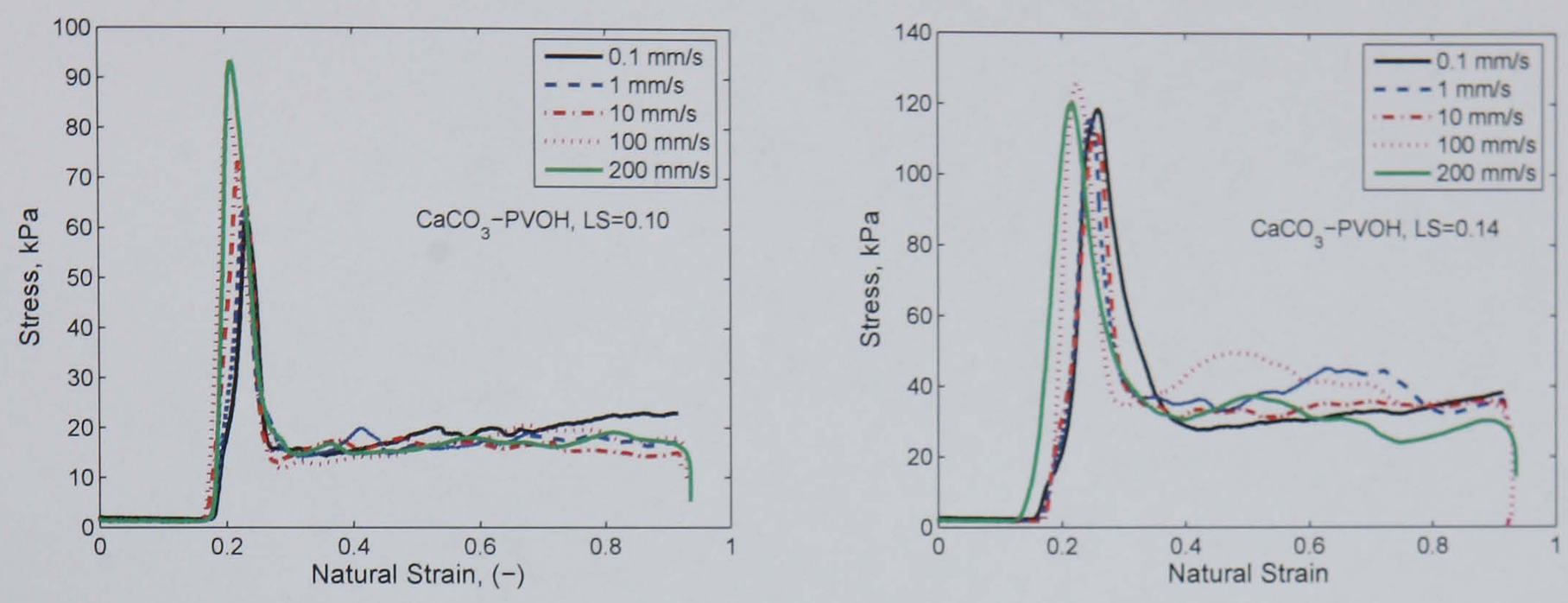

(a) Binder-to-solids ratio = 0.10

(b) Binder-to-solids ratio = 0.14

Figure D.3: Stress versus natural strain profiles for varying platen velocities for binder-to-solids-ratio of 0.10 and 0.14.

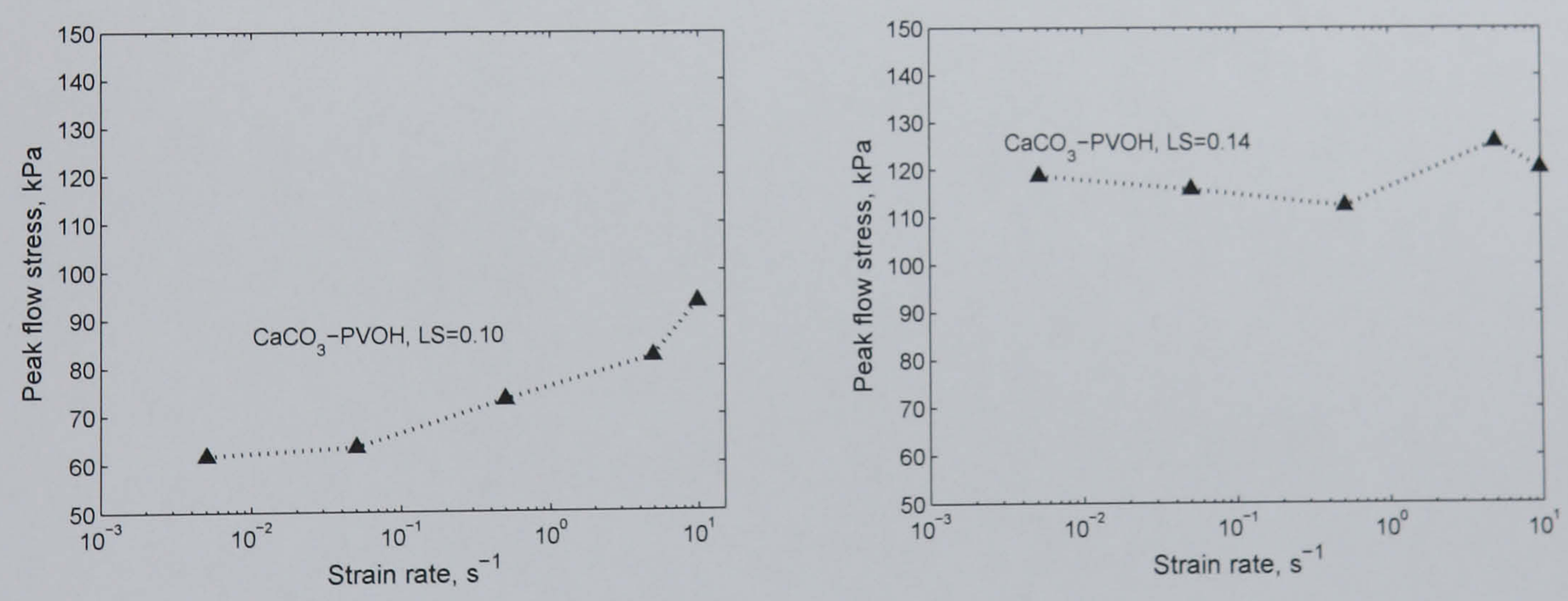

(a) Binder-to-solids ratio = 0.10

(b) Binder-to-solids ratio = 0.14

Figure D.4: Peak flow stress versus strain rate profiles for binder-to-solids-ratio of 0.10 and 0.14.

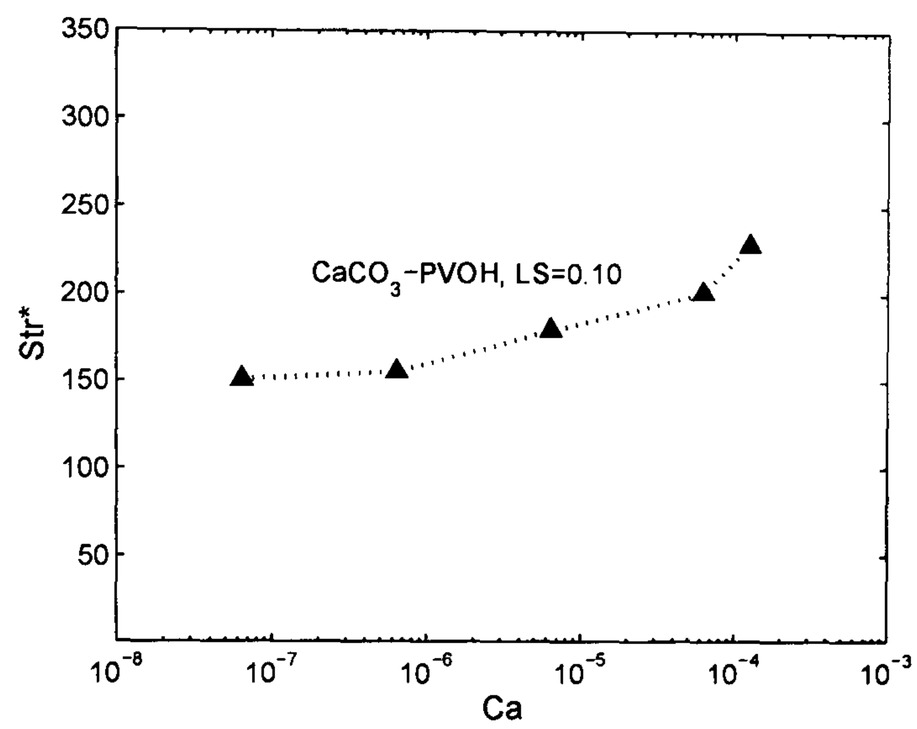

(a) Binder-to-solids ratio = 0.10

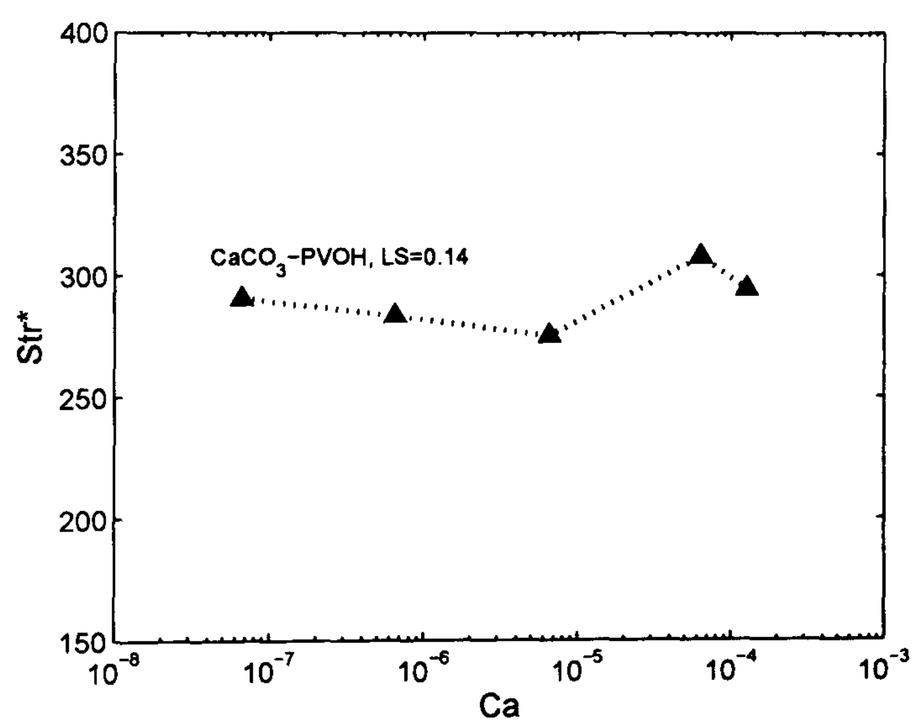

(b) Binder-to-solids ratio = 0.14

Figure D.5: Dimensionless pellet strength versus the dimensionless capillary number for binder-to-solids-ratio of 0.10 and 0.14.

Appendix E

Batch granulation data

Batch granulation experiments were carried out on a laboratory scale batch drum rotary granulator. The granulation recipe consisted of limestone powder (Aglime, Landmark, Australia) with a binder solution of 2% polyvinyl alcohol (PVOH) (Elvanol T66, Du Pont, USA). Granulation experiments pertaining to each of the binder-to-solids ratio and the amount of powder loaded into the drum granulator were performed on a single basis. For each of the experiments, steps were taken to ensure that for cases where the same amount of powder was to be granulated (*i.e.* varying only the binder-to-solids ratio whilst keeping the amount of powder used for granulation fixed). A calibrated balance was used to weigh 1.5 kg and 1.75 kg of powder for each experiment. The delivery of the liquid binder was via a pressure pot arrangement attached to a flat-fan spray nozzle. Consistency with respect to maintaining the pressure was determined by the laboratory supply taps. The choice in using a binder solution with concentration of 2.5% w/w provided a good balance in terms of providing continuous spray without incurring nozzle blockages and granulation.

A scoop sampling procedure was used in the experiments. The method involves plunging a scoop into the tumbling powder bed and extracting the sample. A particular feature of this method that was not conducive to accurate sampling was, to ensure an equal likelihood of all particles in the tumbling powder being sampled. It was observed via visual inspection that, larger granules tended to move towards the periphery of the drum interior whilst smaller granules remained near the center of the powder bed. To account for for this, six sub-samples were taken from different locations on the powder bed (see Figure E.1). These six sub-samples were pooled together to form representative sample of the powder bed for a particular time instant. Processing conditions pertaining to the granule samples after extraction from the

drum granulator, such as the drying time in the oven and the duration on the sieve shaker were maintained for all granulation experiments. The consistency in the procedures used for the granulation experiments pertaining to the sampling method, binder flow rate, drum filling and the post analysis of the samples helped to ensure minimising errors. In retrospect, a minimum of three experiments would need to be carried out for each granulation condition for demonstration of reproducibility.

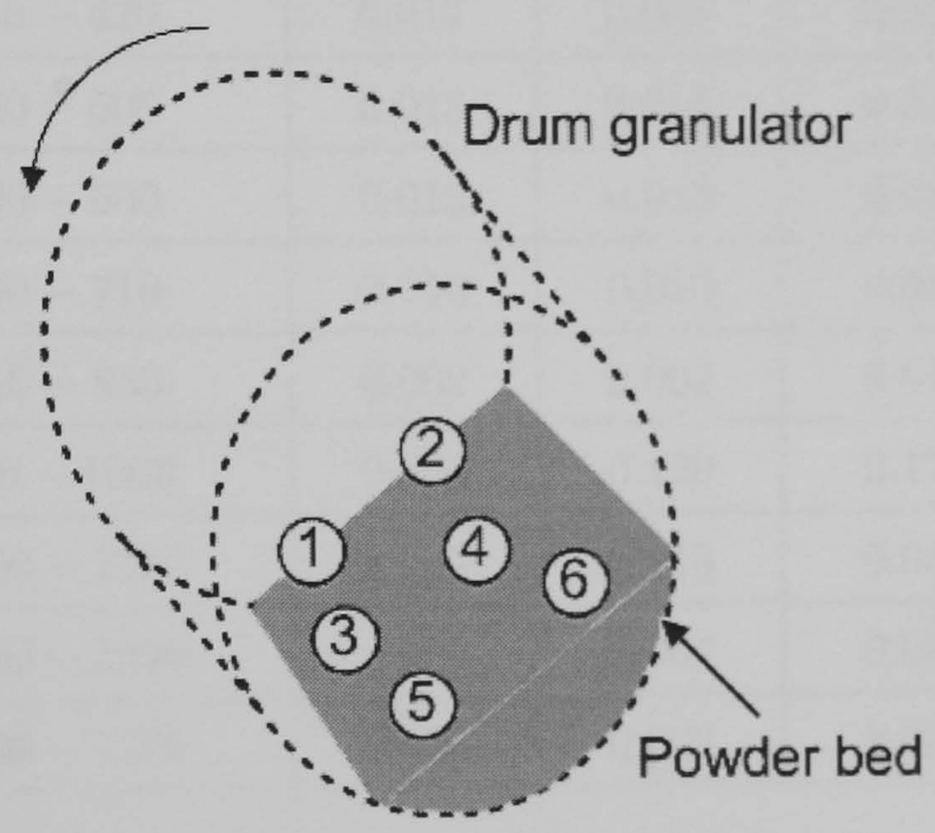

Figure E.1: Illustration of the locations of the six sample locations.

Table E.1: Normalised GSD for binder-to-solids ratio of 0.11 and 1.5 kg of powder–Set 1.

No.	Sieve fraction (μm)	t = 3 min	t = 5 min	t = 10 min	t = 15 min
1	< 250	0.746	0.713	0.598	0.518
2	250 – 300	0.081	0.078	0.095	0.091
3	300 – 355	0.021	0.021	0.025	0.021
4	355 – 420	0.017	0.008	0.015	0.015
5	420 – 500	0.015	0.015	0.014	0.015
6	500 – 600	0.013	0.013	0.013	0.013
7	600 – 710	0.010	0.010	0.010	0.010
8	710 – 850	0.002	0.002	0.021	0.020
9	850 – 1000	0.080	0.120	0.172	0.170
10	1000 – 1180	0.004	0.013	0.035	0.122
11	1180 – 1400	0.006	0.004	0.001	0.003
12	1400 – 1700	0.005	0.003	0.001	0.002

Table E.2: Normalised GSD for binder-to-solids ratio of 0.11 and 1.5 kg of powder–Set 2.

No.	Sieve fraction (μm)	t = 3 min	t = 5 min	t = 10 min	t = 15 min
1	< 250	0.778	0.717	0.603	0.503
2	250 – 300	0.073	0.084	0.097	.0101
3	300 – 355	0.019	0.019	0.029	0.018
4	355 – 420	0.010	0.011	0.012	0.017
5	420 – 500	0.012	0.012	0.018	0.013
6	500 – 600	0.012	0.010	0.016	0.011
7	600 – 710	0.008	0.012	0.011	0.012
8	710 – 850	0.001	0.004	0.028	0.023
9	850 – 1000	0.077	0.112	0.157	0.166
10	1000 – 1180	0.002	0.013	0.027	0.129
11	1180 – 1400	0.005	0.002	0.001	0.004
12	1400 – 1700	0.003	0.004	0.001	0.003

Table E.3: Normalised GSD for binder-to-solids ratio of 0.11 and 1.5 kg of powder–Set 3.

No.	Sieve fraction (μm)	t = 3 min	t = 5 min	t = 10 min	t = 15 min
1	< 250	0.764	0.699	0.589	0.509
2	250 – 300	0.080	0.085	0.088	0.093
3	300 – 355	0.021	0.021	0.022	0.020
4	355 – 420	0.015	0.015	0.017	0.015
5	420 – 500	0.015	0.014	0.015	0.016
6	500 – 600	0.013	0.011	0.013	0.013
7	600 – 710	0.010	0.014	0.014	0.012
8	710 – 850	0.002	0.002	0.031	0.020
9	850 – 1000	0.067	0.104	0.170	0.169
10	1000 – 1180	0.002	0.028	0.039	0.125
11	1180 – 1400	0.006	0.005	0.001	0.005
12	1400 – 1700	0.006	0.002	0.001	0.003

Table E.4: Granule porosity for binder-to-solids ratio of 0.11 and 1.5 kg of powder–Set 1.

No.	Sieve fraction (μm)	t = 3 min	t = 5 min	t = 10 min	t = 15 min
1	< 250	0.149	0.146	0.139	0.139
2	300 – 355	0.148	0.145	0.139	0.139
3	420 – 500	0.147	0.144	0.136	0.135
4	500 – 600	0.146	0.141	0.134	0.129
5	850 – 1000	0.141	0.136	0.131	0.125
6	1180 – 1400	0.138	0.134	0.128	0.122

Table E.5: Granule porosity for binder-to-solids ratio of 0.11 and 1.5 kg of powder–Set 2.

No.	Sieve fraction (μm)	t = 3 min	t = 5 min	t = 10 min	t = 15 min
1	< 250	0.149	0.145	0.139	0.139
2	300 – 355	0.148	0.145	0.138	0.139
3	420 – 500	0.146	0.144	0.135	0.135
4	500 – 600	0.145	0.140	0.134	0.130
5	850 – 1000	0.140	0.136	0.130	0.125
6	1180 – 1400	0.137	0.135	0.127	0.121

Table E.6: Granule porosity for binder-to-solids ratio of 0.11 and 1.5 kg of powder–Set 3.

No.	Sieve fraction (μm)	t = 3 min	t = 5 min	t = 10 min	t = 15 min
1	< 250	0.149	0.145	0.140	0.139
2	300 – 355	0.148	0.144	0.138	0.139
3	420 – 500	0.147	0.144	0.136	0.135
4	500 – 600	0.145	0.140	0.133	0.129
5	850 – 1000	0.140	0.136	0.131	0.125
6	1180 – 1400	0.137	0.135	0.127	0.122

Table E.7: Fractional binder content of granules for target binder-to-solids ratio of 0.11 with 1.5 kg of powder–Set 1.

No.	Sieve fraction (μm)	t = 3 min	t = 5 min	t = 10 min	t = 15 min
1	< 250	5.6	8.3	6.1	5.9
2	250 – 300	6.4	9.3	7.7	6.7
3	300 – 355	7.5	-	8.1	-
4	355 – 420	7.7	10.6	8.3	7.4
5	420 – 500	-	10.7	8.4	7.9
6	500 – 600	6.8	10.4	7.9	7.8
7	600 – 710	7.9	11.1	8.4	9.3
8	710 – 850	8.1	11.2	8.9	8.9
9	850 – 1000	7.3	11.5	-	8.2
10	1000 – 1180	7.8	12.2	-	9.1
11	1180 – 1400	8.3	11.1	9.4	8.8
12	1400 – 1700	8.2	11.6	9.4	8.9

Table E.8: Fractional binder content of granules for target binder-to-solids ratio of 0.11 with 1.5 kg of powder–Set 2.

No.	Sieve fraction (μm)	t = 3 min	t = 5 min	t = 10 min	t = 15 min
1	< 250	6.2	8.0	6.4	6.2
2	250 – 300	6.4	9.6	7.5	6.4
3	300 – 355	7.0	-	8.3	-
4	355 – 420	7.8	10.0	8.6	7.2
5	420 – 500	7.0	10.5	7.9	7.5
6	500 – 600	7.2	10.2	8.1	8.0
7	600 – 710	8.3	10.9	9.0	8.7
8	710 – 850	8.0	11.2	8.4	8.8
9	850 – 1000	8.1	11.3	8.6	8.7
10	1000 – 1180	7.9	11.8	-	9.1
11	1180 – 1400	8.0	12.0	8.7	9.0
12	1400 – 1700	8.4	11.8	9.3	9.2

Table E.9: Fractional binder content of granules for target binder-to-solids ratio of 0.11 with 1.5 kg of powder–Set 3.

No.	Sieve fraction (μm)	t = 3 min	t = 5 min	t = 10 min	t = 15 min
1	< 250	5.8	7.9	6.7	6.0
2	250 – 300	6.3	8.8	7.7	6.5
3	300 – 355	6.9	9.0	8.3	7.0
4	355 – 420	7.2	10.4	8.5	7.2
5	420 – 500	-	10.7	8.0	7.8
6	500 – 600	7.6	11.0	8.0	7.7
7	600 – 710	7.4	11.3	8.6	9.2
8	710 – 850	8.1	10.9	8.7	9.0
9	850 – 1000	8.0	11.1	9.1	8.7
10	1000 – 1180	7.5	11.8	-	8.8
11	1180 – 1400	8.2	11.5	9.0	9.2
12	1400 – 1700	8.4	11.7	9.1	9.2

Table E.10: Normalised GSD for binder-to-solids ratio of 0.12 and 1.5 kg of powder.

No.	Sieve fraction (μm)	t = 3 min	t = 5 min	t = 10 min	t = 15 min
1	< 250	0.530	0.432	0.363	0.212
2	250 – 300	0.074	0.073	0.073	0.073
3	300 – 355	0.025	0.024	0.024	0.025
4	355 – 420	0.015	0.015	0.014	0.015
5	420 – 500	0.015	0.015	0.015	0.025
6	500 – 600	0.013	0.013	0.013	0.023
7	600 – 710	0.010	0.010	0.010	0.010
8	710 – 850	0.002	0.002	0.002	0.002
9	850 – 1000	0.100	0.100	0.130	0.200
10	1000 – 1180	0.170	0.270	0.310	0.350
11	1180 – 1400	0.027	0.027	0.027	0.046
12	1400 – 1700	0.019	0.019	0.019	0.019

Table E.11: Granule porosity for binder-to-solids ratio of 0.12 and 1.5 kg of powder.

No.	Sieve fraction (μm)	t = 3 min	t = 5 min	t = 10 min	t = 15 min
1	< 250	0.149	0.145	0.138	0.138
2	300 – 355	0.147	0.143	0.138	0.138
3	420 – 500	0.147	0.143	0.135	0.135
4	500 – 600	0.145	0.140	0.133	0.129
5	850 – 1000	0.138	0.135	0.129	0.126
6	1180 – 1400	0.137	0.133	0.127	0.121

Table E.12: Fractional binder content of granules for target binder-to-solids ratio of 0.12 with 1.5 kg of powder.

No.	Sieve fraction (μm)	t = 3 min	t = 5 min	t = 10 min	t = 15 min
1	< 250	6.4	8.7	9.1	11.1
2	250 – 300	12.5	10.0	10.9	12.5
3	300 – 355	9.0	13.1	11.2	13.3
4	355 – 420	-	12.9	11.5	13.0
5	420 – 500	8.5	12.6	11.6	12.9
6	500 – 600	8.8	12.1	11.7	9.9
7	600 – 710	8.8	12.4	11.6	9.9
8	710 – 850	9.5	12.4	11.6	12.5
9	850 – 1000	9.5	12.6	11.7	12.3
10	1000 – 1180	8.5	12.0	11.9	11.7
11	1180 – 1400	8.6	12.0	12.1	10.1
12	1400 – 1700	7.9	12.1	12.3	9.4

Table E.13: Normalised GSD for binder-to-solids ratio of 0.11 and 1.75 kg of powder.

No.	Sieve fraction (μm)	t = 3 min	t = 5 min	t = 10 min	t = 15 min
1	< 250	0.719	0.688	0.581	0.481
2	250 – 300	0.101	0.091	0.100	0.097
3	300 – 355	0.020	0.021	0.025	0.021
4	355 – 420	0.015	0.014	0.013	0.015
5	420 – 500	0.014	0.014	0.013	0.016
6	500 – 600	0.012	0.012	0.011	0.013
7	600 – 710	0.010	0.013	0.010	0.010
8	710 – 850	0.002	0.011	0.018	0.020
9	850 – 1000	0.100	0.002	0.200	0.210
10	1000 – 1180	0.002	0.013	0.027	0.112
11	1180 – 1400	0.003	0.003	0.002	0.003
12	1400 – 1700	0.002	0.002	0.001	0.003

Table E.14: Granule porosity for binder-to-solids ratio of 0.11 and 1.75 kg of powder.

No.	Sieve fraction (μm)	t = 3 min	t = 5 min	t = 10 min	t = 15 min
1	< 250	0.142	0.138	0.133	0.136
2	300 – 355	0.141	0.137	0.133	0.136
3	420 – 500	0.140	0.136	0.129	0.132
4	500 – 600	0.137	0.132	0.128	0.126
5	850 – 1000	0.132	0.128	0.125	0.122
6	1180 – 1400	0.130	0.127	0.122	0.119

Table E.15: Fractional binder content of granules for target binder-to-solids ratio of 0.11 with 1.75 kg of powder.

No.	Sieve fraction (μm)	t = 3 min	t = 5 min	t = 10 min	t = 15 min
1	< 250	-	8.7	9.1	11.1
2	250 – 300	7.5	10.0	10.9	12.5
3	300 – 355	8.6	13.1	11.2	13.3
4	355 – 420	7.7	12.9	11.5	13.0
5	420 – 500	-	12.6	11.6	12.9
6	500 – 600	9.7	12.1	11.7	9.9
7	600 – 710	8.7	12.4	11.6	9.9
8	710 – 850	9.0	12.4	11.6	12.5
9	850 – 1000	9.4	12.6	11.7	12.3
10	1000 – 1180	-	12.0	11.9	11.7
11	1180 – 1400	-	12.0	12.1	10.1
12	1400 – 1700	10.1	12.1	12.3	9.4

Table E.16: Normalised GSD for binder-to-solids ratio of 0.13 and 1.5 kg of powder.

No.	Sieve fraction (μm)	t = 5 min	t = 10 min	t = 15 min
1	< 250	0.157	0.124	0.091
2	250 – 300	0.042	0.034	0.028
3	300 – 355	0.016	0.020	0.022
4	355 – 420	0.019	0.013	0.014
5	420 – 500	0.031	0.047	0.044
6	500 – 600	0.027	0.027	0.022
7	600 – 710	0.081	0.120	0.053
8	710 – 850	0.072	0.118	0.027
9	850 – 1000	0.128	0.135	0.095
10	1000 – 1180	0.089	0.054	0.028
11	1180 – 1400	0.060	0.038	0.016
12	1400 – 1700	0.075	0.043	0.019
13	1700 – 2360	0.074	0.052	0.025
14	2360 – 2800	0.027	0.024	0.034
15	2800 – 3350	0.024	0.022	0.046
16	3350 – 4000	0.019	0.023	0.046
17	4000 – 4750	0.020	0.012	0.050
18	> 4750	0.038	0.092	0.342

Table E.17: Normalised GSD for binder-to-solids ratio of 0.14 and 1.5 kg of powder.

No.	Sieve fraction (μm)	t = 5 min	t = 10 min	t = 15 min
1	< 250	0	-	-
2	250 – 300	0.001	-	-
3	300 – 355	0.001	-	-
4	355 – 420	0.002	-	-
5	420 – 500	0.002	-	-
6	500 – 600	0.002	-	-
7	600 – 710	0.004	-	-
8	710 – 850	0.004	0.022	-
9	850 – 1000	0.003	-	-
10	1000 – 1180	0.006	-	-
11	1180 – 1400	0.008	-	-
12	1400 – 1700	0.012	-	-
13	1700 – 2360	0.030	-	-
14	2360 – 2800	0.028	-	-
15	2800 – 3350	0.042	-	-
16	3350 – 4000	0.060	0.010	-
17	4000 – 4750	0.102	0.040	-
18	> 4750	0.692	0.929	1

* Sieve fractions (1-15) were combined in this size range at t = 10 min.

** For sieve fractions (1-17) there were no granules in this size range at t = 15 min.

Table E.18: Normalised GSD for binder-to-solids ratio of 0.13 and 1.75 kg of powder.

No.	Sieve fraction (μm)	t = 5 min	t = 10 min	t = 15 min
1	< 250	0.189	0.081	0.051
2	250 – 300	0.026	0.024	0.017
3	300 – 355	0.019	0.012	0.010
4	355 – 420	0.015	0.016	0.011
5	420 – 500	0.028	0.023	0.020
6	500 – 600	0.033	0.030	0.028
7	600 – 710	0.046	0.036	0.035
8	710 – 850	0.060	0.054	0.048
9	850 – 1000	0.086	0.082	0.068
10	1000 – 1180	0.082	0.109	0.109
11	1180 – 1400	0.098	0.114	0.120
12	1400 – 1700	0.082	0.100	0.118
13	1700 – 2360	0.099	0.134	0.137
14	2360 – 2800	0.038	0.046	0.052
15	2800 – 3350	0.034	0.040	0.043
16	3350 – 4000	0.029	0.039	0.041
17	4000 – 4750	0.015	0.027	0.029
18	> 4750	0.021	0.033	0.063

Table E.19: Normalised GSD for binder-to-solids ratio of 0.14 and 1.75 kg of powder.

No.	Sieve fraction (μm)	t = 5 min	t = 10 min	t = 15 min
1	< 250	0.045	-	-
2	250 – 300	-	-	-
3	300 – 355	-	-	-
4	355 – 420	-	-	-
5	420 – 500	-	-	-
6	500 – 600	-	-	-
7	600 – 710	-	0.028	-
8	710 – 850	-	-	0.012
9	850 – 1000	-	-	-
10	1000 – 1180	0.006	-	-
11	1180 – 1400	-	-	-
12	1400 – 1700	-	-	-
13	1700 – 2360	0.015	0.002	-
14	2360 – 2800	0.016	0.008	-
15	2800 – 3350	0.038	0.032	-
16	3350 – 4000	0.063	0.064	0.021
17	4000 – 4750	0.123	0.105	0.094
18	> 4750	0.694	0.760	0.874

* For sieve fractions (2-9) and (11-12) there were no granules corresponding to t = 5 min.

** Sieve fractions (1-12) were combined corresponding to t = 10 min.

*** Sieve fractions (1-15) were combined corresponding to t = 15 min.

Appendix F

Population balance model

F.1 Determination of phenomenological kernel parameters

In this section, an outline is given for the procedure adopted in this study for determining the adjustable parameters present in the model expressions for the considered granulation phenomena. In addition, a suggested method is given which proposes that an optimisation criterion be used in determining these unknown parameters.

The model that has been developed for the granulation process incorporates mechanistic representations for the nucleation phenomenon and the aggregation phenomenon whilst an exponential relationship is employed for describing granule consolidation. The method adopted in determining the sensitivity of the adjustable parameters, pertaining to each of the considered rate processes was based on the examination of the magnitude of the changes in the response variable (*i.e.* particle size). This was computed using a finite-difference approximation and is defined in Equation (F.1) in which small perturbations are made to the parameters required to be determined for different time instances. This process is repeated for each perturbation and for each of the parameters under consideration.

$$\frac{\partial \mathbf{y}(t)}{\partial x_i} \approx \frac{\mathbf{y}\left(t; \mathbf{x} + \Delta x_i\right) - \mathbf{y}(t; \mathbf{x})}{\Delta x_i} \tag{F.1}$$

Where, $\mathbf{y}$ is the response variable, $\mathbf{x} = [A_0\ c_1\ c]^{\mathsf{T}}$ is the vector of the parameters under consideration (*i.e.* A_0 corresponds to the parameter present in the nucleation kernel, c_1 corresponds to the parameter present in the aggregation kernel and c corresponds to the parameter present in the exponential relation for granule consolidation) and x_i is the ith element of $\mathbf{x}$.

Table E.6: Granule porosity for binder-to-solids ratio of 0.11 and 1.5 kg of powder–Set 3.

No.	Sieve fraction (μm)	t = 3 min	t = 5 min	t = 10 min	t = 15 min
1	< 250	0.149	0.145	0.140	0.139
2	300 – 355	0.148	0.144	0.138	0.139
3	420 – 500	0.147	0.144	0.136	0.135
4	500 – 600	0.145	0.140	0.133	0.129
5	850 – 1000	0.140	0.136	0.131	0.125
6	1180 – 1400	0.137	0.135	0.127	0.122

Table E.7: Fractional binder content of granules for target binder-to-solids ratio of 0.11 with 1.5 kg of powder–Set 1.

No.	Sieve fraction (μm)	t = 3 min	t = 5 min	t = 10 min	t = 15 min
1	< 250	5.6	8.3	6.1	5.9
2	250 – 300	6.4	9.3	7.7	6.7
3	300 – 355	7.5	-	8.1	-
4	355 – 420	7.7	10.6	8.3	7.4
5	420 – 500	-	10.7	8.4	7.9
6	500 – 600	6.8	10.4	7.9	7.8
7	600 – 710	7.9	11.1	8.4	9.3
8	710 – 850	8.1	11.2	8.9	8.9
9	850 – 1000	7.3	11.5	-	8.2
10	1000 – 1180	7.8	12.2	-	9.1
11	1180 – 1400	8.3	11.1	9.4	8.8
12	1400 – 1700	8.2	11.6	9.4	8.9

Table E.8: Fractional binder content of granules for target binder-to-solids ratio of 0.11 with 1.5 kg of powder–Set 2.

No.	Sieve fraction (μm)	t = 3 min	t = 5 min	t = 10 min	t = 15 min
1	< 250	6.2	8.0	6.4	6.2
2	250 – 300	6.4	9.6	7.5	6.4
3	300 – 355	7.0	-	8.3	-
4	355 – 420	7.8	10.0	8.6	7.2
5	420 – 500	7.0	10.5	7.9	7.5
6	500 – 600	7.2	10.2	8.1	8.0
7	600 – 710	8.3	10.9	9.0	8.7
8	710 – 850	8.0	11.2	8.4	8.8
9	850 – 1000	8.1	11.3	8.6	8.7
10	1000 – 1180	7.9	11.8	-	9.1
11	1180 – 1400	8.0	12.0	8.7	9.0
12	1400 – 1700	8.4	11.8	9.3	9.2

Table E.9: Fractional binder content of granules for target binder-to-solids ratio of 0.11 with 1.5 kg of powder–Set 3.

No.	Sieve fraction (μm)	t = 3 min	t = 5 min	t = 10 min	t = 15 min
1	< 250	5.8	7.9	6.7	6.0
2	250 – 300	6.3	8.8	7.7	6.5
3	300 – 355	6.9	9.0	8.3	7.0
4	355 – 420	7.2	10.4	8.5	7.2
5	420 – 500	-	10.7	8.0	7.8
6	500 – 600	7.6	11.0	8.0	7.7
7	600 – 710	7.4	11.3	8.6	9.2
8	710 – 850	8.1	10.9	8.7	9.0
9	850 – 1000	8.0	11.1	9.1	8.7
10	1000 – 1180	7.5	11.8	-	8.8
11	1180 – 1400	8.2	11.5	9.0	9.2
12	1400 – 1700	8.4	11.7	9.1	9.2

Table E.10: Normalised GSD for binder-to-solids ratio of 0.12 and 1.5 kg of powder.

No.	Sieve fraction (μm)	t = 3 min	t = 5 min	t = 10 min	t = 15 min
1	< 250	0.530	0.432	0.363	0.212
2	250 – 300	0.074	0.073	0.073	0.073
3	300 – 355	0.025	0.024	0.024	0.025
4	355 – 420	0.015	0.015	0.014	0.015
5	420 – 500	0.015	0.015	0.015	0.025
6	500 – 600	0.013	0.013	0.013	0.023
7	600 – 710	0.010	0.010	0.010	0.010
8	710 – 850	0.002	0.002	0.002	0.002
9	850 – 1000	0.100	0.100	0.130	0.200
10	1000 – 1180	0.170	0.270	0.310	0.350
11	1180 – 1400	0.027	0.027	0.027	0.046
12	1400 – 1700	0.019	0.019	0.019	0.019

Table E.11: Granule porosity for binder-to-solids ratio of 0.12 and 1.5 kg of powder.

No.	Sieve fraction (μm)	t = 3 min	t = 5 min	t = 10 min	t = 15 min
1	< 250	0.149	0.145	0.138	0.138
2	300 – 355	0.147	0.143	0.138	0.138
3	420 – 500	0.147	0.143	0.135	0.135
4	500 – 600	0.145	0.140	0.133	0.129
5	850 – 1000	0.138	0.135	0.129	0.126
6	1180 – 1400	0.137	0.133	0.127	0.121

Table E.12: Fractional binder content of granules for target binder-to-solids ratio of 0.12 with 1.5 kg of powder.

No.	Sieve fraction (μm)	t = 3 min	t = 5 min	t = 10 min	t = 15 min
1	< 250	6.4	8.7	9.1	11.1
2	250 – 300	12.5	10.0	10.9	12.5
3	300 – 355	9.0	13.1	11.2	13.3
4	355 – 420	-	12.9	11.5	13.0
5	420 – 500	8.5	12.6	11.6	12.9
6	500 – 600	8.8	12.1	11.7	9.9
7	600 – 710	8.8	12.4	11.6	9.9
8	710 – 850	9.5	12.4	11.6	12.5
9	850 – 1000	9.5	12.6	11.7	12.3
10	1000 – 1180	8.5	12.0	11.9	11.7
11	1180 – 1400	8.6	12.0	12.1	10.1
12	1400 – 1700	7.9	12.1	12.3	9.4

Table E.13: Normalised GSD for binder-to-solids ratio of 0.11 and 1.75 kg of powder.

No.	Sieve fraction (μm)	t = 3 min	t = 5 min	t = 10 min	t = 15 min
1	< 250	0.719	0.688	0.581	0.481
2	250 – 300	0.101	0.091	0.100	0.097
3	300 – 355	0.020	0.021	0.025	0.021
4	355 – 420	0.015	0.014	0.013	0.015
5	420 – 500	0.014	0.014	0.013	0.016
6	500 – 600	0.012	0.012	0.011	0.013
7	600 – 710	0.010	0.013	0.010	0.010
8	710 – 850	0.002	0.011	0.018	0.020
9	850 – 1000	0.100	0.002	0.200	0.210
10	1000 – 1180	0.002	0.013	0.027	0.112
11	1180 – 1400	0.003	0.003	0.002	0.003
12	1400 – 1700	0.002	0.002	0.001	0.003

Table E.16: Normalised GSD for binder-to-solids ratio of 0.13 and 1.5 kg of powder.

No.	Sieve fraction (μm)	t = 5 min	t = 10 min	t = 15 min
1	< 250	0.157	0.124	0.091
2	250 – 300	0.042	0.034	0.028
3	300 – 355	0.016	0.020	0.022
4	355 – 420	0.019	0.013	0.014
5	420 – 500	0.031	0.047	0.044
6	500 – 600	0.027	0.027	0.022
7	600 – 710	0.081	0.120	0.053
8	710 – 850	0.072	0.118	0.027
9	850 – 1000	0.128	0.135	0.095
10	1000 – 1180	0.089	0.054	0.028
11	1180 – 1400	0.060	0.038	0.016
12	1400 – 1700	0.075	0.043	0.019
13	1700 – 2360	0.074	0.052	0.025
14	2360 – 2800	0.027	0.024	0.034
15	2800 – 3350	0.024	0.022	0.046
16	3350 – 4000	0.019	0.023	0.046
17	4000 – 4750	0.020	0.012	0.050
18	> 4750	0.038	0.092	0.342

Table E.17: Normalised GSD for binder-to-solids ratio of 0.14 and 1.5 kg of powder.

No.	Sieve fraction (μm)	t = 5 min	t = 10 min	t = 15 min
1	< 250	0	-	-
2	250 – 300	0.001	-	-
3	300 – 355	0.001	-	-
4	355 – 420	0.002	-	-
5	420 – 500	0.002	-	-
6	500 – 600	0.002	-	-
7	600 – 710	0.004	-	-
8	710 – 850	0.004	0.022	-
9	850 – 1000	0.003	-	-
10	1000 – 1180	0.006	-	-
11	1180 – 1400	0.008	-	-
12	1400 – 1700	0.012	-	-
13	1700 – 2360	0.030	-	-
14	2360 – 2800	0.028	-	-
15	2800 – 3350	0.042	-	-
16	3350 – 4000	0.060	0.010	-
17	4000 – 4750	0.102	0.040	-
18	> 4750	0.692	0.929	1

* Sieve fractions (1-15) were combined in this size range at t = 10 min.

** For sieve fractions (1-17) there were no granules in this size range at t = 15 min.

Table E.18: Normalised GSD for binder-to-solids ratio of 0.13 and 1.75 kg of powder.

No.	Sieve fraction (μm)	t = 5 min	t = 10 min	t = 15 min
1	< 250	0.189	0.081	0.051
2	250 – 300	0.026	0.024	0.017
3	300 – 355	0.019	0.012	0.010
4	355 – 420	0.015	0.016	0.011
5	420 – 500	0.028	0.023	0.020
6	500 – 600	0.033	0.030	0.028
7	600 – 710	0.046	0.036	0.035
8	710 – 850	0.060	0.054	0.048
9	850 – 1000	0.086	0.082	0.068
10	1000 – 1180	0.082	0.109	0.109
11	1180 – 1400	0.098	0.114	0.120
12	1400 – 1700	0.082	0.100	0.118
13	1700 – 2360	0.099	0.134	0.137
14	2360 – 2800	0.038	0.046	0.052
15	2800 – 3350	0.034	0.040	0.043
16	3350 – 4000	0.029	0.039	0.041
17	4000 – 4750	0.015	0.027	0.029
18	> 4750	0.021	0.033	0.063

Table E.19: Normalised GSD for binder-to-solids ratio of 0.14 and 1.75 kg of powder.

No.	Sieve fraction (μm)	t = 5 min	t = 10 min	t = 15 min
1	< 250	0.045	-	-
2	250 – 300	-	-	-
3	300 – 355	-	-	-
4	355 – 420	-	-	-
5	420 – 500	-	-	-
6	500 – 600	-	-	-
7	600 – 710	-	0.028	-
8	710 – 850	-	-	0.012
9	850 – 1000	-	-	-
10	1000 – 1180	0.006	-	-
11	1180 – 1400	-	-	-
12	1400 – 1700	-	-	-
13	1700 – 2360	0.015	0.002	-
14	2360 – 2800	0.016	0.008	-
15	2800 – 3350	0.038	0.032	-
16	3350 – 4000	0.063	0.064	0.021
17	4000 – 4750	0.123	0.105	0.094
18	> 4750	0.694	0.760	0.874

* For sieve fractions (2-9) and (11-12) there were no granules corresponding to t = 5 min.

** Sieve fractions (1-12) were combined corresponding to t = 10 min.

*** Sieve fractions (1-15) were combined corresponding to t = 15 min.

Appendix F

Population balance model

F.1 Determination of phenomenological kernel parameters

In this section, an outline is given for the procedure adopted in this study for determining the adjustable parameters present in the model expressions for the considered granulation phenomena. In addition, a suggested method is given which proposes that an optimisation criterion be used in determining these unknown parameters.

The model that has been developed for the granulation process incorporates mechanistic representations for the nucleation phenomenon and the aggregation phenomenon whilst an exponential relationship is employed for describing granule consolidation. The method adopted in determining the sensitivity of the adjustable parameters, pertaining to each of the considered rate processes was based on the examination of the magnitude of the changes in the response variable (*i.e.* particle size). This was computed using a finite-difference approximation and is defined in Equation (F.1) in which small perturbations are made to the parameters required to be determined for different time instances. This process is repeated for each perturbation and for each of the parameters under consideration.

$$\frac{\partial \mathbf{y}(t)}{\partial x_i} \approx \frac{\mathbf{y}\left(t; \mathbf{x} + \Delta x_i\right) - \mathbf{y}(t; \mathbf{x})}{\Delta x_i} \tag{F.1}$$

Where, $\mathbf{y}$ is the response variable, $\mathbf{x} = [A_0\ c_1\ c]^{\mathsf{T}}$ is the vector of the parameters under consideration (*i.e.* A_0 corresponds to the parameter present in the nucleation kernel, c_1 corresponds to the parameter present in the aggregation kernel and c corresponds to the parameter present in the exponential relation for granule consolidation) and x_i is the ith element of $\mathbf{x}$.

The minimisation of the sum of squared errors ($\Phi(\mathbf{x})$) is used as the optimisation criterion and is defined in Equation (F.2).

$$\Phi(\mathbf{x}) = \sum_{t=1}^{N_t}\sum_{i=1}^{N_s}\left(N_{t,i} - \hat{N}_{t,i}(\mathbf{x})\right)^2 \tag{F.2}$$

Where, $N_{t,i}$ and $\hat{N}_{t,i}$ are the experimental and model predicted values for the number of particles in particle size class i at a time instant of t, N_s is the maximum number of particle size classes and N_t is the total number of time instances used for sampling, the vector of the unknown parameters $\mathbf{x}$. The criterion given in Equation (F.2) is based on minimising the sum of squared errors between the model prediction and the measured output quantity obtained from experimental measurements. Solving this optimisation problem whereby, the aim is to minimise the objective function, the overall sum of squared error can be performed by using Sequential Quadratic Programming (SQP) method. Providing an initial value for the parameters in the vector $\mathbf{x}$ will be an important first step and information providing engineering insight of the process will aid in this regard, in addition to literature values as a guide if available. Testing the sensitivity of the objective function on each of the initial parameter values before, commencing optimisation can be performed by perturbing each value separately by an arbitrarily small value such as 1% and observing the difference in the objective function whether it is greater than the optimisation tolerance (*e.g.* 1×10^{-3}).

F.2 Population balance model degrees of freedom

Granulation processes poses a particular challenge to control as there are a limited number of potential manipulated variables, available to use by the operator. The liquid flow rates represent prime candidates as manipulated variables, owing to the sensitivity of the granule size distribution to the moisture content.

In the present study, the population balance model used utilises three manipulated variables which correspond to the three liquid binder flow rates for each spray nozzle placed in different locations along the granulator. The population balance model is formulated with respect to the three internal coordinates, namely the volume of solid, the volume of liquid and the volume of gas in the granules. Thus, each granule is considered to be comprised of the three aforementioned component volumes. A more meaningful interpretation of the granule behaviour is to consider instead, the particle size, granule liquid binder content and the granule porosity (relation to bulk density) which can be determined from knowledge of

the three volumes making up the granule (see Figure 3.2). The rate of aggregation is particularly affected by multiple particle properties of which. the granule size and the liquid binder content exert a strong influence on particle growth. Hence, during experimentation collecting data based on these measurable quantities will prove helpful in controlling the quality of the granules, whilst minimising the the production of out-of-spec granules.

LONDON